Investigation of HLA-E intracellular transport and antigen presentation

Wanlin He

Jesus College

University of Oxford

A thesis submitted for the degree of

Doctor of Philosophy

Trinity 2023

Acknowledgements

My deepest appreciation goes to my dear supervisors Prof. Andrew McMichael, Prof. Persephone Borrow and Dr. Simon Brackenridge. Their unwavering support and invaluable guidance have been instrumental in both this project and my personal growth. Their infectious passion for science, pivotal mentorship, and constant encouragement have sustained me throughout this challenging yet rewarding journey of DPhil study.

I offer my sincere gratitude to Prof. Geraldine Gillespie for her enlightening discussions related to the project as well as professional development. I am also grateful to the past and present members of the McMichael group, Borrow group and Gillespie group for their constructive advice and support, which have greatly enriched my experience in research as well as in life. In addition, I would like to acknowledge the generosity of other members within our department for their support in providing access to resources, facilities, and research opportunities.

My academic pursuit was made possible through the generous support of the China Scholarship Council and the Nuffield Department of Medicine, who provided me with a funded studentship. Without their assistance, my studies at Oxford would not have been attainable.

Finally, I extend my profound gratitude to my cherished family and friends for their constant support throughout this academic journey, with special thanks to my parents for their enduring love and encouragement throughout my time in the UK.

Abstract

Apart from its primary role in presenting signal peptides derived from major histocompatibility complex (MHC) class I molecules to natural killer (NK) cells, MHC-E can also present pathogen-derived peptides to CD8+ T cells to inhibit pathogenesis upon infection. Recent discoveries demonstrated the effectiveness of MHC-E-restricted CD8+ T cell responses in controlling simian immunodeficiency virus (SIV) infection within a vaccine model, which has generated considerable interest in this non-canonical immune pathway.

MHC-E is an appealing target for immunotherapies and vaccine design due to its low genetic diversity and resistance to downregulation in response to pathogen infections and cancers. However, to fully exploit the potential of the unconventional human MHC-E (HLA-E)-restricted CD8+ T cell responses for therapeutic purposes, a comprehensive understanding of the intricate pathways governing HLA-E transport and antigen presentation is necessary, which has remained unclear thus far.

In this thesis, I delineated the basic trafficking patterns of HLA-E and explored the underlying mechanisms. The retention in the endoplasmic reticulum (ER) and the fast surface internalisation are the two major characteristics of HLA-E trafficking, which are predominantly shaped by its cytoplasmic tail and peptide repertoire. The ER retention of HLA-E primarily arises from the scarcity of high-affinity peptides and is further intensified by the absence of a C-terminal ER export motif. The fast internalisation of HLA-E results from a lysine/tryptophan-based endocytic motif on its cytoplasmic tail, while the lack of optimal peptides further decreased the surface stability of HLA-E.

Collectively, these findings unveil unique transport patterns and intricate regulatory mechanisms governing HLA-E trafficking, which not only advances our

understanding of how HLA-E accomplishes its immunological roles through precise transport regulation but also provides valuable insights for the future development of immunotherapies and vaccines targeting the atypical HLA-E-restricted CD8+ T cell responses.

Table of Contents

List of Figures

List of Tables

List of Abbreviations

1G4	TCR specific for HLA-A*0201-restricted NY–ESO-1 peptide
β2m	β2-microglobulin
APC	Antigen presenting cell
BCR	B cell receptor
BFA	Brefeldin A
C62	ChAdOx1.HIVconsv62
CD74 KK10	CD74 with the CLIP region replaced with KK10 peptide
ChAdOx1	Chimpanzee adenoviral vector created by University of Oxford
CLIP	Class II associated invariant chain peptide
CNX	Chaperone calnexin
co-IP	co-immunoprecipitation
CRT	Calreticulin
CTD	C-terminal domain
CTL	Cytotoxic T lymphocyte
DMSO	Dimethyl sulfoxide
DPBS	Dulbecco's Phosphate-Buffered Saline
DSF	Differential scanning fluorimetry
EBV	Epstein-Barr virus
ELISA	Enzyme-linked immunosorbent assay
Endo H	Endoglycosidase H
ERC	Endocytic recycling compartment
ERAP	ER aminopeptidase
FACS	Fluorescence-activated cell sorting
FBS	Fetal bovine serum
HBV	Hepatitis B virus
HC	Heavy chain
HCV	Hepatitis C virus
HCMV	Human cytomegalovirus
HeLa.E cells	HeLa cell line stably transfected with HLA-E*01:03
HeLa.A3 cells	HeLa cell line stably transfected with HLA-A*03:01
HIV	Human immunodeficiency virus
HIV-1(VSVG-BAL)	VSVG-pseudotyped HIV-1 NL4.3-BaL strain
HLA	Human Leukocyte Antigen
hrs	hours
IF	Immunofluorescence
IFN	Interferon
ILT	Ig-like transcript
iNKT cells	Invariant natural killer T cells
IONO	Ionomycin

IP	Immunoprecipitation
K562E cells	K562 cells stably transfected with HLA-E*01:03
KIR	Killer cell immunoglobulin-like receptor
KK10-TCR	TCR specific for HLA-B*2705-restricted HIV-1 KK10 peptide
KSHV	Kaposi's sarcoma-associated herpesvirus
LCMV	Lymphocytic choriomeningitis virus
M4	MVA.tHIVconsv4
MAIT cells	Mucosal-associated invariant T cells
MFI	Mean fluorescence intensity
MHC	Major histocompatibility complex
mins	minutes
MOI	Multiplicity of Infection
MR1	MHC-related protein 1
Mtb	Mycobacterium tuberculosis
MVA	Modified vaccinia Ankara virus
NK cells	Natural killer cells
NTD	N-terminal domain
O.N.	Overnight
PAMP	Pathogen-associated molecular pattern
PBMC	Peripheral blood mononuclear cells
PCC	Pearson's correlation coefficient
PLC	Peptide loading complex
PMA	Phorbol 12-myristate 13-acetate
RhCMV	Rhesus Cytomegalovirus
RL9-TCR	TCR specific for HLA-E-restricted HIV-1 RL9 peptide
RM	Rhesus macaques
RT	Room temperature
RUSH	Retention Using Selective Hooks
SBP	Streptavidin binding protein
SCT	Single-chain peptide-β2m-MHC-I trimer
SCD	Single-chain β2m-MHC-I dimer
SIV	Simian immunodeficiency virus
str	streptavidin
S.typhi	Salmonella typhi
TAP	Transporter associated with antigen processing
TAPBPR	TAP-binding protein-related
TCR	T cell receptor
Tfh cells	Follicular helper T cells
Th cells	Helper T cells
TMD	Transmembrane domain
TGN	Trans-Golgi network
TNF	Tumour necrosis factor

Treg cells	Regulatory T cells
UGT1	UDP-glucose:glycoprotein glucosyltransferase 1
WB	Western blotting (also known as Immunoblotting)

Chapter 1: Introduction

1.1 Immune response overview

The immune system is a sophisticated network of cells, tissues, and organs that protect the host from different diseases. It detects and defends against harmful invaders, including bacteria, viruses, parasites, abnormal cells, and toxic substances (Murphy et al. 2016). The innate immune system and the adaptive immune system are the main branches of the immune system. While the response of the innate immune system is rapid, pre-existing, and broad, the response of the adaptive immune system is more specific and develops over time (Marshall et al. 2018).

The innate immune system is the body's first line of defence, providing immediate and non-specific responses to eliminate harmful pathogens or substances and continuous surveillance for maintaining homeostasis (Riera Romo et al. 2016). It comprises surface barriers, specialised immune cells, and soluble mediators. Surface barriers are the frontline shields to prevent the entry of pathogens and harmful substances, including the physical barriers like the skin and mucous membranes, the chemical barriers such as different antimicrobial peptides and enzymes, and the biological barriers termed microbiota (Antonini et al. 2019). Innate immune cells like neutrophils, macrophages, and NK cells can detect and destroy foreign invaders through different mechanisms, including phagocytosis and the release of antimicrobial proteins and chemical mediators (Marshall et al. 2018). The soluble mediators, which contain a variety of cytokines, chemokines, and complement proteins, provide rapid defence against potential threats and facilitate the coordination of the innate immune response (Riera Romo et al. 2016). The innate immune system enables initial recognition of invading pathogens by identifying common pathogen-associated molecular patterns (PAMPs) (Tang et al. 2012), which not only trigger rapid innate

immune responses but also induce a more targeted adaptive immune response via the presentation of specific antigens (Marshall et al. 2018).

The adaptive immune system complements the innate immune system by providing specialised and long-lasting protection against invading pathogens or harmful substances (Murphy et al. 2016). It consists of humoral and cellular immunity, with B cells and T cells playing the primary roles. B cells are central to humoral immunity, producing antigen-specific antibodies that directly neutralise pathogens or label them for destruction upon antigen recognition through B cell receptors (BCRs) (Marshall et al. 2018). T cells can recognise infected or abnormal cells via antigen-specific T cell receptors (TCRs) on their surfaces (Riera Romo et al. 2016) and can be generally divided into CD8+ cells and CD4+ T cells. CD8+ T cells, also known as cytotoxic T cells, contribute to cellular immunity by directly eliminating target cells upon antigen recognition (Raskov et al. 2021). CD4+ T cells play a crucial role in coordinating different immune responses and are thus referred to as helper T (Th) cells (Borst et al. 2018). Th1 and Th2 cells are the two classical types that promote immune responses against intracellular and extracellular pathogens, respectively (Romagnani 1995). There are also many more recently identified subsets such as Th17 cells, which contribute to the defence against extracellular pathogens and the regulation of autoimmune diseases (Harrington et al. 2005; Singh et al. 2013). Other subsets of CD4+ T cells are also crucial for the orchestration of adaptive immune responses, including the regulatory T (Treg) cells, which suppress autoimmune reactions, as well as the follicular helper T (Tfh) cells, which can migrate to B cell follicles in secondary lymphoid organs to facilitate the development of B cells (Breitfeld et al. 2000; Sakaguchi et al. 1985; Schaerli et al. 2000). Following the initial exposure to a target antigen, the adaptive immune system generates memory cells, ensuring a faster and more robust response upon subsequent encounters with the same antigen, ultimately providing long-term protection (Liu et al. 2020).

1.2 MHC overview

1.2.1 Discovery of MHC

The major histocompatibility complex (MHC) was initially discovered during efforts to understand the genetic factors influencing tumour transplantability in mice (Gorer et al. 1948). Subsequently, the polymorphic human leukocyte antigens (HLA), equivalent to the human MHC, were identified through serological methods (Dausset 1958). Though recognised initially to play a part in alloreactivity, MHC was later found to control critical immune responses (McDevitt and Sela 1967), and MHC

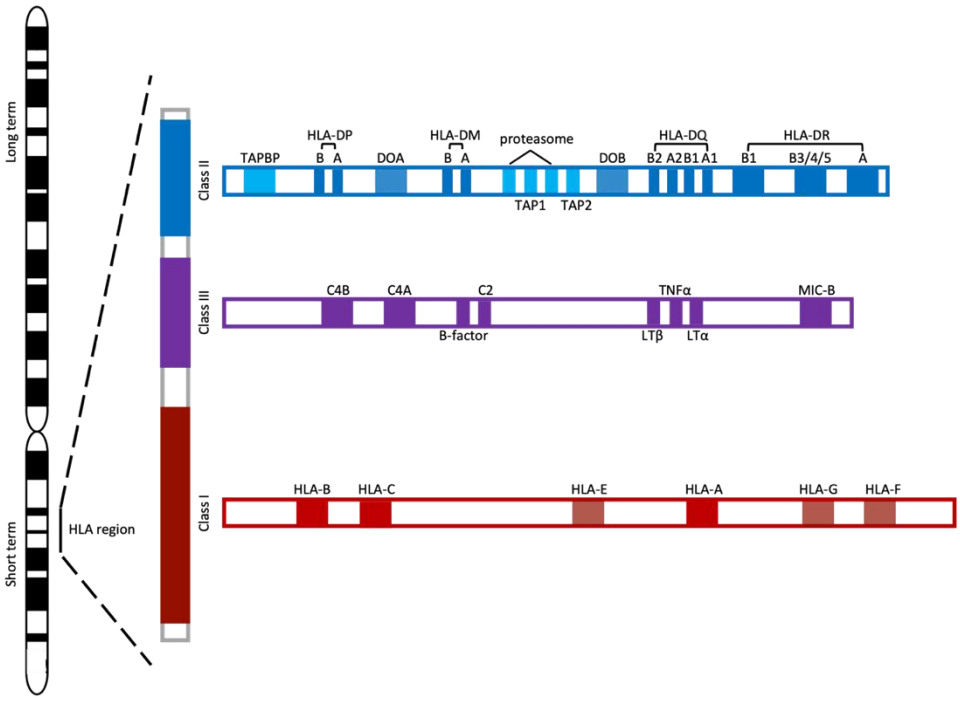

Figure 1.1 Schematic representation of the main genes encoded within the HLA region on chromosome 6
Figure adapted from (Lima-Junior and Pratt-Riccio 2016).

allotype was associated with disease susceptibility (Amiel 1967; LILLY et al. 1964).

The concept of MHC restriction was introduced in studies demonstrating that viral-specific cytotoxic T lymphocytes (CTLs) could only target lymphocytic choriomeningitis virus (LCMV)-infected cells with the same MHC allotype in a murine model (Zinkernagel and Doherty 1974b). CD8+T cells and CD4+ T cells were

found to be restricted by MHC-I and MHC-II molecules, respectively (Goulmy et al. 1977; Zinkernagel and Doherty 1974a). Later on, MHC molecules were shown to bind to foreign peptides and present them to T cells (Allen et al. 1985; Babbitt et al. 1985; Townsend et al. 1986), and the crystal structure of HLA-A2 revealed the peptide's location within the binding groove of MHC-I molecules (Bjorkman et al. 1987a; 1987b). These pioneering studies underscored the central role of MHC in adaptive immunity.

1.2.2 MHC gene region

The human MHC gene region, located on the short arm of chromosome 6, comprises over two hundred genes essential for immune system functions, which can be categorised into three classes based on their locus (Complete sequence and gene map of a human major histocompatibility complex. The mhc sequencing consortium 1999) (Fig.1.1). Class I genes encode HLA-I molecules that are expressed universally and are mainly responsible for presenting endogenous antigens to cytotoxic T cells (Medhasi and Chantratita 2022). They can be further divided into the classical HLA-Ia group, including HLA-A, HLA-B, and HLA-C, which are highly polymorphic, and the non-classical HLA-Ib group containing HLA-E, HLA-F, HLA-G, and HLA-H which exhibit limited polymorphism (Shiina et al. 2009). Class II genes encode HLA-II molecules, which are primarily expressed by antigen presenting cells (APCs) and mainly present exogenous antigens to Th cells. HLA-DR, HLA-DP, and HLA-DQ are the three primary HLA-II genes, each with multiple alleles (Shiina et al. 2009). HLA-DM and HLA-DO, critical for peptide loading of HLA-II proteins, are also located in this region (Mellins and Stern 2014). They are often referred to as non-classical HLA-II molecules and are less variable. Proteins involved in HLA-I peptide loading, such as transporter associated with antigen processing (TAP) and TAP-binding protein-related (TAPBPR), also lay in this region. Class III genes encode secreted proteins that are not directly involved in antigen

presentation but have essential immunological functions, including complement factors and various cytokines (Milner and Campbell 2001).

There are also genes outside these regions that resemble HLA molecules both structurally and functionally, including HLA-I-like molecules CD1 and MHC-related protein 1 (MR1), which can present lipids and metabolites, respectively (Shiina et al. 2001). There are also other proteins important for antigen presentation outside the MHC region. The light chain of the HLA-I heterodimer β-2- microglobulin (β2m) lies on chromosome 15. Tapasin, which is vital for the peptide loading of HLA-I molecules, is found on chromosome 12.

Polymorphism is one of the major features of MHC molecules, with over 35000 HLA alleles reported to date, though the degree of variation differs between different MHC molecules (Barker et al. 2023). Such genetic diversity is likely to be driven by the selection of different pathogens on MHC-peptide binding over millions of years, which explains why the variation differs across different populations (Shankarkumar 2010). This extreme polymorphism prevents pathogens from escaping immune surveillance across different individuals and thereby promotes the overall survival of

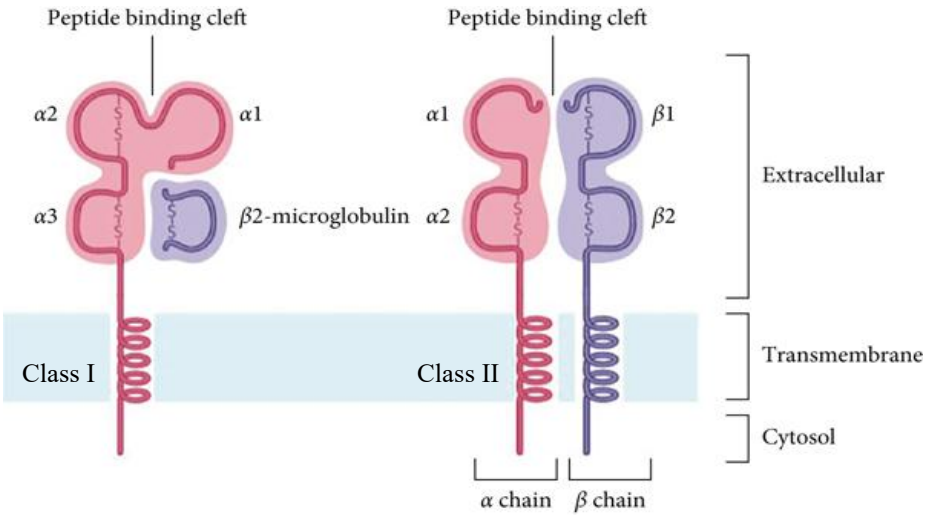

Figure 1.2 Schematic representation of the structure of HLA-I and HLA-II heterodimers
Figure reproduced from (Medhasi and Chantratita 2022)

the species.

1.2.3 Central role of MHC in the immune system

MHC molecules are essential components of the immune system, playing pivotal roles in immune recognition and regulation (Medhasi and Chantratita 2022). They serve as central players in both innate and adaptive immunity, enabling effective orchestration of immune responses against pathogens and abnormal cells.

HLA-specific receptors are essential for the self/non-self discrimination of the immune system, especially in the modulation of NK cell activity. The “missing self hypothesis” is a key concept explaining how NK cells distinguish between self and abnormal cells (Ljunggren and Kärre 1990). The inhibitory receptors on NK cells interact with intact MHC-I molecules on healthy cells, preventing NK cells from attacking self-cells. However, the surface MHC-I expression is often altered when a cell undergoes stress, infection, or transformation, which signals abnormality. NK cells can recognise the “missing self” signal and initiate the elimination of the aberrant cells. Killer cell immunoglobulin-like receptors (KIRs), which are highly polymorphic and include both activating and inhibitory receptors, can directly monitor the expression of classical HLA-I molecules on target cells (Trowsdale 2001). The inhibitory receptors Ig-like transcript 2(ILT-2) and ILT-4 also interact with HLA molecules, with a preference for HLA-G binding (Shiroishi et al. 2003). The inhibitory CD94/NKG2A/B receptors and the activating CD94/NKG2C/E receptors recognise the MHC-E molecules loaded with peptides derived from MHC-I signal sequences (Borrego et al. 1998; Braud et al. 1998a; Kaiser et al. 2008; Lee et al. 1998b). NKG2D/DAP10 receptors can identify MICA/B, induced in response to cell stress, and trigger the elimination of the abnormal cells (Bauer et al. 1999). This fine-tuned regulation contributes to immune homeostasis and the body's ability to defend against infections, tumours, and other threats.

MHC molecules are central in bridging innate and adaptive immunity by facilitating antigen presentation to T cells, thereby initiating specific and highly targeted immune responses. This crucial function enables the immune system to recognise and efficiently eliminate pathogens and abnormal cells. There are two primary classes of MHC molecules, in which Class I molecules largely present intracellular antigens to CD8+ cytotoxic T cells for the specific elimination of infected or abnormal cells, while Class II molecules commonly present extracellular antigens to CD4+ Th cells to promote immune regulation (Rock et al. 2016). In addition, the non-classical MHC-Ib molecules CD1 and MR1 present non-peptide antigens to invariant natural killer T cells (iNKT cells) and mucosal-associated invariant T cells (MAIT cells), respectively (Murphy et al. 2016). The central role of MHC in orchestrating immune responses has broad applications in various immunotherapies and vaccine development.

1.3 MHC-I transport and antigen presentation

1.3.1 Classical antigen presentation pathway of MHC-I molecules

The HLA-I heavy chain (HC) is a type I protein that contains three extracellular domains consisting of three extracellular domains referred to as α1, α2, and α3, as well as a short transmembrane region and an intracellular cytoplasmic tail (Fig.1.2). The α1 and α2 domains form the peptide-binding groove, while the α3 domain binds to β2m (Bjorkman et al. 1987a; Collins et al. 1995). Most polymorphisms in HLA-I are associated with residues located within the peptide-binding cleft or those that interact with the TCR (Parham 1988; Reche and Reinherz 2003). Such genetic diversity was driven to evolve immune responses against pathogens, optimising the immune system's ability to combat infections and threats.

The HC typically forms the heterotrimer with β2m and peptide in the ER and then traffics to the cell surface and presents the peptide. The newly-synthesised HLA-I HC firstly associates with the transmembrane chaperone calnexin (CNX) and ERp57 in

the ER (Morrice and Powis 1998) (Fig.1.3). CNX promotes the proper folding of HCs and retains unassembled HCs in the ER (Jackson et al. 1994). ERp57 facilitates the formation of HC disulfides (Farmery et al. 2000). HC then associates with β2m and dissociates from CNX. The unstable heterodimer, guarded by calreticulin (CRT) (Sadasivan et al. 1996), is further recruited to the peptide loading complex (PLC) containing ERp57, tapasin, and the ABC transporter associated with antigen processing (TAP) (Hughes and Cresswell 1998; Sadasivan et al. 1996). PLC helps with the transport and loading of proteasome-generated peptides onto MHC-I/β2m dimers (Donaldson and Williams 2009). Once loaded with high-affinity peptides, MHC-I molecules exit the ER and traffic through the Golgi to the cell surface (Fig.1.3).

MHC-I is not a static plasma membrane resident and is continually internalised by endocytosis through a clathrin- and dynamin-independent endocytic pathway with the help of Arf6 (Naslavsky et al. 2004). CD74 (also named invariant chain (Ii)), which is the key chaperone for MHC-II trafficking, is also reported to chaperone MHC-I molecules from the ER to the endosomes (Basha et al. 2012; Sugita and Brenner 1995), though the exact pathways remain understudied (Fig.1.3). MHC-I in different conformations follow distinct trafficking pathways. MHC-I trimers with low-affinity peptides or empty MHC-I dimers (open MHC-I conformers) are internalised much faster than MHC-I trimers with high-affinity peptides (closed MHC-I conformers) (Mahmutefendić et al. 2007). After endocytosis, vesicles containing MHC-I molecules merge with the Rab5-associated early sorting endosomes (Naslavsky et al. 2004). From there, closed MHC-I conformers can be sorted to three destinations: a fast recycling pathway which directly recycles proteins from the sorting endosomes to the cell surface, a slow recycling pathway transporting MHC-I molecules to the tubular endocytic recycling compartment (ERC) with the help of Rab11 and then to the surface, and a third pathway to late endosomes for degradation, though a small

fraction may escape to the cell surface (van Endert 2016). In contrast, open MHC-I conformers all remain in endosomes that mature into acidic late endosomes and multi-vesicular bodies where most of them get degraded (Mahmutefendić et al. 2011;

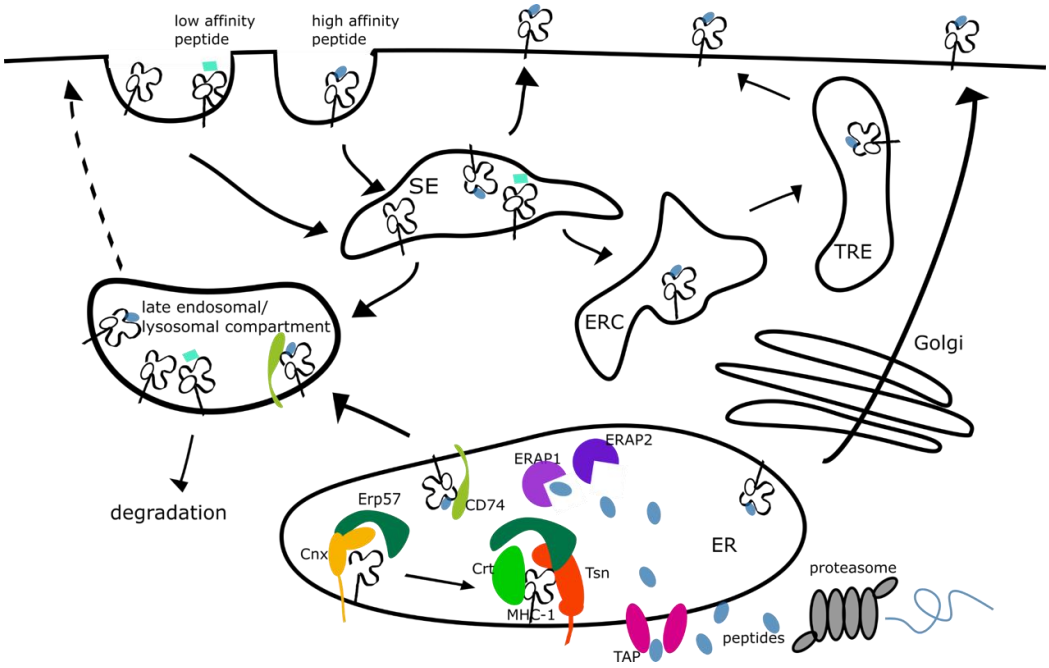

Figure 1.3 Overview of the assembly and trafficking of MHC-I molecules
In the ER, CNX and Erp57 facilitates the binding of ß2m to newly synthesised MHC-I HC, and the PLC further promotes the loading of peptides. Proteasome-generated peptides are transported into the ER via TAP and are further trimmed by ERAP. While most optimally folded MHC-I molecules traffic through the Golgi to the cell surface, some could potentially directly go the endosomes. Surface MHC-I is directed to sorting endosomes after internalisation and is either recycled back to the cell surface or undergoes degradation. Figure adapted from (Adiko et al. 2015).

Mahmutefendić et al. 2017; Zagorac et al. 2012). However, a fraction of open conformers may escape from degradation and be recycled to the cell surface loaded with peptides independent of Rab11 (Mahmutefendic et al. 2013). Most of the studies on MHC recycling have been carried out in non-professional APCs, so the trafficking pathway in specialised APCs like DCs may be different.

1.3.2 Antigen processing for MHC-I molecules

Proteasomes constantly generate peptides from intact or misfolded proteins that are ubiquitinated in the cytoplasm (Hershko 1988). TAP transports peptides, mainly 8~16 residues in length, from the cytosol into the ER lumen (Androlewicz et al. 1993; Androlewicz and Cresswell 1994; Neefjes et al. 1993), with some preferences for

selection on the C termini (Momburg et al. 1994). After import, the peptides are further polished by ER aminopeptidase (ERAP) to 8~10 residues for optical MHC-I binding (Saric et al. 2002; Serwold et al. 2002) (Fig.1.3). Peptides that fail to bind to MHC-I molecules are either degraded or translocated back to the cytosol probably through the sec61b channel (Lehner et al. 2000).

Although the proteasome/TAP-dependent peptide processing is the dominant pathway, alternative, unconventional peptide generation pathways were also reported. Signal peptidase and signal peptide peptidase together liberate the signal peptides of MHC-I molecules on the ER membrane, which constitute the dominant peptide repertoire for HLA-E (Lemberg et al. 2001). Peptides could be generated in the cytosol by proteolytic enzymes like tripeptidyl peptidase II (TPPII) (Seifert et al. 2003), in the trans-Golgi network by furin (Medina et al. 2009), or in the endosomal pathways by cathepsins (Shen et al. 2004). These unconventional peptide processing pathways produce immunogenetic peptides with more diversity both in length and in sequence compared to the conventional pathway (Oliveira and van Hall 2015), thus contributing to the peptide repertoire for alternative MHC-I peptide presentation, like cross-presentation (Shen et al. 2004). These alternative methods also compensate for the peptide repertoire, especially under abnormal conditions where the classical peptide processing pathway is blocked, like viral infections.

1.3.3 Peptide proofreading by tapasin and TAPBPR

The chaperones tapasin and TAPBPR facilitate MHC-I peptide loading and high-affinity epitope selection. Tapasin is an integral component of the PLC (Sadasivan et al. 1996), which not only promotes the association between MHC-I molecules with TAP for access to high-affinity peptides (Grandea et al. 1997; Ortmann et al. 1997) but also assists the recruitment of ERp57 to the PLC, helping to stabilise the PLC and recruit MHC-I molecules (Garbi et al. 2006). Tapasin samples

the quality of peptides loaded onto MHC-I by scanning a structural element in the α2-1-helix region at the C terminus of the peptide (F pocket) (Chen and Bouvier 2007; Thomas and Tampe 2017). When MHC-I molecules are loaded with low-affinity peptides, tapasin stabilises a widened conformation of MHC-I, inducing dissociation of the peptides (Thomas and Tampe 2017). The binding of high-affinity peptides switches the conformation of the α2-1 helix from an open conformation to a closed one and triggers the release of tapasin.

In contrast to tapasin, TAPBPR can function beyond the ER and associate with MHC-I in the Golgi (Boyle et al. 2013). Several studies have shown that TAPBPR promotes the dissociation of low-affinity peptides and stabilises peptide-receptive MHC-I by inserting its K22-D35 "scoop loop" into MHC-I binding groove, a process that depends on the F-pocket specificity of MHC-I allotypes (Ilca et al. 2018; Sagert et al. 2020; Thomas and Tampe 2017). However, a loop-independent editing process might also exist, as some allotypes seem to be loop-independent (Ilca et al. 2018), other interactions like the "jack hairpin" also affect the conformation of the peptide binding groove (Thomas and Tampe 2017), and that an NMR-based study suggests a negative allosteric coupling model (McShan et al. 2018). Apart from peptide editing, TAPBPR also facilitates the transport of sub-optimally folded MHC-I back to the ER (Neerincx et al. 2017). TAPBPR promotes the interaction of UDP-glucose:glycoprotein glucosyltransferase 1(UGT1) to sub-optimally folded MHC-I for reglucosylation, thus promoting the interaction of MHC-I with PLC (Neerincx et al. 2017).

The influence of peptide editors seems to be allotype-dependent (Bashirova et al. 2020; Garstka et al. 2011; Ilca et al. 2019). The existence of two peptide editors might ensure the editing power despite the polymorphism of MHC-I molecules, though the mechanism of how they cooperate to shape the peptide repertoire of different MHC-I alleles remains unclear (Hafstrand et al. 2021).

1.3.4 Cross-presentation of MHC-I molecules

In addition to its classical role in presenting endogenous peptides, MHC-I can also present antigens internalised exogenously through cross-presentation (Ackerman and Cresswell 2003). Exogenous antigens can be ingested into phagosomes/endosomes through phagocytosis, receptor-mediated endocytosis or pinocytosis (Colbert et al. 2020). These antigens are either translocated into the cytosol through the

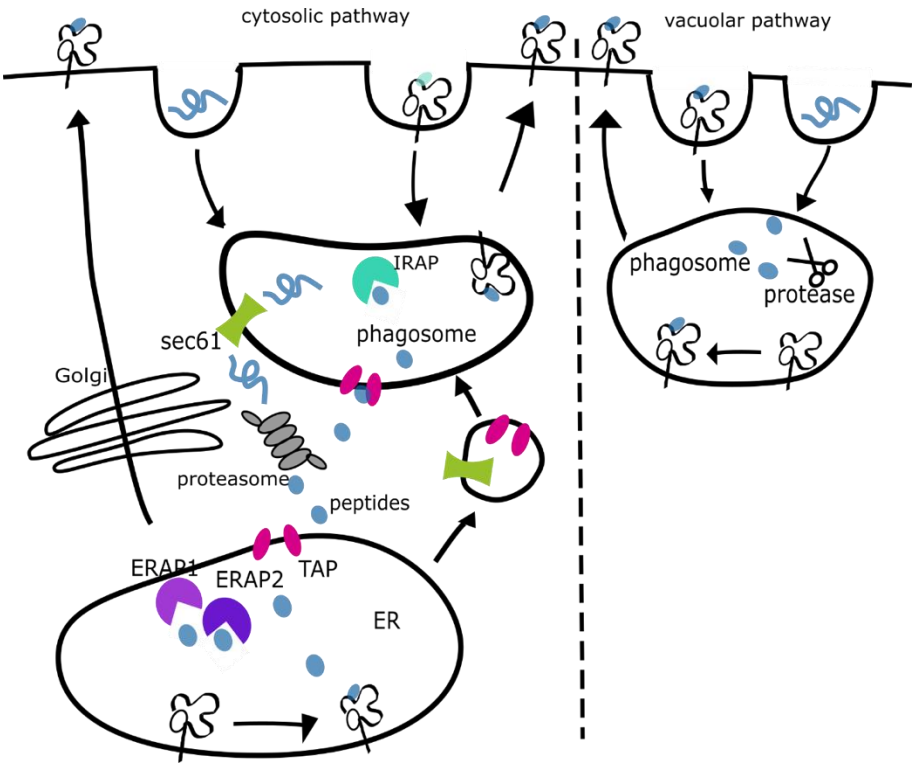

Figure 1.4 Overview of the cross-presentation process of MHC-I molecules
In the cytosolic pathway, exogenous peptides are translocated to the cytosol via sec61 after endocytosis, processed by the proteasome transported to the ER or phagosomes/endosomes by TAP where they are loaded onto MHC-I complex. In the vacuolar pathway, antigen processing and loading occurs entirely in the endocytic pathway and is independent of TAP and proteasome. Figure adapted from (Adiko et al. 2015).

ER-associated degradation pathway, where they are degraded by proteasomes (Kovacsovics-Bankowski and Rock 1995; Kreer et al. 2011), or they stay in the phagosomes/endosomes, where they get degraded by proteases there or by proteasomes translocated into these compartments(Shen et al. 2004).

Many surface receptors on APCs, especially in DCs, are involved in capturing and transporting exogenous proteins for cross-presentation. FcγR assists in the

cross-presentation of exogenous proteins (Schuurhuis et al. 2002) and can even initiate potent cross-presentation in non-APCs (Giodini et al. 2009). Many members of C-type lectin receptors are essential in protein uptake, including mannose receptor (Burgdorf et al. 2006), DEC-205 (Bonifaz et al. 2002), DC-SIGN (Moris et al. 2004), DCIR (Klechevsky et al. 2010) CLEC9A (Schreibelt et al. 2012), and langerin (Farrand et al. 2009). Scavenger receptors are also reported to play a role in antigen uptake for cross-presentation, including LOX-1 (Delneste et al. 2002), $\alpha_v\beta_5$ and CD36 (Shakushiro et al. 2004). The intracellular trafficking of internalised proteins is largely dependent on the receptors they associate with. Proteins internalised via MR-mediated endocytosis are targeted to early endosomes, where they are later processed for cross-presentation (Burgdorf et al. 2007), while DEC-205 mostly delivers proteins to late endosomes or lysosomes (Figdor et al. 2002). DEC-205 and Dectin-1 can both increase the uptake of exogenous protein in DCs, but DEC-205 can effectively elicit CD8+ T cell response, while Dectin-1 is much better at activating CD4+ T cells (Carter et al. 2006). Besides, the nature and the place of the interaction between the receptor and the protein are also fundamental, indicating a complicated and delicate regulation for the trafficking of internalised proteins (Kreer et al. 2011).

There are two main pathways for cross-presentation (Fig.1.4). In the cytosolic pathway, which is TAP- and proteasome-dependent, antigens are translocated to the cytosol after internalisation with the help of the sec61 translocon (Zehner et al. 2015), and then degraded by the proteasome. Loading occurs in the ER or phagosomes/endosomes, to which ER proteins that assist the loading of recycling MHC-I molecules are recruited (Gagnon et al. 2002; Houde et al. 2003). A second 'vacuolar' pathway resembles the trafficking of MHC-II molecules (Song and Harding 1996). It is TAP-independent but needs some specific ER proteins recruited by sec22b for loading (Cebrian et al. 2011). Most studies refer to this process as proteasome-independent, claiming that recycling MHC-I molecules are loaded with

peptides directly produced in maturing endosomes or phagosomes by endolysosomal proteases such as cathepsin S (Shen et al. 2004). However, a later study shows that active proteasomes transported into endosomes or phagosomes also play an important role in peptide generation in this pathway (Sengupta et al. 2019). Insulin-regulated aminopeptidase performs the final trimming of peptides in endosomes, resembling the function of ERAP in ER (Saveanu et al. 2009). Both recycling and neo-synthesised class I molecules can be loaded with cross-presented peptides, but current concepts hold that MHC-I recycled from the cell surface is the principal source in these pathways (van Endert 2016).

During the cross-presentation, tapasin helps to stabilise MHC-I in acidic conditions (Chefalo et al. 2003). TAPBPR may be involved in peptide selection for recycling MHC-I molecules during cross-presentation, as it can facilitate peptide loading outside the ER independently of the PLC (Thomas and Tampe 2017).

1.4 MHC-II transport and antigen presentation

The HLA-II heterodimer comprises an α and a β chain, which share similar structures, with two extracellular domains and a cytoplasmic tail connected by a transmembrane domain (Brown et al. 1993; Jardetzky et al. 1994). α1 and β1 domains from α and β chains, respectively, together form the peptide-binding groove. As the antigen binding groove is open at both ends (Brown et al. 1993), the length of peptides presented by MHC-II molecules is longer than MHC-I molecules, generally 13-25 residues (ten Broeke et al., 2013). Similar to MHC-I, the genetic diversity of MHC-II is enriched in residues in contact with the peptide and the TCR (Reche and Reinherz 2003), which is crucial for recognising a wide range of extracellular antigens.

MHC-II molecules are assembled in the ER together with CD74 (also called invariant chain (Ii))(Jones et al. 1979; Machamer and Cresswell 1982). CD74 not only stabilises the dimers and blocks the peptide-binding site(Roche and Cresswell 1990)

but also chaperones MHC-II via the trans-Golgi network (TGN) to endosomes (Lamb et al. 1991; Lotteau et al. 1990). While a direct route from the TGN to endosomes may exist, most MHC-II molecules are first sorted to the plasma membrane and then internalised in an AP-2-dependent manner driven by the sorting signals LI and ML, which is located in the cytoplasmic tail of CD74 (Bremnes et al. 1994; ten Broeke et al. 2013). In the endocytic pathway, CD74 is degraded sequentially until only the Class II associated invariant chain peptide (CLIP) remains bound to the peptide-binding groove of MHC-II molecules (Berger and Roche 2009). MHC-II-like chaperone protein HLA-DM removes CLIP and stabilises the empty MHC-II molecule until a high-affinity peptide is loaded to the peptide-binding groove (Denzin and Cresswell 1995; Kropshofer et al. 1996; Sherman et al. 1995; Sloan et al. 1995). In contrast to tapasin and TAPBPR, HLA-DM interacts with the MHC-II molecule at the N-terminus of the peptide, inducing structural changes in the P1 and P2 pockets of the peptide binding groove (Pos et al. 2012). The function of HLA-DM is further regulated by HLA-DO, another MHC-II-like molecule (Denzin et al. 1997), but its function is currently controversial. While some studies show that HLA-DO functions as a competitive inhibitor of DM (Guce et al. 2013), other findings imply that HLA-DO works in concert with HLA-DM and stabilises empty MHC-II molecules (Poluektov et al. 2013). Antigens are mostly processed in late endosomes/lysosomes where proteases can be activated for antigen proteolysis by the low pH (Roche and Furuta 2015). MHC-II molecules loaded with peptides are then transported from endosomal membranes to the plasma membrane via MHC-II transport tubules and

vesicles.

The recycling of MHC-II molecules is complicated and less studied. Different from newly synthesised CD74-associated MHC-II molecules, recycling MHC-II molecules follows a distinct endocytic pathway independent of clathrin and AP-2 (Walseng et al. 2008). Recycling MHC-II might exchange peptides in early endosomes, which are not accessed by newly synthesised MHC-II molecules due to the association of CD74, thus increasing the repertoire of antigenic peptides (Walseng et al. 2008).

While immature DCs mostly use newly synthesised MHC-II to load antigens in late endosomes, mature DCs prefer recycling MHC-II molecules with access to antigens in both early and late endosomes (Cho et al. 2020). MHC-II molecules are recycled poorly in immature DCs but much more efficiently in mature DCs. In immature DCs, MHC-II molecules accumulate in antigen-processing compartments (Kleijmeer et al. 1995), and most of the newly formed MHC-II molecules are rapidly ubiquitinated by the E3 ubiquitin ligase MARCH1, which targets these complexes for lysosomal

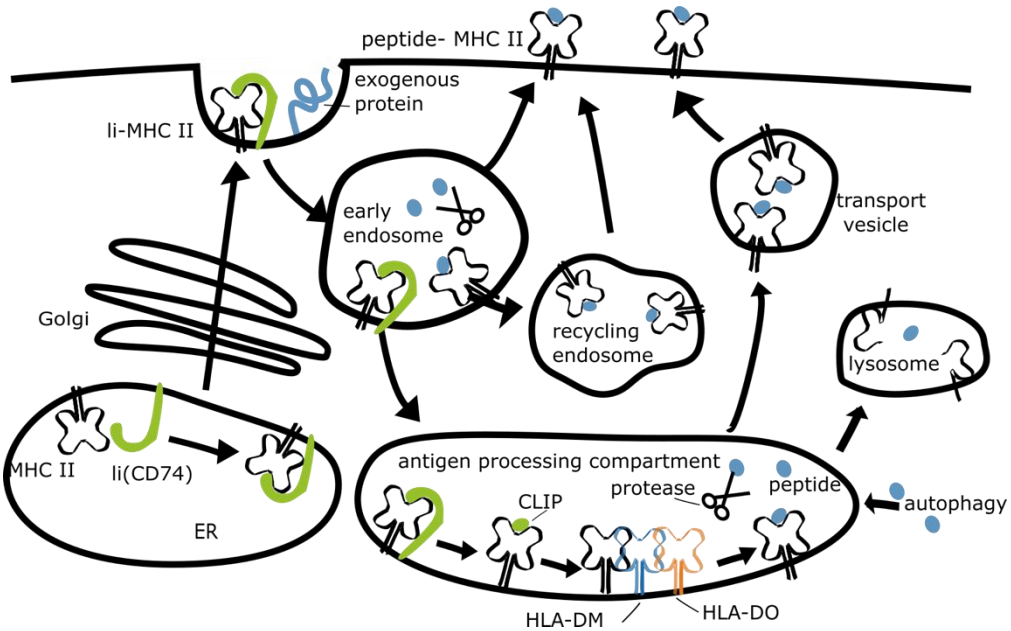

Figure 1.5 Overview of the assembly and trafficking of MHC-II molecules
CD74 binds to the MHC-II dimer in the ER and target it to the cell surface via the ER. CD74 then chaperones MHC-II to the endosomes and get degraded. Endosomal MHC-II is either degraded or get loaded with the antigen with the help of HLA-DM and HLA-DO and get recycled back to the cell surface. Figure adapted from (Roche and Furuta 2015).

degradation (De Gassart et al. 2008). In mature DCs, most MHC-II molecules reside

on the plasma membrane (Pierre et al. 1997; Shin et al. 2006). Ubiquitination of MHC-II molecules is inhibited, and internalised MHC-II molecules are mainly redirected back to the plasma membrane (Shin et al. 2006; van Niel et al. 2006). Such a mechanism could be important for generating a rapidly changing peptide–MHC class II repertoire in immature DCs that can be 'fixed' upon DC activation.

Antigens can enter the endocytic pathway of APCs through receptor-mediated endocytosis via clathrin-coated vesicles, which results in their internalisation into early endosomes, through macropinocytosis which is non-specific and facilitates the uptake of soluble material into macropinosomes, or through phagocytosis in which opsonised particles enter cells in phagosomes (Roche and Furuta 2015). Cytosolic antigens can also enter the endocytic pathway through autophagy, in which intracellular proteins and invading microorganisms are enveloped in autophagosomes (Schmid et al. 2007). These early endosomes eventually fuse with multivesicular late endosomal–lysosomal antigen-processing compartments where internalised antigen proteolysis and peptide-MHC complex formation occur. The mechanism for antigen uptake varies between different APCs. Among all the APCs, B cells are unique in that they have BCRs, which are antigen-specific. BCRs can recognise and internalise a trace amount of antigens and are much more efficient in antigen processing than other non-specific receptors (Barroso et al. 2015). Macropinocytosis and phagocytosis are very important for antigen uptake of DCs (Sallusto et al. 1995), while these are inefficient in B cells. Similar to MHC-I, many receptors are reported to enhance antigen presentation of MHC-II, including DEC-205 (Mahnke et al. 2000), DC-SIGN (Engering et al. 2002), dectin-1 (Ma et al. 2012), MGL (van Vliet et al. 2007), surface complement receptors (Perrin-Cocon et al. 2004), FcγR (Amigorena et al. 1992), etc.

1.5 HLA-E transport and antigen presentation

1.5.1 Classical transport and antigen presentation of HLA-E

HLA-E exhibits very limited polymorphism, which is in striking contrast to HLA-Ia molecules. There are only two major functional HLA-E alleles in humans, which are present at similar frequencies and differ by one amino acid at position 107 (Geraghty et al. 1992). Such low genetic diversity in HLA-E is likely due to its classical role in the regulation of NK cells, in which the highly conserved VL9 peptide (VMAPRTL/VV/L/FL) from the leader sequence of HLA-I molecules is presented (Borrego et al. 1998; Braud et al. 1998a).

Despite its broad expression across various cell types, HLA-E typically maintains a relatively low surface expression level compared to classical HLA-Ia alleles (Braud et al. 1998b). Under normal conditions, VL9 dominates the HLA-E peptidome, and HLA-E traffics to the cell surface following the classical transport pathway after VL9 peptide loading in the ER (Braud et al. 1998b; Lee et al. 1998a; O'Callaghan et al. 1998). Therefore, HLA-E surface expression relies on both the functional integrity of the transport machinery and the VL9 peptide supply from HLA-I leader sequences.

HLA-E binding peptide needs to occupy more pockets in the binding groove than HLA-Ia molecules (O'Callaghan et al. 1998). Such structural constraints impose sequence restrictions and reduce the peptide repertoire, resulting in a biased preference of HLA-E towards VL9 binding (O'Callaghan et al. 1998). VL9 binding facilitates the refolding of HLA-E, which is crucial for its ER export (Walters et al. 2018; Walters et al. 2022). Most other HLA-E peptides are of low affinity, which can’t stabilise HLA-E trimer and therefore can’t effectively transport HLA-E out of the ER due to the failure of passing the proofreading steps (Walters et al. 2018; Walters et al. 2022). Although the generation of VL9 peptide is universal, its supply level is normally far from saturating all the newly synthesised HLA-E in the ER, leading to the ER retention and low surface expression of HLA-E (Camilli et al. 2016). Besides, the affinity of VL9 is not very high compared to high-affinity HLA-Ia peptides, as shown by the lower thermal stability of HLA-E refolded with VL9

(Fahnestock et al. 1992; Morgan et al. 1997; Strong et al. 2003; Walters et al. 2022). This leads to a comparatively short surface lifetime of HLA-E, which further leads to its decreased expression on the cell surface.

1.5.2 Unconventional trafficking process of HLA-E

Under abnormal conditions like pathogen infection, HLA-Ia downregulation and blockage of the classical antigen presentation pathway are common strategies to escape T cell recognition (Antoniou and Powis 2008). However, HLA-E is usually not downregulated and is even upregulated in some cases (Nattermann et al. 2005; Tomasec et al. 2000), which helps the target cells avoid NK cell killing. Though the details are far from clear, several lines of evidence suggest that HLA-E can be transported to the cell surface in a nonclassical manner.

Upon infection, Mycobacterium tuberculosis (Mtb) resides in a membrane-bound vacuole that is relatively impermeable (Clemens et al. 2002). In contrast to class Ia molecules, Mtb peptide presentation primarily uses recycling HLA-E molecules instead of newly synthesised ones (Grotzke et al. 2009). HLA-E molecules are enriched in Mtb phagosomes where peptide loading occurs. The presentation requires proteasome processing and TAP transport of peptides but does not go through the ER-Golgi pathway (Grotzke et al. 2009). Instead, ER proteins necessary for peptide loading are transported to these phagosomes (Grotzke et al. 2009).

After infection, S.typhi (Salmonella typhi) stays and proliferates in the *Salmonella*-containing vacuole (SCV), which is a specialised membrane-bound compartment (Steele-Mortimer 2008). Besides, S.typhi reorganises the host endosomal system and forms extensive membrane tubules called *Salmonella*-induced filaments (Krieger et al. 2014), gaining access to components in different endosomal compartments (Liss et al. 2017). Considering these unique properties, it's likely that

S.typhi-derived peptides are loaded onto HLA-E and are presented at the surface following a non-classical pathway.

Human cytomegalovirus (HCMV) expresses multiple proteins to downregulate HLA-Ia expression for immune escape. US2 and US11 target newly synthesised HLA-I molecules to the cytosol, where they are degraded by proteasomes through different methods (Powers et al. 2008; Stagg et al. 2009; van den Boomen et al. 2014; Wiertz et al. 1996a; Wiertz et al. 1996b), US3 interrupts peptide loading through association with the HC and PLC and inhibition of the function of tapasin (Park et al. 2004a), and US6 targets TAP to inhibit peptide translocation (Hewitt et al. 2001; Lehner et al. 1997). Although subtle sequence difference makes HLA-E insensitive to the regulation of US2 and US11 (Barel et al. 2006), HCMV UL40 protein plays a major role in helping HLA-E escape from downregulation and maintain its surface expression level (Tomasec et al. 2000). UL40 contains a VL9 peptide which highly mimics HLA-I leader sequences (Ulbrecht et al. 2000), compensating for the decrease of HLA-E peptide availability due to HLA-I downregulation. The UL40-derived peptide is loaded onto HLA-E in a TAP-independent manner (Powers et al. 2008; Tomasec et al. 2000), bypassing the blockage of the classical presentation pathway, though the exact mechanism remains unclear.

Human immunodeficiency virus (HIV) can downregulate HLA-I surface expression through different methods, among which Nef plays an important role. Nef not only directly promotes the endocytosis of surface HLA-I molecules, which are further targeted for degradation (Schwartz et al. 1996), but also prevents newly synthesised ones from reaching the cell surface by targeting them directly from TGN to the endosomal pathway (Kasper et al. 2005). HLA-E is not targeted for lack of certain motifs on its cytoplasmic tail that are necessary for the interaction (Le Gall et al. 1998; Williams et al. 2002). Besides, a peptide derived from the gag protein can bind to HLA-E and may thus further maintain its surface expression (Nattermann et al. 2005).

However, the influence of HIV infection on HLA-E surface expression varies from strain to strain, and downmodulation of HLA-E surface expression by Nef is also reported (van Stigt Thans et al. 2019). This suggests a more complicated regulatory network of HIV in modulating HLA-E expression.

Tumour cells not only upregulate surface HLA-E expression for self-protection (Abd Hamid et al. 2019; de Kruijf et al. 2010; Seliger et al. 2016) but also release soluble HLA-E molecules to protect bystander cells (Allard et al. 2011; Morandi et al. 2013; Wagner et al. 2017). These manipulations of HLA-E expression facilitate tumour escape and are associated with poor prognoses. However, the precise mechanism is not well studied.

1.6 Transport and antigen presentation of other non-classical MHC-I molecules

1.6.1 CD1

CD1 is a non-classical MHC-related molecule with five isoforms whose major role is involved in the presentation of lipid antigens. CD1 HC is firstly folded and assembled with β2m in the ER with the assistance of many chaperones, including CNX, CRT and ERp57 (Van Kaer et al. 2016). ER-derived lipids are then loaded onto CD1 dimers, probably with the help of microsomal triglyceride transfer protein (Gumperz 2006). However, it is unknown what the molecular mechanism behind loading is, what kinds of lipids bound to CD1 are and whether there is any difference between CD1 isoforms (Moody and Cotton 2017; Teyton 2018). After the formation of the CD1-lipid complex, CD1a, CD1b, CD1c and CD1d molecules traffic from the ER through the Golgi and finally to the cell surface.

After reaching the cell surface, CD1a-d molecules can be internalised and transported into the endosomal vesicular system. The trafficking pathway after internalisation

depends mainly on the amino acid sequences of their cytoplasmic tails, which differ between CD1 isoforms (Gumperz 2006). While most CD1a molecules remain at the surface, a small fraction is transported to early endosomes and follows a shallow recycling pathway (Sugita et al. 1999). CD1b molecules traffic transiently through early endosomes and accumulate predominantly in late endosomes and lysosomes with the help of both AP-2 and AP-3 (Sugita et al. 2002). CD1c and CD1d molecules are mainly delivered to early and late endosomes via an AP-2-dependent pathway (Moody and Cotton 2017). The trafficking of CD1d may also be altered by MHC-II and CD74 (Kang and Cresswell 2002). How recycling CD1 isoforms travel from endosomes back to the cell surface remains unclear. CD1 isoforms specialise in surveying different compartments, enlarging the lipid antigens repertoire presented (De Libero and Mori 2012).

Unlike other CD1 molecules, CD1e localises intracellularly and does not directly present antigens itself (Angenieux et al. 2000). It is involved in the processing of complex antigens, as well as lipid loading and exchange of other CD1 molecules (De Libero and Mori 2012). CD1e accumulates in the Golgi in immature DCs and is directly relocated into lysosomes upon the maturation of DCs (Angenieux et al. 2000; Angénieux et al. 2005).

While at the cell surface, some CD1 isoforms (e.g., CD1a) can readily capture exogenous lipids (Van Kaer et al. 2016), CD1 molecules predominantly acquire lipid antigens in the endosomal pathways, exhibiting similarities to the antigen processing pathway of MHC-II molecules (Teyton 2018). Extracellular lipids, including both self and foreign origin, associate with different lipid-binding proteins and are delivered to different locations in the endosomal system for loading (De Libero and Mori 2012).

CD1 isoforms adopt different structures for lipid loading. CD1b has a large cleft consisting of 4 pockets, A', F', C' and T', and can bind lipids up to C80 in length

(Briken et al. 2002). CD1a, CD1c, and CD1d have an A' pocket and an F' pocket and can load lipids with an overall chain length of C36-42 (Koch et al. 2005; Scharf et al. 2010; Zajonc et al. 2003). However, the shape and interconnectedness of the A' and F' pockets are different between these CD1 isoforms, facilitating the accommodation of different lipids. CD1e has a wider binding groove, which ensures rapid lipid association and disassociation, contributing to its lipid exchange with CD1b molecules in endosomes (Garcia-Alles et al. 2011). The details of what lipids different CD1 isoforms are specialised in presenting remain unclear.

An acidic environment favours lipid antigen loading of CD1 molecules, as partial denaturation favours the access of lipid antigens to the binding clefts (Cuevas-Zuviría et al. 2020). CD1e is comparatively more resistant to acidic pH, which might be crucial for facilitating lipid exchange/editing (Bushmarina et al. 2011). Although the mechanism is unclear, it's likely that CD1e functions similarly to HLA-DM, which enables endosomal peptide loading of HLA-II molecules in a pH-dependent way (Kropshofer et al. 1997). In addition, the acidic environment activates acid-dependent proteases like cathepsins, which cleave prosaposin to activate lipid transfer proteins (Winau et al. 2004; Zhou et al. 2004).

1.6.2 MR1

MR1 is a non-classical MHC-I molecule that is monomorphic, universally expressed, and highly conserved among mammals (Franciszkiewicz et al. 2016). MR1 binds to two classes of vitamin B-derived ligands, in which metabolites derived from riboflavin (vitamin B2) can activate MAIT cells, while folic acid derivatives (vitamin B9) cannot (McWilliam et al. 2015; Napier et al. 2015). MR1-dependent MAIT cell response can be elicited both in vitro and during bacterial infection (Hinks and Zhang 2020). Many studies have revealed that MAIT cells play a unique and vital role against bacterial infection in mice (Chua et al. 2012; Georgel et al. 2011; Le Bourhis

et al. 2010), but more studies are required to reveal their anti-bacterial roles in humans fully.

MR1 is mainly retained in the ER with a small fraction in late endosomal compartments (Harriff et al. 2016; McWilliam et al. 2016). MR1 has a very low surface expression level and low surface stability (Chua et al. 2011; McWilliam et al. 2016). The ER retention of MR1 is mainly caused by the limited repertoire of MR1 ligands, as increased surface stability and expression level can be observed upon ligand provision either via exogenous addition or bacterial infection (Grotzke et al. 2009; McWilliam et al. 2016; Napier et al. 2015). Nevertheless, there is also a class of ligands that can inhibit the ER egress and the surface expression of MR1 (Salio et al. 2020).

MR1 trafficking is different from the classical MHC-I pathway, as its surface expression is independent of PLC components, including proteasome, TAP, tapasin and CRT (Huang et al. 2008), though association with PLC was reported (Lion et al. 2013; Miley et al. 2003). In contrast to other HLA-I molecules, the MR1 HC must bind to a ligand before it can effectively refold and associate with β2m in the ER (McWilliam et al. 2016). This is probably because the α3 domain of MR1 only interacts weakly with β2m (Miley et al. 2003). In the absence of ligands, most MR1 molecules are retained in ER (McWilliam and Villadangos 2018). After exiting from the ER, MR1-ligand complexes either traffic through the Golgi and then to the cell surface or remain intracellularly (Karamooz et al. 2018).

After antigen presentation at the surface, MR1 molecules are internalised and transported to the endosomal system, where most of them get degraded (Lamichhane and Ussher 2017; McWilliam et al. 2016). Some MR1 molecules can escape degradation, get loaded with new ligands, and get recycled back to the cell surface (Lamichhane and Ussher 2017). CD74 and HLA-DM can associate with MR1,

influence its surface expression, and promote MR1 transport to late endosomes, a process critical for MAIT cell activation (Huang et al. 2008). Although the details remain unclear, this suggests that the trafficking of MR1 through the endosomal system may resemble MHC-II trafficking.

Ligands can be loaded onto MR1 in the ER, in endosomal compartments or at the cell surface (McWilliam and Villadangos 2017). The binding of soluble ligands in the ER is the most dominant pathway, but how these ligands enter the ER remains unclear (Lamichhane and Ussher 2017). MR1 can also exchange ligands in endosomes, and MR1 reloaded with ligands from endocytosis, phagocytosis or autophagy can be recycled back to the cell surface (Lamichhane and Ussher 2017). This alternative pathway enlarges the ligand repertoire. However, recent studies suggest that the endosomal ligand loading of MR1 differs between soluble antigens delivered exogenously and derived from intracellular infection (e.g., Mtb) *in vitro* (Harriff et al. 2016; Karamooz et al. 2019). Soluble ligands may also bind to MR1 at the cell surface either by replacing bound ligands or accessing a small fraction of open MR1 molecules without ligands (Le Bourhis et al. 2010; McWilliam et al. 2016), though this pathway is probably very inefficient.

MR1 has spontaneous high expression of different spliced isoforms generated via alternative slicing (Lion et al. 2013). Although the functions of these truncated versions of full-length MR1A are not well characterised, it was reported that MR1B could present ligands at the plasma membrane and activate MAIT cells *in vitro* as homodimers without the association with β2m (Lion et al. 2013). This may result from the conformational difference between MR1A and MR1B, as MR1B lacks the α3 domain. Besides, MR1B may also fine-tune the MAIT activation elicited by MR1A (McWilliam et al. 2016). This suggests different MR1 isoforms may have specific features, and they together regulate MAIT cell activity, paralleling HLA-G isoforms (Rajagopalan et al. 2006).

1.6.3 HLA-F

HLA-F has an MHC-II-like, partially open-ended peptide-binding groove that can accommodate long peptides (Dulberger et al. 2017). The immunological roles of HLA-F include regulating NK cells via interaction with a range of NKRs as well as presenting peptides to T cells, though the exact functions of the latter remain primarily unexplored (Dulberger et al. 2017). HLA-F has a protective immune function in pregnancy and the peripheral nervous system (Burrows et al. 2016; Garcia-Beltran et al. 2016; Song et al. 2016) and is also reported to inhibit viral replication (Lunemann et al. 2018). HLA-F can bind to HLA-I open conformers, including HLA-E (Goodridge et al. 2010) and is reported to facilitate the cross-presentation of HLA-Ia molecules (Goodridge et al. 2013).

HLA-F mostly stays intracellularly, but its surface expression can be induced upon cell activation (Lin and Yan 2019). HLA-I HC, but not fully-conformed trimers, can interact with HLA-F and regulate its surface level (Goodridge et al. 2010). Unlike other HLA-I molecules, ER exit of newly synthesised HLA-F does not require peptide loading, as its surface expression seems to be TAP-independent (Lee and Geraghty 2003), though interaction with TAP was reported (Wainwright et al. 2000). Instead, HLA-F ER export depends on a C-terminal valine motif as well as an RXR motif on its cytoplasmic tail (Boyle et al. 2006). Given the peptide independence of HLA-F expression and the relative stability of HLA-F open conformers (Dulberger et al. 2017), surface HLA-F can be found both as open conformers and trimer complexes bound to β2m and peptide. HLA-F with distinct conformations differ in their binding affinity to different receptors (Burian et al. 2016; Dulberger et al. 2017; Garcia-Beltran et al. 2016). Details of the peptide loading and presentation pathway of HLA-F remain to be characterised.

1.6.4 HLA-G

HLA-G is important in maternal-fetal and graft tolerance after transplantation (Rouas-Freiss et al. 1997). The expression of HLA-G is highly restricted in healthy tissues but can be induced in cancers (Bukur et al. 2003; Davidson et al. 2005; Ye et al. 2007; Zhu et al. 2011), transplantations (Lila et al. 2000), viral infections (Lafon et al. 2005; Lila et al. 2000) and many other different diseases (HoWangYin et al. 2012). HLA-G inhibits the immunological functions of a wide range of immune cells by binding to different inhibitory receptors expressed on them (HoWangYin et al. 2012). Due to its immunosuppressive role, HLA-G is often induced and upregulated in cancers and infectious diseases (Rashidi et al. 2022).

One of the most unique characteristics of HLA-G is that it has seven isoforms generated via alternative splicing, among which four are membrane-bound while the other three are soluble (Djurisic and Hviid 2014). Soluble HLA-G binds to the surface receptors on the target cells and gets endocytosed into the endosomal compartments, allowing for a more flexible immune regulation without cell contact (Rajagopalan et al. 2006; Schwich et al. 2020). Besides, soluble HLA-G is a promising biomarker for cancer diagnosis, as its expression level is usually upregulated by tumour cells to escape immune recognition (Kirana et al. 2017; Li et al. 2021; Lázaro-Sánchez et al. 2020; Martín-Villa et al. 2022). Only HLA-G1 and G5 contain all three domains of the HC and can, therefore, bind to β2m (Morales et al. 2003). Apart from HLA-G3, most isoforms can form homodimers (HoWangYin et al. 2012). Different conformations and isoforms of HLA-G have different binding preferences for different receptors (HoWangYin et al. 2012). Though the details are unclear, these studies suggest a complex regulatory picture of HLA-G.

HLA-G is mainly retained in the early secretory pathway, which is regulated by its C-terminal dilysine-based ER retrieval motif (Park et al. 2001). The binding of high-affinity peptides promotes the ER exit of HLA-G and increases its surface expression (Park et al. 2001). Both TAP-dependent and independent pathways of

peptide loading exist for HLA-G (Moreau et al. 2002). In contrast to HLA-Ia molecules, most surface HLA-G molecules are sensitive to endoglycosidase H (endo H), implying an unconventional transport pathway for newly synthesised HLA-G to get to the cell surface (Riteau et al. 2001). Soluble isoforms of HLA-G lack the ER-retrieval motif, which is essential for its secretion (Fujii et al. 1994). The truncated cytoplasmic tail of HLA-G lacks the tyrosine-based endocytosis signal that is conserved in most HLA-I molecules, thus increasing the surface stability of HLA-G (Park et al. 2001).

1.7 CD8+ T cell response in cancer and pathogen infection

CD8+ T cells, also known as cytotoxic T lymphocytes (CTLs), are critical for the immune defence against cancers and intracellular pathogens. T cell activation requires the recognition of specific antigens presented by MHC-I molecules by TCR as well as the interaction of co-stimulatory molecules (Reina-Campos et al. 2021). Upon the recognition of target cells, activated CD8+ T cells exert three major cytotoxic functions to kill them (Reina-Campos et al. 2021). Activated CD8+ T cells release cytotoxic granules, which contain perforin and granzymes (Bolitho et al. 2007). After perforins form pores on the membrane of the target cells, granzymes enter and exert their role as serine proteases, leading to the apoptosis of these malignant cells (Lopez et al. 2013). CD8+ T cells express Fas ligand, which interacts with Fas on the cell surface of target cells, leading to a caspase cascade that kills the target cells (Strasser et al. 2009). Activated CD8+ T cells also secrete a range of cytokines that have anti-tumour and anti-microbial effects, of which tumour necrosis factor (TNF)-α and cytokines interferon (IFN)-γ are the most important ones (Brehm et al. 2005; Gocher et al. 2022; Shankaran et al. 2001).

Given the specificity and effectiveness of CD8+ T cell response, they have become a key target in vaccines and immunotherapies. Pre-exposure to pathogen-specific

antigens provided by vaccines enables the immune system to recognise and eliminate bacteria and viruses upon infection quickly and is an effective tool to prevent diseases caused by these pathogens (Hurwitz 2018; Osterloh 2022). Cancer vaccines are also a promising therapeutic strategy to elicit effective CTL-mediated anti-tumour immune response, though their development is challenging and is at the early stages (Gupta et al. 2022). Apart from vaccine development, other CTL-targeting immunotherapies, including adaptive cell transfer and immune checkpoint blockade, are effective and promising in cancer treatment (Durgeau et al. 2018).

One of the primary immune escape methods adopted by pathogens or tumours is inhibiting the presentation of pathogen/tumour-specific antigens by HLA-I molecules, resulting in poor recognition of T cells (Jhunjhunwala et al. 2021). This renders the effectiveness of CTL-targeting therapies. Besides, MHC restriction also limits the clinical application of CTL-targeting immunotherapies to a subset of patients (Haworth et al. 2015). CTL-targeting therapies seem to be even more challenging for cancer treatment, given that selecting tumour-specific antigen targets is hard, and it's difficult for CTLs to persist and penetrate the tumour microenvironment to eradicate tumours (Sambi et al. 2019).

1.8 MHC-E-restricted CD8+ T cell response

Apart from the conventional role of presenting HLA-Ia leader peptides to NK cells, HLA-E can also present pathogen-derived peptides and activate CD8+ T cells. Although this field remains largely understudied, existing reports suggest that HLA-E-restricted unconventional CD8+ T cell response is universal and can be found in bacteria, viruses and cancer.

HLA-E-restricted presentation of peptides derived from Mtb can activate CD8+ T cells that inhibit Mtb outgrowth in infected patients (Heinzel et al. 2002; van Meijgaarden et al. 2015). 36 out of 69 Mtb-derived peptides predicted using motif

scores can bind to HLA-E, of which 11 can activate CD8+ T cells (Joosten et al. 2010). Five of the predicted Mtb-derived peptides can stabilise HLA-E surface expression, of which Mtb44 is the most significant (Caccamo et al. 2015). This is probably because of the high affinity of Mtb44, which is comparable to that of VL9 (Walters et al. 2018). In another study, 28 Mtb peptides were identified to be presented by HLA-E using mass spectrometry during intracellular Mtb infection (McMurtrey et al. 2017). 9 peptides could activate CD8+T cells from donors, of which the HLA-E-restricted recognition of the conserved Rv0634A19-29 peptide (EIEVDDDLIQK) is universal, and thus could be a good target for vaccine design (McMurtrey et al. 2017). Unlike most Mtb-reactive CD8+ T cells that characterise Th1 cells, the HLA-E-restricted Mtb-specific CD8+ T cells exhibit an unusual Th2-like profile (Caccamo et al. 2015; Prezzemolo et al. 2018; van Meijgaarden et al. 2015).

HLA-E can present S.typhi peptides to CD8+ T cells, which inhibits S.typhi pathogenesis persistently (Salerno-Goncalves et al. 2004; Salerno-Goncalves et al. 2010). HLA-E-restricted CD8+ T cell response has also been reported for the BZLF1 peptide derived from the Epstein-Barr virus (EBV) (Pietra et al. 2003). HLA-E can bind the YLLPRRGPRL peptide from Hepatitis C virus (HCV) core amino acid 35-44 (Nattermann et al. 2005) and be recognised by CD8 T cells (Schulte et al. 2009). HLA-E-restricted HCV-specific CD8+ T cell responses can be found in around 50% of patients chronically infected with HCV, and a higher frequency is found in patients homozygous for HLA-E01:01 (Schulte et al. 2009). The HCMV protein UL40 contains a peptide in its signal sequence that is identical to the human VL9 peptide. HLA-E loaded with this UL40-derived peptide can activate CD8+ T cells (Pietra et al. 2003) which can effectively kill HCMV-infected target cells (Mazzarino et al. 2005). Persistent unconventional CD8+ T cells that recognise HLA-E loaded with

UL40-derived VL9 peptide can be found in about one-third of HCMV seropositive hosts (Jouand et al. 2018).

Recent studies show that Mamu-E (the rhesus macaque (RM) homolog of HLA-E) can present SIV-derived peptides and activate CD8+ T cells in RMs vaccinated with a Rhesus Cytomegalovirus (RhCMV) 68-1-vectored vaccine containing recombinant SIV genes, which is in correlation with SIV protection (Hansen et al. 2016). RhCMV68-1-vectored vaccine expressing antigens derived from *Plasmodium knowlesi* can elicit MHC-E-restricted CD8+ T cell response and delay parasitemia (Hansen et al. 2019), though the exact functions of these CD8+T cells need further characterisation. The RhCMV68-1-vectored vaccine containing antigens derived from Hepatitis B virus (HBV) can also elicit unconventional HBV-specific, MHC-E-restricted CD8+ T cells that can target HBV-infected primary hepatocytes from humans as well as RMs (Burwitz et al. 2020).

HLA-E-restricted CD8+T cell response against the RL9 peptide (RMYSPTSIL), which is from the HIV gag protein, can be effectively primed in vitro and has demonstrated the ability to suppress HIV replication (Yang et al. 2021). Some other HIV-derived peptides can also bind to HLA-E and stabilise its surface expression (Hannoun et al. 2018). Although the first structure of HLA-E in complex with HIV-derived peptide has been solved (Walters et al. 2018), further work is needed on whether HLA-E can elicit CD8+ T cell activation in vivo by presenting HIV-derived peptides and its significance in protection against HIV.

As Mamu-E and HLA-E are highly similar in terms of expression, sequence, and peptide binding and presentation (Wu et al. 2018), it is possible that a vaccine eliciting protective HLA-E-restricted CD8+T cell responses against pathogens like HIV could be developed. Like HLA-E, the surface expression level of Mamu-E is low and can be similarly upregulated by viral pathogens (Wu et al. 2018). The sequences

of Mamu-E and HLA-E are similar and highly conserved, especially at places where MHC-E binds the peptide or contacts the TCR (Wu et al. 2018). The amino acids in the five binding pockets are almost identical (Walters et al. 2018; Wu et al. 2018). HLA-E can present SIV-derived peptides and activate SIV-specific rhesus CD8+ T cells (Hansen et al. 2016). Furthermore, Mamu-E and HLA-E present several HLA-E-restricted peptides, including RL9HIV and Mtb44, to rhesus CD8+ T cells with similar magnitude (Walters et al. 2018).

Several advantages make HLA-E-bound pathogen-derived epitopes attractive targets for vaccine-elicited CD8+T cell responses. Many pathogens downregulate the surface expression of HLA-Ia but not HLA-E to avoid NK cell killing (McMichael and Picker 2017). The low polymorphism of HLA-E makes it likely that HLA-E-restricted CD8+T cell responses will be shared among individuals. In the case of HIV infection, as HLA-E-restricted CD8+ T cell responses aren't thought to be induced in natural HIV infection, the persisting virus won't contain escape-conferring mutations in HLA-E-bound peptides. Given the recent success of eliciting protective MHC-E-restricted CD8+ T cell response in RMs for different infections via the RhCMV68-1-vectored vaccine (Burwitz et al. 2020; Hansen et al. 2019; Hansen et al. 2016), it's promising that HLA-E could be exploited to make vaccines eliciting protective CD8+ T cells against many different infections.

1.9 MHC-I transport regulation via its cytoplasmic tail

1.9.1 Intracellular transport regulation of MHC-I via its cytoplasmic tail

Previous studies have shown that the cytoplasmic tail of MHC-I molecules regulates its intracellular trafficking in various aspects, including endocytosis (Vega and Strominger 1989), degradation (Park et al. 2001) and ER retrieval (Boyle et al. 2006; Cho et al. 2011).

The C-terminal valine in the cytoplasmic tail is crucial for the ER export of the non-classical MHC-Ib molecule HLA-F (Boyle et al. 2006; Cho et al. 2011). Although HLA-A/B/C can exit the ER through bulk flow, the C-terminal valine/alanine motif makes this process more efficient by facilitating association with the sec23/24 complex, thus promoting a COPII-mediated ER export pathway(Cho et al. 2011). The C-terminal valine/alanine motif might be a universal regulator of ER export, as it can be found in around 10% of type I membrane proteins (Nufer et al. 2002). Apart from regulating ER export of HLA-I proteins (Boyle et al. 2006; Cho et al. 2011), the C-terminal motif is also important for efficient ER export of several other crucial membrane proteins of the immune system, including proTGF-α (Briley et al. 1997; Ureña et al. 1999), MT1-MMP (Ureña et al. 1999), and CD8α (Iodice et al. 2001). This suggests that the C-terminal ER export motif provides additional fine-tuning of the surface expression of important immune proteins.

The RxR motif in the HLA-F cytoplasmic tail, which is not present in other HLA-I molecules, also contributes to its antegrade transport via the interaction with 14-3-3 proteins (Boyle et al. 2006). HLA-G contains a unique dilysine-based C-terminal ER-retrieval motif, which retains HLA-G in the early secretory pathway unless it binds to high-affinity peptides (Park et al. 2001). Soluble HLA-G isoforms do not contain this ER-retrieval motif but have a unique C-terminal sequence which confers solubility (Fujii et al. 1994).

How the cytoplasmic tail affects endocytic trafficking has been well-studied for CD1. The trafficking pathway after internalisation largely depends on the cytoplasmic tail of CD1, whose sequences differ between isoforms (Gumperz 2006). Most CD1 molecules contain the Yxxφ (X =any amino acid, Φ = a bulky hydrophobic amino acid) endosomal sorting signal (Sugita et al. 2004). This tyrosine-based signal recruits AP2, thus promoting the internalisation of surface CD1 molecules through a clathrin-dependent pathway. CD1a has a truncated cytoplasmic tail and does not

contain this motif (Sugita et al. 1999), which may explain why most CD1a molecules remain at the surface, with only a tiny fraction transported to early endosomes and follow a shallow recycling pathway (Van Kaer et al. 2016). While CD1c and CD1d molecules are mainly delivered to early and late endosomes via AP-2 (Moody and Cotton 2017), CD1b molecules accumulate predominantly in late endosomes and lysosomes via the interaction of its cytoplasmic tail with AP-3 (Sugita et al. 2002). The cytoplasmic tail of CD1e plays a crucial role in controlling its Golgi accumulation in immature DCs as well as its direct transport to endosomes upon DC maturation (Maître et al. 2008).

HLA-A/B/E/F molecules contain a highly conserved YXXA sequence, which is highly similar to the well-characterised Yxxφ endosomal targeting motif. A non-classical tyrosine-based motif important for endolysosomal targeting exists, as tyrosine mutation disrupts endosomal peptide loading of MHC-I molecules and abrogates cross-presentation in DCs (Lizée et al. 2003). HLA-C lacks the tyrosine-based endosomal targeting motif but contains a dileucine-based motif (LI) in its cytoplasmic tail, which promotes its internalisation and endolysosomal transport (Bonifacino and Traub 2003; Schaefer et al. 2008). HLA-G has a truncated cytoplasmic tail without the endocytosis motif, which helps to prolong its surface lifetime (Park et al. 2001).

Ubiquitination also controls the endocytosis of surface HLA-I molecules. At the trans-Golgi network, the E3-ligase MARCH9 could recognise the lysines on the cytoplasmic tails of HLA-I molecules and target them to endosomal compartments, thus reducing their surface expression level (De Angelis Rigotti et al. 2017). For CD1e, ubiquitination on the cytoplasmic tail also provides the crucial signal for its direct trafficking from TGN to endosomes (Maître et al. 2008).

The C-terminal exon7 of MHC-I was also reported to be involved in the regulation of endocytosis, though the corresponding motifs and mechanisms were not thoroughly studied (Rodríguez-Cruz et al. 2011). The serine at position 335 in the MHC-I cytoplasmic tail is a conserved phosphorylation site (Guild and Strominger 1984; Pober et al. 1978), which might also be involved in the regulation of internalisation.

1.9.2 Pathogens can modulate MHC-I transport by targeting its cytoplasmic tail

Many pathogens are known to downregulate surface HLA molecules by targeting the cytoplasmic tail, including HIV-1(Cohen et al. 1999; Le Gall et al. 1998; Roeth et al. 2004; Williams et al. 2002; Wonderlich et al. 2008), EBV(Griffin et al. 2013) and Kaposi's sarcoma-associated herpesvirus (KSHV) (Coscoy et al. 2001; Hewitt et al. 2002). Many cancer cells also modulate MHC-I distribution by targeting its cytoplasmic tail (Bradley et al. 2015; Wang et al. 2008).

Viral proteins can utilise the ubiquitination pathway and target MHC-I molecules for degradation by recognising the lysines on the cytoplasmic tail. K3 and K5 from KSHV could act like E3-ligase and promote the endocytosis of surface MHC-I through a clathrin-dependent pathway (Coscoy and Ganem 2000; Coscoy et al. 2001; Hewitt et al. 2002). MK3 protein from MHV-68 not only directly downregulates surface MHC-I by ubiquitinating newly synthesised MHC-I in the ER and promotes its degradation (Boname and Stevenson 2001) but also triggers the degradation of MHC-I loading complex (Boname et al. 2004).

Different motifs on the cytoplasmic tail allow for selective downregulation of HLA-I molecules by viruses or pathogens. HIV Nef reroutes the trafficking of HLA-A and HLA-B by recruiting AP1 to their cytoplasmic tail, thus downregulating their surface expression (Roeth et al. 2004). Tyr320, Ala324 and Asp327 are the critical amino acids required for AP1-binding (Le Gall et al. 1998; Wonderlich et al. 2008). HLA-C and HLA-E lack some of these binding sites, and their surface expression is thus not

affected by Nef (Cohen et al. 1999; Le Gall et al. 1998). BILF protein from EBV can downregulate surface HLA-A/B/E, in which three amino acids in the HLA-I cytoplasmic tail are essential for such downregulation (Griffin et al. 2013). HLA-C escapes from BILF-mediated downregulation due to its difference in these crucial residues. HCMV protein US11 could selectively target HLA-A/B for degradation, in which the C-terminal lysine and valine are important (Barel et al. 2006; Story et al. 1999). HLA-C/E/G escapes from such allele-specific downregulation for their subtle sequence variation in the cytoplasmic tail.

1.10 Objectives

The unique characteristics of HLA-E make it an attractive target for immunotherapies against pathogen infection and cancers. Previous studies have suggested that HLA-E follows an unconventional pathway for antigen presentation, and such a transport pathway is crucial for eliciting effective HLA-E-restricted CD8+ T cell response. However, there has been a lack of study in the unusual transport pathways of HLA-E and the regulatory factors, which are fundamental for further manipulation of this HLA-E-restricted CD8+ T cell response for potential therapeutic purposes.

Therefore, I aimed to explore the following questions in my thesis:

- How is the intracellular distribution, and what are the trafficking pathways of HLA-E? How is it different from HLA-Ia molecules? Can such differences be observed in different cell types? (Chapter 3)
- What fundamental regulatory factors shape the intracellular distribution and transport process of HLA-E? What mechanisms are adopted by these different factors to regulate the trafficking of HLA-E? (Chapter 4)
- Is it possible to establish a robust system to enable sensitive examination of the presentation pathway of peptides delivered via different systems? (Chapter 5)

Chapter 2: Materials and Methods

2.1 Peptides

All peptides were purchased from GenScript at a purity of 85% in lyophilized powder. After reconstitution to a final concentration of 200mM in dimethyl sulfoxide (DMSO), peptides were aliquoted and stored at -80°C. Sequences of the peptides used are listed in Table 7.4.

2.2 Plasmid construction

All plasmids were prepared using the QIAprep Spin Miniprep kit (Qiagen, UK) or the NucleoBond Xtra Maxi kit (Macherey-Nagel) following the manufacturer's instructions. Primers (Table 7.1) and GeneArt Strings were purchased from Life Technologies. All sequences were confirmed by Sanger sequencing using an ABI 3770.

pGEN_EGFP, pGEN_HLA-E_EGFP, pGEN_HLA-A3_EGFP were generated previously. The original Retention Using Selective Hooks (RUSH) plasmids were created by inserting HLA-E or HLA-A3b fragment between the AscI and EcoRI sites in pIRESneo3 Str-Ii+CD44-SBP-EGFP (a kind gift of Frances Brodsky). The β2-microglobulin expression (β2m) plasmid was created by inserting a GeneArt string encoding β2-microglobulin with a C-terminal Picornavirus 2A "slip" sequence between the HindIII and NotI restriction sites of pGEN so that β2m and EGFP would be expressed as separate proteins in transfected cells. Peptide minigene constructs (VL9/TH9) were generated by annealing complementary oligonucleotides encoding the desired peptide sequences with appropriate overhangs to allow insertion between the HindIII and NotI sites of pGEN. The HLA-E*01:03-β2m-peptide single-chain trimer construct (SCT) encoding VL9, RL9 and AL9, as well as the

HLA-E*01:03-β2m single-chain dimer construct (SCD) were generated as previously described (Hannoun et al. 2018) by inserting the DNA fragments encoding the target peptide between the signal sequence and β2m. All these plasmids mentioned above were generated by Dr Simon Brackenridge in our group. pGEN_HLA-B*2705 and pGEN_Gag were from Dr. Lee Garner in our group.

The str-CD74 hook plasmid was constructed by inserting the HindIII_str-CD74 _NotI fragment (amplified with pGEN HindIII F and pGEN NotI CD74 R from the original RUSH plasmid) between the HindIII and NotI sites in pGEN. The HLA-SBP-EGFP reporter plasmids were created by inserting HindIII-NotI fragments encoding HLA-E (amplified with HLA-E HindIII F and pGEN EGFP NotI R from pIRESneo3 str-CD74+HLA-E-SBP-EGFP) or HLA-A3 (amplified with HLA-A3 HindIII F and pGEN EGFP NotI R from pIRESneo3 str-CD74+HLA-A3-SBP-EGFP) between the HindIII and NotI sites in pGEN. The plasmid expressing the sec61B RUSH hook was created by inserting a GeneArt String encoding a str-sec61B fusion between the HindIII and NotI sites in pGEN.

The following constructs were created by overlap extension PCR using appropriate flanking primers and inserted between the HindIII and NotI sites of pGEN using NEBuilder HiFi DNA Assembly (New England Biolabs) following the manufacturer's instructions. HLA-E, HLA-EA3, HLA-A3, and HLA-A3E without the EGFP tag were amplified from the corresponding EGFP-fusion constructs using pGEN F and corresponding reverse primers (E NotI R for HLA-E and HLA-A3E, A3 NotI R for HLA-EA3 and HLA-A3). HLA-E_L337V and HLA-EA3_V337L were amplified from HLA-E and HLA-EA3 constructs using pGEN F and corresponding reverse primers (E L337V NotI R and A3 L337V NotI R). pGEN_CD74 (p33) was amplified from the pGEN_str-CD74 hook using p33 F and p33 R. All the constructs listed in Table 2.1 were generated by inserting two overlapping fragments into the pGEN. Part 1 was amplified from the Part 1 backbone using pGEN F and Part 1,

while Part 2 was amplified from the Part 2 backbone using pGEN TER R and Part 2 primer.

Table 2.1 Strategies for constructs generation

Construct	Part 1 primer	Part 2 primer	Part 1 backbone	Part 2 backbone
HLA-EA3_EGFP	EA3 R	EA3 F	HLA-E_EGFP	HLA-A3_EGFP
HLA-A3E-EGFP	A3E R	A3E F	HLA-A3_EGFP	HLA-E_EGFP
HLA-E_L337V_EGFP	L337V EGFP R	L337V EGFP F	HLA-E_EGFP	HLA-E_EGFP
HLA-EA3_V337L_EGFP	V337L EGFP R	V337L EGFP F	HLA-EA3_EGFP	HLA-EA3_EGFP
HLA-E_Y320A_EGFP	Y320A R	Y320A F	HLA-E_EGFP	HLA-E_EGFP
HLA-E6A_EGFP	A7E R	A7E F	HLA-EA3_EGFP	HLA-E_EGFP
HLA-E7A_EGFP	E7A R	E7A F	HLA-E_EGFP	HLA-A3_EGFP
HLA-A6E_EGFP	E7A R	E7A F	HLA-A3E_EGFP	HLA-A3_EGFP
HLA-A7E_EGFP	A7E R	A7E F	HLA-A3_EGFP	HLA-E_EGFP
HLA-E_K310R_EGFP	K310R R	K310R F	HLA-E_EGFP	HLA-E_EGFP
HLA-E_K322Q_EGFP	K322Q R	K322Q F	HLA-E_EGFP	HLA-E_EGFP
HLA-E-2K_EGFP	K322Q R	K322Q F	HLA-E_K310R_EGFP	HLA-E_K310R_EGFP
HLA-A3+2K_EGFP	A3+2K R	A3+2K F	HLA-A3_EGFP	HLA-A3_EGFP
HLA-EA3+2K_EGFP	A3+2K R	A3+2K F	HLA-EA3_EGFP	HLA-EA3_EGFP
HLA-E_5C9_EGFP	5C9 R	5C9 F	HLA-E_EGFP	HLA-A3_EGFP
HLA-E_EW_AS_EGFP	EW_AS R	EW_AS F	HLA-E_EGFP	HLA-E_EGFP
HLA-E_E324A_EGFP	E324A R	E324A F	HLA-E_EGFP	HLA-E_EGFP
HLA-E_W325S_EGFP	W325S R	W325S F	HLA-E_EGFP	HLA-E_EGFP
HLA-A3_W	A3_W R	A3_W F	HLA-A3_EGFP	HLA-A3_EGFP
HLA-A3_2KW	A3_2KW R	A3_W F	HLA-A3+2K_EGFP	HLA-A3+2K_EGFP
CD74 KK10	KK10 R	KK10 F	pGEN CD74	pGEN CD74

All newly created lentiviral constructs were also generated by overlap extension PCR using appropriate flanking primers and inserted between the BamHI and SalI sites of pLenti CMV GFP Puro (a gift from Eric Campeau & Paul Kaufman; Addgene plasmid # 17448; (Campeau et al. 2009)). The following inserts were amplified from the corresponding constructs encoded in pGEN, including str-CD74 (pLVX CD74 BamHI F, pLVX CD74 SalI R), HLA-E_SBP_EGFP/ HLA-E_EGFP/ HLA-EA3_EGFP (pLVX HLA-E BamHI F, pLVX EGFP SalI R), HLA-A3_SBP_EGFP/HLA-A3_EGFP/HLA-A3E_EGFP (pLVX HLA-A3 BamHI F, pLVX EGFP SalI R), or HLA-B*27:05 (pLVX B27 BamHI F, pLVX B27 SalI R). The lentiviral constructs co-expressing HLA-B*27:05 and CD74 (pLVX_B27_CD74 WT), CD74 KK10 (pLVX_B27_CD74 KK10) or Gag (pLVX_B27_Gag) separated by the self-cleaving P2A sequence were generated using overlap extension PCR using corresponding constructs encoded in pGEN with primers listed in Table 2.2. Lenti vectors encoding TCRs specific for HLA-E HIV-1 $Gag_{275\text{-}283}$ RL9 peptide (RL9-TCR),

HLA-A*0201 NY–ESO-$1_{157–165}$ peptide (1G4), or HLA-B*2705 HIV-1 $Gag_{263-272}$ KK10 peptide (KK10-TCR) were generated previously on our group (Yang et al. 2021).

Table 2.2 Construction of lentiviral plasmids

Construct	Part 1 primer	Part 2 primer	Part 1 backbone	Part 2 backbone
pLVX_B27_Gag	pLVX B27 BamHI F/ B27 P2A R	P2A Kozak GAG F/ pLVX GAG SalI R	HLA-B27	Gag
pLVX_B27_CD74 WT		P2A_Kozak_CD74_F/ pLVX CD74 SalI R		CD74 WT
pLVX_B27_CD74 KK10				CD74 KK10

2.3 Tetramer generation

Refolding and purification of the HLA-E*01:03-β2m-RL9 complex and the HLA-B*27:05-β2m-KK10 complex was carried out as previously described with minor modifications (Walters et al. 2018). Briefly, β2m was first refolded at 4°C for 30 minutes (mins) (2μM final concentration) before sequential addition of peptide (20-50μM) and HC (1μM final concentration). After refolding at 4°C for 48hrs, refolded complexes were filtered through 1.0 μm cellulose nitrate membranes (Cytiva), followed by buffer exchange into Tris buffer (20mM, pH=8 with 150mM NaCl) (Life Technologies) via PD-10 desalting columns (Cytiva). Refolded HLA-I molecules were then biotinylated overnight via BirA (Avidity) using 875μL BiomixA, 875μL Biomix B, 100μL Bio200, and 5μg BirA enzyme following the manufacturer's instructions. Samples were purified by fast protein liquid chromatography on a Superdex S75 16/60 column in Tris buffer. For tetramer generation, six additions of 20.4μL APC or 22.1μL PE-conjugated to streptavidin (str) (Biolegend) were added to 100μg complex reconstituted in 50μL Tris buffer, with 10-minute intervals in-between where samples were kept on ice and protected from light. All tetramers were generated by Max Quastel in our group.

2.4 Cell lines and cell culture conditions

HEK 293T and HeLa cell lines were maintained in DMEM (Life Technologies), while T2, 721.211, THP-1, SKW-3 and K562 cell lines were cultured in RPMI-1640 (Life Technologies). All culture media were supplemented with 10% heat-inactivated fetal bovine serum (FBS, Sigma) and penicillin/streptomycin (50 units/mL and 50 µg/mL, respectively; Gibco), and cells were maintained at 5% CO_2/37°C. 293T cell lines with TAP or tapasin knocked out were previously constructed in our lab by Simon Brackenridge using the CRISPR/Cas9 system. 721.211 cells stably expressing HLA-E*01:03 or HLA-B*27:05 were previously constructed in our group. K562 cells stably transfected with HLA-E*01:03 (Lampen et al. 2013) (K562E) were generously provided by Thorbald van Hall (Leiden University Medical Centre). K562 cells transduced with HLA-E*01:03 SCT encoding VL9 or RL9 were previously constructed in our group (Yang et al. 2021). SKW-3 cells were purchased from DMSZ. THP-1 cells were differentiated into macrophages by overnight incubation in the presence of 50ng/mL phorbol 12-myristate 13-acetate (PMA, Merck), followed by PMA removal with fresh media the following day.

2.5 Plasmid transfection

HEK293T cells and HeLa cells were seeded at 30-50% confluence in 6-well plates 24hrs before transfection so that cell confluence was around 50-80% during transfection. In one well of a 6-well plate, HEK293T cells were transfected with 1µg of plasmid DNA using GeneJuice (Merck), and HeLa cells were transfected with 2µg of plasmid DNA using Lipofectamine™ 3000 (Thermo Fisher Scientific) following the manufacturers' instructions. Transfection carried out in plates of other sizes was scaled up or down accordingly. 24hrs after transfection, cells were harvested for experiments. For immunofluorescence (IF), HeLa cells were seeded in 24-well plates and transfected with 0.5µg of total plasmid DNA. For the RUSH assay, hook and reporter plasmids were transfected at ratios of 5:1 and 10:1 for HLA-E and HLA-A3 respectively, to ensure optimal ER trapping. When plasmids expressing peptides were

included in the RUSH assay, an equal amount of the peptide minigene plasmid and the RUSH plasmids were transfected. In HEK293T cells co-transfected with HLA-E and different amounts of peptide minigene plasmid or β2m plasmid, 0.2 μg HLA-E plasmid was transfected for each sample, and the total amount of plasmid is topped up to 1 μg by addition of EGFP plasmid. Equal amounts of different plasmids were transfected in all the other co-transfections.

2.6 Isolation and culture of CD8+ primary cells

Peripheral blood mononuclear cells (PBMCs) were selected from leukocyte cones derived from healthy donors (NHS Blood and Transplant, UK) by density gradient separation. Cones were slowly added on top of an equal amount of Ficoll-Paque Plus layer (Merck) and centrifuged at 2300rpm for 23 mins at room temperature (RT) with a slow deceleration program. The PBMC interface was collected using a transfer pipette (Sarstedt) and washed twice with HBSS (Hank's Balance Salt Solution, Gibco). CD8+ T cells were enriched from PBMC by positive selection using CD8 microbeads and LS columns according to the manufacturer's instructions (Miltenyi Biotec). Briefly, $1x10^8$ PBMCs were resuspended in 800μL MACS buffer (5%FBS (Sigma), 2mM EDTA (Invitrogen) diluted in PBS), mixed with 200μL CD8 microbeads, and incubated at 4°C for 20 mins. Cells were washed with 10mL MACS buffer and resuspended in 500μL MACS buffer. Cells were then loaded onto pre-washed LS columns, washed 3 times with 3mL MACS buffer each, and eluted with 5mL MACS buffer. $8x10^6$ Cells were then resuspended in 4mL RH5 media (RPMI medium (Life Technologies) supplemented with 5% AB Human Sera (UK National Blood Service), 1% non-essential amino acids (Gibco), 1% sodium pyruvate (Gibco), 1% glutamine (Gibco), 1% HEPES (Gibco), 0.1% β-mercaptoethanol (Invitrogen), penicillin/streptomycin (50 units/mL and 50 μg/mL, respectively; Gibco)) supplemented with 1000 IU/mL IL-2 (produced in house from hybridomas) and 10ng/mL IL-15 (R&D Systems). CD3/CD28 Dynabeads (Gibco) were washed with

MACS buffer, resuspended in RH5 media, and added to CD8+ T cells at 1:1 beads:cell ratio following the manufacturer's protocol. CD8+T cells were activated for two days before TCR transduction. Primary CD8+ T cells were cultured in RH5 media supplemented with IL-2 and IL-15 after transduction.

2.7 Stable cell line construction

All stable cell lines were constructed using the lentiviral transduction system.

2.7.1 Lentivirus production

Lentivirus was produced as previously described (He et al. 2023). Briefly, lentiviruses were generated via transient transfection in HEK293T cells using GeneJuice (Merck) following the manufacturer's instructions. For each well in a six-well plate, 1µg transfer plasmid was co-transfected with 0.5µg pQ8.91 packaging plasmid and 0.5µg pMD2.G envelope plasmid (a gift from Didier Trono (Addgene plasmid # 12259)). Viral supernatants were collected 48hrs after transfection and filtered via a 0.45µM syringe filter (Fisherbrand) and were directly used for infection.

2.7.2 Lentiviral transduction in adherent cells

HeLa cell lines stably expressing HLA-E, HLA-EA3, HLA-A3, or HLA-A3E with EGFP tagging on the C-terminus were constructed following the protocol below. WT HeLa cells were seeded in 6-well plates at 30% confluency 24hrs before lentiviral transduction. An extra well was seeded as untransduced control. 0.5mL filtered lentiviral supernatant was added to 1.5mL pre-warmed antibiotic-free media, and polybrene (Santa Cruz Biotechnology) was then added to a final concentration of 10 µg/mL and mixed well. The supernatant of HeLa cells was then replaced with the diluted viral supernatant with polybrene, and the cells were then centrifuged at 800xg for 30 mins at 32°C. 24hrs after transduction, viral supernatant was replaced with

fresh media. 72hrs after transduction, puromycin (Life Technologies) was added for selection with a final concentration of 2ng/mL. The supernatant was replaced with fresh media with puromycin every three days, and cells were subcultured if confluent. EGFP expression and cell viability were observed every day. When most of the untransduced cells in the control well died, and most of the transduced cells were resistant to puromycin selection, which usually took a week, cells were collected for flow cytometry analysis to verify the protein expression level and cell viability. Stable cell lines were further expanded and stored in liquid nitrogen or used for experiments.

HeLa cells stably expressing the RUSH system were constructed with minor modifications. str-CD74 were firstly transduced into HeLa cells using the lentiviral system at a Multiplicity of Infection (MOI) of 3. After puromycin selection and cell sorting, HeLa cells stably expressing CD74_str were then transduced with HLA-A3_SBP_EGFP or HLA-E_SBP_EGFP at a MOI of 0.3. Cells were assessed 48hrs after transduction with the reporter protein.

2.7.3 Lentiviral transduction in suspension cells

The following cell lines were constructed following the protocol below：

- THP1 cells stably expressing HLA-B*27:05 (THP1_B27), or co-expressing HLA-B*27:05 and CD74 (THP1_B27_CD74 WT), CD74 KK10 (THP1_B27_CD74 KK10) or Gag (THP1_B27_Gag).
- SKW-3 cells stably expressing 1G4, KK10-TCR or RL9-TCR.
- Primary CD8+ T cells transduced with 1G4 or RL9-TCR.

For suspension cell lines like SKW-3 cells, THP1 cells, and primary CD8+ T cells, transduction was carried out in 24-well plate non-tissue culture treated plates (Starlabs). Each well was preincubated with 300μL PBS containing 25μg/mL retronectin (Takara Bio). After gently shaking to ensure that the bottom of each well was covered with liquid, the plate was sealed with the cling film and kept at 4°C for at least 24hrs. On the day of transduction, each retronectin-coated well was blocked with 300μL PBS containing 2% bovine serum albumin (BSA, Merck) for 30 mins at RT. After washing with 300μL PBS, 2mL filtered viral supernatant was added to each

well, and the plate was centrifuged at 2000xg for 90 mins at 4°C. Viral supernatant was then mostly removed, leaving behind around 100 µL so that the plate did not dry out. 0.5 million cells resuspended in 2mL media were added to each well, and the plate was centrifuged at 2000rpm for 1 minute at RT. Cells were then incubated for another four days and were subcultured as required. THP1 cells were subsequently resuspended in fresh media supplemented with puromycin at a final concentration of 1ng/µL, with media replaced every 2-3 days. The antibiotic selection continued until most of the untransduced cells in the control well died, and the majority of the transduced cells were resistant to puromycin selection, which usually took about a week. THP1 cells were then collected for flow cytometry analysis to verify the protein expression level and cell viability before sorting the HLA-B27 positive cells. SKW-3 cells and primary CD8+ T cells were directly assessed for protein expression without antibiotic selection, followed by Fluorescence-activated cell sorting (FACS) as described in section 2.8. Sorted cells were further expanded in fresh media and then stored in liquid nitrogen or used for experiments.

2.7.4 Surface staining of TCR-transduced SKW-3 cells and primary CD8+ T cells for FACS

All staining procedures were carried out at RT and protected from light. After washing with MACS buffer (5%FBS (Sigma), 2mM EDTA (Invitrogen) diluted in PBS), cells transduced with the RL9/KK10 TCRs were first co-stained with APC/PE-conjugated tetramers diluted in MACS buffer for 40 mins. Tetramers were generated as described in section 2.3 with 20µg HLA-E-RL9 tetramer or 1µg HLA-B27-KK10 tetramer added for each fluorescence. KK10-TCR transduced cells were washed once with MACS buffer and stained with Live/Dead Fixable Aqua dye (Invitrogen), CD8-BV421, CD3-APC_cy7 and TCRβ-FITC diluted MACS buffer for 30 mins. These antibodies were directly added to RL9-TCR transduced cells without the removal of the RL9-tetramers. Cells transduced with 1G4 were washed and

directly stained with the antibodies without tetramer staining. Cells were washed once and resuspended in MACS buffer, followed by sorting of CD3+CD8+TCR+ cells. Sorted SKW-3 cells or primary CD8+ cells were further expanded in R10 media or RH5 media supplemented with IL-2 and IL-15 (as described in section 2.4) for two weeks before they were ready for experiments.

2.8 Flow cytometry

Surface staining for the sorting of TCR-transduced cells, intracellular p24 staining and cytokine secretion evaluation were carried out as described in section 2.7.4 and 2.20, respectively. For other experiments, flow cytometry was carried out as previously described (He et al. 2023). The samples were kept at 4°C and protected from light throughout the staining process. Briefly, for surface staining, cells were stained with antibody diluted in 100µL DPBS (Dulbecco's Phosphate-Buffered Saline) for 20 mins, washed twice with DPBS, and fixed with 100µL Cytofix (BD Biosciences) for 20 mins. For intracellular staining, cells were fixed and permeabilised with 100µL Cytofix/Cytoperm Solution (BD Biosciences) for 20 mins, washed twice with Perm/Wash buffer (BD Biosciences), and then stained with antibody diluted in 100µL Perm/Wash buffer for 20 mins. After washing with Perm/Wash buffer and DPBS, samples were resuspended in DPBS and acquired using a Cyan ADP Analyser (Beckman Coulter) or an Attune NxT Flow Cytometer (Thermo Fisher Scientific), and data were analysed using FlowJo 10.4. Single-stained compensation beads (BD biosciences) were used to generate the compensation matrix if required following the manufacturer's guidance. Details of the antibodies used are listed in Table 7.2.

2.9 Brefeldin A (BFA) decay assay

Cells were incubated with 10µg/mL BFA (Cambridge Bioscience) diluted in prewarmed media for different time points, and the surface expression of different HLA-I molecules was assessed by flow cytometry. In some experiments, primaquine

(0.3mM final, Enzo Life Sciences) and/or peptides (100μM, final) were added simultaneously to the media or the cells were pre-incubated with peptides (100μM, final) before BFA addition, as specified in each experiment. To stop further protein transport during the staining process, samples were maintained at 4°C. Surface stability was measured by the percentage of HLA-E remaining on the cell surface after BFA incubation, which was calculated as the percentage of the initial surface signal without BFA incubation. Details of the antibodies used are listed in Table 7.2.

2.10 Immunoblotting

Cells were lysed in RIPA buffer (10X RIPA Lysis buffer (Merck) diluted in ddH2O, with the addition of protease inhibitor cocktail (Roche), PhosSTOP (Roche) and PMSF (Stratech Scientific)) for 20 mins on ice. Cells were then centrifuged at 13000 rpm for 15 mins at 4°C, and the supernatant was transferred to a new tube and kept on ice. The lysates directly used for immunoblotting were mixed with NuPAGE™ LDS Sample Buffer and Sample Reducing Agent (Invitrogen), heated for 10 mins at 70 °C, and then used for immunoblotting. Cell lysates used for endo H essay or immunoprecipitation (IP) were treated as described in corresponding sections before immunoblotting. All steps were carried out at RT during immunoblotting.

Protein samples were loaded onto 4-12% Bis-Tris gels (Life Technologies). Precision Plus Protein Kaleidoscope Standards (Bio-Rad) was loaded simultaneously, and the loading buffer was added to all empty wells left. Samples were run in NuPAGE™ MOPS running buffer (Invitrogen) at 100W for 10 mins and then at 150W for 90 mins. PVDF membrane (Merck) was activated for 30 seconds in methanol (Sigma) and then equilibrated in 2X transfer buffer (20x NuPAGE™ Transfer Buffer (Invitrogen) was diluted in ddH2O to 2x concentration with 10% methanol added). Gels were washed with ultra-pure water and then equilibrated in 2X transfer buffer. Filter papers were also soaked with the 2X transfer buffer. A semi-dry transfer was then carried out on

Trans-Blot SD (Bio-Rad) at 15V for 60 mins. Membranes were blocked in the blocking buffer (5% skim milk (VMR) 0.05% Tween-20 (Sigma) diluted in DPBS) for one hour and then incubated with primary antibodies diluted in the blocking buffer for another hour. Membranes were washed three times in washing buffer (0.05% Tween-20 (Sigma) diluted in DPBS) (10 mins each), followed by incubation with secondary antibodies diluted in the blocking buffer. After three washings with washing buffer (10 mins each), membranes were washed once more with DPBS and imaged on a LICOR Odyssey X instrument following the manufacturer's instructions.

2.11 Endoglycosidase H (Endo H) treatment

Cell lysates were generated as described in section 2.10 and were then used for endo H assay via protein digestion with endo Hf (New England Biolabs) following the manufacturer's protocol. Briefly, after denaturation of heating at 100°C for 10 mins, lysates were treated with 1000 U of endo Hf (New England Biolabs) for 2hrs at 37°C. A digestion control group was set up simultaneously with an equal amount of cell lysate without endo H addition. After mixing with the loading buffer, lysates were assessed with immunoblotting.

2.12 Co-immunoprecipitation (co-IP)

Co-immunoprecipitation was carried out using Dynabeads Protein G (Invitrogen, referred to as beads) following the manufacturer's protocol with minor alterations. For all the washing steps, immunoprecipitates were reconstituted in 1mL washing buffer (0.05% Tween-20 (Sigma) diluted in DPBS), and the beads were then separated from the wash buffer using the DynaMag™-2 Magnet (Invitrogen). Briefly, 30µL beads were washed once with DPBS and resuspended with the cell lysate. Cell lysates were generated as described in section 2.10. Input samples were taken out from the lysates before mixing with the beads if necessary. 1 µg antibody was then added, and the samples were incubated with rotation for 3hrs at 4°C. After three washings, samples

were resuspended with loading buffer, heated for 10 mins at 70°C, and the protein elution was taken for immunoblotting. Details of the antibodies used are listed in Table 7.3.

2.13 Immunofluorescence (IF)

Cells were seeded into a 24-well plate with coverslips (VMR) placed at the bottom, and IF was carried out as previously described (He et al. 2023). Briefly, samples were fixed with 4% formaldehyde (16%formaldehyde (Thermo Fisher Scientific) diluted in DPBS) for 15mins, washed with DPBS, and then blocked and permeabilised with the blocking buffer (DPBS containing 0.5% saponin (Merck) and 2% bovine serum albumin (Merck)) for 1h. For the RUSH assay, cells were fixed at different time points after the addition of biotin (Sigma-Aldrich). For surface staining, saponin was excluded from the blocking buffer. Samples were then incubated in primary antibody diluted in the blocking buffer for 1.5hrs, washed with the blocking buffer, and then incubated in secondary antibody diluted in the blocking buffer for 2hrs. After washing with the blocking buffer and then with DPBS, coverslips were mounted onto microscope slides (Scientific Laboratory Supplies) with DAPI fluoromount-G (Cambridge Bioscience). Images were obtained using an inverted confocal microscope (Zeiss LSM880) equipped with a Plan-Apochromat 63x/1.4 oil objective. Images were processed and analysed in Fiji/ImageJ, and the Coloc2 plug-in was used to calculate the Pearson correlation coefficient (PCC) values. Details of the antibodies used are listed in Table 7.3.

2.14 Live-cell imaging

Live-cell imaging was carried out as previously described (He et al. 2023). Briefly, HeLa cells were seeded on μ-Slide 8 well-high glass bottom plate (Thistle Scientific), and live-cell imaging was carried out in a thermostat-controlled chamber using an inverted confocal microscope (Zeiss LSM880) equipped with a Plan-Apochromat

63x/1.4 oil objective. Images were acquired every minute upon biotin addition (50μM final) up to 2hrs and were processed further in Fiji/ImageJ.

2.15 Acid stripping assay

Acid stripping assays were carried out as previously described (He et al. 2023). Briefly, to explore the antegrade transport of HLA-I proteins in THP1-derived macrophages, cells were incubated with the citric acid buffer (pH 3.0) for 3 mins to strip off surface HLA-I proteins, neutralised with chilled media, and resuspended with pre-warmed media. BFA was added to some samples as indicated. Cells recovered for different time lengths were collected, and surface HLA-I proteins were assessed with flow cytometry. To examine the internalisation rates of HLA-I proteins, surface HLA-I proteins were antibody-labelled before resuspension in pre-warmed media with primaquine added. Cells were collected after internalisation for different time lengths, and the uninternalised surface antibody-HLA-I complex was stripped off as described above. The signal of each sample was normalised to the surface signal without acid stripping. Details of the antibodies used are listed in Table 7.2.

2.16 Surface biotinylation assay

Surface biotinylation was carried out following as previously described with minor modifications (Turvy and Blum 2001). Briefly, cells were washed twice with HBSS (Gibco) and labelled with 0.5mg/mL EZ-Link™ sulfo-NHS-S-S-biotin (Thermo Fisher Scientific) diluted in HBSS for 30 mins at 4°C with rotation. A non-labelled sample was used as the negative control. Cells were then washed twice with 20mM glycine (MP Biomedicals) diluted in HBSS, resuspended in media, and incubated at 37°C to allow for internalisation. Cells were collected at different time points, washed twice with chilled HBSS, and lysed as described in section 2.10.

Enzyme-linked immunosorbent assay (ELISA) was then applied to quantitate the biotin signal based on the previous protocol with modifications (Turvy and Blum 2001). Briefly, ELISA plates (Life Technologies) were pre-coated with 50µL of antibody diluted to 10µg/mL in ELISA coating buffer (Biolegend) overnight at 4°C. After washing three times with DPBS, 300µL blocking buffer (2% BSA (Sigma) in DPBS) was added to each well, and the plate was blocked for 2hrs at 4°C. After washing three times with PBST (0.05% Tween-20 (Sigma) diluted in DPBS), 100µL lysate was added to each well, and the plate was incubated for 2hrs at 4°C. After washing five times with PBST, 100µL 2.5µg/mL HRP-conjugated str (Thermo Scientific) diluted in the blocking buffer was added to each well and incubated for 30 mins at RT. The plate was washed five times with PBST and then developed using the Tetramethyl benzidine system (TMB Substrate Set, Biolegend) following the manufacturer's protocol. Absorbance at 450nm was then obtained on a FLUOstar OMEGA plate reader, and the signal was normalised as the percentage of the uninternalised sample. Details of the antibodies used are listed in Table 7.3.

2.17 T cell activation assay

K562 cells or THP1 cells were treated as specified in each experiment before co-incubation with TCR-transduced SKW-3 cells or primary CD8+ T cells at an E:T ratio of 1:1 unless otherwise specified. Primary CD8+ T cells were rested for 24hrs in RH5 media without cytokine before co-incubation. In some experiments, THP1 cells were pre-stimulated with IFN-γ (final 100ng/mL) (Petrotech) or PMA (final 50ng/mL) (Merck) for 24hrs followed by extensive washing with media. For peptide pulsing, RL9 (RMYSPTSIL) was used at a final concentration of 100µM and was kept in media during the co-incubation. NY-ESO-1 (SLLMWITQC) and KK10 (KRWIILGLNK) were used at a final concentration of 1µM unless otherwise specified, and the peptides were removed during the co-incubation. Cells were co-incubated in a 96-well round-bottom plate (Corning) with two replicates for each condition for 16hrs

unless otherwise specified. Each well contains 10^5 CD8+T cells and 10^5 or $5x10^5$ APCs in 200μL media. SKW-3 directly stimulated with PMA (final 50ng/mL) (Merck) and ionomycin (IONO) (final 40ng/mL) (Merck) was used as the positive control as indicated.

For the evaluation of the upregulation of the surface activation markers, cells were stained with Live/Dead Fixable Aqua dye, APC- Cy7, CD8-BV421, CD25-BV711, CD69-APC, and CD137-PE (section 2.8). The assessment of cytokine secretion was carried out as previously described with minor modifications (Yang et al. 2021). Briefly, after peptide pulsing for 2hrs, THP1 cells were co-incubated with T cells for 8hrs in the presence of 5μg/mL BFA (Biolegend) and 5μg/mL GolgiStop (BD Biosciences). After washing with DPBS, cells were firstly surface stained Live/Dead Fixable Aqua dye, APC- Cy7, CD8-BV421 to select live CD8+ T cells, followed by intracellular staining with TNF-α-PE, IFN-γ-BV711 and MIP-1β-APC (section 2.8). Details of the antibodies used are listed in Table 7.2.

2.18 Production of HIV-1 (VSVG-BaL) virus

The HIV-1 lab-adapted strains NL4.3 BaL plasmid were kindly provided by Drs John Kappes and Christina Ochsenbauer (University of Alabama at Birmingham). To produce the virus stocks for the VSVG-pseudotyped HIV NL4.3 BaL stain (HIV-1 VSVG-BaL), plasmid DNA and the lentiviral packaging plasmid pMD2.G (a gift from Didier Trono (Addgene plasmid # 12259)) were co-transfected into HEK293T cells using 1μg/μL polyethylenimine (PEI, Polysciences) at ratio 3:1 in Opti-MEM (Gibco). Viral supernatants were harvested 72hrs later, clarified by centrifugation at 1500 × g for 10 mins, filtered through a 0.45μm syringe filter (Fisherbrand), and stored at −80 °C. The infectivity of viral stocks was determined using a colorimetric reverse transcriptase assay following the manufacturer's instructions (Roche Life Sciences). All viral stocks were generated by Anna Kliszczak in our group.

2.19 Viral infection

2.19.1 HIV infection

$1x10^6$ THP1 cells were resuspended in media containing 50ng HIV-1 (VSVG-BaL) virus, followed by centrifugation at 2000rpm at 27°C for 2hrs. THP1 cells were resuspended in 2mL fresh media, transferred to a 6-well plate, and incubated for three days. Infection rate was then determined via intracellular p24 staining (section 2.20). The presentation of the KK10 peptide was evaluated via T cell activation assay (section 2.16).

2.19.2 M4/C62 infection

MVA.tHIVconsv4 (M4) and ChAdOx1.HIVconsv62 (C62) were provided by Tomas Hanke (University of Oxford), and the details of the constructs were described previously (Wee et al. 2021). HeLa cells were seeded the day before at 30-50% confluence in a 6-well plate so that cell confluence was around 50-80% during transfection. M4/C62 was diluted in DMEM at the indicated MOI before addition to HeLa cells with media replaced by 1mL DMEM. Cells were incubated with the virus for 2hrs at 37°C, and the supernatant containing the virus was replaced by 3mL fresh media. For THP1 cells, M4/C62 was diluted in RPMI before addition to 10^6 cells resuspended in 500µL RPMI at the indicated MOI. THP1 cells were then centrifuged at 800xg at 32°C for 2hrs, resuspended in 1mL media and transferred to a 24-well plate. The infection rate of M4 was then determined via intracellular p24 staining (section 2.20), while the infection rate of C62 was evaluated via immunoblotting using SV5-Pk1 antibody and IRDye 800CW donkey anti-mouse antibody sequentially (section 2.10).

2.20 Intracellular p24 staining

Intracellular p24 staining was adapted from a published protocol (Yang et al. 2013). All staining steps required keeping the samples in dark, all washing steps used 5mL PBS and all centrifugation steps were done at 2000rpm for 3 mins at 4°C. $1x10^6$ THP1 cells were resuspended in 100µL PBS containing 0.5µL Live/Dead Fixable Aqua dye and incubated at RT for 20 mins. After washing twice, cells were resuspended in 500µL 20 µg/mL lysolecithin (Sigma) in 4% paraformaldehyde (PFA, Santa Cruz), briefly vortexed to mix, and then incubated at RT for 2 mins for fixation. Cells were pelleted and resuspended in 1mL chilled 50% methanol (Sigma, diluted in PBS) and incubated at 4°C for 15 mins. Cells were pelleted and resuspended in 500µL 0.1% NP-40 (Sigma, diluted in PBS) and incubated at 4°C for 5 mins. Cells were washed once, resuspended in 100µL PBS containing 2µL anti-p24 antibody (KC-57-FITC, Beckman Coulter), and incubated at RT for 20 mins. Cells were washed twice and resuspended in 300µL PBS and then acquired and analysed as described in section 2.8.

2.21 Statistic analysis

Data were analyzed in GraphPad Prism 9 and were presented as mean ± SD (ns, not significant; *, $P < 0.05$; **, $P < 0.01$; and ****, $P < 0.0001$). Two-tailed student's t-test with Welch's correction (two groups, unpaired or paired) or one-way ANOVA with Tukey's post-hoc test (three or more groups) was performed for comparison between groups.

Chapter 3: Characterisation of HLA-E trafficking patterns

Part of the data presented in this chapter has been published in (He et al. 2023).

3.1 Introduction

CD8+ T cell activation is enabled by the antigen presentation of HLA-I molecules. The high polymorphism of HLA-I molecules restricts the application of CD8+ T cell targeting immunotherapies to a subset of patients (Haworth et al. 2015), and the common downregulation of HLA-I molecules by pathogens and in cancers further renders the effectiveness of these therapies (Jhunjhunwala et al. 2021). In contrast, HLA-E has very low polymorphism and is resistant to the downregulation by most pathogens (McMichael and Picker 2017), and these advantages make it an attractive target for immunotherapies.

The unconventional HLA-E-restricted CD8+ T cell response has been found in different pathogens and is shown to be potentially highly effective against these infections, including Mtb, S.typhi, HCMV, HCV, and HIV (Caccamo et al. 2015; Mazzarino et al. 2005; Salerno-Gonçalves et al. 2004; Schulte et al. 2009; Yang et al. 2021). To inform the rational design of methods to elicit HLA-E-restricted CD8+T cell responses, understanding how HLA-E traffics and presents pathogen-derived peptides is very important. However, this field is largely unexplored, and many basic questions remain unanswered. Therefore, in this chapter, I aim to carry out a complete characterisation of the trafficking patterns of HLA-E, including both its intracellular distribution and the dynamic transport process.

3.2 Intracellular distribution of HLA-E

To explore the intracellular distribution and transport of HLA-E, I constructed a Hela cell line stably expressing HLA-E*01:03 tagged with EGFP (HeLa.E). Another Hela

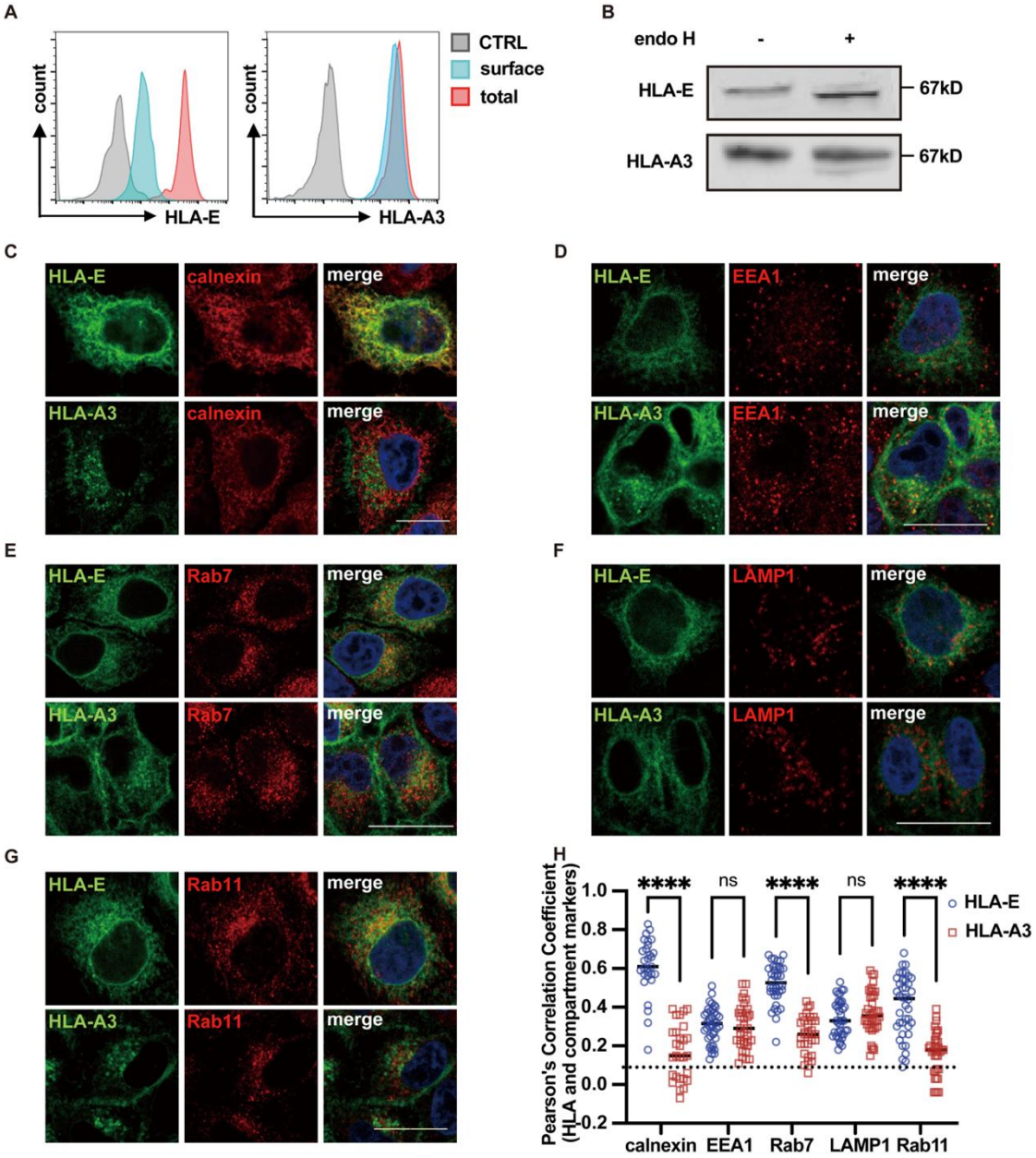

Figure 3.2.1 Intracellular distribution of HLA-E in HeLa cells

A. HeLa.E or HeLa.A3 were collected for flow cytometry analysis (gated on GFP+ cells). Expression of HLA molecules was assessed with either anti-HLA-A3 antibody (GAP.A3) or anti-HLA-E antibody (3D12). Representative graphs of total expression (red) and surface expression (blue) of HLA-E or HLA-A3 are shown. MFI of the unstained sample (grey) was used as the negative control. MFIs shown here are representative of observations made in six experiments.

B. Lysates of HeLa.E or HeLa.A3 were treated with Endo H for 2hrs at 37°C, followed by detection with immunoblotting using an anti-EGFP antibody.

C, D, E, F, G. Representative micrographs of HeLa.E or HeLa.A3. After fixation and permeabilization, cells were stained with antibodies against marker proteins for ER (calnexin, C), early endosome (EEA1, D), late endosome (Rab7, E), lysosome (LAMP1, F), and recycling endosome (Rab11, G), followed by detection with Alexa568-conjugated secondary antibody. Scale bars = 20 μm.

H. Quantification of co-localization of HLA-E or HLA-A3 with different marker proteins from Fig1.C-G.

The PCC values of each cell and the mean values are shown with 20-40 cells per sample. Statistical analysis was performed using unpaired two-tailed student's t-test with Welch's correction. Asterisks show the statistical significance between indicated groups: ns, not significant; ****, $P < 0.0001$.

cell line stably expressing HLA-A*03:01 tagged with EGFP (HeLa.A3) was constructed as a control, as HLA-A3 is not known to share the binding of peptides

with HLA-E. As the intracellular accumulation of HLA-E was reported previously (Camilli et al. 2016; Coupel et al. 2007; Lee et al. 1998a), I examined the proportion of HLA-E on the cell surface by comparing the Mean fluorescence intensity (MFI) of HLA-E surface staining to that of the intracellular staining (Fig.3.2.1A). Consistent with previous data, while most HLA-A3 stayed on the cell surface, only around 5% of total HLA-E was present on the cell surface. Endoglycosidase H (Endo H) assay was carried out to examine whether most intracellular HLA-E stays in the early secretory pathway. Immature proteins in the early secretory pathways consist of N-linked glycans that are sensitive to endo H cleavage, which can be detected by a shift of protein band of a lower molecular weight in western blot. While most HLA-A3 was resistant to endo H cleavage, most HLA-E was sensitive to endo H cleavage (Fig.3.2.1B). This reconfirms our conclusion that the majority of HLA-A3 stays on the plasma membrane, while most HLA-E stays in the early secretory pathway.

To further explore if most intracellular HLA-E in the early secretory pathway stays in the ER, I used confocal microscopy to co-localise HLA-E with the ER marker protein calnexin. Pearson correlation coefficient (PCC) was used to quantify the degree of co-localisation (Dunn et al. 2011). The maximal PCC value goes up to 1 when the fluorescence intensities of the two channels are exactly linearly related to each other. The minimal PCC value is -1, which happens when signals from the two channels are perfectly but inversely linearly related. HLA-E co-localised strongly with the ER, as indicated by the high PCC value with the mean value at around 0.6 (Fig.3.2.1C, H). In contrast, HLA-A3 co-localised poorly with the ER, with an average PCC value of around 0.1. Most HLA-E stayed intracellularly, and the surface signal was undetectable under microscopy (Fig.3.2.1C), which is consistent with previous results showing the low surface expression of HLA-E. In contrast, the bright surface signal could be observed for HLA-A3 (Fig.3.2.1C), implying that a large proportion of

HLA-A3 stayed on the cell surface. The signal for intracellular HLA-A3 appeared like bright green spots under the microscope, which resembled endosomal compartments.

I then explored whether HLA-E could be found in different endosomal compartments, as endosomal peptide loading of HLA-E might be crucial for the presentation of pathogen-derived peptides (Grotzke et al. 2009; Verweij et al. 2021). HLA-E was found in early endosomes (EEA1), late endosomes (Rab7), recycling endosomes (Rab11) and lysosomes (LAMP1), as evidenced by the co-localisation with different endosomal markers (Fig.3.2.1D-H). HLA-A3 could also be found in all these endosomal compartments. While no difference in PCC values with EEA1 and LAMP1 was observed between HLA-E and HLA-A3, the PCC values with Rab7 and Rab11 were higher for HLA-E (Fig.3.2.1H). This implies that HLA-E is more enriched in late endosomes and recycling endosomes compared to HLA-A3.

As overexpression, EGFP tagging and cell line specificity might potentially introduce systematic bias, I further tested the intracellular distribution of endogenous HLA-E and HLA-Ia in PMA-differentiated THP1 cells that resemble macrophages (Fig.3.2.2). Similarly, the majority of the endogenous HLA-E in THP1-derived macrophages stayed intracellularly, as shown by the low surface expression (Fig.3.2.2A). The sensitivity to endo H cleavage showed that most HLA-E remained in the early secretory pathway (Fig.3.2.2B). Good co-localisation with ER was observed for endogenous HLA-E (Fig.3.2.2C, H), which further confirmed the intrinsic ER accumulating effect of HLA-E. Most HLA-Ia stayed on the cell surface and was thus insensitive to endo H cleavage. As regards endosomal distribution, HLA-E was more enriched in late endosomes and recycling endosomes than HLA-Ia (Fig.3.2.2D-H). Therefore, all the characters of HLA-E static distribution were recaptured in PMA-differentiated THP1 cells.

In conclusion, while most HLA-Ia molecules stay on the cell surface, most HLA-E molecules accumulate intracellularly, mostly in the ER. HLA-Ia and HLA-E can be found in all endosomal structures, but HLA-E molecules are more enriched in late endosomes and recycling endosomes.

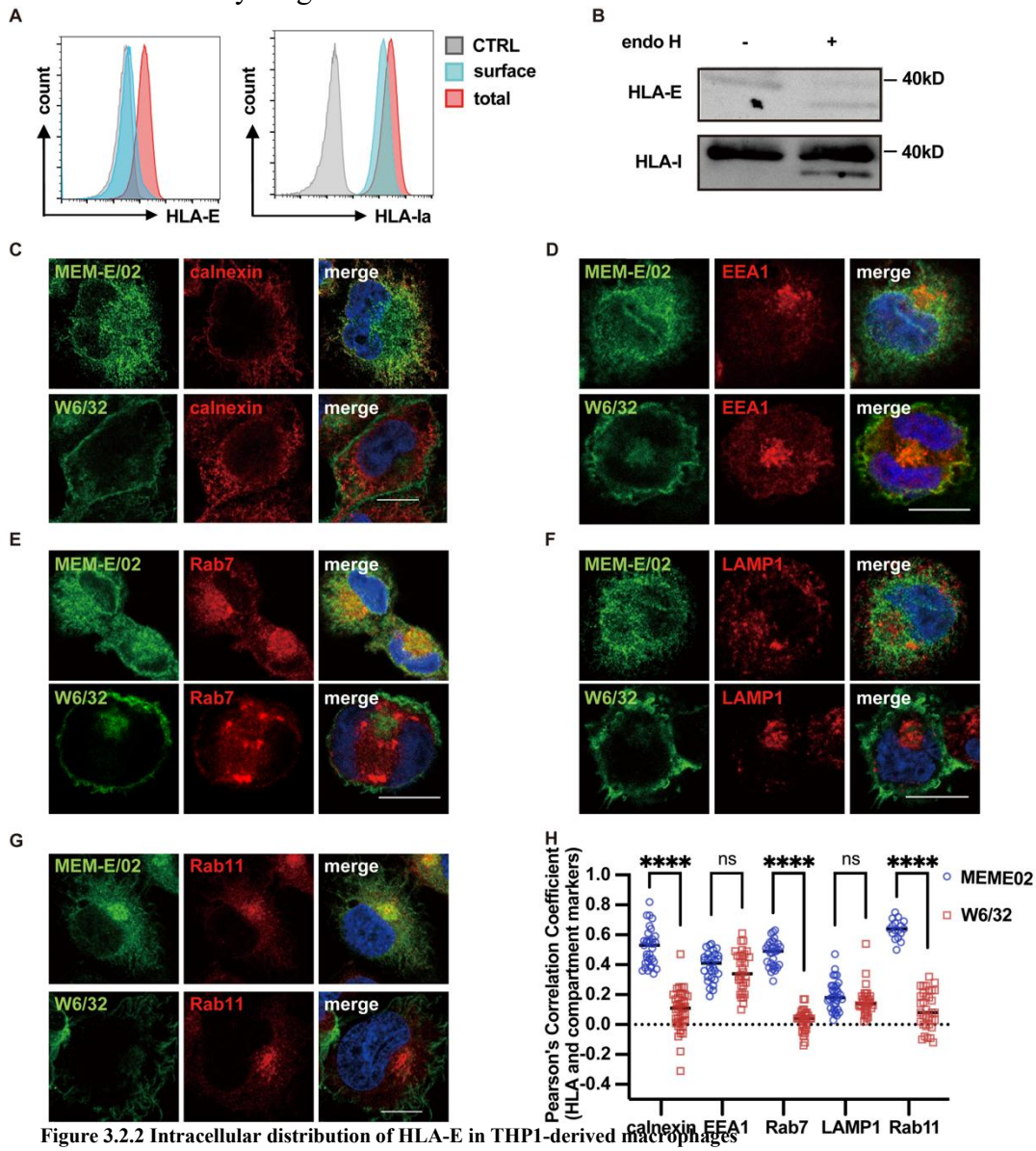

Figure 3.2.2 Intracellular distribution of HLA-E in THP1-derived macrophages

A. THP1-derived macrophages were collected for flow cytometry analysis. Expression of HLA molecules was assessed with either anti-HLA-E antibody (3D12) or anti-HLA-I antibody (W6/32). Representative graphs of total expression (red) and surface expression (blue) of HLA-E or HLA-Ia are shown. MFI of the unstained sample (grey) was used as the negative control. MFIs shown here are representative of observations made in six experiments.

B. Lysates of THP1-derived macrophages were treated with Endo H H for 2hrs at 37°C before western blot analysis, followed by detection with immunoblotting.

C, D, E, F, G. Representative micrographs of THP1-derived macrophages. Cells were fixed, permeabilized, and co-stained with rabbit antibodies against different marker proteins [ER (calnexin, C), early endosome (EEA1, D), late endosome (Rab7, E), lysosome (LAMP1, F), recycling endosome (Rab11, G)] and mouse antibodies against different HLA-I molecules [HLA-E (MEM-E/02), HLA-Ia (W6/32)]. Cells were then stained with anti-Rabbit Alexa568 and anti-mouse Alexa488 secondary antibodies. Scale bars = 10 μm.

H. Quantification of co-localization of HLA-E or HLA-Ia with different marker proteins from FigS1.C-G. The PCC values of each cell and the mean values are shown with 30-40 cells per sample. Statistical analysis was performed using unpaired two-tailed student's t-test with Welch's correction. Asterisks show the statistical significance between indicated groups: ns, not significant; ****, $P < 0.0001$.

3.3 Dynamic transport of HLA-E

3.3.1 Development of the Retentions Using Selective Hook (RUSH) system to study HLA-E antegrade transport

As ER retention of HLA-E may be caused by a slow antegrade transport process, I first explored the antegrade transport of HLA-E. I applied the RUSH system, which can synchronise the release of proteins from the ER and is a useful tool to get an overview of the antegrade trafficking route of HLA-E in physiological conditions (Boncompain et al. 2012) (Fig.3.3.1). The system is made up of a hook and a reporter. The hook consists of an ER-resident protein fused to streptavidin (str) and a reporter that contains the target protein with streptavidin binding protein (SBP) and EGFP fused to its cytoplasmic tail. When the two parts are co-expressed, the reporter protein can be trapped in the ER. Biotin addition disrupts the interaction between str and SBP and leads to the simultaneous release of the reporter protein from the ER.

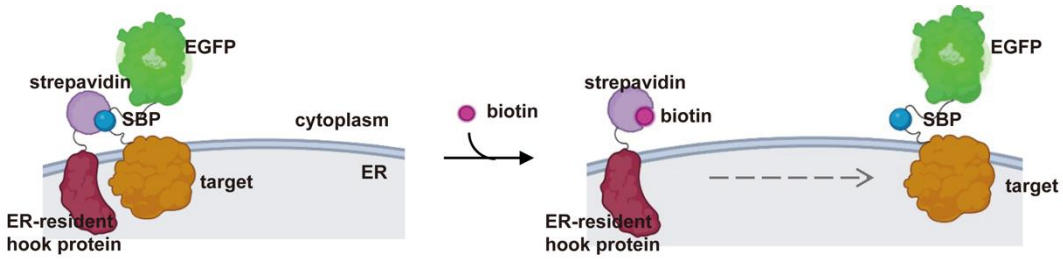

Figure 3.3.1 Schematic diagram of the RUSH system
The reporter complex contains the target protein (HLA-E or HLA-A3) with SBP and EGFP fused to the C terminus. The hook contains str fused to the N-terminus of the ER-resident protein, which retains the reporter complex in the ER through the interaction between SBP and str. Biotin binds to str and enables the trafficking of the target protein out of the ER. The figure was adapted from (Boncompain et al., 2012) and created with BioRender.com.

3.3.1.1 Testing of the initial HLA-E RUSH system

The initial HLA-E RUSH plasmid with CD74 as the hook was constructed previously by Simon Brackenridge in our group by replacing the CD44 coding sequence in the original RUSH plasmid pIRESneo3 Str-Ii+CD44-SBP-EGFP with HLA-E (CD74 is also known as the invariant chain (Ii)). I further constructed an HLA-A3 RUSH plasmid as the control following the same method.

The effectiveness of this initial RUSH system was first validated via surface staining. There was no detectable surface HLA-E signal in 293T cells transfected with the HLA-E RUSH plasmid without biotin addition (Fig.3.3.2A), indicating that all HLA-E was nicely trapped in ER. Surface HLA-E could be detected after biotin addition (Fig.3.3.2A, B), implying that HLA-E was successfully released from the ER. Similar results were observed for the HLA-A3 RUSH plasmid, though the system was slightly leaky, as a small amount of HLA-A3 could be detected on the cell surface even before biotin addition (Fig.3.3.2C, D). As most HLA-A3 got out of the ER quickly after synthesis, it is possible that some HLA-A3 escaped ER retention by trafficking quickly out of the ER after synthesis or that the hook expression level was too low to trap HLA-A3 effectively in the early stages after transfection. In

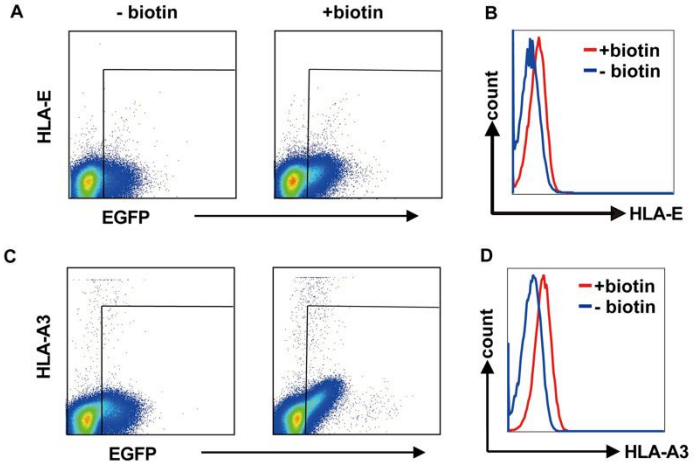

Figure 3.3.2 The original RUSH system works for HLA-E and HLA-A3
HEK 293T cells were transiently transfected with the original RUSH plasmids co-expressing the CD74 hook and HLA-E_SBP_EGFP (A, B) or HLA-A3_SBP_EGFP (C, D). +biotin samples were incubated with biotin (final 50μM) overnight for complete biotin release. 24hrs after transfection, cells were collected for flow cytometry analysis (gated on GFP+ cells), and surface expression of HLA molecules was assessed with either anti-HLA-E antibody (3D12) or anti-HLA-A3 antibody (GAP.A3). Dotplots and histograms shown here are representative of observations made in three independent experiments.

conclusion, the initial RUSH system works.

3.3.1.2 Separation of the hook from the reporter

As the EGFP expression level was low in the initial RUSH system (Fig.3.3.2), the gating of transfected cells was challenging. To explore whether this was due to the misfolding of EGFP in the fusion protein, I constructed plasmids expressing the HLA-E reporter fusion protein (HLA-E_SBP_EGFP) or with EGFP directly fused to HLA-E (HLA-E_EGFP) (Fig.3.3.3A). EGFP expression level was similar in 293T

cells transfected with these two constructs and was higher than that in the original RUSH plasmid (Fig.3.3.3B, Fig.3.3.2A). Therefore, protein fusion did not seem to affect the folding of EGFP and was thus not the main reason for the low signal of EGFP in the RUSH plasmid. As a low EGFP level was also seen in the HLA-A3 RUSH construct (Fig.3.3.2C), this problem could be due to the bicistronic plasmid design. It seems likely that the expression level of the reporter proteins in the original design was made very low artificially compared to the hook protein to ensure efficient ER retention.

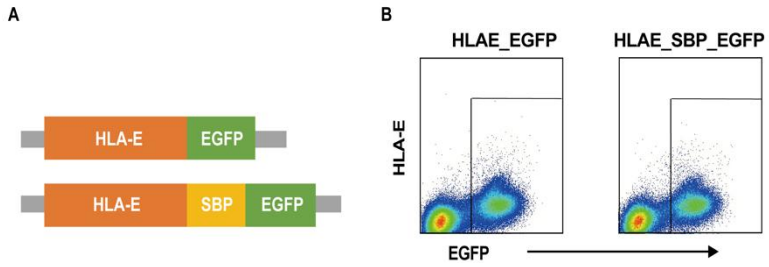

Figure 3.3.3 Protein fusion does not affect EGFP folding
A. Schematic diagram of the constructs HLA-E_EGFP and HLA-E_SBP_EGFP.
B. HEK 293T cells were transiently transfected with HLA-E_EGFP or HLA-E_SBP_EGFP. Cells were incubated with biotin (final 50µM) overnight for complete biotin release. 24hrs after transfection, cells were collected for flow cytometry analysis (gated on GFP+ cells), and surface expression of HLA-E molecules was assessed with the anti-HLA-E antibody 3D12. Dotplots shown here are representative of observations made in three independent experiments.

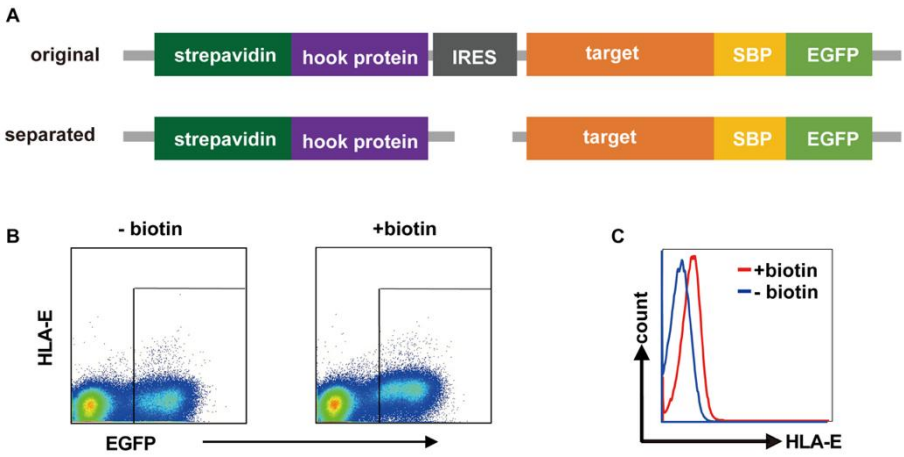

Figure 3.3.4 Separation of the hook and the reporter rescues EGFP expression
A. Schematic diagram comparing the design of the old RUSH system (original) and the new RUSH system (separated).
B, C. HEK 293T cells were transiently co-transfected with the CD74 hook and HLA-E_SBP_EGFP. +biotin sample was incubated with biotin (final 50µM) overnight for complete biotin release. 24hrs after transfection, cells were collected for flow cytometry analysis (gated on GFP+ cells), and surface expression of HLA-E molecules was assessed with the anti-HLA-E antibody 3D12. Dotplots and histogram shown here are representative of observations made in three independent experiments.

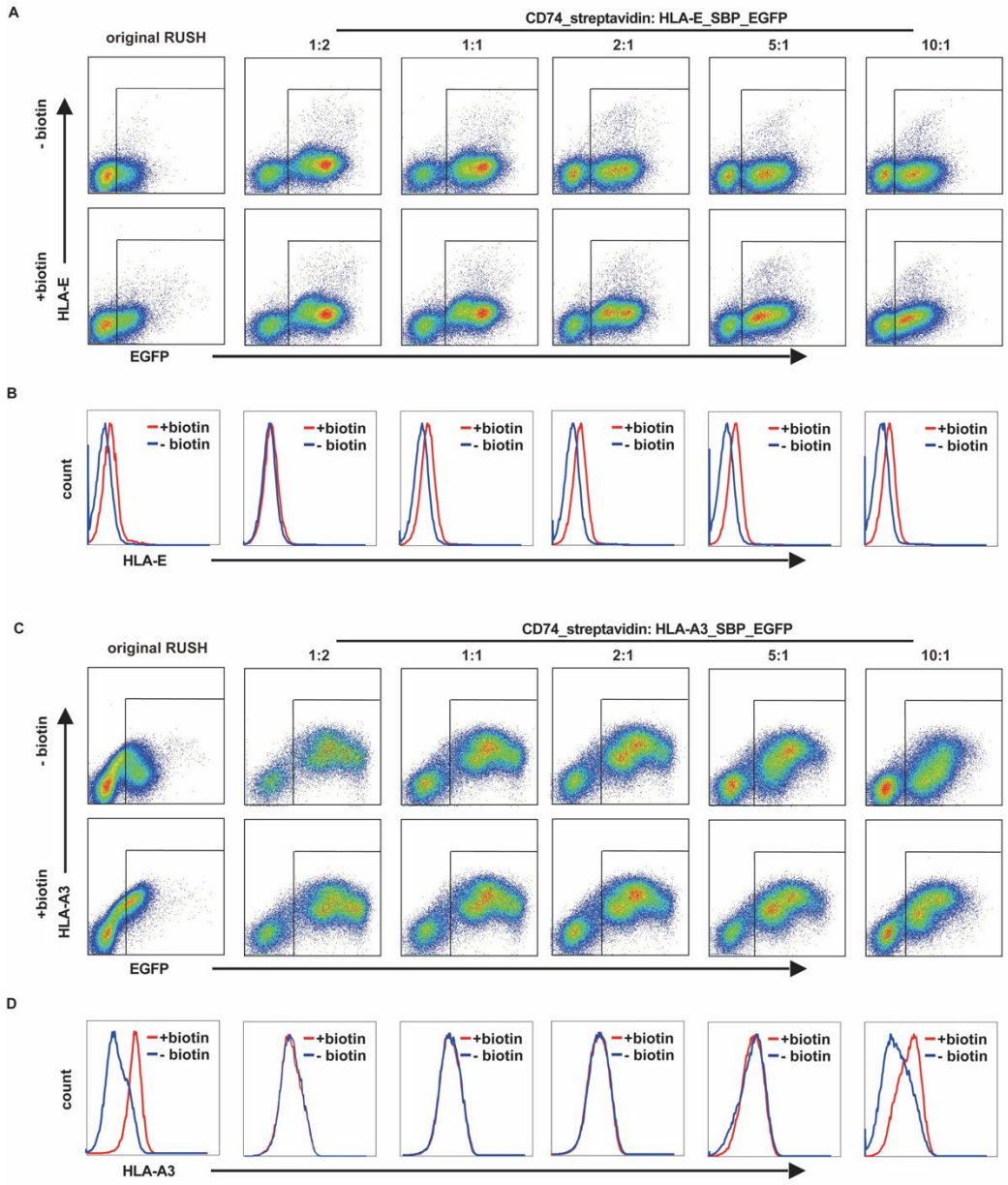

Figure 3.3.5 Test the efficiency of the RUSH system at different hook:reporter ratios
HEK 293T cells were transiently co-transfected with the CD74 hook and HLA-E_SBP_EGFP (A, B) or HLA-A3_SBP_EGFP (C, D) at different ratios. 1μg total plasmids were used for each transfection per well in a 6-well plate. +biotin samples were incubated with biotin (final 50μM) overnight for complete biotin release. The original RUSH plasmids were included as controls. 24hrs after transfection, cells were collected for flow cytometry analysis (gated on GFP+ cells), and surface expression of HLA molecules was assessed with either anti-HLA-E antibody (3D12) or anti-HLA-A3 antibody (GAP.A3). Dotplots and histograms shown here are representative of observations made in three independent experiments.

To better control the expression level of the hook and the reporter, I modified the RUSH system by separating the CD74 hook and the reporter into different plasmids (Fig.3.3.4A). When the hook plasmid and HLA-E reporter plasmid were co-transfected at a 1:1 ratio into HEK 293T cells, a satisfactory EGFP signal could be detected (Fig.3.3.4B). EGFP expression was rescued in this new RUSH system,

making the gating for cells transfected with the RUSH system much easier and more accurate. The new RUSH system was also effective, as HLA-E was still effectively trapped in the ER by the hook and was released after biotin addition (Fig.3.3.4B, C).

3.3.1.3 Optimisation of hook/reporter ratio for HLA-E and HLA-A3

Although the co-transfection of the hook plasmid and reporter plasmid at a 1:1 ratio worked for HLA-E, the system might be leaky for HLA-A3, as observed in the original RUSH system. While most HLA-A3 traffics out of the ER quickly after synthesis, most HLA-E tends to stay longer in the ER (Fig.3.2.1). Therefore, it might be easier for HLA-E to encounter the hook in the ER and get trapped there, and a higher hook: reporter ratio may be required to trap HLA-A3 in the ER efficiently.

To test this hypothesis, I co-transfected the CD74 hook plasmid and the HLA-E or HLA-A3 reporter plasmids at different ratios into HEK293T cells (Fig.3.3.5). The initial RUSH plasmids were used as control. The RUSH system worked well for HLA-E when the hook:reporter ratio was between 1:1 and 5:1 (Fig.3.3.5A, B). When the ratio was at 10:1, the system still worked, but the surface HLA-E level after biotin addition decreased, indicating that HLA-E was probably not released efficiently after biotin addition, which might be due to the oversupply of the hook protein. A decrease in the EGFP signal could be observed with the increase in the hook:reporter ratio, which supported our previous hypothesis that the expression level of the reporter protein in the original RUSH protein may be very low. When the hook:reporter ratio was 1:2, the system was very leaky, and the surface HLA-E level was similar with or without biotin addition. This is likely due to inefficient trapping, as the HLA-E expression level may be higher than that of the hook. Therefore, a 1:1 hook:reporter ratio is good for the HLA-E RUSH system.

In comparison, the RUSH system for HLA-A3 was very leaky when the hook:reporter ratio is between 1:2 to 5:1 (Fig.3.3.5C, D), and no apparent difference in HLA-A3

surface expression was observed with or without biotin addition under these conditions. When the hook: reporter ratio was 10:1, the trapping was effective as a higher HLA-A3 level could be seen after biotin addition, though the system was still leaky. This suggests that HLA-A3 requires a higher level of hook for effective ER trapping compared to HLA-E.

3.3.1.4 Sequential transfection does not work well for the RUSH system

Further increase of the hook:reporter ratio might not completely prevent the leakiness of the HLA-A3 RUSH system. As most HLA-A3 is transported out of the ER quickly after synthesis, some early synthesised HLA-A3 may escape the hook trapping when the hook level is low in the early stages after the co-transfection. Besides, a further increase of the hook:reporter ratio adds difficulty to accurate co-transfection and EGFP gating. Sequential transfection might solve the problem, as the hook could be allowed to express and accumulate in the ER before the introduction of the reporter proteins. Therefore, I transfected the hook plasmid firstly into HEK 293T cells before a second round of transfection of the HLA-A3_SBP_EGFP reporter plasmid 24hrs later. However, the RUSH system for HLA-A3 became even leakier in sequential transfection (Fig.3.3.6A, B), as even a hook:reporter ratio of 10:1 could not effectively trap HLA-A3 in the ER.

A possible explanation is that a hook:reporter ratio of 10:1 was not achieved as expected in many cells during the sequential transfection. There were probably not enough hooks for ER trapping in many cells transfected with HLA-A3. To examine this hypothesis, I did intracellular staining for HEK293T cells co-transfected with the CD74_hook and HLA-A3-SBP-EGFP at a ratio of 10:1 either simultaneously (co-transfection) or in a sequential manner (sequential transfection) (Fig.3.3.6C). During the sequential transfection, getting the CD74_hook plasmid in the first round did not seem to affect the chances of cells getting the HLA-A3-SBP-EGFP plasmid in

the second round. Therefore, about 50% of cells transfected with HLA-A3 did not contain the hook plasmid. In comparison, when the hook and the reporter plasmids

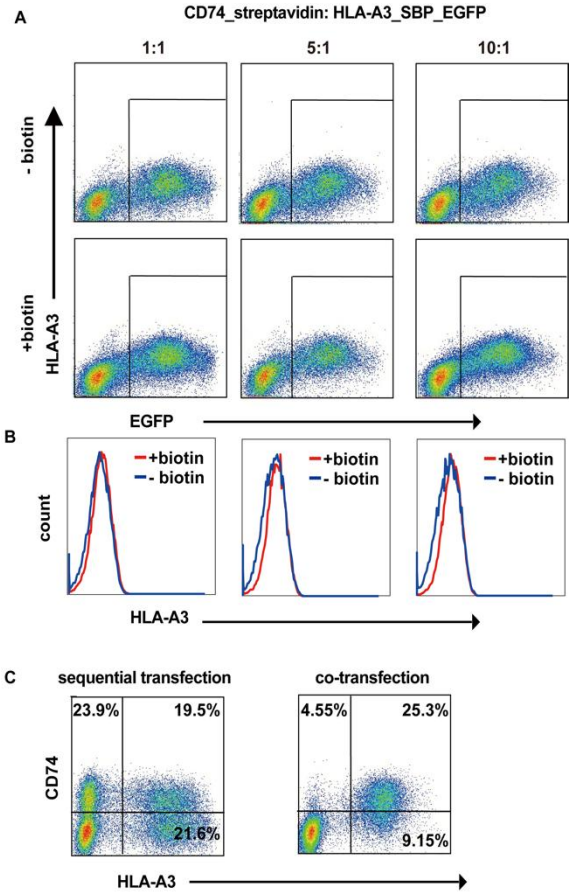

Figure 3.3.6 Sequential transfection does not work well for the RUSH system
A, B. HEK 293T cells were firstly transfected with the CD74 hook, and then transfected with HLA-A3_SBP_EGFP 24hrs later. 1μg total plasmid amount was used per well in a 6-well plate. +biotin samples were incubated with biotin (final 50μM) overnight for complete biotin release. 24hrs after the transfection of the second plasmid, cells were collected for flow cytometry analysis (gated on GFP+ cells), and surface expression of HLA-A3 molecules was assessed with the anti-HLA-A3 antibody GAP.A3. Dotplots and histograms shown here are representative of observations made in three independent experiments.
C. HEK 293T cells were either firstly transfected with the CD74 hook, and then transfected with HLA-A3_SBP_EGFP 24hrs later (sequential transfection, left), or co-transfected with the CD74 hook and HLA-A3_SBP_EGFP simultaneously (co-transfection, right). 24hrs after the last transfection, cells were collected for flow cytometry analysis, and intracellular expression of CD74 was assessed with the anti-CD74 antibody LN2. Dotplots shown here are representative of observations made in three

were co-transfected, a strong tendency of co-expression was observed, as the cells either got no plasmids or both plasmids. Therefore, sequential transfection is not a good option.

3.3.1.5 Stable hook expression does not improve the RUSH system

To get around the problem in the sequential transfection, I used the lentiviral system to construct a HeLa cell line stably expressing the CD74 hook. In this way, all the cells have the hook expressed in them before further introduction of the reporter proteins. Reporter plasmids were then transduced via the lentiviral system, and reporter proteins were allowed to express for two days. Transient transfection was not used to express the reporter proteins to avoid overexpression. To reduce the possibility of leakiness, a Multiplicity of Infection (MOI) of 3 and 0.3 were used for the hook and reporter during transduction, respectively.

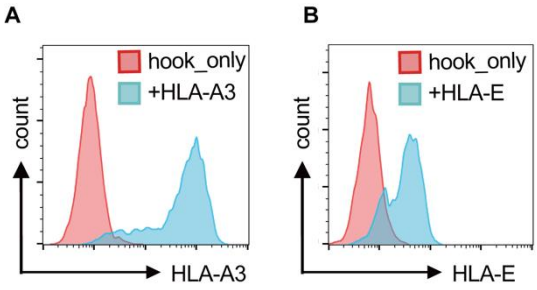

Figure 3.3.7 Stable hook expression does not improve the RUSH system
HeLa cells stably expressing the CD74 hook were transduced with the reporter protein HLA-A3_SBP_EGFP (A) or HLA-E_SBP_EGFP (B) (blue) using the lentiviral system. 2 days after the transduction of the reporter protein, cells were collected for flow cytometry analysis to test the efficiency of ER trapping (gated on GFP+ cells). Surface expression of HLA molecules was assessed with either anti-HLA-E antibody (3D12) or anti-HLA-A3 antibody (GAP.A3), and HeLa cells only expressing the CD74 hook was used as the negative control. Histograms shown here are representative of observations made in three independent experiments.

However, this system turned out to be very leaky, as a lot of HLA-A3 and HLA-E could be found on the cell surface even without biotin addition (Fig.3.3.7). Two peaks were present on the histogram for HLA-E, where the small peak on the left overlapped with the peak of the sample without reporter expression (Fig.3.3.7B). This indicates that only a small amount of HLA-E was trapped in the ER. For HLA-A3, there was only one peak with an elongated tail on the left side (Fig.3.3.7A). This implies that the hook expression did decrease the HLA-A3 surface expression in some cells, but the whole system was very leaky and was far from complete ER trapping. The improper hook:reporter ratios in these cells are the most likely explanation, as it's hard to overexpress the CD74 hook extensively in a stable cell line constructed via the lentiviral system, unlike in transient transfection. Therefore, the hook:reporter ratio might not be even high enough to effectively trap HLA-E in the ER, let alone HLA-A3.

3.3.1.6 Design a new sec61B hook for the RUSH system

Although CD74 was widely used in the RUSH system as the hook protein (Boncompain et al. 2012), it is previously reported to associate with and modify the trafficking of MHC class I molecules (Basha et al. 2012; Reber et al. 2002; Sugita and Brenner 1995; Vigna et al. 1996), and therefore may potentially affect HLA-E trafficking. Therefore, it would be worth testing another ER hook. In my system, the ER hook needs to be a transmembrane protein with a short sequence on the

cytoplasmic side. In this way, the str fused to the hook can interact with the SBP fused to the cytoplasmic tail of HLA proteins on the ER cytoplasmic side. Unfortunately,

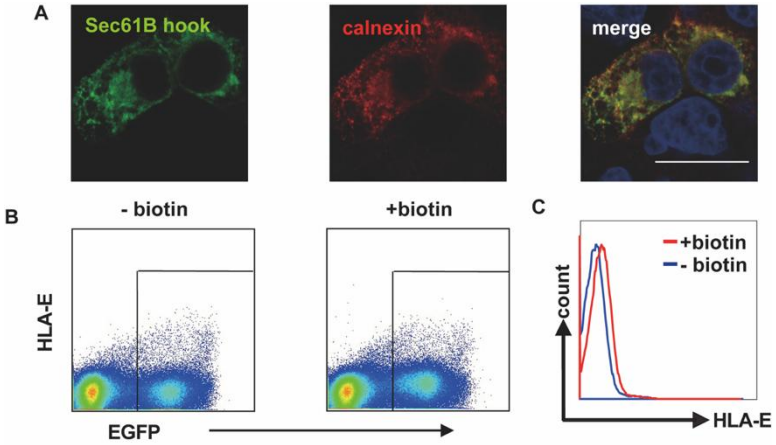

Figure 3.3.8 sec61B hook could be nicely trapped in the ER
A. Representative micrograph of HeLa cells transiently expressing the hook sec61B_str. Cells were fixed, permeabilised, and stained with a mouse antibody against str and a rabbit antibody against the ER marker protein calnexin, followed by detection with anti-mouse Alexa488 and anti-Rabbit Alexa568 secondary antibodies. Scale bar = 20 µm. Micrographs shown here are representative of two independent experiments.
B, C. HEK 293T cells were transiently co-transfected with the sec61B hook and HLA-E_SBP_EGFP at a 1:1 ratio. +biotin sample was incubated with biotin (final 50µM) overnight for complete biotin release. 24hrs after transfection, cells were collected for flow cytometry analysis (gated on GFP+ cells), and surface expression of HLA-E molecules was assessed with the anti-HLA-E antibody 3D12. Dotplots and histogram shown here are representative of observations made in three independent experiments.

other published ER hooks, like the KDEL or STIM1-NN hook (Boncompain et al. 2012), are not suitable for our study.

Therefore, I designed a new RUSH hook plasmid with str fused to the C-terminus of sec61B. Although not previously used for the RUSH system, sec61B is a type II single-pass ER transmembrane protein with a well-known topology, with the N-terminal fusion keeping target proteins on the ER luminal side (Lee et al. 2016). Confocal imaging was then applied to confirm the intracellular localisation of the sec61B hook. The perfect co-localisation with the ER marker calnexin validated that the sec61B hooks all stayed in the ER (Fig.3.3.8A). I then tested the potency in ER trapping for this new sec61B hook. Similar to the CD74 hook, the sec61B hook could also effectively trap HLA-E in the ER when the hook and reporter plasmids were co-expressed at a 1:1 ratio, and surface HLA-E could also be detected after biotin addition (Fig.3.3.8B, C). Therefore, sec61B could be a suitable alternative hook to use in our studies.

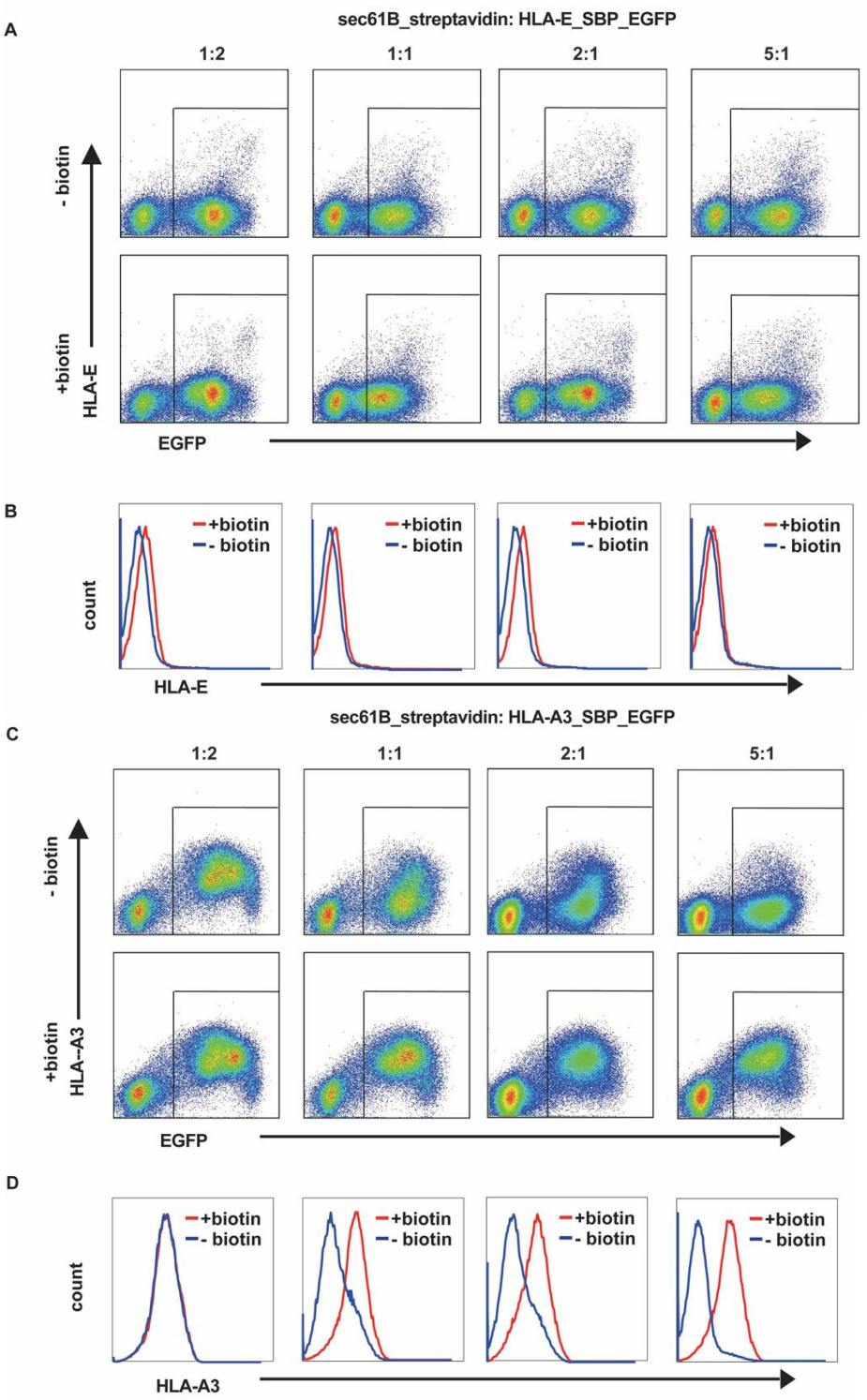

Figure 3.3.9 Optimise the hook:reporter ratios for HLA-E and HLA-A3 using sec61B as the hook
HEK 293T cells were transiently co-transfected with the sec61B hook and HLA-E_SBP_EGFP (A, B) or HLA-A3_SBP_EGFP (C, D) at different ratios. 1μg total plasmids were used for each transfection per well in a 6-well plate. +biotin samples were incubated with biotin (final 50μM) overnight for complete biotin release. 24h after transfection, cells were collected for flow cytometry analysis (gated on GFP+ cells), and surface expression of HLA molecules was assessed with either anti-HLA-E antibody (3D12) or anti-HLA-A3 antibody (GAP.A3). Dotplots and histograms shown here are representative of observations made in three independent experiments.

When the hook:reporter ratio was 1:1, the surface HLA-E level was lower after biotin

addition for the sec61B hook compared to the CD74 hook (Fig.3.3.4B, C). This suggests that sec61B might be a more potent hook, and the current hook:reporter ratio might not be optimal. To test this hypothesis, I co-transfected the sec61B hook plasmid and the HLA-E or HLA-A3 reporter plasmids at different ratios into HEK293T cells. For HLA-E, inefficient ER release after biotin addition was obvious when the hook:reporter ratio reached 5:1 (Fig.3.3.9A, B). Effective ER trapping could be observed even when the hook:reporter ratio is 1:2. For HLA-A3, the RUSH system worked even when the hook:reporter ratio is 1:1 (Fig.3.3.8C, D), though leaky. When the hook:reporter ratio reached 5:1, the ER trapping was very efficient, and the system was no longer leaky. These data indicate that sec61B is a more efficient hook compared to CD74 and is, therefore, a better hook for our studies.

Our data also imply that the hook:reporter ratio in the RUSH system should be optimised not only for different reporter proteins but also for different hooks, as different ER resident proteins may vary in their potency in ER trapping. A RUSH system with the hook and the reporter in separate plasmids is thus much more flexible than the original design.

3.3.1.7 Optimise the suitable biotin concentration

As most HLA-E stayed in the ER for a long time even after biotin addition, it may get trapped by the hook again after biotin release if there was no sufficient biotin.

Incomplete biotin release may make the weak HLA-E surface signal even harder to detect. Therefore, before using the RUSH system to explore HLA-E antegrade transport, it is crucial to ensure that HLA-E can be completely released after biotin addition. To test if the current biotin concentration is enough for efficient ER release, I compared the surface HLA-E level after overnight incubation with biotin of different concentrations. The increase of biotin final concentration from 50μM to 500μM did not lead to any detectable increase of surface HLA-E level (Fig.3.3.10A), indicating

that the biotin concentration was not a limitation for HLA-E surface signal detection and that the original 50μM biotin concentration should be sufficient. Besides, after overnight biotin release, the surface HLA-E level of cells transfected with the RUSH system was similar to that of cells transfected with HLA-E_SBP_EGFP alone (Fig.3.3.10B). These results confirmed that the RUSH system could completely release HLA-E after biotin addition.

To conclude, I have optimised the original RUSH system via a combination of various strategies, including separation of the hook from the reporter, design of a new hook, comparison of different transfection methods, optimisation of the hook: reporter ratio, and biotin concentration.

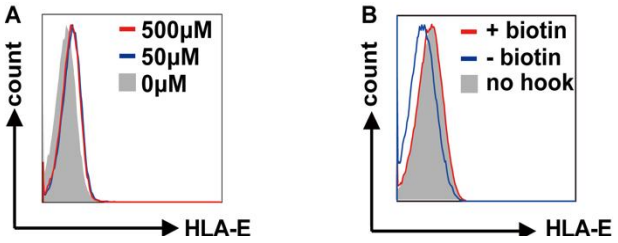

Figure 3.3.10 Confirmation of complete HLA-E release of the RUSH system after biotin addition
A. HEK 293T cells were transiently co-transfected with sec61B-str and HLA-E_SBP_EGFP. Samples were incubated with biotin at different concentrations overnight. 24hrs after transfection, cells were collected for flow cytometry analysis (gated on GFP+ cells), and surface expression of HLA-E molecules was assessed with the anti-HLA-E antibody 3D12. MFIs shown here are representative of observations made in three experiments.
B. HEK 293T cells were transiently transfected with HLA-E_SBP_EGFP (gray area) or co-transfected with sec61B-str and HLA-E_SBP_EGFP (lines). +biotin sample (red line) were incubated with biotin (final 50μM) overnight. 24hrs after transfection, cells were collected for flow cytometry analysis (gated on GFP+ cells), and surface expression of HLA-E molecules was assessed with the anti-HLA-E antibody 3D12. MFIs shown here are representative of observations made in three experiments.

3.3.2 The antegrade transport of HLA-E

3.3.2.1 Explore the antegrade transport process in HeLa cells using the RUSH system

A 1:1 and 5:1 hook:reporter ratios were used for the RUSH system of HLA-E and HLA-A3 using sec61B as the hook protein in the following studies. After the co-transfection of the hook and reporter plasmids, both HLA-E and HLA-A3 were nicely trapped in the ER, as the EGFP signal resembled the typical tubular ER structure (Fig.3.3.11A, B). Through confocal microscopy, I then tracked the

intracellular distribution of HLA-E and HLA-A3 at different time points after synchronous release from the ER via biotin addition. Both HLA-E and HLA-A3 could get out of the ER quickly after biotin addition, as strong signals of both were detected in the Golgi compartment within 5 minutes (mins) upon biotin release. While most HLA-A3 trafficked out of the ER after biotin addition, only a small fraction of HLA-E managed to do so. Both HLA-E and HLA-A3 continued to accumulate in the Golgi from 10 mins to 30 mins upon biotin release, as indicated by the increase of co-localisation with the Golgi marker protein GM130. Golgi accumulation started to decrease one hour after ER release for both HLA-E and HLA-A3, though the enrichment was still significant. After overnight biotin release, the intracellular distribution of HLA-E and HLA-A3 reached a steady state, and they were no longer enriched in the Golgi.

To describe the transport process more accurately and statistically, I calculated the PCC values to analyse the co-localisation of GM130 with HLA-E or HLA-A3 (Fig.3.3.11C, D). A significant rise in PCC values implies that both HLA-E and HLA-A3 were enriched in Golgi as early as 5 mins after biotin release, as indicated in the confocal images. As most HLA-E was retained in the ER after biotin addition, the PCC value of HLA-E was lower than that of HLA-A3 at early time points. The PCC values of HLA-A3 plateaued 10 mins after ER release, though it continued to accumulate in the Golgi until 30 mins. The decrease of PCC value for HLA-A3 from 10 to 30 mins despite its continuous Golgi accumulation could be due to its surface accumulation, as indicated by the strong surface signal in confocal images (Fig.3.3.11B, D).

Given the continuous strong ER signal, the antegrade transport process of HLA-E was less clear compared to HLA-A3. Therefore, I further applied live-cell imaging to track HLA-E transport upon ER release (video). Similarly, I observed that HLA-E trafficked quickly out of the ER, and evident Golgi enrichment could be observed as

early as 5 mins after biotin addition. Golgi enrichment was pronounced for HLA-E and continued for 2hrs after biotin addition, though the peak signal came at around 30 mins upon biotin release. Therefore, while only a tiny amount of HLA-E exits the ER, the dynamics of its antegrade trafficking process resembles that of HLA-A3.

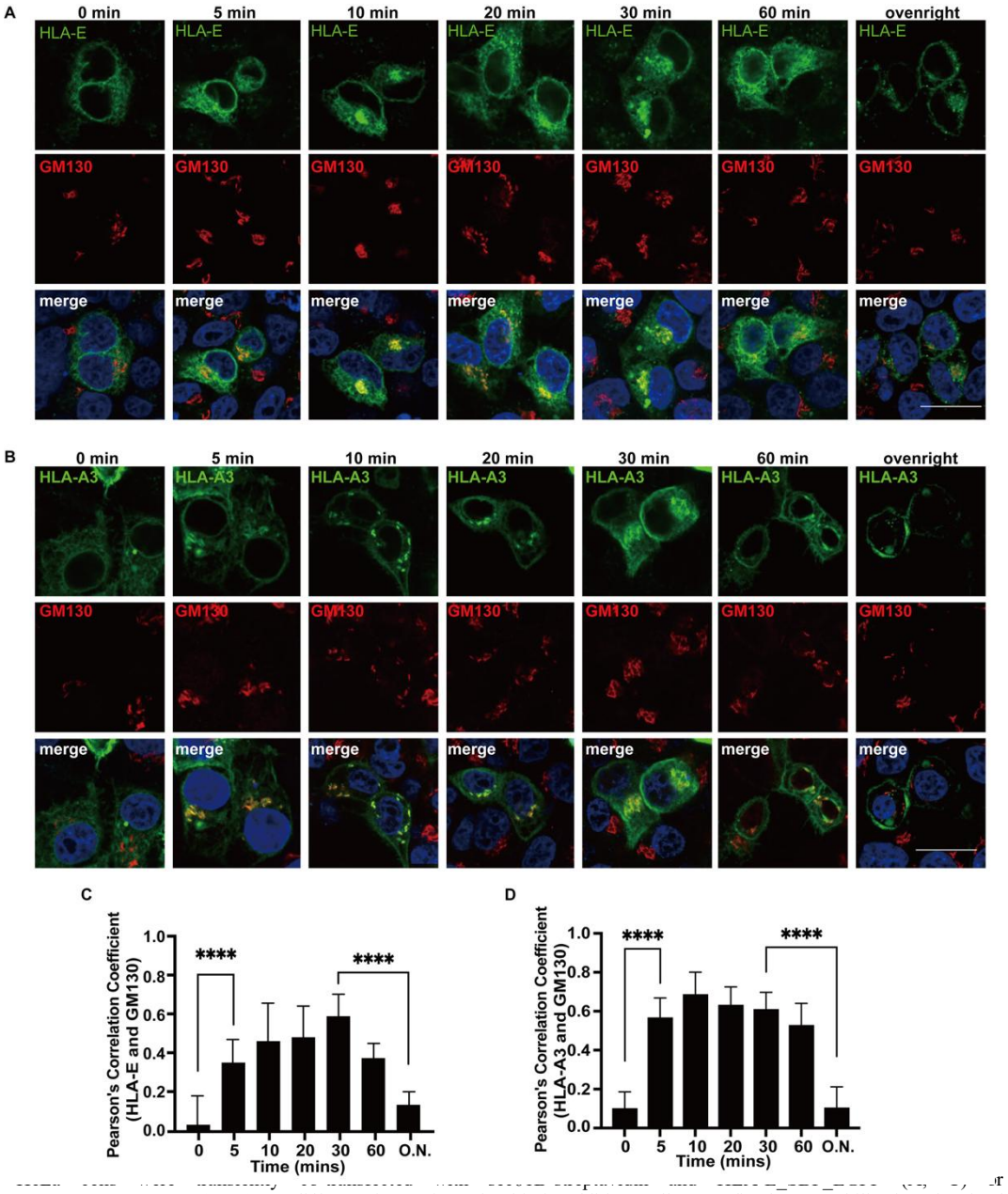

HLA-A3_SBP_EGFP (B, D). At different time points after biotin addition, cells were fixed, permeabilized, and stained with an antibody against the Golgi marker protein GM130, followed by detection with an Alexa568-conjugated secondary antibody. A, B, Representative micrographs of HeLa cells. Scale bars = 20 μm. C, D, Quantification of Golgi co-localization for HLA-E (C) or HLA-A3 (D). O.N. is short for overnight. At each time point, PCC value was calculated for 10-20 individual cells, and the data are shown as mean ± SD (error bars). Statistical analysis was performed using unpaired two-tailed student's t-test with Welch's correction. Asterisks show the statistical significance between indicated groups: ****, $P < 0.0001$.

As surface HLA-E was almost undetectable under the microscope, flow cytometry was used to examine the surface arrival of HLA-E and HLA-A3, which is more sensitive and quantitative compared to imaging. Both HLA-E and HLA-A3 could be

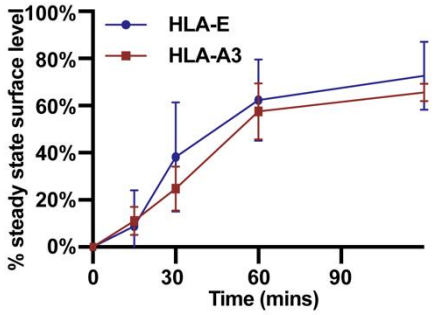

Figure 3.3.12 HLA-E and HLA-A3 traffic from the ER to the surface with similar velocity
HEK 293T cells were transiently co-transfected with Sec61B-streptavidin and HLA-E_SBP_EGFP (blue circle) or HLA-A3_SBP_EGFP (red square). At different time points after biotin addition, cells were collected for flow cytometry analysis. The stable cell surface MFI after the biotin addition overnight was set to 100%, the MFI before biotin addition was set to 0%, and the other values were normalised accordingly. Data were collected for three biological runs and are shown as mean ± SD

detected on the cell surface 15 mins after biotin addition, which is consistent with the fast antegrade transport observed (Fig.3.3.12). Surface HLA-E and HLA-A3 continued to accumulate quickly from 15 mins to 1h after biotin release at similar rates. These results further confirm the parallel antegrade trafficking dynamics of HLA-E and HLA-A3.

3.3.2.2 Explore the antegrade transport process in THP1-derived macrophages

To rule out the potential systematic bias of the RUSH system on HLA-E transport, I applied the acid stripping assay to further analyse the antegrade transport dynamics of

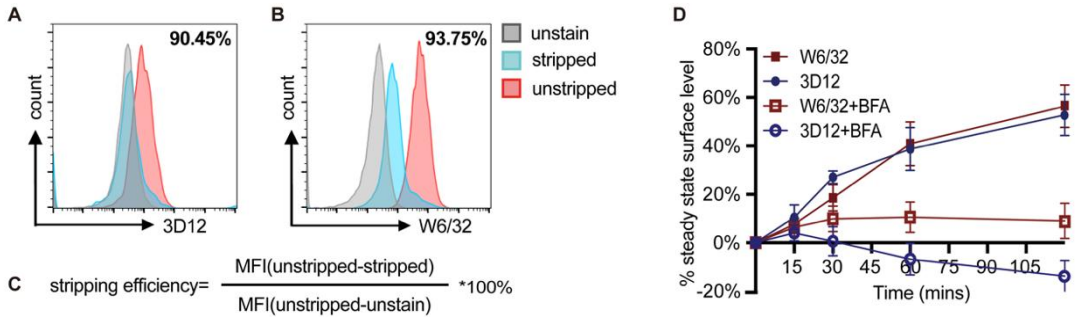

Figure 3.3.13 Antegrade transport of endogenous HLA-E and HLA-Ia are alike in THP1 cells
A, B. THP1-derived macrophages **with endogenous expression of HLA-Ia and HLA-E** were exposed to citric acid for 3mins to strip off surface proteins (blue). After neutralisation and washing, cells were collected for flow cytometry and surface level of HLA molecules was assessed with either anti-HLA-E antibody (3D12) or anti-HLA-I antibody (W6/32). Unstripped samples (red) and unstained samples (gray) were used as positive and negative controls respectively. MFIs shown here are representative of observations made in three experiments. The stripping efficiency is shown on the upper right corner of each histogram.
C. The formula for the calulcation of the stripping efficiency.
D. Surface HLA molecules on THP1-derived macrophages were stripped off by citric acid, and then cells were incubated in media with (hollow) or without (solid) BFA for different time points before flow cytometry analysis for surface MFI of HLA-E (3D12, blue) and HLA-Ia (W6/32, red). The average cell surface MFI for timepoint zero was set to 0%, the average cell surface MFI without acid stripping was set to 100%, and the following values were normalized as its percentage. Data were collected for three biological runs and are shown as mean ± SD (error bars).

endogenous HLA-E in THP1-derived macrophages. The efficiency of acid stripping was firstly tested (Fig.3.3.13A-C), and I found that a three-minute incubation with mild citric acid (pH=3) could effectively strip off the surface HLA-E and HLA-Ia in THP1 cells without affecting the cell viability. After acid stripping, cells were then washed and incubated in fresh media to allow for the recovery of surface proteins, and the surface expression levels of both HLA-E and HLA-Ia were measured at different time points. Similar to the results from previous RUSH assays, both HLA-E and HLA-Ia could be detected as quickly as 15 mins after acid stripping (Fig.3.3.13D). Surface recovery was very fast between 15 mins and 60 mins. A 60% recovery rate was achieved after one hour, which is consistent with the antegrade trafficking speed detected in the RUSH system. No noticeable difference in terms of surface recovery was observed between HLA-E and HLA-Ia.

Control groups with Brefeldin A (BFA) addition were included simultaneously to examine the contribution of the recycling pathway to the recovery of surface proteins (Fig.3.3.13D). BFA inhibits the transport of protein beyond the early secretory pathway, and no newly synthesised protein could arrive at the cell surface upon BFA addition. No surface recovery was detected when the antegrade transport was blocked via BFA addition, suggesting that the recycling pathway is at least not the major pathway contributing to the surface recovery of HLA-E and HLA-Ia. The surface MFI of HLA-E dropped even below the initial level during BFA incubation, which could be due to the internalisation of the minor fraction of surface HLA-E that was not stripped off completely by the acid. A slight and quick surface recovery was observed for HLA-Ia after BFA incubation. This is possibly because some HLA-Ia has trafficked beyond the early secretory pathway but has not yet arrived at the cell surface at the moment of acid stripping. This is further confirmed by the result that no further surface recovery was seen after 30 mins. In conclusion, antegrade transport is

the primary source of surface protein for both HLA-E and HLA-Ia, and their trafficking dynamics are similar.

Thus, HLA-E traffics quickly to the cell surface upon ER release, a process comparable to that of HLA-A3. ER retention, but not the slow antegrade transport, contributes to the low surface expression of HLA-E.

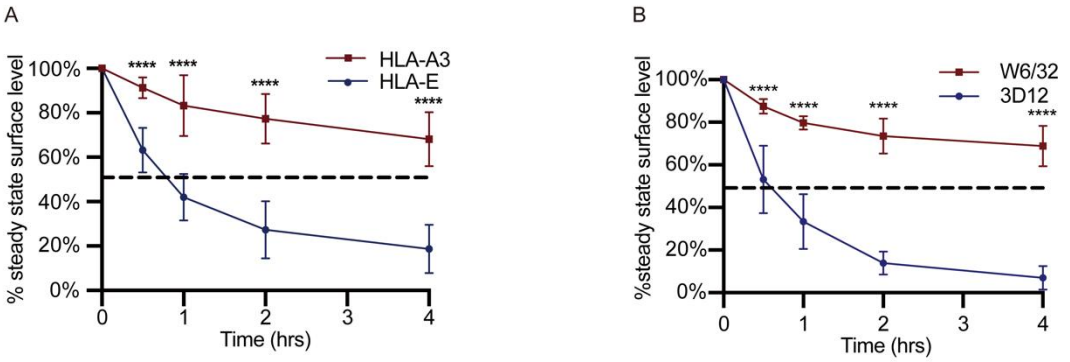

Figure 3.3.14 HLA-E is unstable on the cell surface
HeLa cells stably expressing HLA-A3 (red square) or HLA-E (blue circle) (A) or THP1-derived macrophages **with endogenous expression of HLA-Ia and HLA-E** (B) were incubated in media containing BFA for different time points before flow cytometry analysis for surface MFI of HLA-E (3D12), HLA-A3 (GAP.A3) or HLA-Ia (W6/32). The average cell surface MFI for timepoint zero was set to 100% and the following values were normalised as its percentage. The dashed lines represent 50%. Data were collected for three biological runs and are shown as mean ± SD (error bars). Statistical analysis was performed using unpaired two-tailed student's t-test with Welch's correction. Asterisks show the statistical significance between indicated groups: ****, $P < 0.0001$.

3.3.3 Turnover of surface HLA-E

3.3.3.1 Surface HLA-E is unstable

Apart from ER retention, fast surface turnover might also contribute to the low surface level of HLA-E. In the RUSH assay, Golgi enrichment declined for HLA-E after around one hour upon biotin addition, indicating that most of the HLA-E released from the ER has trafficked beyond the Golgi (Fig.3.3.11A, C, video). HLA-E appeared around one hour after ER release and accumulated quickly in endosomal structures (video). While some HLA-E in endosomes could directly come from the Golgi, the majority of the endosomal HLA-E seemed to come from the surface HLA-E that was quickly internalised upon surface arrival, as HLA-E accumulated in endosomes following surface accumulation. Besides, HLA-E moved quickly through

these endosomal structures (video), implying that HLA-E might undergo quick turnover and recycling. This is consistent with our previous data that HLA-E was enriched in late endosomes and recycling endosomes.

BFA decay assay was then applied to analyse the surface stability of HLA-E (Fig.3.3.14). BFA inhibits the surface arrival of newly synthesised proteins, which is the main source of surface protein for HLA-I molecules. Therefore, the surface lifetime of HLA-I proteins could be measured easily through surface staining. In Hela stable cell lines, surface HLA-E disappeared quickly upon BFA addition, and only around 40% remained on the cell surface after one hour (Fig.3.3.14A). HLA-A3 was much more stable, with over 60% remaining on the cell surface even after 4hrs. Therefore, the surface stability of HLA-A3 is higher than that of HLA-E.

The surface instability of endogenous HLA-E was also explored in THP1-derived macrophages (Fig.3.3.14B). Similarly, about half of the surface HLA-E disappeared from the surface within 30 mins, while around 70% of surface HLA-Ia remained at the cell surface after 4hrs. Thus, surface HLA-E is very unstable compared to HLA-Ia molecules.

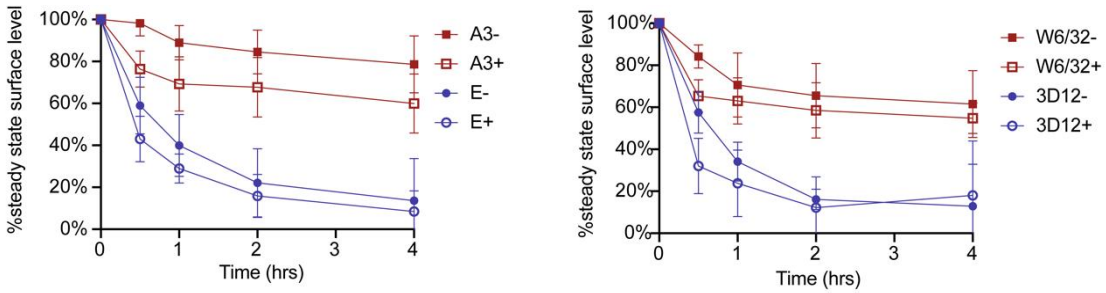

Figure 3.3.15 Recycling contributes to a small fraction of surface HLA molecules
HeLa cells stably expressing HLA-E_EGFP (blue circle) or HLA-A3_EGFP (red square) (A) or THP1-derived macrophages **with endogenous expression of HLA-Ia and HLA-E** (B) were incubated in media containing BFA with (solid) or without (hollow) primaquine before flow cytometry analysis for surface MFI of HLA-E (3D12), HLA-A3 (GAP.A3) or HLA-Ia (W6/32). The average cell surface MFI for timepoint zero was set to 100% and the following values were normalised as its percentage. Data were collected for four biological runs and are shown as mean ± SD (error bars).

3.3.3.2 Most internalised HLA-E is not recycled back to the cell surface

As surface stability is influenced by both internalisation and recycling, I further explored how the addition of primaquine (PQ), a drug that inhibits the recycling process, affected the surface stability of HLA-E (Fig.3.3.15). In HeLa cells, both HLA-E and HLA-A3 became less stable upon PQ addition (Fig.3.3.15A), implying that a small amount of HLA-E and HLA-A3 could be recycled back to the cell surface. While an obvious effect of PQ on the surface stability of HLA-A3 could be observed over time, the impact on HLA-E was not apparent at later time points, indicating that most HLA-E was not recycled back to the cell surface. A similar trend was observed in THP1-derived macrophages (Fig.3.3.15B), which further supported the conclusion that the recycling pathway makes a small contribution to the surface expression of HLA molecules. These results agree with the acid stripping assay in THP1-derived macrophages (Fig.3.1.13D), which reconfirms the antegrade transport pathway as the major source of surface HLA molecules.

3.3.3.3 Surface HLA-E is quickly internalised

Surface HLA-E seemed to get internalised more quickly than HLA-A3, as the disappearance of surface HLA-E signal was still much faster when both the antegrade trafficking pathway and the recycling pathway were inhibited (Fig.3.3.15A). Therefore, I measured the internalisation rate of HLA-E and HLA-A3 via an acid stripping method, which is similar to what has been described in section 3.3.2.2. The surface proteins are first labelled with specific antibodies, and the protein-Ab complexes are allowed for internalisation for different time lengths before acid stripping. The internalised protein-Ab complexes are protected from stripping, while the uninternalised ones are stripped off. The level of Ab signal after acid stripping enables a quantitative measurement of the internalisation rate of the target protein.

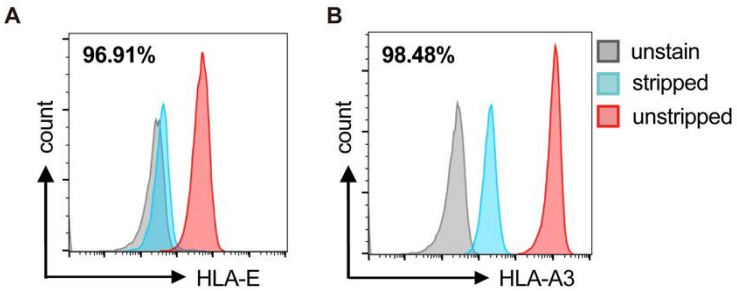

Figure 3.3.16 Measurement of acid stripping efficiency in HeLa cells
HeLa.E or HeLa.A3 cells were exposed to citric acid for 3mins to strip off surface proteins (blue). After neutralisation and washing, cells were collected for flow cytometry and surface level of HLA molecules was assessed with either anti-HLA-E antibody (3D12, A) or HLA-A3 (GAP.A3, B). Unstripped samples (red) and unstained samples (gray) were used as positive and negative controls respectively. MFIs shown here are representative of observations made in three experiments. The stripping efficiency was calculated as shown in Fig.3.3.13(C) and is shown on the upper left corner of each histogram.

The efficiency of acid stripping was first tested as described in section 3.3.2.2 (Fig.3.3.16). A three-minute incubation with mild citric acid (pH=3) could effectively strip off the surface HLA-E and HLA-A3 in HeLa cells without affecting the cell viability. Prolongation of incubation of cells with citric acid did not seem to further increase the stripping efficiency but decreased the viability of cells. Therefore, a three-minute acid incubation is an optimal condition for HeLa cells. The internalisation rates of HLA-E and HLA-A3 were then measured in HeLa cells, and a faster internalisation rate was observed for HLA-E (Fig.3.3.17A, B). While approximately 30% of HLA-E was internalised after one hour, only about 5% of HLA-A3 was internalised in the same time frame. The fast recycling of HLA-A3 could be ruled out, as PQ was added to the media during recovery, which inhibits the recycling process.

The acid stripping assay was then repeated in THP1-derived macrophages, and a similar trend was detected (Fig.3.3.17C, D). While over 15% of HLA-E was internalised in one hour, only 5% of HLA-Ia was internalised in the same time frame. The internalisation rate for HLA-E is slightly lower in THP1 cells than in HeLa cells. A possible explanation is that the overexpression of HLA-E in HeLa cells may aggravate the deficiency of high-affinity HLA-E-binding peptides, thus decreasing the

overall HLA-E surface stability. This hypothesis is further supported by the data on exploring how HLA-E binding peptides affect its transport in section 4.3.

To conclude, compared to HLA-Ia molecules, HLA-E is less stable on the cell surface and is quickly internalised upon surface arrival.

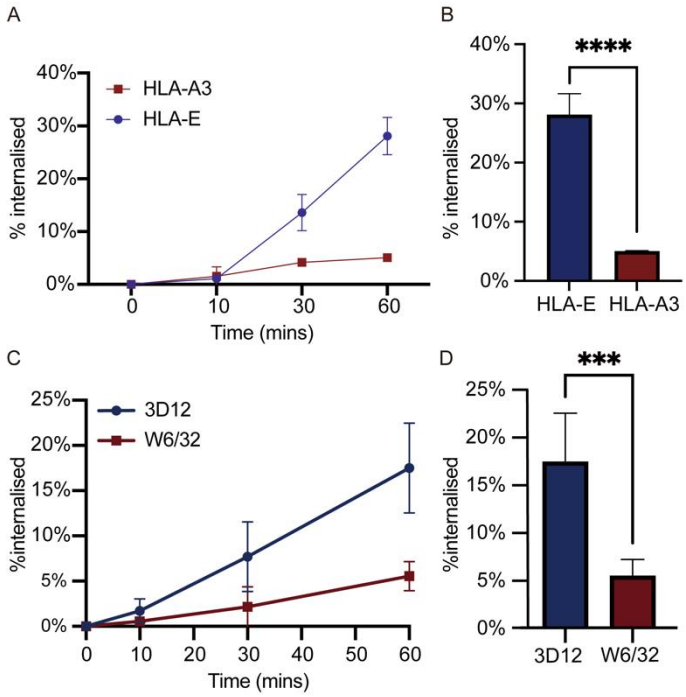

Figure 3.3.17 Quick internalisation of surface HLA-E
Surface HLA molecules of Hela stable cell lines (A, B) or THP1-derived macrophages (C, D) were labelled antibodies, and then the cells were incubated in media containing primaquine. After different time points of internalisation, samples were collected, and uninternalised surface antibody-HLA complexes were stripped off using citric acid. A, C. The MFI of antibody-labeled cells without acid stripping was set to 100%, and the MFI of antibody-labeled cells with acid stripping but without internalisation was set to 0%. The percentage of internalisation was quantified by the normalisation of MFI increase accordingly. B, D. The percentage of HLA internalised after one hour. Data were collected for three biological runs and are shown as mean ± SD (error bars). Statistical analysis was performed using unpaired two-tailed student's t-test with Welch's correction. Asterisks show the statistical significance between indicated groups: ***, $P < 0.001$; ****, $P < 0.0001$.

3.3.3.4 Surface HLA-E is quickly degraded

The above results showed that most internalised HLA-E molecules are not recycled back to the cell surface, so they are likely to be stored intracellularly or degraded. Therefore, I tested the degradation rate of surface HLA proteins by following the signal intensity of labelled surface HLA molecules over time. Surface biotinylation was used to measure the degradation rate of surface HLA-E and HLA-A3. Surface proteins were first labelled with biotin, and the remaining signal of labelled HLA molecules after different time lengths were measured by the ELISA assay. As expected, the HLA-E biotin signal disappeared rapidly, with only 70% of the initial signal remaining after 30 mins (Fig.3.3.18A). In contrast, the degradation rate of surface HLA-A3 was slower, with more than 90% signal remaining after 30 mins. To

rule out the systematic bias of the assay in HeLa cells, I then repeated the assay in THP1-derived macrophages (Fig.3.3.18B). The similar fast degradation of endogenous HLA-E further confirms the conclusion.

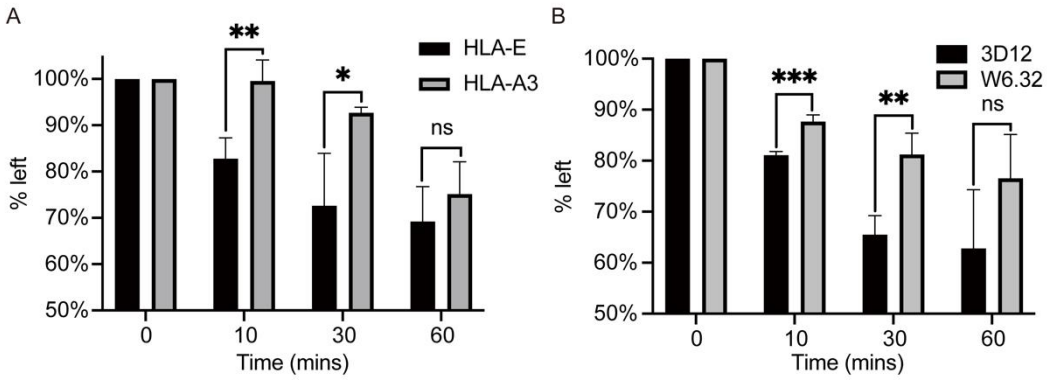

Figure 3.3.18 Surface HLA-E was degraded quickly after internalisation
Surface proteins of Hela stable cell lines (A) or THP1-derived macrophages **with endogenous expression of HLA-Ia and HLA-E** (B) were biotin-labeled, and then the cells were incubated in fresh media for different timepoints. Equal number of cells were collected and lysed after different time points and signal of labelled HLA molecules were measured via the ELISA assay. (A) In HeLa cells, HLA-E and HLA-A3 signal was detected using an anti-EGFP antibody. (B) In THP1 cells, HLA-E and HLA-Ia were detected using 3D12 and W6/32 respectively. The signal of biotin-labeled cells without acid stripping was set to 100%, and the signal of biotin-labeled cells with acid stripping but without internalisation was set to 0%. The percentage of internalisation was quantified by the normalisation of signal increase accordingly. Data were collected for three biological runs and are shown as mean ± SD (error bars). Statistical analysis was performed using unpaired two-tailed student's t-test with Welch's correction. Asterisks show the statistical significance between indicated groups: ns, not significant; *, $P < 0.05$; **, $P < 0.01$; ***, $P < 0.001$.

3.3.3.5 The enrichment of HLA-E in late endosomes and recycling endosomes is independent of the acidic environment in these compartments

As HLA-E is relatively more stable in a mildly acidic environment compared to other HLA-Ia molecules (Camilli et al. 2016), I tested how acidification affected the endosomal distribution of HLA-E molecules. HeLa.E and HeLa.A3 cells were incubated with chloroquine (CQ), a drug which inhibits the acidification of the endosomes, and the endosomal distribution of HLA-E and HLA-A3 was assessed under the confocal microscope (Fig.3.3.19). CQ incubation did not seem to affect the transport of HLA-E and HLA-A3 through early endosomes, late endosomes, or recycling endosomes, as no change in terms of co-localisation with these compartments was observed between the samples with or without CQ incubation

(Fig.3.3.19A-C). However, CQ incubation significantly increased the co-localisation of both HLA-E and HLA-A3 with lysosomes (Fig.3.3.19D, E). This is probably because the elevation of pH in lysosomes inhibited degradation, thus leading to the accumulation of undegraded HLA proteins in lysosomes. More HLA-E and HLA-A3 could be seen in endosomal structures, which appear like bright green spots and co-localises very well with lysosomes (Fig.3.3.19E), which further supported the idea that the degradative pathway is less effective in an environment with elevated pH. Therefore, the enrichment of HLA-E in late endosomes and recycling endosomes is independent of the acidic environment in these compartments.

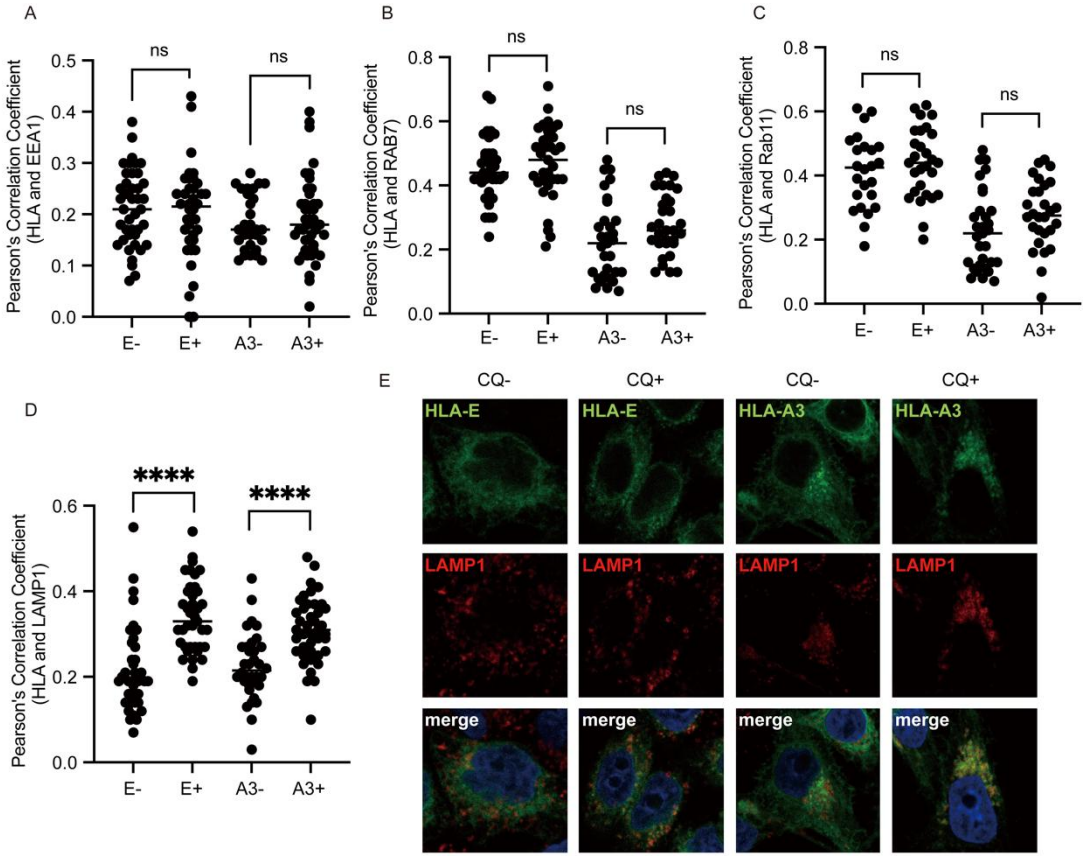

Figure 3.3.19 Inhibition of endosome acidification leads to the accumulation of both HLA-E and HLA-A3 in lysosomes

HeLa cells stably expressing HLA-E and HLA-A3 were incubated in media with (+) or without (-) chloroquine (CQ, finial concentration 100μM) for 3hrs. Cells were then fixed, permeabilised, and stained with antibodies against protein markers for early endosome (EEA1, A), late endosome (Rab7, B), recycling endosome (Rab11, C), or lysosome (LAMP1, D). Cells were then stained with Alexa568-conjugated secondary antibody. A, B, C, D. The co-localization of HLA-E or HLA-A3 with different endosomal compartment markers was quantified using PCC, with 20-40 cells per sample. The PCC values of each cell and the mean values are shown. Statistical analysis was performed using one-way ANOVA with Tukey's post-hoc test. Asterisks show the statistical significance between indicated groups: ns, not significant; ****, $P < 0.0001$. E, Representative images of col-localization of HLA-E or HLA-A3 with lysosomes are shown.

To conclude, surface HLA-E is less stable compared to classical HLA-Ia molecules. HLA-E molecules are quickly internalised upon surface arrival, with only a small fraction recycled back to the cell surface and most directed to the degradation pathway. The acidic environment in the endosomal compartment is essential for the degradation of internalised HLA-E but does not affect its trafficking process in internalisation and recycling.

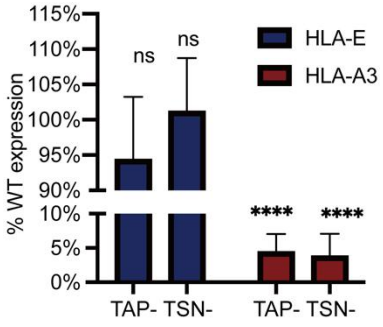

Figure 3.3.20 HLA-E surface expression is indepedent of TAP and tapasin
A. HLA-E_EGFP or HLA-A3_EGFP were transiently transfected into WT HEK293T cells or HEK293T cells with TAP or tapasin (TSN) knocked out. 24hrs after transfection, cells were collected for flow cytometry analysis (gated on GFP+ cells), and surface expression of HLA molecules was assessed with either anti-HLA-E antibody (3D12) or anti-HLA-A3 antibody (GAP.A3). Surface MFI of HLA-E or HLA-A3 in WT HEK293T cells was set to 100%, and their surface expression in HEK293T with TAP/TSN knocked out was normalised as its percentage. Data were collected for four biological runs and are shown as mean ± SD (error bars). Statistical analysis was performed using unpaired two-tailed student's t-test with Welch's correction. Asterisks show the statistical significance between indicated groups: ns, not

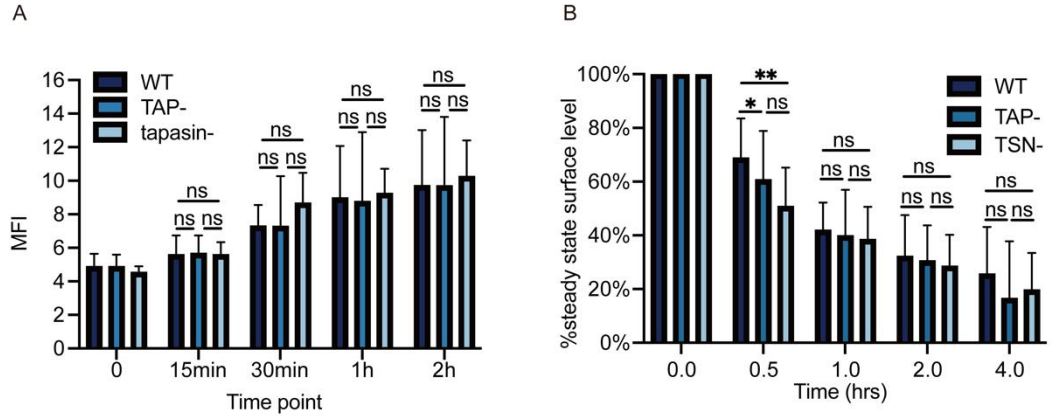

Figure 3.3.21 Influence of TAP and tapasin on the antegrade transport and surface stability of HLA-E
A. Sec61B_str and HLA-E_SBP_EGFP were transiently transfected into WT HEK293T cells or HEK293T cells with TAP or TSN knocked out. At different time points after biotin addition, cells were collected for flow cytometry analysis and surface HLA-E was assessed with the anti-HLA-E antibody 3D12. The stable cell surface MFI after the biotin addition overnight was set to 100%, the MFI before biotin addition was set to 0%, and the other values were normalised accordingly. Data were collected for five biological runs and are shown as mean ± SD (error bars).
B. HLA-E_EGFP was transiently transfected into WT HEK293T cells or HEK293T cells with TAP or TSN knocked out. 24hrs after transfection, cells were incubated in media containing BFA for different time points before flow cytometry analysis for surface MFI of HLA-E. The average cell surface MFI for timepoint zero was set to 100% and the following values were normalised as its percentage. Data were collected for five biological runs and are shown as mean ± SD (error bars).
Statistical analysis was performed using one-way ANOVA with Tukey's post-hoc test. Asterisks show the statistical significance between indicated groups: ns, not significant; *, $P < 0.05$; **, $P < 0.01$.

3.3.4 HLA-E trafficking is independent of TAP and tapasin

I also explored how TAP and tapasin affect HLA-E surface expression and intracellular transport, which are both key regulatory elements for HLA-I trafficking.

HLA-E and HLA-A3 were transfected into WT HEK293T cells or HEK293T cells with TAP or tapasin knocked out (Fig.3.3.20). While HLA-A3 surface level dropped to less than 5% of its original level without TAP or tapasin, HLA-E surface expression did not seem to be affected, implying that surface expression of HLA-E is independent of TAP and tapasin.

To further analyse whether TAP or tapasin might influence HLA-E trafficking, RUSH assay and BFA surface decay assay were carried out for HLA-E in these different HEK293T cell lines (Fig.3.3.21). In the RUSH assay, no difference was observed between the surface accumulation of HLA-E proteins upon biotin addition between WT HEK293T cells and HEK293T cells with TAP or tapasin knocked out (Fig.3.3.21A), suggesting that either TAP or tapasin affect the antegrade transport of HLA-E. In the BFA decay assay, a slight decrease of surface stability could be observed thirty mins after BFA addition in the cell lines with TAP or tapasin knocked out, but not later time points (Fig.3.3.21B). This suggests that the shortage of TAP and tapasin could further decrease the surface stability of HLA-E, though the effect is trivial.

In summary, while the surface expression of HLA-A3 is significantly blocked in the absence of TAP or tapasin, HLA-E surface expression and antegrade transport are independent of TAP and tapasin expression. Although TAP and tapasin could affect the surface stability of HLA-E, the effect is minor.

3.4 Discussion

In this chapter, I characterised the intracellular distribution and dynamic transport process of HLA-E. While most HLA-Ia molecules stay on the cell surface, HLA-E mainly stays in the early secretory pathway, mostly in the ER. Apart from ER retention, HLA-E is also more enriched in late endosomes and recycling endosomes compared to HLA-Ia. To characterise the trafficking of HLA-E, I first optimised the

RUSH assay and applied this system to explore the antegrade transport process of HLA molecules. Although most HLA-E is retained in the ER, its trafficking to the cell surface upon ER exit is fast and does not differ from that of HLA-Ia in terms of both pathways and dynamics. I then explored the turnover of surface HLA-E, including surface stability, internalisation, recycling and degradation. Compared to HLA-Ia molecules, HLA-E is less stable and gets internalised quickly. Although further studies are required to give a more accurate and solid delineation of the recycling pathway of HLA-E, results here suggest that most internalised HLA-E seem to be degraded quickly, and only a tiny amount could be recycled back to the cell surface.

Although some characteristics of HLA-E intracellular localisation have been reported in previous studies, including both ER retention and low surface expression (Camilli et al. 2016; Coupel et al. 2007; Lee et al. 1998a), the complete picture of its distribution is far from clear, let alone the dynamic trafficking progress. Here I made a thorough characterisation of HLA-E intracellular distribution and trafficking dynamics. To ensure the reliability of the results, I applied various methods including flow cytometry, imaging, and western blotting, as well as verified the conclusions in different cell lines. The low surface expression of HLA-E results from ER retention and fast surface turnover, but not from slow antegrade transport, as HLA-E traffics to the cell surface with similar dynamics to HLA-Ia molecules upon ER exit. Apart from intracellular accumulation, I further found that HLA-E is more enriched in late endosomes and recycling endosomes compared to HLA-Ia, which has not been reported previously to my knowledge. The endosomal accumulation of HLA-E may result from fast internalisation upon surface arrival (Fig.3.3.17) and its comparative resistance to the acidic endosomal environment (Camilli et al. 2016). The endosomal enrichment of HLA-E might be crucial for its unconventional antigen presentation to CD8+ T cells upon pathogen infection, as pathogen-derived peptides could be loaded

onto HLA-E in late endosomal structures and subsequently presented to CD8+ T cells via the recycling pathway (Grotzke et al. 2009).

The characterisation of the HLA-E intracellular distribution and trafficking process was carried out in both HeLa cells and THP1-derived macrophages. HeLa cells are the ideal cell line to start with, as it's in HeLa that many previous studies on HLA transport were obtained and many methods were established. Different methods were applied to ensure the robustness of the results. For example, imaging captures all the HLA molecules as they are tagged with EGFP, which rules out the potential bias introduced by the conformation preference of antibodies. However, the results on HLA-E trafficking obtained solely in HeLa cells are not reliable enough. As the endogenous HLA-E is almost undetectable in HeLa cells, if any, HLA-E was introduced exogenously and overexpressed in them. EGFP tagging may also distort the trafficking of HLA-E. Besides, protein localisation and transport may be cell-line specific. Therefore, I also characterised the HLA-E intracellular distribution and trafficking process in THP1-derived macrophages. Endogenous HLA-E was evaluated in THP1-derived macrophages, which excludes the possible bias of artificial overexpression of tagged HLA-E. THP1 is a myeloid cell line, and HLA-E is upregulated in THP1-derived macrophages which can function as APCs (Camilli et al. 2016). Recent studies imply that myeloid-derived macrophages may be important for the priming of MHC-E-restricted T cells (Hansen et al. 2022; Malouli et al. 2021). Consistent with my data (Fig.3.2.2), HLA-E is enriched in autophagosomal pathways during the monocyte-macrophage differentiation (Camilli et al. 2016), which further implies the importance of the unconventional endosomal pathways in myeloid cells to present pathogen-derived antigens to CD8+ T cells. Therefore, the results obtained in THP1-derived macrophages better mimic the physiological conditions.

The RUSH system can control and synchronise the release of the target protein from the ER (Boncompain et al. 2012) and is thus a useful system to monitor the trafficking

routes and the kinetics of HLA-E upon ER exit. Although most HLA-E is retained in the ER, the synchronisation of ER exit ensures high sensitivity of robust detection of the HLA-E transport process (Fig.3.3.11-12). The coupling of the RUSH system with imaging allows for direct visualisation and precise calculation of the dynamic trafficking of HLA-E at different time points (Fig.3.3.11, video). Although the surface arrival of HLA-E is hardly detectable under the microscope due to its low level, flow cytometry could offer an accurate readout, enabling quantitative analysis of the time required for HLA-E to traffic to the cell surface.

Although the original design of the RUSH system worked for HLA-E (Fig.3.3.2), several problems exist. As the low expression of the reporter protein resulting from the bicistronic design of the original plasmid makes the gating of RUSH-positive cells difficult, I established a modified version of the RUSH system by separating the hook and the reporter protein into two plasmids (Fig.3.3.4). To rule out the potential influence of the hook protein CD74 on HLA-E trafficking, a new hook with sec61B was constructed (Fig.3.3.8). The effectiveness of the new hook was validated, and the hook:reporter ratios were optimised for HLA-E and HLA-A3 respectively so that the reporter protein expression reached a satisfactory level in the RUSH system while the effectiveness of ER trapping was preserved (Fig.3.3.8-10). The optimised RUSH system is not only more sensitive and contains less background, but also is easier to manipulate and optimise for different reporter proteins. Such an optimisation process might not be necessary for a rough overview of the trafficking process for proteins with high surface expression levels (Boncompain et al. 2012), but is critical if a thorough characterisation of the trafficking dynamics is required or if the target has a low surface expression like HLA-E where very high sensitivity of the assay is needed for robust detection of the tiny fraction of HLA-E that traffics out of the ER.

It’s not clear why the new sec61b hook is more effective at ER trapping compared to the original CD74 hook in the RUSH assay (Fig.3.3.5, 3.3.9). Sec61 complex is

located in both ER and ER-Golgi intermediate complex(Greenfield and High 1999), which may enable the sec61b hook to trap reporter proteins that escape from the ER but are still in the early secretory pathway. The overexpression of the sec61b hook may affect the antigen translocating function of the sec61 translocon which inhibits the peptide transport and decreases the efficiency of HLA-A3 ER export, thus allowing for easier ER trapping. Certain characteristics of CD74 itself, including the conformation, self-trimerisation and protein interactome, may inhibit the interaction between str and SBP which reduces the potency of the CD74 hook (Schröder 2016).

Although live imaging seems to be the most direct and ideal way to track the transport of HLA molecules, its usage is limited by some technical difficulties. Cells transfected with a proper ratio of the hook and the reporter were selected under the microscope. Co-transfection of a third plasmid expressing a fluorescence-tagged compartment marker protein at a proper level is necessary to accurately localise HLA-E molecules at different time points, as overexpression of some compartment markers may distort the HLA-E transport process. As the chances of getting 3 different plasmids (hook, reporter, marker) co-transfected at the right ratio are very low, very few representative cells could be found within one field. Both high resolution and high magnification are required for accurate tracking and intracellular localisation of HLA-E molecules, which limits the number of cells in the field. As HLA-E traffics out of the ER quickly upon biotin addition, pictures have to be taken at high frequencies to catch the dynamic transport process, which makes it impossible for the microscope to take turns to take pictures from different fields. For fixed samples, it is easier to collect sufficient representative samples for quantitative analysis and to label different compartments easily through antibody staining. Therefore, I mainly used fixed samples for analysis of HLA-E antegrade transport (Fig.3.3.11) and only used live cell imaging to confirm the conclusions drawn from fixed samples (video).

In the measurement of the degradation rate of surface HLA proteins, I used biotin to label the proteins rather than antibodies as adopted in other assays (Fig.3.3.18). Direct antibody labelling is not ideal, as antibodies may survive after the degradation of HLA molecules and antibodies may disassociate from target proteins and thus cannot accurately inform the location of HLA molecules. Antibody binding may also change the endosomal trafficking of target proteins. Besides, the acidic endosomal environment may lead to misfolding of antibodies or a change in the intensity of the fluorescence signal. An anti-EGFP antibody was then used in the ELISA readout, as it could capture HLA-E or HLA-A3 in all conformations, circumventing possible bias introduced by antibodies specific to different conformations. Furthermore, as EGFP was tagged on the C-terminal, biotinylation did not affect antibody binding.

Although the enrichment of HLA-E in recycling endosomes was observed in both HeLa cells and PMA-differentiated, macrophage-like THP1 cells (Fig.3.2.1-2), the PCC value in the latter is more significant, with the mean value over 0.6. This is probably because macrophages are professional APCs that are highly capable of using recycling MHC-I molecules for antigen presentation (Hansen et al. 2022; Malouli et al. 2021). Besides, overexpression of HLA-E may artificially lead to a higher proportion of HLA-E targeted to the degradation pathway after internalisation, which might contribute to the lower co-localisation with recycling endosomes in HeLa cells.

The similar surface accumulating rates of HLA-E and HLA-Ia seem counterintuitive at first glance (Fig3.3.12-13), as the comparatively tiny amount of HLA-E released from the ER suggests a longer accumulation time for surface HLA-E to reach the steady state. However, the short surface lifetime and the low steady-state surface expression level favour the surface HLA-E to reach equilibrium quickly. These factors together explain why HLA-E reached the steady-state level as quickly as HLA-Ia.

In the presence of BFA and PQ, the decrease of surface HLA expression should be equivalent to the internalisation rate (Fig.3.3.15), as the arrival of newly synthesiSed molecules and recycling ones are blocked. However, the disappearance of the surface signal detected in the surface decay assay is faster than the internalisation rate calculated in the acid stripping assay, though a similar trend was observed (Fig.3.3.17). Similarly, the degradation rates measured are higher than the internalisation rates (Fig.3.3.18). The systematic bias of the acid-stripping assay might be the major reason for this. As the HLA-antibody complex may fall apart or get degraded after internalisation, the fluorescent intensity may be affected by the acidic endosomal environment, and the cells might need some time to recover from acid stripping before efficient internalisation could initiate, the internalisation rate is likely underestimated in the acid stripping assay. Besides, internalisation rates may be overestimated in the surface decay assay and the degradation assay. Drug addition in the surface decay assay may lead to a certain level of cell stress, which could potentially increase the internalisation rate, though no obvious toxic effects were observed here. Biotinylation in the degradation assay may promote the internalisation of surface proteins. Apart from internalisation, proteolytic shedding of surface HLA molecules may also contribute to the disappearance of surface signal (Demaria et al. 1994; Derré et al. 2006; Park et al. 2004b), though this should not be a significant pathway in cell lines under normal conditions.

Primaquine had an obvious effect on the stability of classical HLA-I molecules over time, indicating the recycling pathway constantly contributes to a small portion of surface HLA molecules (Fig.3.3.15). While the effect of primaquine is significant at early time points for HLA-E, the effect decreased over time, and there's no obvious difference in samples with or without PQ addition at later time points. HLA-E may be retained in the endosomal pathway, as it is enriched in late and recycling endosomes compared to HLA-Ia (Fig.3.2.1-2). Thus, the recycling pathway might contribute less

to HLA-E on surface expression. Besides, the amount of HLA-E in the recycling pathway may be very small at later time points, as the surface HLA-E level is already very low, and only a tiny fraction of internalised HLA-E could enter the recycling pathway. Furthermore, as the remaining surface level of HLA-E is already very low at later time points, further decrease of the surface signal may not significantly change the normalised expression values calculated here.

As there's likely a lack of good HLA-E peptides in HEK293T cells (which will be explored and discussed further in Chapter 4), the surface HLA-E may mostly come from a non-classical, TAP/tapasin-independent pathway, which explains why the absence of TAP or tapasin did not affect HLA-E surface expression in HEK293T cells (Fig.3.3.20). This is consistent with previous results that surface HLA-E was detectable and was not downregulated by the TAP inhibitor UL49.5 in K562E cells, which lacks endogenous VL9 peptides for the absence of HLA-Ia expression (Lampen et al. 2013). Similarly, TAP inhibition did not reduce the surface level of Mamu-E (Abdulhaqq et al. 2019) or Qa1 (van Hall et al. 2007)

Although the surface level of HLA-E is unaffected in HEK293T cells without TAP or tapasin, the slight decrease of surface stability suggests a lower binding affinity of the peptide repertoire presented by HLA-E via the non-classical, TAP-independent pathway (Fig.3.3.21). Previous studies in K562E cells also suggested an alternative TAP-independent, broad peptide repertoire presented by HLA-E (Lampen et al. 2013). Although the presentation of signal sequence-derived peptides is inhibited by the TAP inhibitor UL49.5, other non-dominant peptides substitute the peptide repertoire in the absence of TAP (van Hall et al. 2007).

However, there were also studies showing that HLA-E surface expression entirely depends on the classical TAP/tapasin-dependent pathway and requires the binding of VL9 peptide derived from HLA-I signal sequences in 721.221 cells (Braud et al.

1998b; Lee et al. 1998a). A possible explanation is that the TAP/tapasin-independent transport of HLA-E is cell line-specific and does not exist or at least is hard to detect in 721.221 cells. Therefore, it is necessary to further characterise how TAP and tapasin regulate the transport and peptide loading of HLA-E in different cell types.

Different antibodies may introduce some systematic bias here. Antibody cross-linking may change the behaviour of surface HLA proteins. The antibody signals may not truly represent the internalisation process of target proteins, as antibodies with lower affinity or more sensitive to low pH may fall apart more easily in the endosomal pathway. Besides, antibodies have preferences for different conformations of the target protein. W6/32 is known to bind to fully conformed HLA-I molecules, but the conformation preference of the HLA-E-binding antibody 3D12 and the HLA-A3-binding antibody GAP.A3 is not well characterised. MHC-I molecules of distinct conformations follow different trafficking pathways (Mahmutefendić et al. 2013). Open conformers are unstable on the cell surface and have a higher internalisation rate (Mahmutefendić et al. 2011; Zagorac et al. 2012). After internalisation, open conformers follow a different endosomal pathway from fully conformed MHC-I molecules, with a higher degradation rate and poor recycling (Mahmutefendić et al. 2007; Mahmutefendić et al. 2011; Zagorac et al. 2012). Different from HLA-Ia, the majority of HLA-E molecules are not optimally folded due to the lack of high-affinity peptides, which may partially explain why the intracellular distribution and trafficking patterns of HLA-E resemble that of open MHC-I conformers. However, it is difficult to characterise the trafficking pathways of HLA-E of different conformations due to the lack of antibodies available to distinguish between them.

As the addition of PQ in the surface decay assay only provides some indirect description of the recycling pathway, I attempted to examine the amount of HLA-E recycled back to the cell surface as previously described (Turvy and Blum 2001).

Briefly, biotin-labelled surface HLA-E is allowed for internalisation for a certain time length, and the uninternalised HLA-E is stripped off by citric acid. The internalised pool was then allowed for recycling for different time points, and the acid stripping was applied to strip of the HLA-E recycled back to the cell surface. However, this method is not sensitive enough for HLA-E molecules, as the amount of surface HLA-E is already very small and only a very tiny fraction of internalised surface HLA-E is recycled back.

Although I have explored the static intracellular distribution as well as the dynamic transport of HLA-E in a detailed and systematic way and delineated an overall picture of the trafficking patterns of HLA-E, future work is necessary to answer some important questions. Given the importance of HLA-E-restricted endosomal peptide loading during pathogen infection (Grotzke et al. 2009; Verweij et al. 2021), further characterisation of the endosomal transport of HLA-E molecules is necessary. However, the tiny amount of surface HLA-E makes it very difficult to study its transport beyond surface arrival, and assays with higher sensitivity are required. I have characterised the general trafficking progress of HLA-E molecules, but it would be informative if the trafficking of HLA-E of different conformations could be studied separately, as previous studies reported that the transport of HLA-I molecules of different conformations might be different (Mahmutefendić et al. 2011; Mahmutefendić et al. 2013; Zagorac et al. 2012). The development of antibodies targeting HLA-E of different conformations would be crucial for such exploration, and other members of the group are currently working on this. Pathogen infection could change HLA-E transport pathways and I will also explore HLA-E trafficking and antigen presentation upon pathogen infection in the future.

Chapter 4: Mechanistic exploration of HLA-E trafficking regulation

Part of the data presented in this chapter has been published in (He et al. 2023)

4.1 Introduction

The RhCMV-vectored vaccine expressing SIV-derived antigens has exhibited effective, long-term protection in over 50% of vaccinated RMs following the SIV challenge (Hansen et al. 2011; Hansen et al. 2013a; Hansen et al. 2016). The efficacy of the vaccine relies on the initiation of unconventional MHC-E-restricted CD8+ T cell responses, which requires careful modulation of MHC-E transport (Hansen et al. 2016; Verweij et al. 2021). Non-canonical antigen presentation pathways also appear crucial for the efficacy of HLA-E-restricted CD8+ T cell responses against M.tb infection (Grotzke et al. 2009). Therefore, an in-depth exploration into the regulatory mechanisms governing HLA-E transport could serve as the fundamental basis for not only advancing the transformation of this efficacious SIV vaccine into an HIV vaccine but also for developing other potential immunotherapies centred around HLA-E targeting.

β2m and peptide together with HLA-E HC form the functional trimer complex. β2m availability was reported to be necessary for the surface expression of HLA-E (Marín et al. 2003; Ulbrecht et al. 1999; Ulbrecht et al. 1992). The dominant VL9 peptide derived from the HLA-I signal sequence also affects HLA-E transport (Braud et al. 1997; Braud et al. 1998b), and the increase in VL9 supply could promote the surface expression of HLA-E (Lee et al. 1998a). HCMV upregulates the HLA-E surface level via the enhancement of VL9 availability from the UL40 signal sequence to avoid the recognition by NK cells (Tomasec et al. 2000). However, no detailed characterisation of how peptide availability shapes HLA-E intracellular distribution and transport was done.

The existence of different motifs on the cytoplasmic tail is required for the precise regulation of the specific intracellular trafficking pathways of different non-classical HLA-I molecules, as has been reported for HLA-F (Boyle et al. 2006; Cho et al. 2011), HLA-G (Fujii et al. 1994; Park et al. 2001), and CD1 (Gumperz 2006; Maître et al. 2008; Sugita et al. 2002). Many viruses target the cytoplasmic tail of MHC-I for degradation to downregulate its surface level, including HIV (Le Gall et al. 1998; Wonderlich et al. 2008), EBV (Griffin et al. 2013), KSHV (Coscoy et al. 2001; Hewitt et al. 2002) and HCMV (Barel et al. 2006; Story et al. 1999). Cytoplasmic tail-mediated downregulation of MHC-I molecules is also common in cancers (Bradley et al. 2015; Wang et al. 2008). Though the cytoplasmic tail of HLA-E is understudied, it seems likely to play a crucial role in shaping its unique trafficking patterns.

In Chapter 3, I have characterised the intracellular localisation and trafficking process of HLA-E, in which the unique trafficking patterns of HLA-E suggest non-canonical regulatory mechanisms. Therefore, in this chapter, I aim to explore the following questions:

- How β2m availability affects HLA-E surface level
- How peptide affinity and availability affect HLA-E intracellular distribution and transport
- How the cytoplasmic tail of HLA-E regulates its intracellular distribution and transport, and the functional motifs contributing to the regulatory effects

4.2 How β2m availability affects HLA-E transport

As the inefficient pairing between HLA-E and β2m may be a reason for ER retention, I co-transfected β2m plasmid and HLA-E plasmid at different ratios in HEK293T cells and examined how the availability of β2m affects HLA-E transport (Fig 4.2). Consistent with previous studies (Marín et al. 2003), β2m overexpression led to a modest increase of surface HLA-E (Fig 4.2A), and a higher surface HLA-E level was observed with more β2m plasmids co-transfected. When the amount of β2m plasmid

transfected is four-fold of that of HLA-E, a two-fold increase of surface HLA-E level was observed. A slight but not significant increase of surface HLA-E was seen when the amount of β2m plasmid co-transfected was between 0.5 to two-fold of that of HLA-E plasmid. This implies that while the supply of β2m influences HLA-E transport and surface expression level, it is not the only, and may not be, the major regulatory factor of HLA-E trafficking. The surface MFI of endogenous HLA-A2 was examined simultaneously, and I found that the surface HLA-A2 level was not affected by the transfection of β2m plasmid (Fig.4.2B).

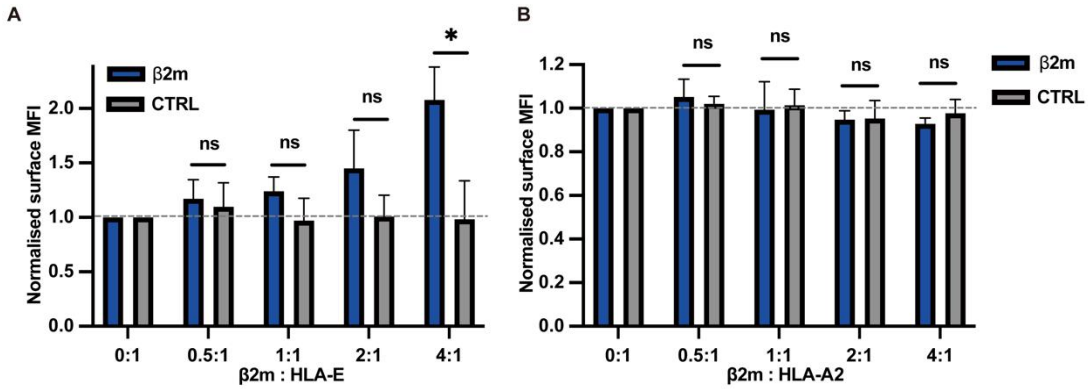

Figure 4.2 The effect of β2m on HLA-E surface expression
HEK 293T cells were transiently co-transfected with HLA-E_EGFP and β2m_EGFP or EGFP (CTRL). The same amount of HLA-E plasmid was transfected under different conditions. The total plasmid amount is adjusted to the same across all conditions by the addition of the irrelevant EGFP plasmid. Expression of HLA-E (A) and endogenous HLA-A2 (B) were assessed. The surface level was normalised to the MFI of the sample only transfected with HLA-E_EGFP. MFIs were collected for three biological runs, and data are shown as mean ± SD (error bars). Statistical analysis was performed using unpaired two-tailed student's t-test with Welch's correction. Asterisks show the statistical significance between indicated groups: ns, not significant; *, $P < 0.05$.

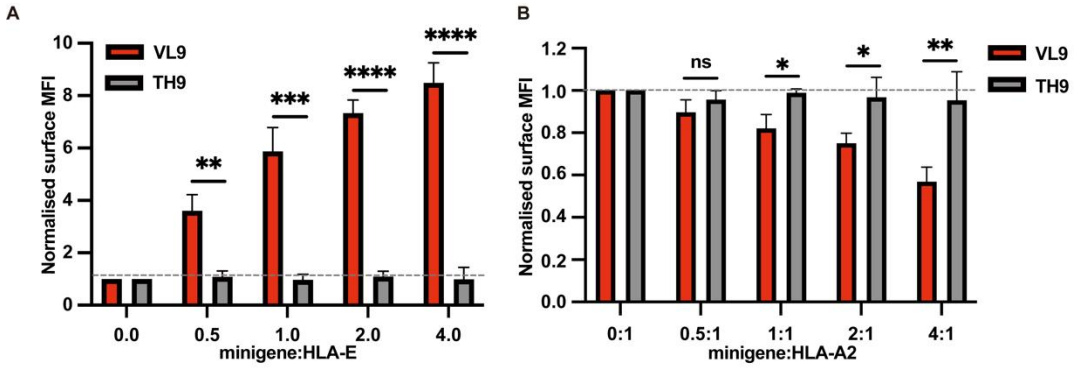

Figure 4.3.1 The effect of peptides on HLA-E surface expression
HEK 293T cells were transiently co-transfected with HLA-E_EGFP and different peptide minigenes. The same amount of HLA-E plasmid was transfected under different conditions. The total plasmid amount is adjusted to the same across all conditions by addition of the irrelevant EGFP plasmid. Expression of HLA-E (A) and endogenous HLA-A2 (B) were assessed. The surface level was normalised to the MFI of the sample only transfected with HLA-E_EGFP. MFIs were collected for three biological runs, and data are shown as mean ± SD (error bars). Statistical analysis was performed using unpaired two-tailed student's t-test with Welch's correction. Asterisks show the statistical significance between indicated groups: ns, not significant; *, $P < 0.05$; **, $P < 0.01$; ***, $P < 0.001$; ****, $P < 0.0001$.

4.3 How HLA-E peptide regulates its transport

4.3.1 HLA-E binding peptides play an important role in regulating HLA-E surface expression

The low competency of HLA-E for β2m and the modest effect of β2m overexpression on promoting HLA-E surface expression suggest that HLA-E binding peptides, which are crucial for the stability of the HLA-E complex (Walters et al. 2018; Walters et al. 2022; Wu et al. 2018), may play a deciding role in controlling HLA-E transport. To explore the effect of HLA-E peptide supply, I co-transfected the HLA-E plasmid with different minigene plasmids at different ratios into HEK293T cells (Fig 4.3.1). The VL9 peptide (VMAPRTLLL) derived from the signal sequence of HLA-A*01 molecules (Sharpe et al. 2019) was used as the representative of a strong HLA-E-binding peptide. The TH9 peptide (TVCVIWCIH) did not bind to HLA-E (Hannoun et al. 2018; Wu et al. 2018) and was used here as the negative control.

Consistent with previous reports (Lee et al. 1998a), VL9 minigene overexpression led to a significant increase of surface HLA-E (Fig 4.3.1A), as a four-fold increase of surface HLA-E was observed when the amount of VL9 minigene transfected was half of that of HLA-E plasmid. When the amount of VL9 minigene plasmid co-transfected was less than that of the HLA-E plasmid, there was a near-linear relationship between the amount of VL9 plasmid transfected and the surface expression level of HLA-E. This indicates that the lack of good peptides is a major limiting step for HLA-E surface expression. The surface HLA-E MFI continued to increase when the amount of VL9 minigene plasmid co-transfected was more than that of HLA-E plasmid, though at a lower accumulating velocity, with an eight-fold increase of surface HLA-E when the minigene:HLA-E ratio was 4:1. The co-expression of the non-binder TH9 peptide did not affect HLA-E surface level. These results suggest that the lack of good peptides is a major contributor to the low surface expression of HLA-E. The

surface expression level of endogenous HLA-A2 molecules was examined simultaneously, and a gradual decrease of surface HLA-A2 was observed with more VL9 minigene expressed (Fig 4.3.1B). The surface HLA-A2 was reduced by over 40% when the minigene:HLA-E ratio was 4:1. The VL9 minigene expression likely affected the binding of β2m to HLA-A2. The co-expression of the non-binder TH9 peptide did not affect the HLA-A2 level.

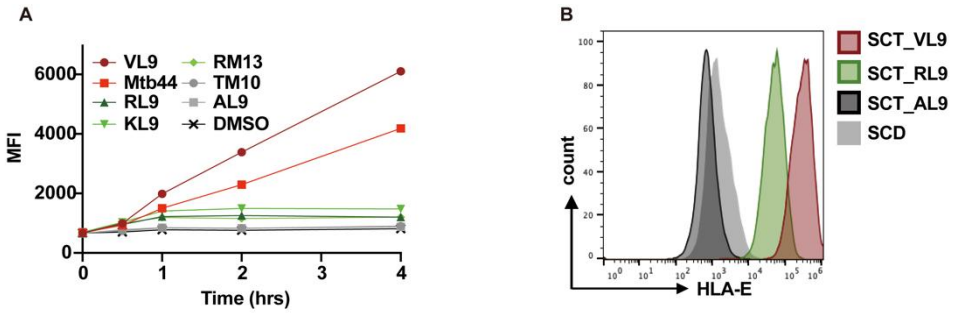

Figure 4.3.2 Peptides of different affinity affect HLA-E surface level differently
A. K562E was incubated in media containing different peptides (100μM final), and surface expression of HLA-E molecules was assessed with flow cytometry at different timepoints. Peptides labelled in red, green and gray are good peptides, weak peptides, and non-binders respectively. DMSO is used as control. Graph shown here is representative of 4 biological replicates.
B. HEK 293T cells were transiently transfected with 3 different HLA-E SCTs, or a HLA-E SCD (light grey). 24hrs after transfection, surface expression of HLA-E molecules was assessed with flow cytometry. MFIs shown here are representative of observations made in four experiments.

4.3.2 Peptide binding affinity determines the effectiveness in promoting HLA-E surface level

As high-affinity peptides are more efficient at promoting the refolding of HLA-E trimers (Walters et al. 2022), I explored how peptides of different affinities affect HLA-E surface expression. I incubated K562E cells (K562 cells stably expressing HLA-E*0103) with high-affinity peptides (red), weak-binding peptides (green), or non-binding peptides (grey) (Walters et al. 2018) and examined the surface expression of HLA-E at different points (Fig.4.3.2A). The HLA-E binding affinity of these peptides has been characterised through different methods, and the sequence and affinity of these peptides are listed in Table 7.4. A rapid surface accumulation of HLA-E was observed for the high-affinity peptides VL9 and Mtb44, as the surface MFI increased around eight to ten-fold after the four-hour incubation. Weak peptides

also slightly promoted HLA-E surface expression, but the efficiency was much lower compared to strong peptides, with a two-fold increase of HLA-E surface MFI after the four-hour incubation. Besides, while the increase of surface HLA-E reached a plateau at around one hour after incubation with the weak peptides, the fast increase continued after the four-hour incubation for the strong ones. The non-binders and DMSO failed to increase the surface level of HLA-E. These results suggest a positive correlation between peptide binding affinity and its effectiveness at promoting the HLA-E surface level, which is possibly because only high-affinity peptides can effectively promote the refolding of HLA-E trimers (Walters et al. 2022).

To exclude the potential influence of β2m on the assessment of peptides, I constructed single-chain peptide-β2m-MHC-I trimers (SCT) of HLA-E (Hannoun et al. 2018) with different peptides inserted, in which β2m is covalently linked MHC-E. Single-chain β2m-MHC-I dimer of HLA-E (SCD), which was created by Simon Brackenridge in our group, was used as the control. HLA-E surface expression level matched the binding affinity of peptides (Fig.4.3.2B). While both SCT_VL9 and SCT_RL9 enhanced HLA-E surface expression compared to SCD, the surface-promoting effect was more significant for SCT_VL9. The HLA-E surface level of SCT_AL9 was lower than SCD, which may be because the presence of the non-binder AL9 peptide impeded the binding of HLA-E peptides. Therefore, HLA-E binding peptides could promote its surface expression, and the efficiency matched the peptide binding affinity well.

4.3.3 VL9 peptide increases HLA-E surface expression mainly by promoting ER export

4.3.3.1 VL9 peptide can effectively release HLA-E from the ER

As the binding of high-affinity peptides facilitates the refolding of HLA-E and most HLA-E is retained in ER after synthesis (Fig.3.2.1-2), it is likely that the VL9 peptide

increases HLA-E surface expression by promoting its ER release. To test this hypothesis, HLA-E and different minigenes were co-transfected into HeLa cells, and the co-localisation of HLA-E with the ER was examined via imaging (Fig.4.3.3). The minigene plasmids co-express the mCherry construct, so the cells transfected with the minigene plasmids were selected based on mCherry expression. In HeLa cells co-transfected with HLA-E and the VL9 minigene, no ER enrichment was observed for HLA-E, suggesting that VL9 peptide could effectively promote the ER exit of HLA-E (Fig.4.3.3). In contrast, the co-transfection of the TH9 minigene did not seem to facilitate the ER export of HLA-E, as the level of HLA-E accumulated in the ER was similar to the control sample with no minigene co-transfected (Fig.4.3.3). Apart from a decrease of HLA-E signal in ER, VL9 minigene also led to an increase of HLA-E signal in endosomal structures, as indicated by the bright green spots (Fig.4.3.3A). However, no obvious surface accumulation of HLA-E was observed, which is possibly because the amount of HLA-E on the cell surface is still small, though much bigger than the level without VL9 minigene co-expression.

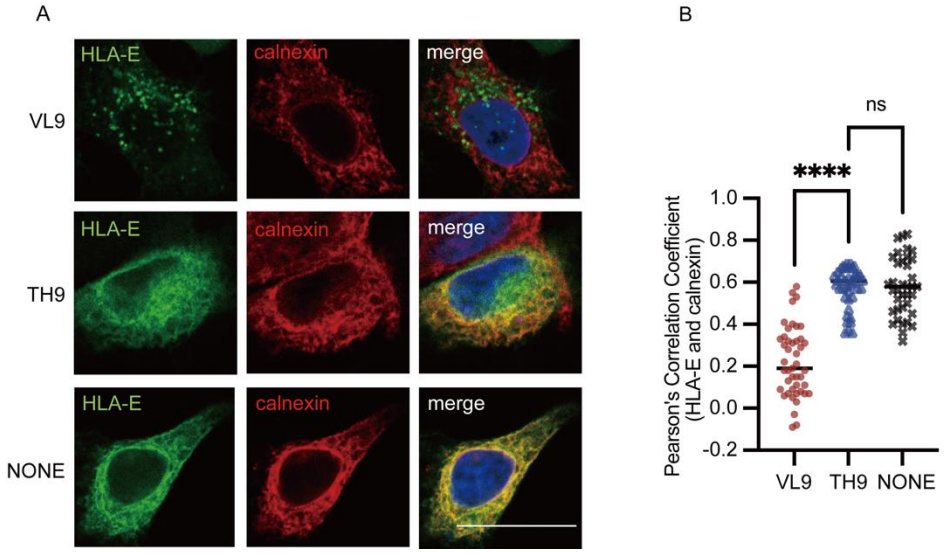

Figure 4.3.3 VL9 minigene peptide can effectively release HLA-E from the ER
HeLa cells were transiently transfected with HLA-E_EGFP or co-transfected with HLA-E_EGFP and different peptide minigenes (selected on mCherry expression, channel not shown). Cells were fixed, permeabilised, and stained with an antibody against the ER marker protein calnexin, followed by detection with an Alexa647-conjugated secondary antibody.
A. Micrographs shown here are representative of two independent experiments. Scale bar = 20 µm.
B. Quantification of ER co-localisation. The PCC values of each cell and the mean values are shown with 30-50 individual cells calculated per sample. Statistical analysis was performed using one-way ANOVA with Tukey's post-hoc test. Asterisks show the statistical significance between indicated groups: ns, not significant; ****, $P < 0.0001$.

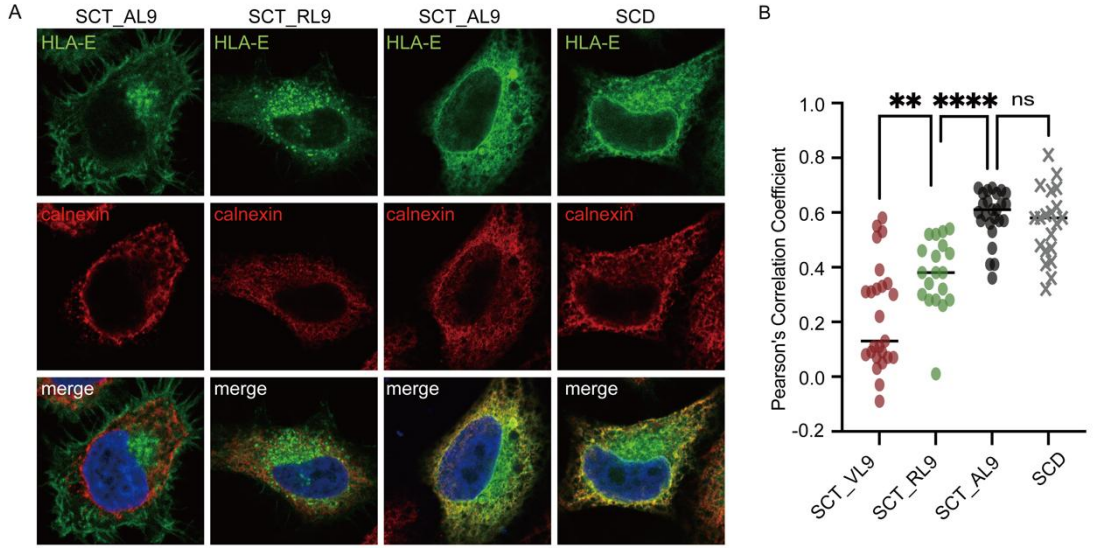

Figure 4.3.4 The efficiency of HLA-E peptides to promote ER export depend on their binding affinity
HeLa cells were transiently transfected with three different HLA-E SCTs or a HLA-E HC SCD. Cells were fixed, permeabilised, and stained with an antibody against the ER marker protein calnexin, followed by detection with an Alexa568-conjugated secondary antibody. A, Micrographs shown here are representative of two independent experiments. B, Quantification of ER co-localisation. The PCC values of each cell and the mean values are shown with 30-50 individual cells calculated per sample. Statistical analysis was performed using one-way ANOVA with Tukey's post-hoc test. Asterisks show the statistical significance between indicated groups: ns, not significant; ** $P < 0.01$; ****, $P < 0.0001$.

4.3.3.2 The binding affinity of peptides determines their effectiveness in promoting HLA-E ER export

Given the difference in surface level between HLA-E SCTs (Fig.4.3.2B), I then examined whether the ER-releasing effect differs between peptides of distinct affinity to HLA-E. Different HLA-E SCTs were transfected into HeLa cells, and their co-localisation with the ER was analysed. SCD was also included as the control (Fig.4.3.4). No ER accumulation was observed for SCT_VL9, and most of it stayed on the cell surface or in endosomes (Fig.4.3.4A). While most SCT_RL9 stayed in endosomes, some could also be observed in the ER. Notably, that the actual peptide affinity of VL9 and RL9 is lower. Without the artificial linkage in the SCT constructs, VL9 fails to stabilise surface HLA-E, and RL9 fails to promote ER export (will be explored further in the chapter). SCT_AL9 and SCD mostly stayed in the ER, and no obvious ER-releasing effect was observed for these two constructs. Therefore, the effectiveness of promoting the ER export of HLA-E depends on the binding affinity

of the peptides. To assess the ER co-localisation statistically, the PCC values of these samples were calculated (Fig.4.3.4B). The results show that high-affinity peptides can completely relieve the ER retention of HLA-E, moderate peptides can promote ER export and decrease the ER enrichment level of HLA-E, and non-binders do not affect the ER retainment of HLA-E.

4.3.3.3 HLA-E peptides do not effectively promote its surface stability under physiological conditions

As peptide supply could facilitate the refolding of the MHC-I trimer complex and that fully conformed MHC-I complex has been reported to be more stable than open conformers (Mahmutefendić et al. 2013), I explored whether peptides could effectively increase HLA-E surface stability. K562E cells were firstly incubated with different peptides provided in excess for 3hrs to saturate surface HLA-E molecules. An equivalent amount of DMSO was used as the control. BFA was then added to block the export of new HLA-E from the ER to the cell surface, and the surface stability of HLA-E was examined (Fig.4.3.5A, B). Excessive good HLA-E peptides like VL9 in media significantly stabilised surface HLA-E, with over 60% remaining on the cell surface after a four-hour BFA incubation. In contrast, weak peptides like RL9 failed to effectively stabilise surface HLA-E, which is probably because the binding affinity of RL9 is not high enough to efficiently help HLA-E refold into a compact and stable conformation (Walters et al. 2022). The surface stability of HLA-E incubated with excessive AL9 was even slightly worse than the control sample without peptide addition.

As excessive peptide supply in the media was comparatively artificial, I then repeated the BFA decay assay with peptides removed after the three-hour incubation before BFA addition (Fig.4.3.5C). The surface HLA-E preincubated with high-affinity peptides was stable in the first hour, supporting the results that these peptides could

help HLA-E refold into a more stable conformation. However, a rapid decrease in surface HLA-E signal was detected after one hour, and the surface level of HLA-E pre-incubated with high-affinity peptides was similar to the sample without peptide incubation after 6hrs. This implies that these HLA-E binding peptides could not stabilise HLA-E very well at the cell surface, which is probably because the affinity of even the best HLA-E peptide VL9 is not very high compared to classical HLA-I peptides (Walters et al. 2022). It's likely that surface HLA-E lost these good peptides after one hour and became very unstable after the collapse of the well-conformed trimer. With an oversupply of good peptides in media (Fig.4.3.5A, B), HLA-E could rebind to good peptides and remain in a folded stable conformation.

To further confirm this in endogenous peptide presentation, the BFA decay assay was carried out for different SCTs and SCD (Fig.4.3.5D, E). SCT_VL9 was stable, with over 60% remaining on the cell surface 4hrs after BFA addition. SCT_RL9 slightly improved the surface stability of HLA-E, while the non-binder AL9 did not seem to promote HLA-E surface stability and even slightly decreased the surface stability compared to SCD. The surface stabilising effect was consistent with the surface expression level of different constructs (Fig.4.3.2), and these results were comparable to the peptide pulsing data with excessive peptide in media (Fig.4.3.5A, B).

To test the surface-stabilising effect of endogenous peptides, I then co-transfected HEK293T cells with HLA-E and different peptide minigenes and carried out the BFA decay assay (Fig.4.3.5D, E). Compared to external peptide pulsing, the endogenous peptide provision through minigenes mimics the physiological conditions. While the co-expression of the VL9 minigene significantly increased HLA-E surface expression compared to the non-binder TH9, it did not significantly enhance HLA-E surface stability, as a rapid decrease of surface expression was observed after BFA addition (Fig.5.3.5F). The decay started earlier compared to peptide pulsing (Fig.4.3.5C), which is possibly because the percentage of surface HLA-E bound to VL9 is lower in

the case of minigenes while most surface HLA-E was saturated with the VL9 peptide before BFA addition in peptide pulsing.

The difference in stabilising surface HLA-E explains why a significant surface signal could only be observed for SCT but not for HLA-E co-expressed with VL9 minigene (Fig.4.3.3A; Fig.4.3.4A), though HLA-E could be completely released from the ER in both cases. To further assess how HLA-E peptides promote its surface stability with the exclusion of the effect of β2m, I co-transfected HEK293T cells with SCD and the VL9 minigene (Fig.4.3.5G). Although VL9 peptide minigene could promote HLA-E SCD surface stability at early time points compared to TH9, the SCD surface level started to drop quickly after about half an hour of BFA incubation. While around 60% of HLA-E remained on the cell surface in the case of SCT_VL9 after the four-hour BFA incubation, around 20% remained in the case of the co-expression of SCD and VL9 minigene. This reinforces our conclusion that even the best HLA-E peptides could not effectively stabilise HLA-E on the cell surface.

As HLA-E is linked to β2m in SCT and SCD, I further co-transfected different minigenes with SCD or with HLA-E HC and β2m plasmid to explore whether β2m binding affects HLA-E surface stability (Fig.4.3.5H). The surface HLA-E level decreased faster when HLA-E and β2m were not covalently linked, suggesting that β2m also plays a role in stabilising surface HLA-E. HLA-E SCD seemed to be more stable than HLA-E HC after around 1.5hrs even when the latter was co-transfected with the VL9 minigene, possibly because the VL9 peptide had already disassociated from surface HLA-E at that time point. These results further confirmed that even the best binding peptide VL9 is not capable of stabilising surface HLA-E under physiological conditions. Enhancing the surface stability is not the main mechanism by which high-affinity HLA-E peptides like VL9 increase the surface level of HLA-E.

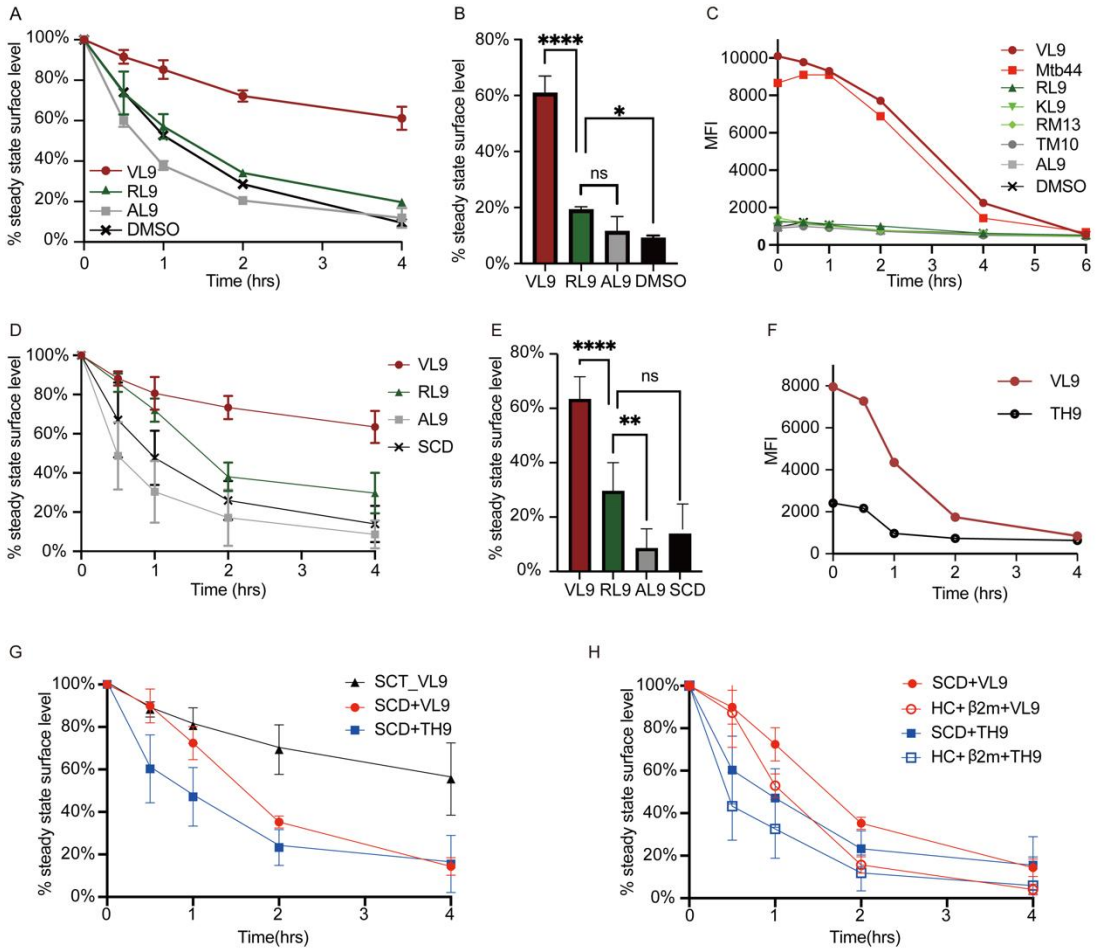

Figure 4.3.5 HLA-E peptides do not effectively promote its surface stability under physiological conditions

A, B. K562E was incubated in media containing different peptides(100uM) for 3hrs, then BFA with peptide kept in media for different timepoints. Surface expression of HLA-E molecules was assessed with anti-HLA-E antibody(3D12). A, The average cell surface MFI for timepoint zero of each sample was set to 100% and the following values were normalised as its percentage. B, Percentage of surface HLA-E after BFA incubation for 4hrs. MFIs were collected and plotted for three biological runs, and data are shown as mean ± SD (error bars).

C. K562E was incubated in media containing different peptides (100uM) for 3hrs, then replaced with fresh media containing BFA with peptides removed for different timepoints. Peptides labelled in red, green and gray are good peptides, weak peptides, and non-binders respectively. DMSO is used as control. Surface expression of HLA-E molecules was assessed with anti-HLA-E antibody (3D12). Graph here shows the average cell surface MFI and is representative of three biological replicates.

D, E. HEK 293T cells were transiently transfected with 3 different SCTs, or a SCD (light grey). 24hrs after transfection, cells were incubated in media containing BFA for different timepoints, and surface expression of HLA-E molecules was assessed with anti-HLA-E antibody(3D12). D. The average cell surface MFI for timepoint zero of each sample was set to 100% and the following values were normalised as its percentage. E, Percentage of surface HLA-E after BFA incubation for 4hrs. MFIs were collected and plotted for three biological runs, and data are shown as mean ± SD (error bars).

F. HEK 293T cells were transiently co-transfected with HLA-E_EGFP and VL9/TH9 peptide minigenes. 24hrs after transfection, cells were incubated in media containing BFA for different timepoints, and surface expression of HLA-E molecules was assessed with anti-HLA-E antibody (3D12). The average cell surface MFI was shown. Graph here shows the average cell surface MFI and is representative of three biological replicates.

G. HEK 293T cells were transiently transfected SCT_VL9, or co-transfected with SCD and different peptide minigenes. 24hrs after transfection, cells were incubated in media containing BFA for different timepoints, and surface expression of HLA-E molecules was assessed with anti-HLA-E antibody (3D12). The average cell surface MFI for timepoint zero of each sample was set to 100% and the following values were normalised as its percentage. MFIs were collected and plotted for three biological runs, and data are shown as mean ± SD (error bars).

H. HEK 293T cells were co-transfected with SCD and different peptide minigenes (solid), or co-transfected with the HLA-E HC, β2m and different peptide minigenes (hollow). 24hrs after transfection, cells were incubated in media containing BFA for different timepoints, and surface expression of HLA-E molecules was assessed with anti-HLA-E antibody (3D12). The average cell surface MFI for timepoint zero of each sample was set to 100% and the following values were normalised as its percentage. MFIs were collected and plotted for three biological runs, and data are shown as mean ± SD (error bars).

Statistical analysis was performed using one-way ANOVA with Tukey's post-hoc test. Asterisks show the statistical significance between indicated groups: ns, not significant; *, $P < 0.05$; **, $P < 0.01$; ****, $P < 0.0001$.

4.3.3.4 VL9 peptide increases HLA-E surface expression mainly by promoting ER export

To further characterise how VL9 peptide affects the surface level of HLA-E, I co-transfected the RUSH system together with different peptide minigenes into HEK293T cells (Fig.4.3.6). After biotin addition, a rapid increase of surface HLA-E signal could be observed in the presence of the VL9 peptide (Fig.4.3.6A). The fast surface accumulation suggests that VL9 was potent in releasing HLA-E from ER. However, the surface expression level started to decrease rapidly after reaching its peak one hour after ER release. As a rapid endosomal accumulation of HLA-E was observed in the RUSH assay (Fig.3.3.11; video), it is likely that HLA-E driven to the cell surface by VL9 was not stable and got internalised quickly, which is consistent with the results from the BFA decay assay (Fig.4.3.5). In the absence of high-affinity peptides, surface HLA-E only accumulated rapidly at early timepoints, and the signal accumulation reached a plateau one hour after biotin addition. In comparison, surface HLA-A3 continued to increase after 4hrs until reaching a stable state (Fig.4.3.6B). The unique dynamic patterns of HLA-E surface expression over time suggest that the VL9 peptide enhances HLA-E surface expression mainly through promoting HLA-E ER export but not via increasing its surface stability.

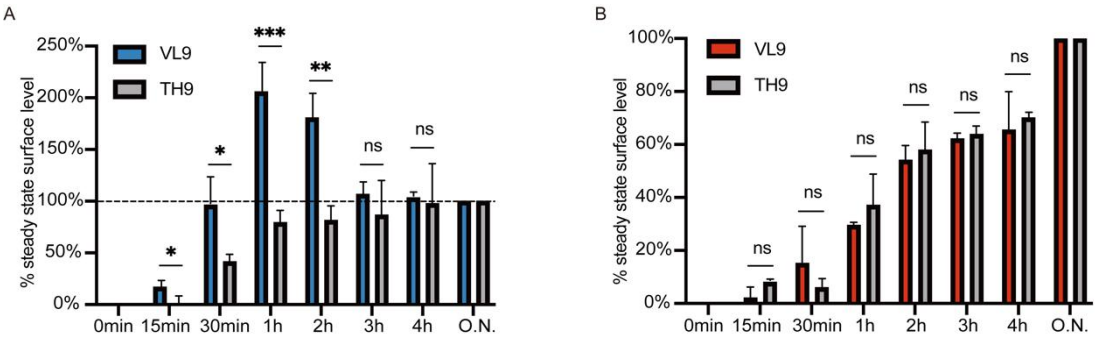

Figure 4.3.6 VL9 minigene can effectively promote the ER export of HLA-E, but not its surface stability
HEK 293T cells were transiently co-transfected with different peptide minigenes and the RUSH system with Sec61B-str as the hook and HLA-E_SBP_EGFP (A) or HLA-A3_SBP_EGFP (B) as the reporter protein. At different time points after biotin addition, the surface expression of HLA-E (A) and HLA-A3 (B) were assessed by anti-HLA-E antibody 3D12 or anti-HLA-A3 antibody GAP.A3 respectively. The stable cell surface MFI after the biotin addition overnight was set to 100%, the MFI before biotin addition was set to 0%, and the other values were normalised accordingly. Data were collected for three biological runs and are shown as mean ± SD (error bars). Statistical analysis was performed using unpaired two-tailed student's t-test with Welch's correction. Asterisks show the statistical significance between indicated groups: ns, not significant; *, $P < 0.05$; ** $P < 0.01$; ***, $P < 0.001$.

4.3.4 HLA-E binding peptides play a major role in shaping its intracellular distribution

Incubation at 26ºC could promote HLA-E surface stability, thus promoting its accumulation on the surface (Ljunggren et al. 1990). However, I did not observe any obvious change in HLA-E intracellular distribution under the confocal microscope after overnight incubation at 26ºC (Fig.4.3.7A, D), as most HLA-E was still in the ER, and no surface signal was detected. Considering that the surface stabilising effect of the low temperature may not be good enough, I then examined the combined effect of the low-temperature incubation and VL9 peptide pulsing, which should effectively increase the surface stability of HLA-E (Fig.4.3.7B, E). Only very weak HLA-E surface signal could be observed in cells incubated with excessive VL9 peptide overnight at 26ºC (Fig.4.3.7E), which is likely due to the ineffectiveness of external VL9 addition at releasing HLA-E from the ER and the potential influence of low temperature on the antegrade transport.

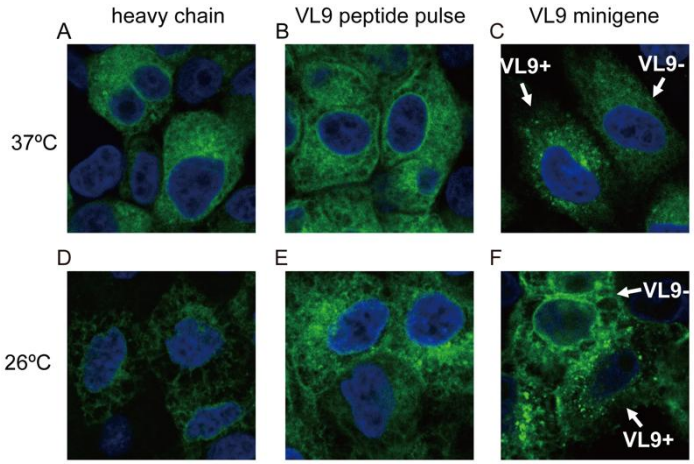

Figure 4.3.7 The affinity of VL9 is not high enough to effectively promote the surface stability of HLA-E
HeLa cells were transiently transfected with HLA-E_EGFP (A, B, D, E) or co-transfected with HLA-E_EGFP and VL9 peptide minigene (C, F). VL9 peptide pulse samples (B, E) were incubated with VL9 peptide (100uM) overnight. Cells were kept at 37ºC (A-C) or kept at 26ºC (D-F) overnight before fixation. VL9+ cells were selected based on the expression of mCherry (C, F, channel not shown). Micrographs shown here are representative of two independent experiments.

The combining effect of the low-temperature incubation and VL9 peptide minigene expression was then examined. VL9 minigene plasmid co-expresses the mCherry fluorescent protein so that the VL9 positive cells were selected by mCherry expression (Fig.4.3.7C, F; channel not shown). While VL9 peptide minigene co-expression could completely release HLA-E from the ER (Fig.4.3.7C), surface

accumulation of HLA-E could only be observed when cells expressing the VL9 minigene was incubated overnight at 26ºC (Fig.4.3.7F). In cells expressing the VL9 minigene, more HLA-E could be observed in endosomal structures when incubated at 37ºC compared to 26ºC. The enrichment of endosomal HLA-E seemed to come from the internalised, unstable HLA-E that was promoted to the surface by endogenous VL9 peptide. These results reconfirmed the conclusion that VL9 peptide could effectively release HLA-E from the ER but not stabilise HLA-E on the cell surface under physiological conditions.

The intracellular distribution of HLA-E might be similar to that of other HLA-I molecules if the affinity and availability of HLA-E binding peptides are similar to that of other HLA-Ia molecules. Therefore, I combined VL9 minigene expression and VL9 peptide pulsing to mimic the effect of HLA-Ia high-affinity peptides (Fig.4.3.8A, B). While minigene expression could lead to efficient ER release of HLA-E, no

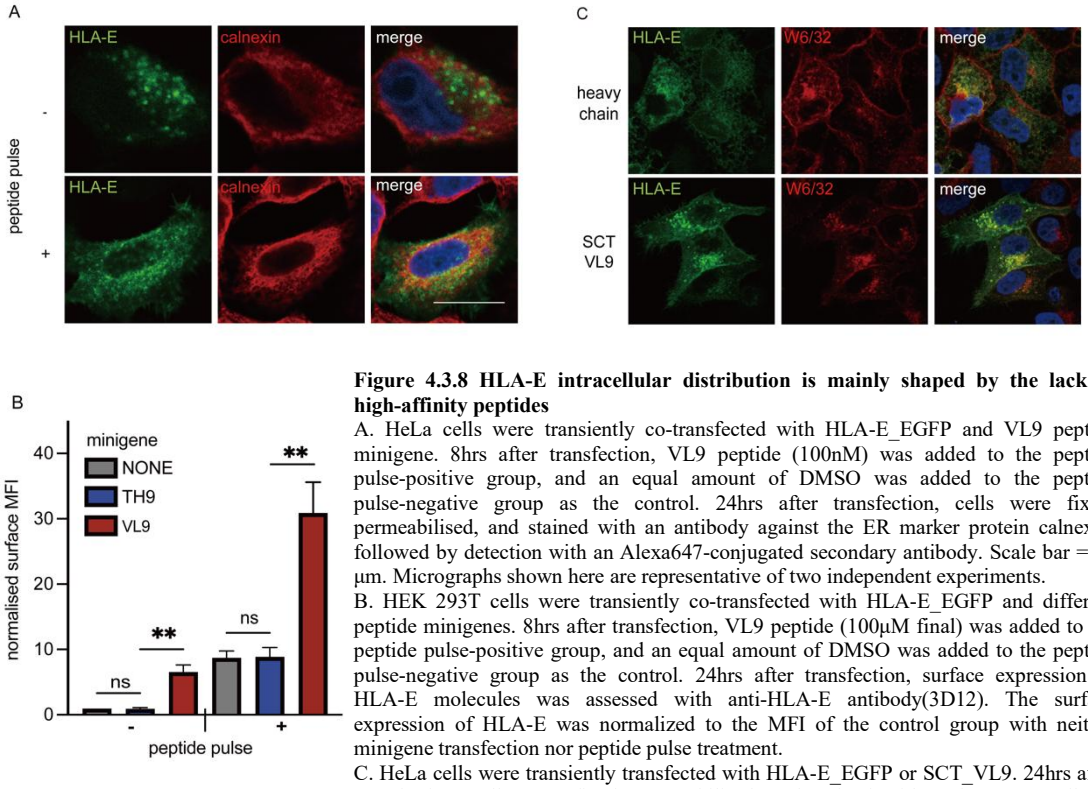

Figure 4.3.8 HLA-E intracellular distribution is mainly shaped by the lack of high-affinity peptides

A. HeLa cells were transiently co-transfected with HLA-E_EGFP and VL9 peptide minigene. 8hrs after transfection, VL9 peptide (100nM) was added to the peptide pulse-positive group, and an equal amount of DMSO was added to the peptide pulse-negative group as the control. 24hrs after transfection, cells were fixed, permeabilised, and stained with an antibody against the ER marker protein calnexin, followed by detection with an Alexa647-conjugated secondary antibody. Scale bar = 20 μm. Micrographs shown here are representative of two independent experiments.

B. HEK 293T cells were transiently co-transfected with HLA-E_EGFP and different peptide minigenes. 8hrs after transfection, VL9 peptide (100μM final) was added to the peptide pulse-positive group, and an equal amount of DMSO was added to the peptide pulse-negative group as the control. 24hrs after transfection, surface expression of HLA-E molecules was assessed with anti-HLA-E antibody(3D12). The surface expression of HLA-E was normalized to the MFI of the control group with neither minigene transfection nor peptide pulse treatment.

C. HeLa cells were transiently transfected with HLA-E_EGFP or SCT_VL9. 24hrs after transfection, cells were fixed, permeabilised, and stained with anti-HLA-I antibody W6/32, followed by detection with an Alexa647-conjugated secondary antibody. Micrographs shown here are representative of two independent experiments.

surface signal could be observed under the microscope (Fig.4.3.8A). With the addition of exogenous VL9 peptide, surface HLA-E became clearly detectable, which is likely because the HLA-E released from the ER by the VL9 peptide minigene was effectively stabilised at the cell surface due to excessive VL9 peptide in media. Besides, VL9 peptide pulsing and VL9 minigene expression had a synergic effect on promoting the HLA-E surface level (Fig.4.3.8B). While peptide pulsing or minigene could lead to an increase of HLA-E surface signal that was close to ten-fold on their own, the combination of the two led to a significant thirty-fold increase of HLA-E surface signal. These results indicate that these two methods promoted HLA-E surface expression via different mechanisms, and an HLA-E binding peptide of real high affinity could greatly increase the HLA-E surface level via simultaneous enhancement of ER release and surface stability.

The intracellular distribution of SCT_VL9 also supported this conclusion (Fig.4.3.4). In the SCT construct, VL9 not only effectively promoted ER release of HLA-E but also stabilised it on the cell surface (Fig.4.3.4). Indeed, SCT_VL9 co-localised very well with HLA-Ia molecules (Fig.4.3.8C), with apparent surface accumulation and a fraction in perinuclear endosomal structures. Therefore, the intracellular distribution of HLA-E was mainly determined by its peptide reservoir, and the unique distribution pattern of HLA-E was largely due to the lack of good peptides.

4.3.5 How the VL9 peptide shapes the endosomal distribution of HLA-E

As VL9 could not effectively stabilise the HLA-E molecules released from the ER at the cell surface under physiological conditions, VL9 expression may lead to the enrichment of HLA-E in endosomal compartments, as HLA-E was clearly detectable in endosomes when co-expressed with the VL9 peptide minigene (Fig.4.3.3A). I then explored the distribution of HLA-E in endosomal structures when co-expressed with the VL9 minigene under the microscope (Fig.4.3.9). While HLA-E could be found in

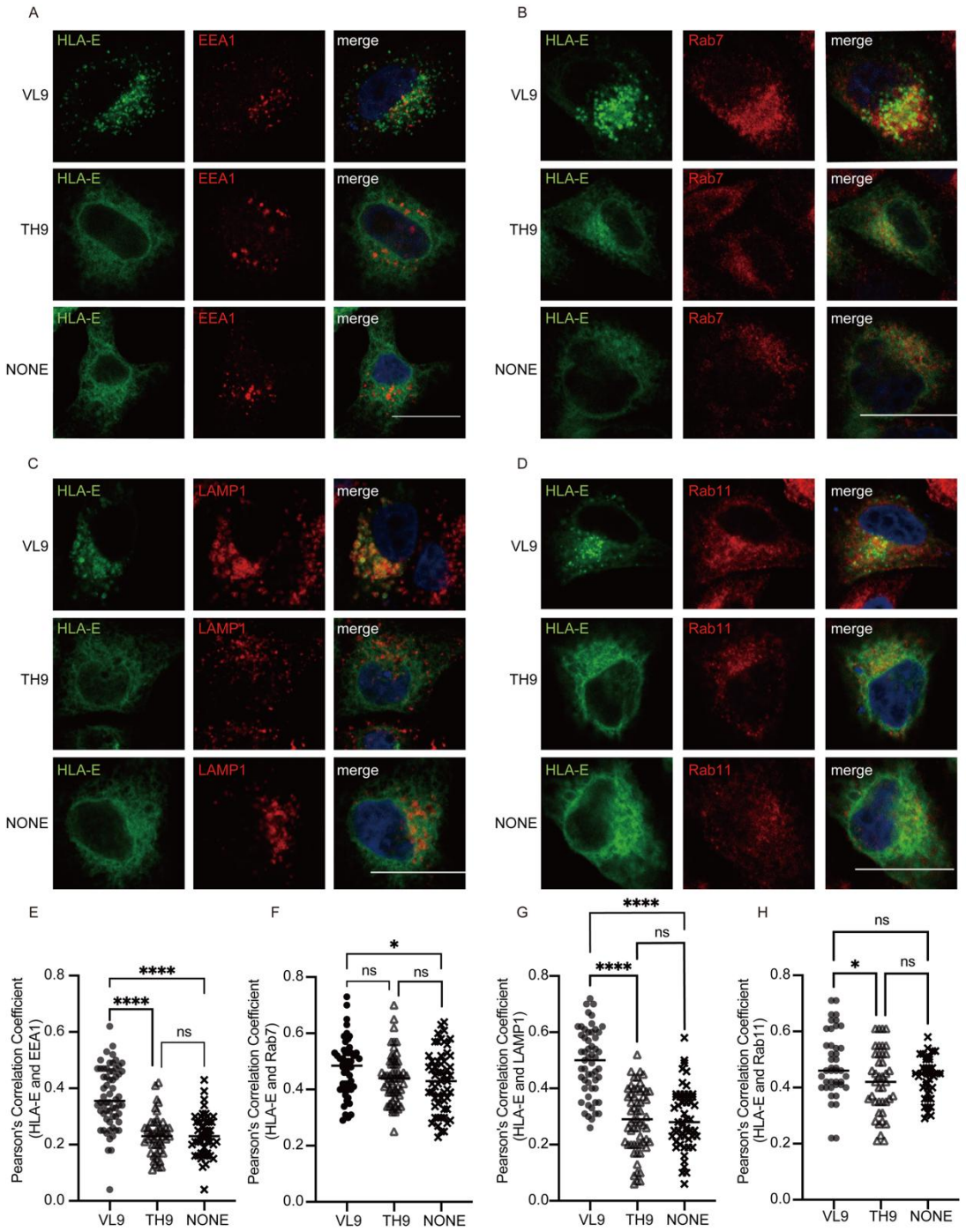

Figure 4.3.9 VL9 peptide enriches HLA-E in early endosomes and lysosomes

HeLa cells were transiently transfected with HLA-E_EGFP (NONE) or co-transfected with HLA-E_EGFP and VL9/TH9 peptide minigenes. Cells were fixed, permeabilised, and stained with antibodies against protein markers of the early endosome (EEA1), late endosome (Rab7), lysosome (LAMP1), or recycling endosome (Rab11). Cells were then stained with Alexa647-conjugated secondary antibody.

A-D. Representative confocal micrographs of HLA-E co-localising with early endosome (A), late endosome (B), lysosome (C) or recycling endosome (D) under different conditions. Scale bar = 20 μm.

E-H. Quantification of co-localisation of HLA-E with early endosome (E), late endosome (F), lysosome (G) or recycling endosome (H). The PCC values of each cell and the mean values are shown with 30-60 cells per sample. Statistical analysis was performed using one-way ANOVA with Tukey's post-hoc test. Asterisks show the statistical significance between indicated groups: ns, not significant; *, $P < 0.05$; ****, $P < 0.0001$. Data shown are representative of two independent experiments.

all endosomal compartments, the co-expression of the VL9 minigene led to the accumulation of HLA-E in early endosomes (Fig.4.3.9A, E) and lysosomes (Fig.4.3.9C, G). Therefore, an oversupply of endogenous VL9 peptide not only increases the HLA-E surface level but also enriches HLA-E in early endosomes and lysosomes.

4.3.6 VL9 minigene promotes the TAP/tapasin-dependent, classical transport of HLA-E

As HLA-E surface expression seemed to be independent of TAP and tapasin under normal conditions in HEK293T cells (Fig.3.3.19; Fig.3.3.20), I explored whether the functions of the VL9 peptide minigene was affected in the absence of TAP or tapasin. HLA-E and different peptide minigenes were co-transfected into different HEK293T cell lines, and the surface HLA-E level was assessed (Fig.4.3.10). In WT HEK293T cells, the surface HLA-E level of the samples co-transfected with the VL9 peptide minigene was over five-fold of the samples co-transfected with the TH9 peptide minigene. However, the effects of the VL9 peptide minigene were blocked in HEK293T cells with TAP or tapasin knocked out, as there was no difference in HLA-E surface expression between samples co-transfected with VL9 or TH9 peptide minigene. This suggests that VL9 peptide minigene promotes ER export of HLA-E through the classical HLA-I transport pathway, where both TAP and tapasin play an important regulatory role.

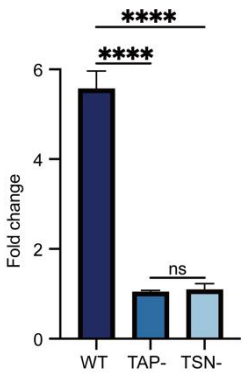

Figure 4.3.10 Increase of surface HLA-E promoted by VL9 minigene peptide depends on TAP and tapasin
HLA-E_EGFP was co-transfected with VL9/TH9 peptide minigenes into WT HEK293T cells or HEK293T cells with TAP or tapasin (TSN) knocked out. 24h after transfection, cells were collected for flow cytometry analysis (gated on GFP+ cells), and surface expression of HLA-E molecules was assessed with 3D12. Fold change in different cell lines was calculated by normalising the surface HLA-E expression in samples co-transfected with the VL9 peptide minigene to that in samples co-transfected with the TH9 peptide minigene. Data were collected for four biological runs and are shown as mean ± SD (error bars). Statistical analysis was performed using one-way ANOVA with Tukey's post-hoc test. Asterisks show the statistical significance between indicated groups: ns, not significant; ****, $P < 0.0001$.

In summary, the intracellular distribution of HLA-E is mainly shaped by the lack of high-affinity peptides. Overexpression of the best HLA-E binding peptide VL9 could completely release HLA-E from the ER via the classical pathway which relies on TAP and tapasin, thus enhancing its surface expression. However, the affinity of VL9 is not high enough to effectively promote the surface stability of HLA-E, leading to its fast surface turnover and enrichment in early endosomes and lysosomes.

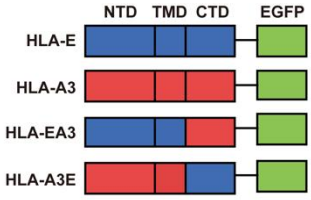

Figure 4.4.1 Schematic representation of different HLA constructs
HLA-EA3 has the N-terminal domain (NTD) and transmembrane domain (TMD) of HLA-E and the cytoplasmic tail (CTD) of HLA-A3. HLA-A3E has the NTD and TMD of HLA-A3 and the CTD of HLA-A3. All constructs were tagged with EGFP on the C-terminus.

4.4 How HLA-E cytoplasmic tail regulates its transport

4.4.1 How HLA-E cytoplasmic tail regulates its transport and shapes its intracellular distribution

To explore if HLA-E trafficking is regulated by its cytoplasmic tail, I swapped the cytoplasmic domains of HLA-E and HLA-A3 and created two chimeric proteins HLA-EA3 and HLA-A3E (Fig.4.4.1). Hela cell lines stably expressing these different constructs were then generated for the following experiments.

4.4.1.1 HLA-E cytoplasmic tail facilitates intracellular accumulation

After obtaining the HLA-A3 cytoplasmic tail, an increase in HLA-E surface expression could be observed (Fig.4.4.2A, B), implying that the HLA-E cytoplasmic tail contributed to its low surface level. However, the effect of the cytoplasmic tail on HLA-E surface expression was less significant compared to high-affinity peptides, as the surface level of HLA-EA3 was approximately 1.7-fold that of HLA-E. Meantime, a decrease in HLA-A3 surface expression was seen after the acquisition of the cytoplasmic tail of HLA-E (Fig.4.4.2C, D). Therefore, the HLA-E cytoplasmic tail contributes to its low surface expression, though the effect is modest.

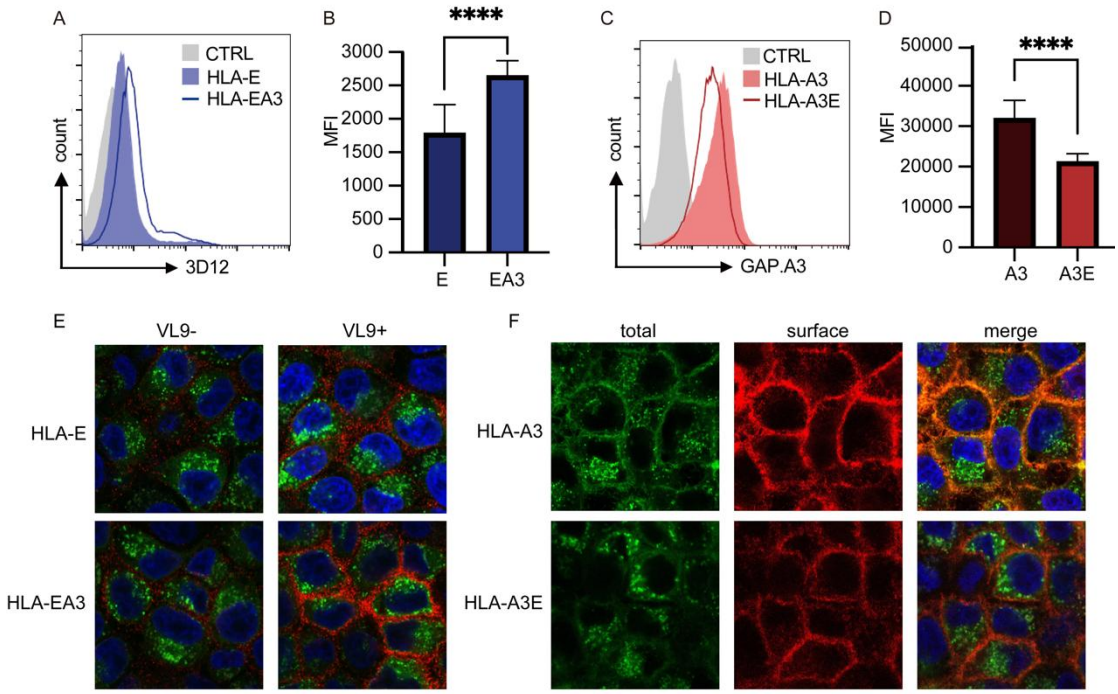

Figure 4.4.2 HLA-E cytoplasmic tail contributes to intracellular accumulation
A-D. HeLa cells stably expressing different HLA molecules were collected for flow cytometry analysis. Surface MFI of HLA-E (light blue area) and HLA-EA3 (dark blue line) assessed using the anti-HLA-E antibody 3D12, and surface MFI of HLA-A3 (light red area) or HLA-A3E (dark red line) assessed using the anti-HLA-A3 antibody GAP.A3. A, C. Histograms are representative of observations made in six experiments. MFI of the unstained sample (grey area) was used as the negative control. B, D. MFIs were collected and plotted for six biological runs, and data are shown as mean ± SD (error bars). Statistical analysis was performed using paired two-tailed student's t-test with Welch's correction. Asterisks show the statistical significance between indicated groups: ****$P < 0.0001$.
E. Hela cells stably expressing different HLA-E or HLA-EA3 were incubated with VL9 peptide (100nM, VL9+) or an equal amount of DMSO (VL9-) overnight. Cells were fixed and surface HLA-E or HLA-EA3 expression was stained with 3D12-APC.
F. Hela cells stably expressing different HLA-A3 or HLA-A3E were fixed and surface HLA-A3 or HLA-A3E expression was stained with GAP.A3-APC.

To confirm this conclusion, I stained the surface HLA-E or HLA-EA3 on HeLa cells stably expressing these constructs and assessed their surface expression level via confocal microscopy (Fig.4.4.2E). Consistent with previous data, the surface signal of HLA-E was almost undetectable. While an increase of surface signal was observed for HLA-EA3, it was still very weak, which is in line with the FACS result that the HLA-EA3 surface level was still low despite being somewhat higher than that of HLA-E (Fig.4.4.2A, B). To increase the sensitivity of the assay, I further incubated these cell lines with the VL9 peptide overnight to enhance the surface expression of HLA-E and HLA-EA3. As expected, a stronger signal detected for HLA-E indicated an increase in its surface level (Fig.4.4.2E). A rise in surface expression was also observed for HLA-EA3, and its surface staining signal was obviously stronger than

that of HLA-E. I also stained the surface HLA-A3 or HLA-A3E on HeLa cells stably expressing these two constructs (Fig.4.4.2E). A very strong surface staining signal was detected for HLA-A3, which was anticipated as most HLA-A3 stays on the cell surface. While HLA-A3E also showed clear surface staining, the signal was lower compared to HLA-A3. To conclude, HLA-E cytoplasmic contributes to its low surface expression and intracellular accumulation.

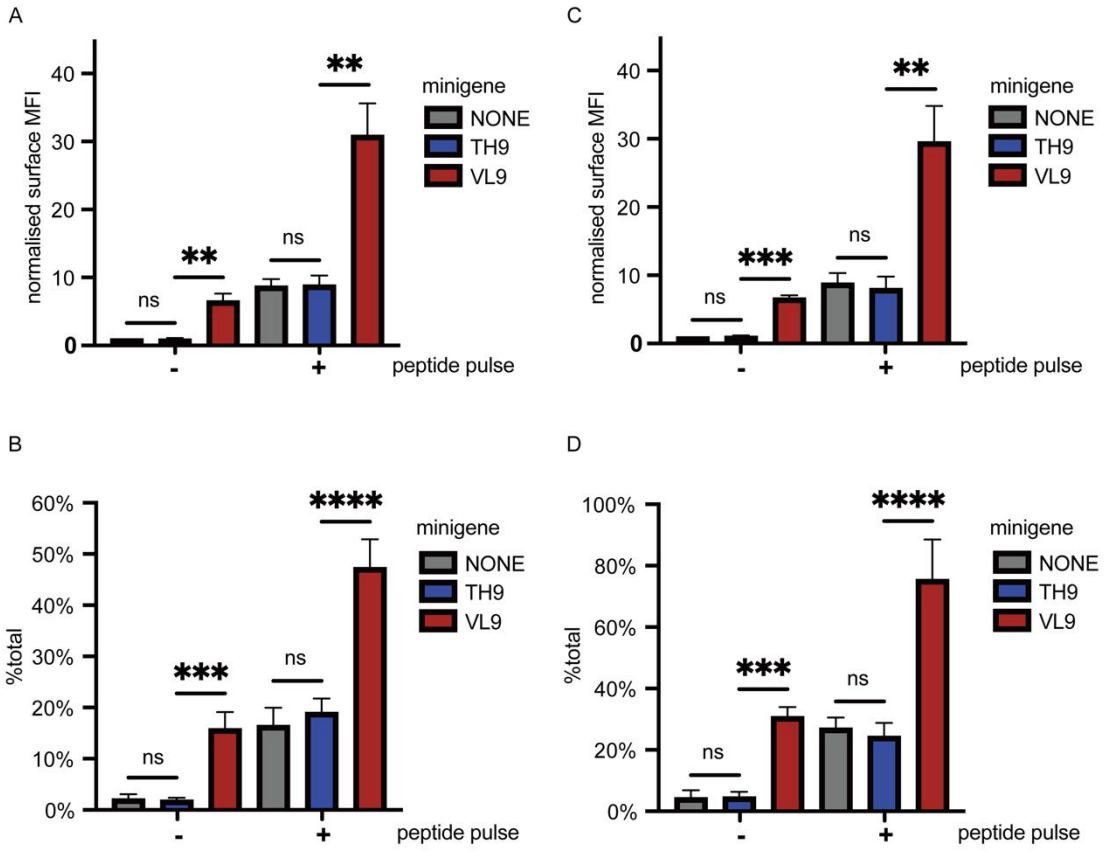

Figure 4.4.3 HLA-E cytoplasmic tail and VL9 peptide affects HLA-E surface expression via different mechanisms
A, B. HEK 293T cells were transiently transfected with HLA-E (NONE, grey), or co-transfected with HLA-E and peptide minigenes VL9 (red) or TH9 (blue). C, D. HEK 293T cells were transiently transfected with HLA-EA3 (NONE, grey), or co-transfected with HLA-EA3 and peptide minigenes VL9 (red) or TH9 (blue). Samples were incubated with VL9 peptide (100nM, peptide pulse+) or an equal amount of DMSO (peptide pulse-) overnight. 24hrs after transfection, cells were collected for flow cytometry analysis (gated on EGFP+ cells). A, C. Surface expression of HLA-E and HLA-EA3 was assessed with anti-HLA-E antibody (3D12), and was normalised to the MFI of the sample with neither minigene co-expression nor peptide pulsing. B, D. The percentage of total HLA-E or HLA-EA3 on the cell surface was calculated by normalising the surface staining signal to that of intracellular staining (total signal), which were both assessed with anti-HLA-E antibody (3D12). MFIs were collected and plotted for four biological runs, and data was shown as mean ± SD (error bars). Statistical analysis was performed using unpaired two-tailed student's t test. Asterisks show the statistical significance between indicated groups, not significant; **, $P < 0.01$; ***, $P < 0.001$; ****, $P < 0.0001$.

4.4.1.2 HLA-E cytoplasmic tail and peptides are the major regulators of HLA-E surface expression level

As tail swapping and VL9 peptide pulsing seemed to have a synergic effect on elevating the surface level of HLA-E (Fig.4.4.2E), I then examined how the combination of high-affinity peptides and tail swapping affect HLA-E surface expression in a quantitative way (Fig.4.4.3). VL9 minigene and VL9 peptide pulsing were used simultaneously to mimic the functions of high-affinity peptides as established in section 4.3.4 (Fig.4.3.8B), which not only effectively promoted the ER exit of HLA-E, but also greatly stabilised HLA-E on the cell surface. Although VL9 minigene and VL9 peptide together resulted in a thirty-fold increase of surface HLA-E level (Fig.4.4.3A), about half of the HLA-E still stayed intracellularly (Fig.4.4.3B), which suggested the existence of other crucial factors contributing to the intracellular accumulation of HLA-E apart from peptide repertoire. As the cytoplasmic tail did not affect peptide binding, tail swapping did not affect the fold change of HLA-E surface level induced by VL9 peptide supply (Fig.4.4.3C). However, around 80% of HLA-EA3 was present on the cell surface given sufficient good peptides (Fig.4.4.3D), which is comparable to that of HLA-Ia. Thus, the shortage of good peptides and the cytoplasmic tail are the two major regulators for the low surface expression of HLA-E.

4.4.1.3 HLA-E cytoplasmic tail contributes to ER retention

To explore whether the HLA-E cytoplasmic tail facilitates its ER retention, which is a major character of the intracellular distribution of HLA-E, I examined the co-localisation of these different chimeric constructs with ER under the confocal microscope (Fig.4.4.4A, B).

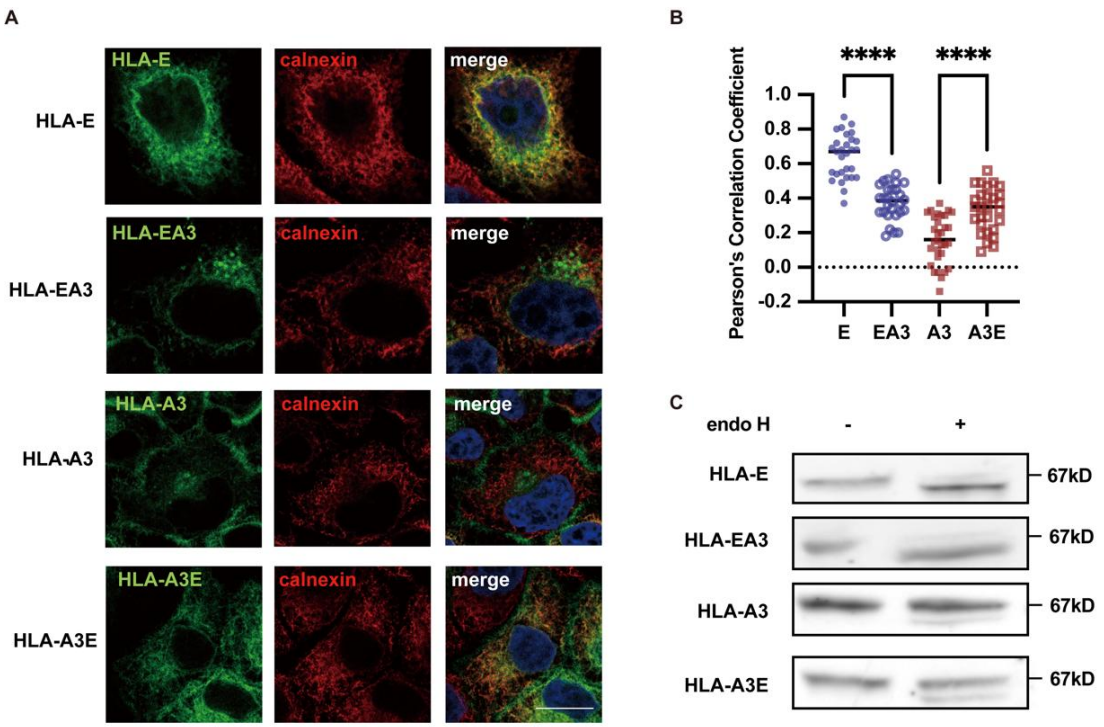

Figure 4.4.4 HLA-E cytoplasmic tail contributes to ER retention
A, B. Hela cells stably expressing different HLA molecules were fixed, permeabilised, and stained with an antibody against the ER marker protein calnexin, followed by detection with an Alexa568-conjugated secondary antibody. A, Representative confocal micrographs of Hela cells stably expressing different HLA molecules. Scale bar = 20 μm. B, Quantification of co-localisation of different constructs with the ER marker protein calnexin. The PCC values of each cell and the mean values are shown with 20-40 cells per sample. Statistical analysis was performed using unpaired two-tailed student's t-test with Welch's correction. Asterisks show the statistical significance between indicated groups: ****P < 0.0001.
C. Lysates of Hela cells stably expressing different HLA molecules were treated with endo H, followed by detection with immunoblotting using an anti-EGFP antibody.

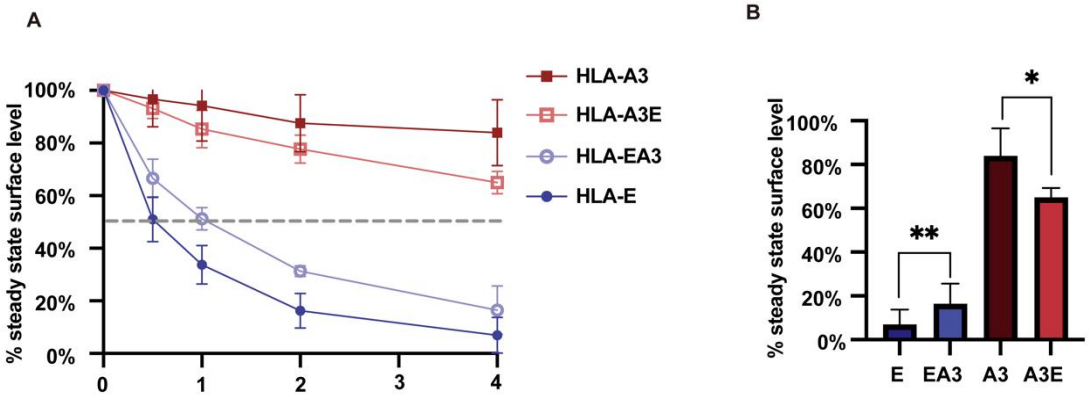

Figure 4.4.5 HLA-E cytoplasmic tail contributes to its surface instability
HeLa cells stably expressing different HLA constructs were incubated in media containing BFA for different time points. Surface expression of HLA-E and HLA-EA3 were assessed using the anti-HLA-E antibody 3D12, and surface MFI of HLA-A3 and HLA-A3E were assessed using the anti-HLA-A3 antibody GAP.A3.
A. The average cell surface MFI for timepoint zero was set to 100% and the following values were normalised as its percentage. The dashed line represents 50%.
B. The percentage of HLA on the cell surface after BFA incubation for 4hrs.
Data were collected for four biological runs and are shown as mean ± SD (error bars). Statistical analysis was performed using unpaired two-tailed student's t-test with Welch's correction. Asterisks show the statistical significance between indicated groups: ns, not significant; *, P < 0.05; **, P < 0.01.

HLA-EA3 was less enriched in the ER compared to HLA-E, implying that HLA-E cytoplasmic tail contributes to its ER retention. However, a significant ER

accumulation was also observed for HLA-EA3, suggesting that while tail swapping could assist HLA-E ER export, other factors are required for its effective ER release, including peptide supply. More HLA-A3E was present in the ER compared to HLA-A3, which further supports the ER-retaining effect of the HLA-E cytoplasmic tail.

ER retention was further verified via the endo H assay (Fig.4.4.4C). As expected, most HLA-E and HLA-EA3 were sensitive to endo H cleavage, implying that most of them are retained in ER, which is consistent with previous results (Fig.4.4.3, Fig.4.4.4A, B). The comparative signal of the cleavage-sensitive band of HLA-EA3 was slighter weaker than that of HLA-E, suggesting that the swapping of the cytoplasmic tail only weakly promoted the ER export of HLA-E. Similarly, while most HLA-A3 and HLA-A3E were insensitive to endo H cleavage, the relative signal of the cleavage insensitive band was stronger for HLA-A3, suggesting that more HLA-A3E was retained in the ER compared to HLA-A3. In conclusion, the HLA-E cytoplasmic tail could facilitate its ER retention, though the effect is moderate.

4.4.1.4 HLA-E cytoplasmic tail contributes to surface instability

Apart from the influence on ER export, how the cytoplasmic tail affects the turnover of surface HLA molecules was also assessed. BFA decay assay was performed for different constructs to determine if the cytoplasmic tails of HLA-A3 and HLA-E affect HLA surface stability differently (Fig.4.4.5). While the half-life of surface HLA-E was around 30 mins, the surface half-life of HLA-EA3 was around one hour, implying that the cytoplasmic tail of HLA-E made HLA molecules less stable on the cell surface compared to that of HLA-A3. In contrast, less than 10% of HLA-A3 was endocytosed after 4hrs, whilst about 30% of HLA-A3E was endocytosed within the same timeframe. Therefore, the cytoplasmic tail of HLA-E contributes to its surface instability.

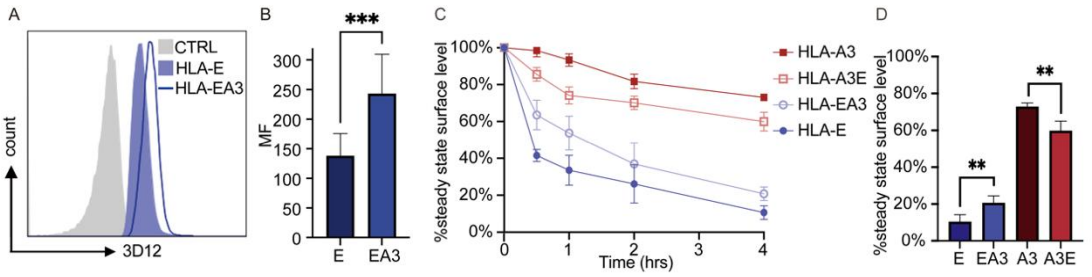

Figure 4.4.6 EGFP tagging does not seem to distort the functions of HLA-E cytoplasmic tail
A, B. HEK293T cells were transiently co-transfected with EGFP and HLA-E or HLA-EA3 constructs without EGFP tagging. 24hrs after transfection, cells were collected for flow cytometry analysis (gated on GFP+ cells), and surface expression of HLA-E and HLA-EA3 were assessed with anti-HLA-E antibody (3D12). A, Representative graph of surface MFI of HLA-E (light blue area) and HLA-EA3 (dark blue line). MFI of unstained samples (grey area) was used as negative control. B, MFIs were collected and plotted for five biological runs, and data was shown as mean ± SD (error bars).
C, D. HEK293T cells were transiently co-transfected with EGFP and different HLA constructs without EGFP tagging. 24hrs after transfection, cells were incubated in media containing BFA for different time points. Surface expression of HLA-E and HLA-EA3 were assessed using the anti-HLA-E antibody 3D12, and surface MFI of HLA-A3 and HLA-A3E were assessed using the anti-HLA-A3 antibody GAP.A3. C, The average cell surface MFI for timepoint zero was set to 100% and the following values were normalised as its percentage. D, The percentage of HLA on the cell surface after BFA incubation for 4hrs. Data were collected for six biological runs and are shown as mean ± SD (error bars).
Statistical analysis was performed using paired (B) or unpaired (D) two-tailed student's t test. Asterisks show the statistical significance between indicated groups: **, $P < 0.01$; ***, $P < 0.001$.

As EGFP tagging might interfere with the interactions involved in the regulation of endocytosis and block the effects of the cytoplasmic tail, I assessed the potential effect of the EGFP tag before further exploration of the functions of the cytoplasmic tail (Fig.4.4.6). Plasmids expressing HLA-E, HLA-EA3, HLA-A3 and HLA-A3E HC alone without EGFP tagging were constructed. I then transiently transfected HLA-E and HLA-EA3 into HEK293T cells and measured their surface expression level (Fig.4.4.6A, B). The surface level of HLA-EA3 is about 1.8-fold that of HLA-E, which resembles the effect of tail swapping between constructs with EGFP tagging (Fig.4.4.2A, B). This suggests that the functions of the motifs potentially involved in regulating HLA-E transport did not seem to be affected by EGFP tagging. I also repeated the BFA decay assay using these constructs without EGFP tagging (Fig.4.4.6C, D), and the result is consistent with that of the constructs with EGFP tagging (Fig.4.4.5). Therefore, the regulatory functions of HLA-E cytoplasmic tail on surface turnover seem to be preserved in the presence of EGFP tagging.

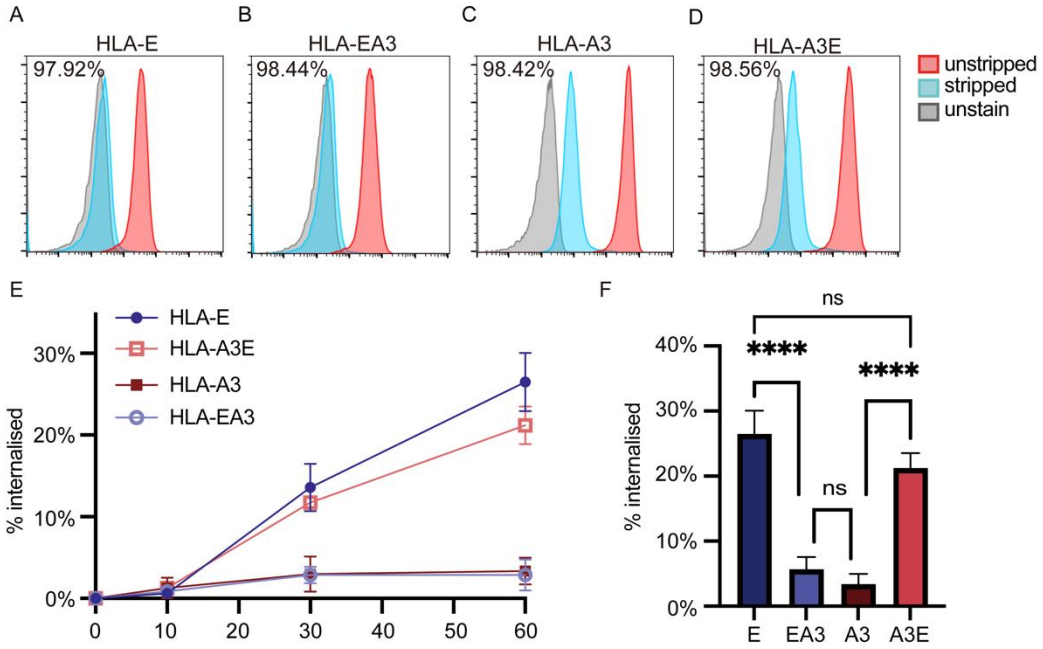

Figure 4.4.7 HLA-E cytoplasmic tail plays a major role in determining its fast internalisation
A-D. Surface HLA molecules of Hela cells stably expressing different constructs were exposed to citric acid for 3mins to strip off surface proteins (blue). After neutralisation and washing, cells were collected for flow cytometry. Surface expression of HLA-E and HLA-EA3 were assessed using the anti-HLA-E antibody 3D12, and surface MFI of HLA-A3 and HLA-A3E were assessed using the anti-HLA-A3 antibody GAP.A3. Unstripped samples (red) and unstained samples (gray) were used as positive and negative controls respectively. The stripping efficiency was calculated as shown in Fig.3.3.13(C) and is shown on the upper left corner of each histogram.
E, F. Surface HLA molecules of Hela stable cell lines were labeled, and then the cells were incubated in media containing primaquine. After different time points of internalisation, samples were collected, and uninternalised surface antibody-HLA complexes were stripped off using citric acid. E, The MFI of antibody-labeled cells without acid stripping was set to 100%, and the MFI of antibody-labeled cells with acid stripping but without internalisation was set to 0%. The percentage of internalisation was quantified by the normalisation of MFI increase accordingly. F, The percentage of HLA internalised after one hour. Data were collected for four biological runs and are shown as mean ± SD (error bars). Statistical analysis was performed using one-way ANOVA with Tukey's post-hoc test. Asterisks show the statistical significance between indicated groups, not significant; ****, $P < 0.0001$.

4.4.1.5 HLA-E cytoplasmic tail promotes fast internalisation and recycling of surface HLA molecules

As fast internalisation might be the major contributor to the fast surface turnover of HLA-E, I employed an acid stripping assay as previously described (Ma et al. 2016) to explore if the cytoplasmic tail of HLA-E affects internalisation (Fig.4.4.7). Efficiency of acid stripping was firstly tested in HeLa cells stably expressing these constructs following the method described in section3.3.3.3 (Fig.3.3.16). Acid stripping was effective in these cell lines, as around 98% of surface HLA could be stripped off without obvious influence on the cell viability (Fig.4.4.7A-D). Rapid internalisation could be observed for both HLA-E and HLA-A3E, with over 20% internalised within one hour (Fig.4.4.7E, F). In contrast, the internalisation rate of

HLA-A3 and HLA-EA3 was much slower, with less than 5% internalised after one hour. The cytoplasmic tail seemed to be the main regulator of the fast internalisation of HLA-E, as tail swapping almost completely reversed the internalisation rate between HLA-E and HLA-A3.

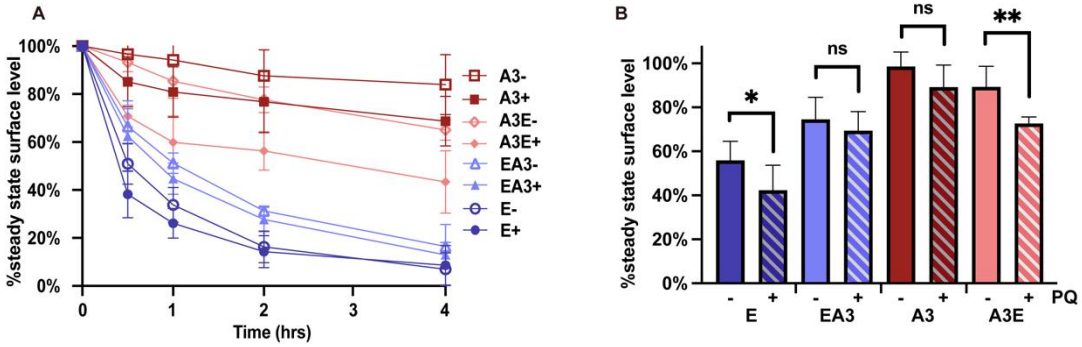

Figure 4.4.8 HLA-E cytoplasmic tail might facilitate the recycling pathway
HeLa cells stably expressing different HLA constructs were incubated in media containing BFA with ("+") or without ("-") primaquine (PQ) for different time points. Surface expression of HLA-E and HLA-EA3 were assessed using the anti-HLA-E antibody 3D12, and surface MFI of HLA-A3 and HLA-A3E were assessed using the anti-HLA-A3 antibody GAP.A3.
A. The average cell surface MFI for timepoint zero was set to 100% and the following values were normalized as its percentage.
B. The percentage of HLA on the cell surface after BFA incubation for 30mins.
Data were collected for six biological runs and are shown as mean ± SD (error bars). Statistical analysis was performed using unpaired two-tailed student's t test. Asterisks show the statistical significance between indicated groups, not significant; *, $P < 0.05$; **, $P < 0.01$.

I also explored how the cytoplasmic tail of HLA-E regulates the recycling of HLA molecules, which is another factor influencing surface stability apart from internalisation. Given the limited surface signal of HLA-E, the acid stripping method (Zagorac et al. 2012) was not sensitive enough to test how the cytoplasmic tail affects the recycling rate of HLA-E. Therefore, I repeated the BFA decay assay with or without the inhibition of the recycling pathway via primaquine (PQ) addition, as described in section 3.3.3.2 (Fig.3.3.15). PQ decreased HLA-E surface stability at early time points but did not seem to significantly affect HLA-E surface stability at later time points (Fig.4.4.8), implying that a fast-recycling pathway might exist for HLA-E. In contrast, PQ did not seem to affect the recycling of HLA-EA3, suggesting that the potential fast recycling of HLA-E seemed to be mainly dependent on its cytoplasmic tail.

HLA-A3 and HLA-A3E seemed more affected by PQ compared to HLA-E and HLA-EA3, as the decrease of surface stability after PQ addition was more significant (Fig.4.4.8A). This suggests that a higher percentage of internalised HLA-A3 and HLA-A3E were recycled back to the cell surface, which is possibly due to a high percentage of fully-conformed HLA-A3 molecules compared to HLA-E (Zagorac et al. 2012). HLA-A3E seemed more sensitive to PQ than HLA-A3 at early time points, suggesting that more HLA-A3E could be recycled back to the cell surface shortly after internalisation. 30 mins after PQ addition, a significant decrease in surface stability could be observed for HLA-E and HLA-A3E, but not for HLA-EA3 and HLA-A3 (Fig.4.4.8B), implying that HLA-E cytoplasmic tail may facilitate a fast-recycling pathway for internalised HLA molecules. However, given the small percentage of surface HLA-I molecules recycled back to the cell surface, the assay was not sensitive enough to allow for a persuasive conclusion here. Further experiments and analysis are required to figure out the effect of the HLA-E cytoplasmic tail on the recycling pathway.

Therefore, while the cytoplasmic tail of HLA-E plays the deciding role in the enhancement of fast internalisation of surface HLA-I molecules, its promotion on a fast recycling pathway is less significant and needs further analysis.

4.4.1.6 HLA-E cytoplasmic tail contributes to its enrichment in late endosomes and recycling endosomes

As the HLA-E cytoplasmic tail is involved in the regulation of endosomal trafficking, I investigated how it influences the intracellular distribution of HLA-I molecules in different endosomal compartments by co-localising these chimeric constructs with different endosomal markers (Fig.4.4.9). While HLA-E was more enriched in late endosomes and recycling endosomes compared to HLA-A3, there was no difference in terms of enrichment in either of these compartments between HLA-E and

HLA-A3E (Fig.4.4.9B, D, F, H). This is in accordance with the functions of the HLA-E cytoplasmic tail, as the increase in internalisation and recycling might lead to the enrichment of late endosomes and recycling endosomes. While HLA-EA3 is less enriched in recycling endosomes compared to HLA-E, the late endosomal enrichment was retained, implying that other factors apart from the cytoplasmic tail could also lead to the enrichment of HLA-E in late endosomes. The slight difference between

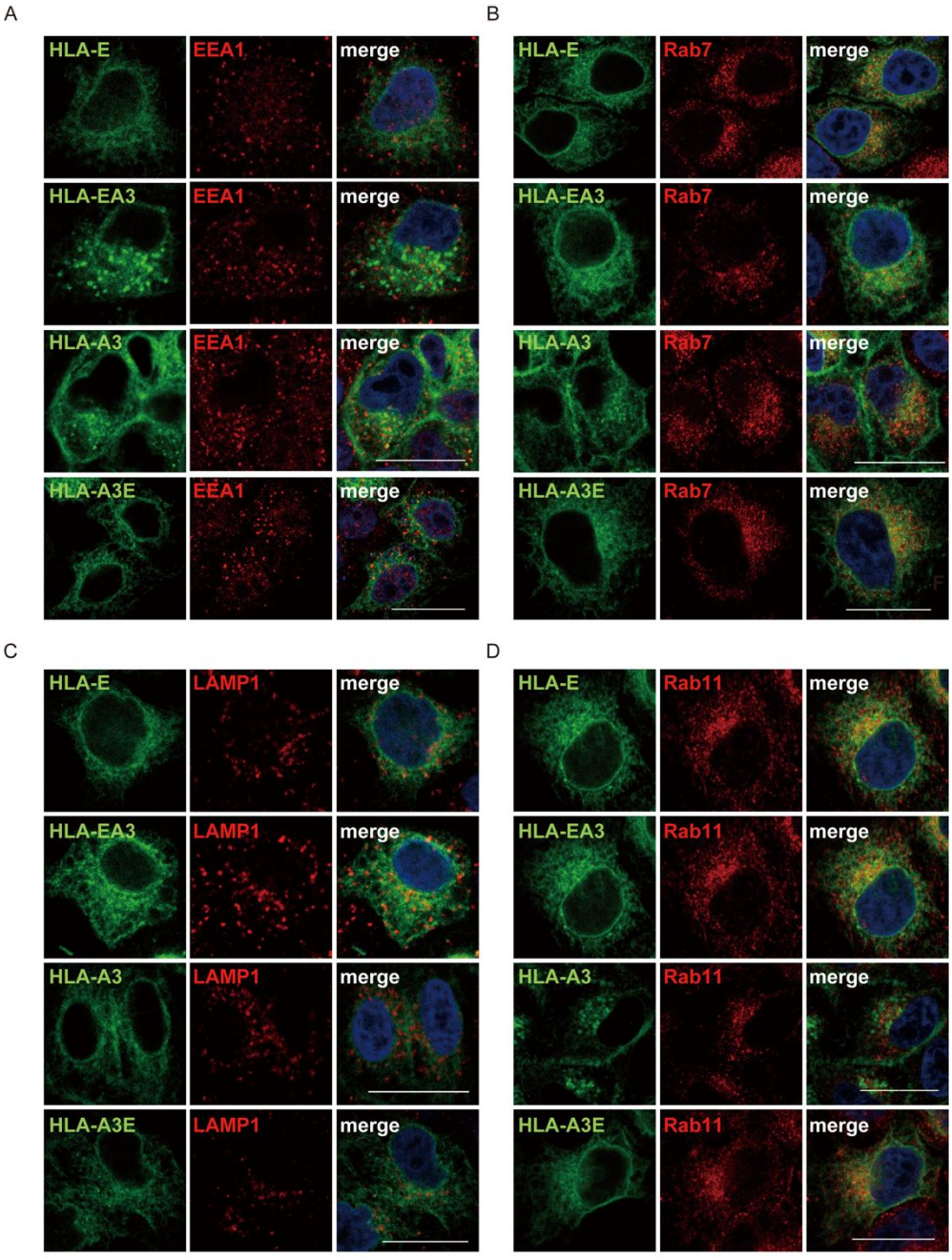

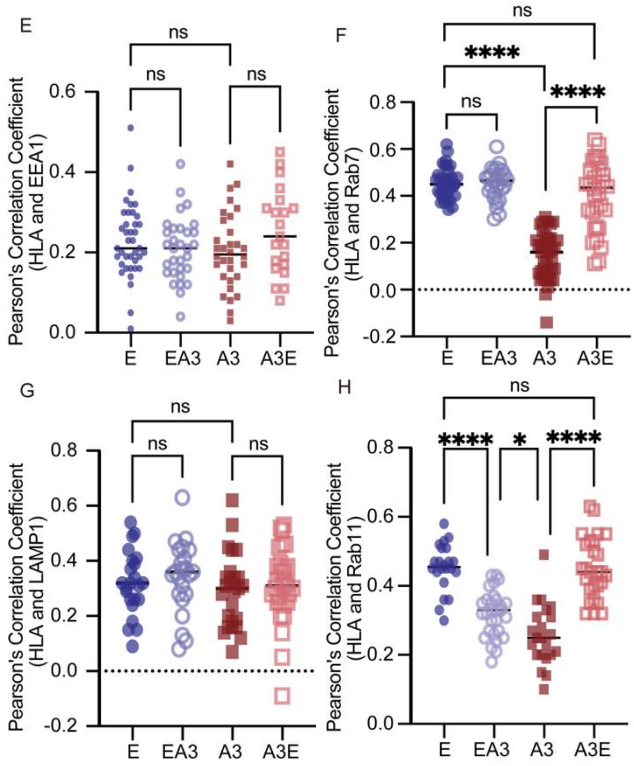

Figure 4.4.9 HLA-E cytoplasmic tail facilitates endosomal enrichment
Hela cells stably expressing different HLA constructs were fixed, permeabilised, and stained with antibodies against protein markers for early endosome (EEA1), late endosome (Rab7), lysosome (LAMP1), or recycling endosome (Rab1). Cells were then stained with Alexa568-conjugated secondary antibody.
A-D. Representative confocal micrographs of different HLA constructs co-localising with early endosome (A), late endosome (B), lysosome (C) or recycling endosome (D) under different conditions. Scale bar = 20 μm.
E-H. Quantification of co-localisation of different HLA constructs with early endosome (E), late endosome (F), lysosome (G) or recycling endosome (H). The PCC values of each cell and the mean values are shown with 20-40 cells per sample.
Statistical analysis was performed using one-way ANOVA with Tukey's post-hoc test. Asterisks show the statistical significance between indicated groups: ns, not significant; *, $P < 0.05$; ****,

HLA-EA3 and HLA-A3 in the enrichment of recycling endosomes also suggests the existence of other regulatory factors in the recycling pathway. No difference was observed for the distribution in early endosomes and lysosomes (Fig.4.4.9A, C, E, G). To conclude, the HLA-E cytoplasmic tail plays a crucial role in shaping the endosomal distribution of HLA-I molecules, contributing to its enrichment in late endosomes and recycling endosomes.

4.4.1.7 The TAP/tapasin-independent surface expression of HLA-E does not require its cytoplasmic tail

Given that the surface expression of HLA-E did not seem to be affected in the absence of TAP or tapasin in WT HEK293T cells (Fig.3.3.19; Fig.3.3.20), I then explored whether such TAP/tapasin-independent surface trafficking of HLA-E is regulated by its cytoplasmic tail. Chimeric HLA constructs were transfected into HEK293T cells with TAP or tapasin knocked out (Fig.4.4.10), and their surface level was measured. The shortage of TAP or tapasin did not seem to affect the surface expression of

HLA-E and HLA-EA3, while the surface expression of HLA-A3 and HLA-A3E was significantly inhibited, which suggests that the TAP/tapasin-independent surface expression of HLA-E does not rely on its cytoplasmic tail. While a small amount of HLA-A3 and HLA-A3E could get to the cell surface in the absence of TAP, no signal could be detected in HEK293T cells with tapasin knocked out. This indicates that the reliance of HLA-A3 on tapasin is higher than that of TAP, though both are required for its normal surface expression. Therefore, the cytoplasmic tail of HLA-E does not seem to contribute to its non-canonical, TAP/tapasin-independent transport.

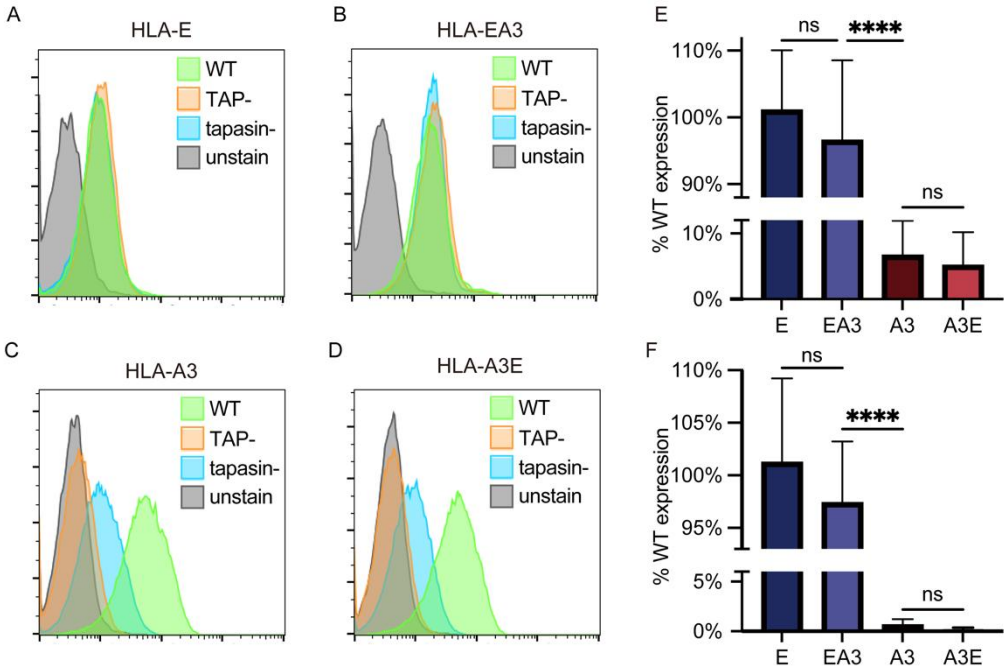

Figure 4.4.10 The TAP/tapasin-independent transport of HLA-E does not depend on its cytoplasmic tail
Chimeric HLA contructs were transiently transfected into WT HEK293T cells or HEK293T cells with TAP or tapasin knocked out. 24hrs after transfection, cells were collected for flow cytometry analysis (gated on EGFP+ cells), and surface expression of HLA molecules were assessed with either anti-HLA-E antibody (3D12) or anti-HLA-A3 antibody (GAP.A3).
A-D. Representative histograms of the surface MFI of HLA-E (A), HLA-EA3 (B), HLA-A3 (C) or HLA-A3E (D) in different different HEK293T cells. Unstained samples were used as the negative control.
E, F. Surface MFIs of different constructs in WT HEK293T cells were set to 100%, and their surface expression in HEK293T cells with TAP (E) or tapasin (F) knocked out was normalised as its percentage. Data were collected for three biological runs and are shown as mean ± SD (error bars). Statistical analysis was performed using one-way ANOVA with Tukey's post-hoc test. Asterisks show the statistical significance between indicated groups: ns, not significant; ****, $P < 0.0001$.

Taken together, the ER-retaining effect and surface-destabilising effect of the HLA-E cytoplasmic tail together contribute to the intracellular accumulation of HLA-E, of which the pathways are independent of TAP and tapasin. The cytoplasmic tail of

HLA-E accelerates both the internalisation and recycling of surface HLA molecules, with an overall decrease in surface stability. While it is the major determinant of the internalisation rate of surface HLA-I molecules, its influence on the recycling process seems to be minor. The regulatory effects of HLA-E cytoplasmic tail on the endosomal pathways lead to its enrichment in late endosomes and recycling endosomes.

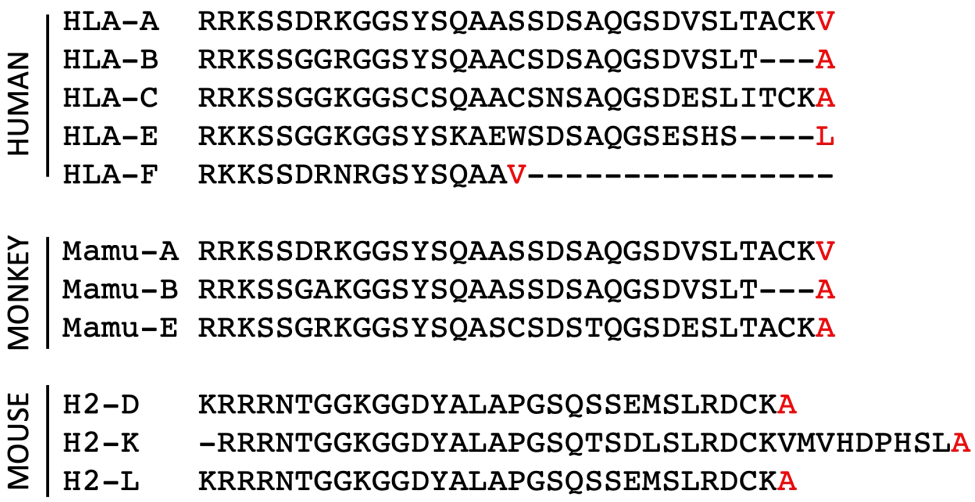

Figure 4.4.11 Sequences of the cytoplasmic tail of different MHC-I molecules in different species

4.4.2 Crucial motifs for the special regulatory functions of HLA-E cytoplasmic tail

4.4.2.1 The ER-retaining effect of the HLA-E cytoplasmic tail results from the lack of a C-terminal ER export motif

ER export of the non-classical MHC-Ib molecule HLA-F is dependent on the C-terminal valine in the cytoplasmic tail (Boyle et al. 2006; Cho et al. 2011). Although HLA-A/B/C can exit the ER through bulk flow, the C-terminal valine/alanine motif makes this process more efficient by binding to structural components of the COPII complex (Cho et al. 2011). Surprisingly, while this C-terminal valine/alanine motif is well-conserved among different MHC-I molecules (Fig.4.4.11), HLA-E possesses a leucine at its C-terminal. To determine whether the

lack of a C-terminal valine/alanine motif contributes to HLA-E ER retention, I mutated the C-terminal leucine of HLA-E to valine (L337V), as well as mutated the C-terminal valine of HLA-EA3 to leucine (V337L) (Fig.4.4.12). EGFP was not linked to the C-terminus of these constructs in case of any potential influence of EGFP tagging on the functions of the C-terminal motif. The obtainment of the C-terminal motif led to a slight increase in HLA-E surface expression (Fig.4.4.13A, B). Similarly, losing the C-terminal motif resulted in a slight decrease in HLA-EA3 surface expression (Fig.4.4.13C, D). Therefore, the lack of a C-terminal motif contributed to the intracellular accumulation of HLA-E.

HLA-E	RKKSSGGKGGSYSKAEWSDSAQCSESHSL
HLA-E L337V	RKKSSGGKGGSYSKAEWSDSAQCSESHSV
HLA-EA3	RRKSSDRKGGSYSQAASSDSAQGSDVSLTACKV
HLA-EA3 V337L	RRKSSDRKGGSYSQAASSDSAQGSDVSLTACKL

Figure 4.4.12 Sequence of the cytoplasmic tail of different constructs
The final amino acids are highlighted in red.

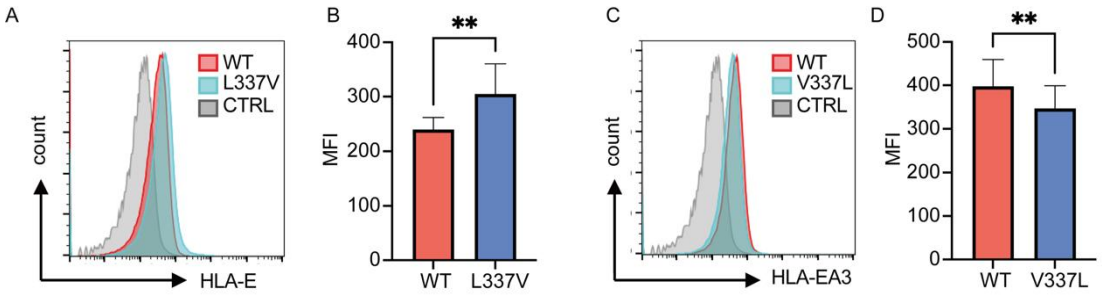

Figure 4.4.13 Lack of the C-terminal amino acid motif contributes to intracellular accumulation of HLA-E
A, B. HEK 293T cells were transiently co-transfected with EGFP and HLA-E WT (red) or HLA-E L337V (blue). 24hrs after transfection, cells were collected for flow cytometry analysis (gated on GFP+ cells), and surface expression of different constructs were assessed with anti-HLA-E antibody (3D12). A, Representative graph of surface MFI of HLA-E WT (red) or HLA-E L337V (blue). MFI of unstained sample (grey area) was used as the negative control. B, MFIs were collected and plotted for six biological runs, and data was shown as mean ± SD (error bars).
C, D. HEK 293T cells were transiently co-transfected with EGFP and HLA-EA3 WT (red) or HLA-EA3 V337L (blue). 24hrs after transfection, cells were collected for flow cytometry analysis (gated on GFP+ cells). Surface expression of different constructs were assessed with anti-HLA-E antibody (3D12). C, Representative graph of surface MFI of HLA-EA3 WT (red) or HLA-EA3 V337L (blue). MFI of unstained sample (grey, CTRL) was used as the negative control. D, MFIs were collected and plotted for six biological runs, and data was shown as mean ± SD (error bars).
Statistical analysis was performed using paired two-tailed student's t-test with Welch's correction. Asterisks show the statistical significance between indicated groups: **P < 0.01.

I then made another version of these constructs with EGFP linked to the C-terminus and tested the effect of EGFP tagging on the C-terminal motif (Fig.4.4.14). Similarly, the L337V mutation in HLA-E increased its surface level, whereas the V337L mutation in HLA-EA3 decreased its surface level. These results suggest that the

functions of the C-terminal motif were preserved in the presence of EGFP tagging, and the constructs with EGFP tagging were therefore applied in the following experiments.

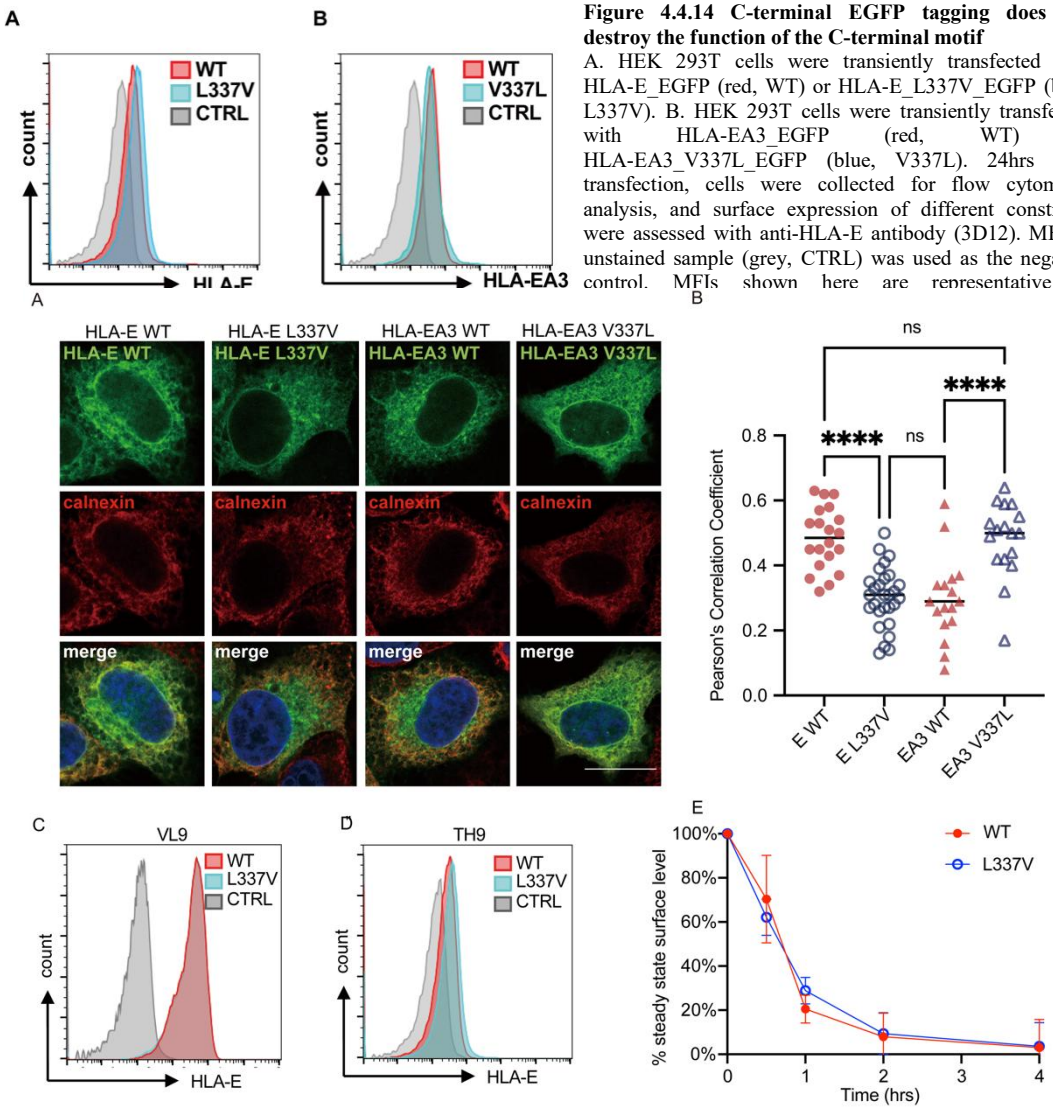

Figure 4.4.14 C-terminal EGFP tagging does not destroy the function of the C-terminal motif
A. HEK 293T cells were transiently transfected with HLA-E_EGFP (red, WT) or HLA-E_L337V_EGFP (blue, L337V). B. HEK 293T cells were transiently transfected with HLA-EA3_EGFP (red, WT) or HLA-EA3_V337L_EGFP (blue, V337L). 24hrs after transfection, cells were collected for flow cytometry analysis, and surface expression of different constructs were assessed with anti-HLA-E antibody (3D12). MFI of unstained sample (grey, CTRL) was used as the negative control. MFIs shown here are representative of

Figure 4.4.15 C-terminal amino acid of HLA-E contributes to its ER retention
A, B. HeLa cells were transiently transfected with HLA-E_EGFP, HLA-E L337V_EGFP, HLA-EA3_EGFP, or HLA-EA3 V337L_EGFP. Cells were fixed, permeabilised, stained with Abs against the ER marker protein calnexin, followed by detection with Alexa568-conjugated secondary antibody. A, Representative confocal micrographs of different constructs. B, Quantification of co-localisation of different constructs with the ER marker protein calnexin. The PCC values of each cell and the mean values are shown with 20-40 cells per sample. Scale bars = 20 µm. Statistical analysis was performed using one-way ANOVA with Tukey's post-hoc test. Asterisks show the statistical significance between indicated groups: ns, not significant; ****, $P < 0.0001$.
C, D. HEK 293T cells were transiently co-transfected with HLA-E WT (red) or HLA-E L337V (blue) with peptide minigene VL9(C) or TH9(D). 24hrs after transfection, cells were collected for flow cytometry analysis (gated on EGFP+ cells), and surface expression of different constructs was assessed with anti-HLA-E antibody (3D12). MFI of unstained sample (grey, CTRL) was used as the negative control. MFIs shown here are representative of observations made in three experiments.
E. HEK 293T cells were transiently transfected with HLA-E_EGFP (red) or HLA-E L337V_EGFP (blue). 24hrs after transfection, cells were incubated in media containing BFA. Surface expression of different constructs (gated on EGFP+ cells) was assessed with anti-HLA-E antibody (3D12). The average cell surface MFI for timepoint zero was set to 100% and the following values were normalised as its percentage. Data were collected and plotted for three biological runs and were shown as mean ± SD (error bars).

To investigate whether the C-terminal valine could facilitate the ER export of HLA-E, I co-localised different constructs with the ER via the confocal microscope (Fig.4.4.15A, B). Although most HLA-E was still in the ER after the obtainment of the C-terminal valine motif, a decrease in enrichment could be observed, suggesting that the C-terminal motif could play a subsidiary role in assisting ER export. Likewise, the loss of the C-terminal motif led to higher ER retention of HLA-EA3. Furthermore, the mutation of the C-terminal amino acid seemed to be sufficient to reverse the ER enrichment level of HLA-E and HLA-EA3, as a similar level of ER co-localisation was observed between HLA-E and HLA-EA3 V337L as well as between HLA-EA3 and HLA-E L337V (Fig.4.4.15B). This implies that the ER-retaining effect of the HLA-E cytoplasmic tail entirely results from the lack of a C-terminal ER export motif.

To further examine the effectiveness of the C-terminal valine motif in releasing HLA-E from the ER, I co-expressed HLA-E WT and HLA-E L337V constructs with different peptide minigenes (Fig.4.4.15C, D). When co-expressed with the VL9 peptide minigene, no difference in surface expression between HLA-E WT and HLA-E L337V was observed (Fig.4.4.15C). As the VL9 peptide minigene could potently enhance HLA-E surface expression by promoting ER release (Fig.4.3.1; Fig.4.3.3), the blockage of the effect of the C-terminal valine motif suggests that this motif functions in the same way to promote HLA-E surface expression but much less efficient compared to the VL9 peptide. The co-expression of the TH9 peptide did not abolish the effect provided by the L337V mutation (Fig.4.4.15D). These results further supported the ER export-promoting effect of the C-terminal valine motif.

To examine whether the C-terminal motif also promotes the HLA-E surface level via promoting its surface stability, a BFA decay assay was carried out (Fig.4.4.15E). The surface stability of HLA-E L337V was similar to that of HLA-E, which excludes the possibility that the leucine-to-valine substitution affects HLA-E surface stability.

Therefore, the C-terminal valine motif increases HLA-E surface expression solely by promoting its ER export.

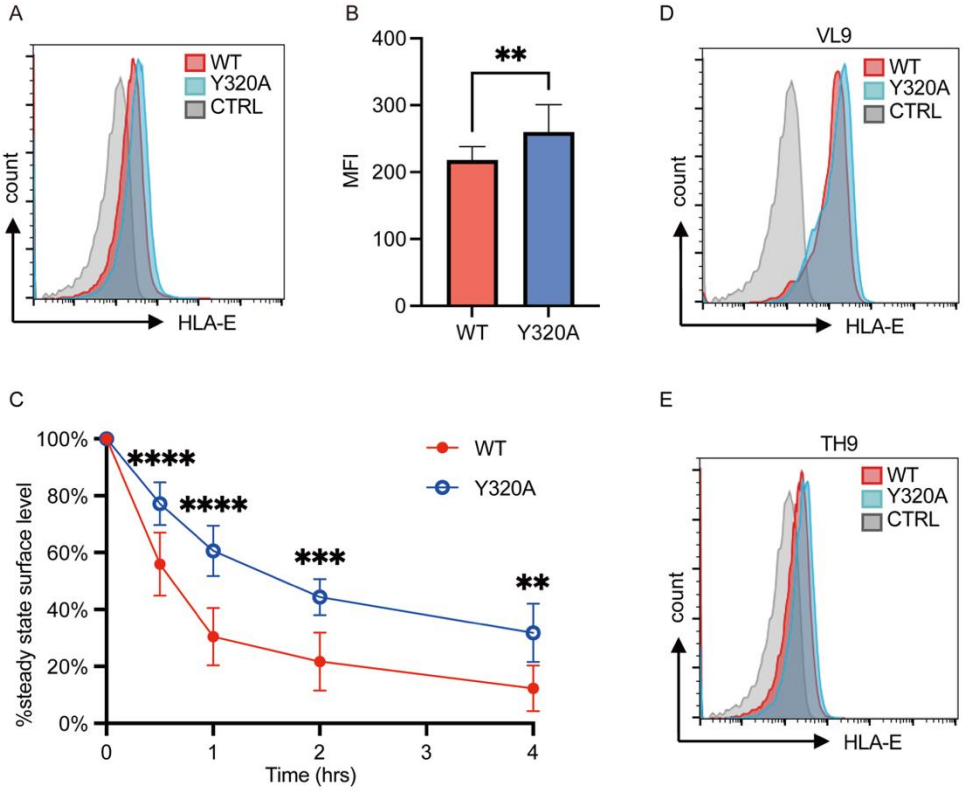

Figure 4.4.16 Function of the tyrosine-based motif in the cytoplasmic tail in the regulation of transport
A, B. HEK 293T cells were transiently transfected with HLA-E (red) or HLA-E Y320A (blue). 24hrs after transfection, cells were collected for flow cytometry analysis (gated on EGFP+ cells), and surface expression of different constructs was assessed with anti-HLA-E antibody (3D12). A, Representative graph of surface MFI of HLA-E WT (red) or HLA-E Y320A (blue). MFI of unstained sample (grey, CTRL) was used as the negative control. MFIs shown here are representative of observations made in three experiments. B, MFIs were collected and plotted for three biological runs, and data was shown as mean ± SD (error bars).
C. HEK 293T cells were transiently transfected with HLA-E (red) or HLA-E Y320A (blue). 24hrs after transfection, cells were incubated in media containing BFA. Surface expression ofdifferent constructs (gated on EGFP+ cells) was assessed with anti-HLA-E antibody (3D12). The average cell surface MFI for timepoint zero was set to 100% and the following values were normalised as its percentage. Data were collected and plotted for ten biological runs and were shown as mean ± SD (error bars).
D, E. HEK 293T cells were transiently co-transfected with HLA-E WT (red) or HLA-E Y320A (blue) with peptide minigene VL9(D) or TH9(E). 24hrs after transfection, cells were collected for flow cytometry analysis (gated on EGFP+ cells), and surface expression of different constructs molecules was assessed with anti-HLA-E antibody (3D12). MFI of unstained samples (grey, CTRL) was used as the negative control. MFIs shown here are representative of observations made in three experiments.
Statistical analysis was performed using paired two-tailed student's t-test with Welch's correction. Asterisks show the statistical significance between indicated groups: **, $P < 0.01$; ***, $P < 0.001$; ****, $P < 0.0001$.

To further validate the methods adopted here to examine the functions of the C-terminal valine, I also mutated the tyrosine at position 320 to arginine in HLA-E (Y320A) and analysed the effects of the mutation (Fig.4.4.16). This mutation disrupts a conserved tyrosine-based motif that is crucial for the endosomal targeting of surface HLA-I molecules and increases HLA-I surface expression (Lizée et al. 2003; Santos et al. 2006). An increase in surface expression and surface stability was observed in HLA-E Y320A compared to HLA-E (Fig.4.4.16A-C), which is in line with the function of the tyrosine-based motif in facilitating endocytosis. In contrast to the L337V mutation, the surface-promoting effect of the Y320A mutation was not diminished by minigene co-expression (Fig.4.4.16A, D, E). The additive surface-promoting effect of Y320A mutation and VL9 peptide expression is in accordance with the fact that they promote HLA-E surface expression via different mechanisms.

Taken together, our data suggest that the moderate ER-retaining effect of the HLA-E cytoplasmic tail results from the lack of a C-terminal valine/alanine motif, and such an effect can be masked in the presence of a good peptide supply.

4.4.2.2 HLA-E cytoplasmic tail requires both exon6 and exon7 to promote internalisation

I explored the motif that is responsible for promoting the fast internalisation of HLA-E in a systematic way, as no well-characterised, HLA-E-unique motifs were found in its cytoplasmic tail. As the cytoplasmic tail of HLA-I molecules contains two exons (Fig.4.4.17), in which exon6 is comparatively more conserved than exon7, I

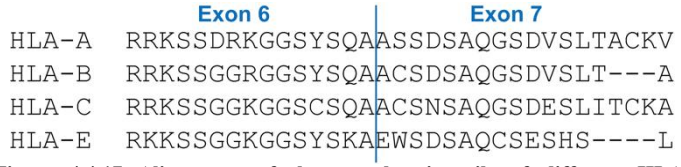

Figure 4.4.17 Alignments of the cytoplasmic tails of different HLA constructs

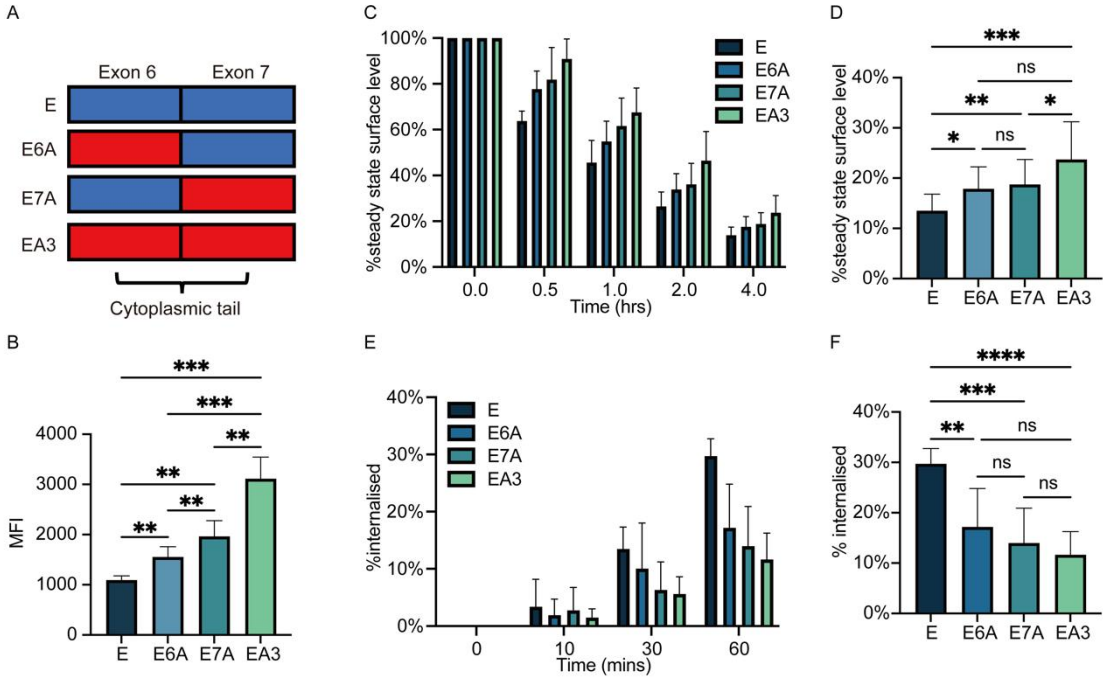

Figure 4.4.18 Both exon6 and exon7 of the cytoplasmic tail contributes to the fast surface turnover of HLA-E
A. Schematic representation of different HLA constructs. Exons from HLA-E and HLA-A3 are indicated in blue and red respectively. The cytoplasmic tail of E6A has exon6 from HLA-E and exon7 from HLA-A3; The cytoplasmic tail of E7A has exon6 from HLA-A3 and exon7 from HLA-E.
B. HEK 293T cells were transiently transfected with different constructs. 24hrs after transfection, cells were collected for flow cytometry analysis (gated on EGFP+ cells), and surface expression of different constructs was assessed with anti-HLA-E antibody (3D12). MFIs were collected and plotted for six biological runs, and data was shown as mean ± SD (error bars).
C, D. HEK 293T cells were transiently transfected with different constructs. 24hrs after transfection, cells were incubated in media containing BFA for different time points, and surface expression of different constructs was assessed with anti-HLA-E antibody (3D12). C, The average cell surface MFI for timepoint zero was set to 100% and the following values were normalised as its percentage. D, The percentage of HLA on the cell surface after BFA incubation for 4hrs. Data were collected for eight biological runs and are shown as mean ± SD (error bars).
E, F. HEK 293T cells were transiently transfected with different constructs. 24hrs after transfection, surface HLA molecules were labeled with anti-HLA-E antibody 3D12, and then the cells were incubated in media containing primaquine. After different time points of internalisation, samples were collected, and uninternalised surface antibody-HLA complexes were stripped off using citric acid. E, The MFI of antibody-labeled cells without acid stripping was set to 100%, and the MFI of antibody-labeled cells with acid stripping but without internalisation was set to 0%. The percentage of internalisation was quantified by the normalisation of MFI increase accordingly. F, The percentage of HLA internalised after one hour. Data were collected for six biological runs and are shown as mean ± SD (error bars).
Statistical analysis was performed using one-way ANOVA with Tukey's post-hoc test. Asterisks show the statistical significance between indicated groups: ns, not significant; *, $P < 0.05$; **, $P < 0.01$; ***, $P < 0.001$; ****, $P < 0.0001$.

firstly explored which exon is crucial for the fast internalisation of HLA-E.

I swapped the exon6 and exon7 of HLA-E to that of HLA-A3 and created two constructs named HLA-E6A and HLA-E7A (Fig.4.4.18A). The obtainment of either exon6 or exon7 from HLA-A3 increased the surface expression level of HLA-E but less effectively than the obtainment of both exons from HLA-A3 (EA3) (Fig.4.4.18B), suggesting that both exons contribute to the intracellular retainment of HLA-E. A BFA decay assay was then carried out to assess how these exons affect the surface

stability of HLA-E (Fig.4.4.18C, D). Both exon6 and exon7 seemed to contribute to the instability of surface HLA-E molecules, as the swapping of either of them to that

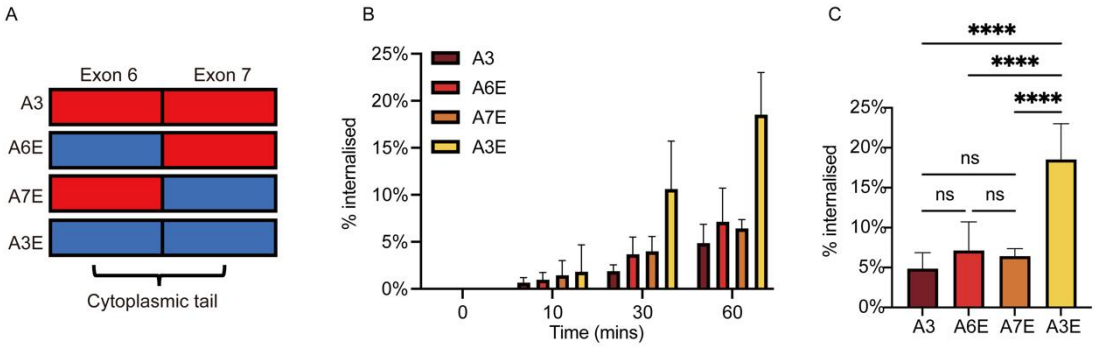

Figure 4.4.19 Both exon6 and exon7 of the cytoplasmic tail are required for the fast surface turnover of HLA molecules

A. Schematic representation of different HLA constructs. Exons from HLA-E and HLA-A3 are indicated in blue and red respectively. The cytoplasmic tail of A6E has exon6 from HLA-E and exon7 from HLA-A3; The cytoplasmic tail of A7E has exon6 from HLA-A3 and exon7 from HLA-E.

B, C. HEK 293T cells were transiently transfected with different constructs. 24hrs after transfection, surface HLA molecules were labeled with anti-HLA-A3 antibody GAP.A3, and then the cells were incubated in media containing primaquine. After different time points of internalisation, samples were collected, and uninternalised surface antibody-HLA complexes were stripped off using citric acid. B, The MFI of antibody-labeled cells without acid stripping was set to 100%, and the MFI of antibody-labeled cells with acid stripping but without internalisation was set to 0%. The percentage of internalisation was quantified by the normalisation of MFI increase accordingly. C, The percentage of HLA internalised after one hour. Data were collected for six biological runs and are shown as mean ± SD (error bars).

Statistical analysis was performed using one-way ANOVA with Tukey's post-hoc test. Asterisks show the statistical significance between indicated groups: ns, not significant; ****, $P < 0.0001$.

of HLA-A3 increased the surface stability of HLA-E. As the surface stability of HLA-EA3 was higher than that of HLA-E6A and HLA-E7A, the two exons on the HLA-E cytoplasmic tail seem to have a synergic effect in facilitating fast surface turnover. An acid stripping assay was then carried out to assess how these two exons affect the internalisation of surface HLA-E (Fig.4.4.18E, F). Changing either of the exons in the HLA-E cytoplasmic tail to that of HLA-A3 inhibited the fast internalisation of HLA-E, suggesting that both exons are required for the internalisation-promoting effect of HLA-E cytoplasmic tail.

To further validate the effects of both exons in the HLA-E cytoplasmic tail, I swapped the exon6 and exon7 of HLA-A3 to that of HLA-E and created two constructs named HLA-A6E and HLA-A7E (Fig.4.4.19A). An acid-stripping assay was then applied to examine the internalisation rates of these constructs (Fig.4.4.19B, C). The internalisation rates of HLA-A6E and HLA-A7E were similar to that of HLA-A3, with less than 10% internalised after one hour. Therefore, the

internalisation-promoting effect of the HLA-E cytoplasmic tail requires both exon6 and exon7.

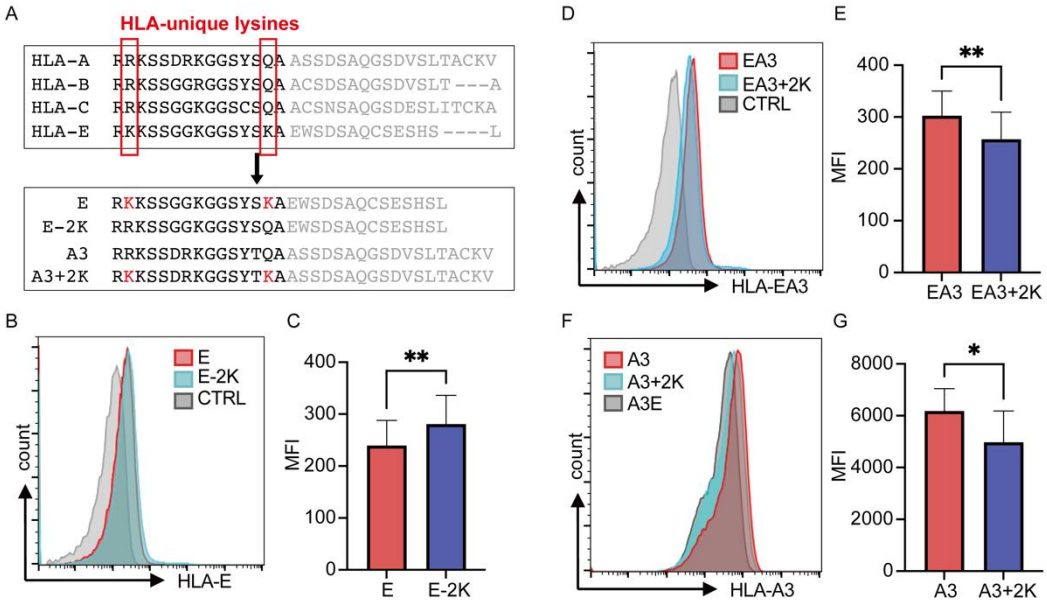

Figure 4.4.20 HLA-E-unique lysines contributes to intracellular accumulation
A. Sequences of the cytoplasmic tail of different constructs. Sequences of exon6 and exon7 are in black and grey respectively, and the positions of HLA-E-unique lysines are highlighted.
B-G. B, C, HEK 293T cells were transiently transfected with HLA-E_EGFP (red) or HLA-E-2K_EGFP (blue). D, E, HEK 293T cells were transiently transfected with HLA-EA3_EGFP (red) or HLA-EA3+2K_EGFP (blue). F, G, HEK 293T cells were transiently transfected with HLA-A3_EGFP (red) or HLA-A3+2K_EGFP (blue). 24hrs after transfection, cells were collected for flow cytometry analysis (gated on EGFP+ cells), and surface expression of different constructs was assessed with anti-HLA-E antibody (3D12, B-E) or anti-HLA-A3 antibody (GAP.A3, F-G). B, D, F, Representative graphs of surface MFI of different constructs. MFI of unstained sample (grey, CTRL) was used as the negative control. C, E, G, MFIs were collected and plotted for five biological runs, and data was shown as mean ± SD (error bars). Statistical analysis was performed using paired two-tailed student's t-test with Welch's correction. Asterisks show the statistical significance between indicated groups: *, $P < 0.05$; **, $P < 0.01$.

4.4.2.3 The internalisation-promoting effect of exon6 requires either HLA-E-unique lysines

As both exon6 and exon7 contribute to the fast internalisation of HLA-E, I then explored these two exons separately to find the potential motifs embedded within. Although the sequence of exon6 is well-conserved across different HLA-I molecules, HLA-E possesses two unique lysines on positions 310 and 322 (Fig.4.4.20A). To explore whether these two HLA-E-unique lysines affect the surface expression and turnover of HLA-E, I mutated the two lysines to arginine and glutamine respectively to create the construct E-2K (Fig.4.4.20A). The loss of these two lysines led to a slight increase in surface HLA-E expression (Fig.4.4.21B, C). I also mutated the arginine and glutamine at positions 310 and 322 to lysines in the cytoplasmic tails of

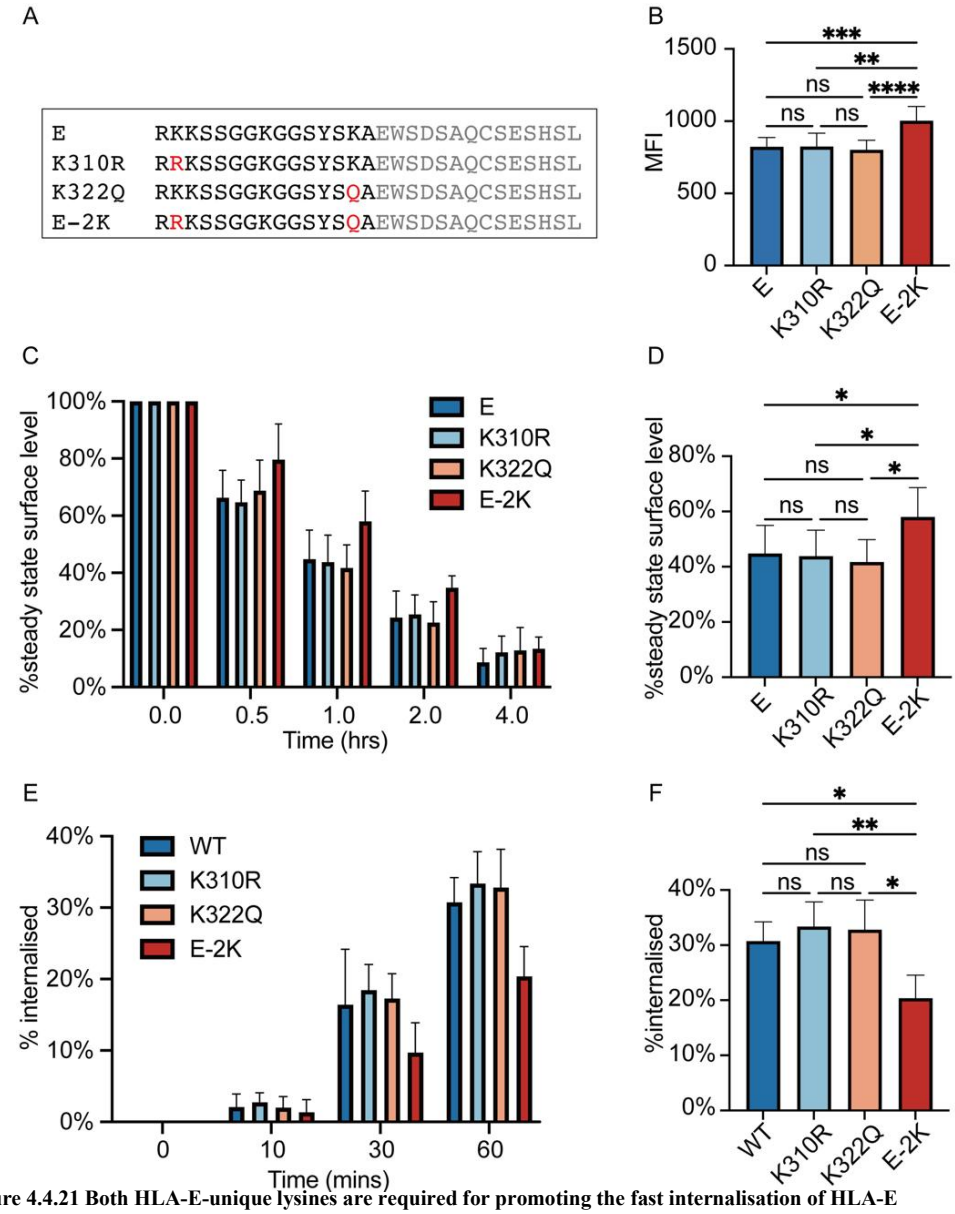

Figure 4.4.21 Both HLA-E-unique lysines are required for promoting the fast internalisation of HLA-E

A. Sequences of the cytoplasmic tail of different constructs with mutations in exon6. The mutations amino acids are highlighted in red.

B. HEK 293T cells were transiently transfected with different constructs. 24hrs after transfection, cells were collected for flow cytometry analysis (gated on EGFP+ cells), and surface expression of different constructs was assessed with anti-HLA-E antibody (3D12). MFIs were collected and plotted for nine biological runs, and data was shown as mean ± SD (error bars).

C, D. HEK 293T cells were transiently transfected with different constructs. 24hrs after transfection, cells were incubated in media containing BFA for different time points, and surface expression of different constructs was assessed with anti-HLA-E antibody (3D12). C, The average cell surface MFI for timepoint zero was set to 100% and the following values were normalised as its percentage. D, The percentage of HLA on the cell surface after BFA incubation for one hour. Data were collected for six biological runs and are shown as mean ± SD (error bars).

E, F. HEK 293T cells were transiently transfected with different constructs. 24hrs after transfection, surface HLA molecules were labeled with anti-HLA-E antibody 3D12, and then the cells were incubated in media containing primaquine. After different time points of internalisation, samples were collected, and uninternalised surface antibody-HLA complexes were stripped off using citric acid. E, The MFI of antibody-labeled cells without acid stripping was set to 100%, and the MFI of antibody-labeled cells with acid stripping but without internalisation was set to 0%. The percentage of internalisation was quantified by the normalisation of MFI increase accordingly. F, The percentage of HLA internalised after one hour. Data were collected for four biological runs and are shown as mean ± SD (error bars).

Statistical analysis was performed using one-way ANOVA with Tukey's post-hoc test. Asterisks show the statistical significance between indicated groups: ns, not significant; *, $P < 0.05$; **, $P < 0.01$; ***, $P < 0.001$; **88, $P < 0.0001$.

HLA-EA3 and HLA-A3 and created two constructs EA3+2K and A3+2K. The

introduction of the two HLA-E-unique lysines resulted in a small decrease in the surface level of HLA-EA3 (Fig.4.4.21D, E) and HLA-A3 (Fig.4.4.21F, G). Therefore, these HLA-E-unique lysines contribute to the intracellular accumulation of HLA proteins.

To examine the potential functions of these two HLA-E-unique lysines, I also made HLA-E constructs with either of these HLA-E-unique lysines mutated and generated the constructs named K310R and K322Q (Fig.4.4.21A). No detectable change of HLA-E surface level was observed for K310R and K322Q (Fig.4.4.21B), suggesting that mutations of both lysines are required to reverse the down-regulating effect of exon6 in HLA-E cytoplasmic tail. In the BFA surface decay assay, I observed that the surface stability of K310R and K322R were similar to that of HLA-E (Fig.4.4.21C, D) and lower than that of E-2K, which implies that either HLA-E-unique lysine was sufficient for the fast surface turnover of HLA-E. In the acid stripping assay, the internalisation rates of K310R and K322R paralleled that of HLA-E and were significantly faster than that of E-2K (Fig.4.4.21E, F). Therefore, while these HLA-E-unique lysines contribute to the fast surface turnover and intracellular accumulation of HLA-E, the system seems redundant, as the acquirement of either HLA-E-unique lysine seems to be sufficient.

4.4.2.4 The internalisation-promoting effect of exon7 depends on a tryptophan-based motif

Compared to exon6, the exon7 of HLA-I molecules are relatively less conserved. Given that the middle part of exon7 (position 326-332) is comparatively conserved, I first explored the positions at the start and the end of exon7 in the HLA-E cytoplasmic tail for potential motifs (Fig.4.4.22A). I swapped the first two amino acids in the exon7 of HLA-E to the corresponding amino acids in HLA-A3 and created a construct called EW_AS. The final five amino acids on exon7 were changed into the final nine

amino acids of HLA-A3 to generate a construct called 5C9. Given that the final amino acid also affects the surface level of HLA-E, I did not compare the surface expression

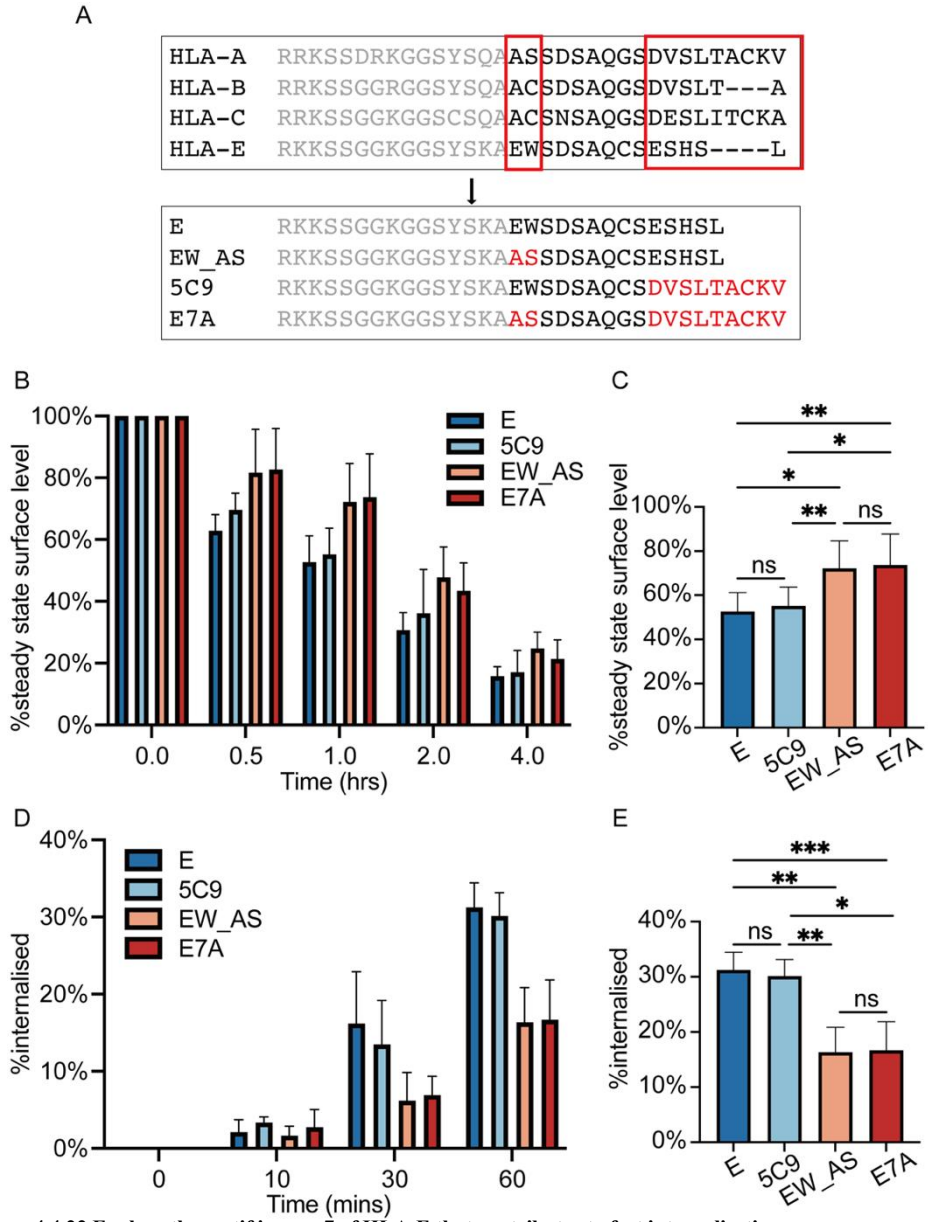

Figure 4.4.22 Explore the motif in exon7 of HLA-E that contributes to fast internalisation

A. Sequences of the cytoplasmic tail of different constructs with mutations in exon7. The mutations amino acids are highlighted in red.

B, C. HEK 293T cells were transiently transfected with different constructs. 24hrs after transfection, cells were incubated in media containing BFA for different time points, and surface expression of different constructs was assessed with anti-HLA-E antibody (3D12). B, The average cell surface MFI for timepoint zero was set to 100% and the following values were normalised as its percentage. C, The percentage of HLA on the cell surface after BFA incubation for one hour. Data were collected for five biological runs and are shown as mean ± SD (error bars).

D, E. HEK 293T cells were transiently transfected with different constructs. 24hrs after transfection, surface HLA molecules were labeled with anti-HLA-E antibody 3D12, and then the cells were incubated in media containing primaquine. After different time points of internalisation, samples were collected, and uninternalised surface antibody-HLA complexes were stripped off using citric acid. D, The MFI of antibody-labeled cells without acid stripping was set to 100%, and the MFI of antibody-labeled cells with acid stripping but without internalisation was set to 0%. The percentage of internalisation was quantified by the normalisation of MFI increase accordingly. E, The percentage of HLA internalised after one hour. Data were collected for five biological runs and are shown as mean ± SD (error bars).

Statistical analysis was performed using one-way ANOVA with Tukey's post-hoc test. Asterisks show the statistical significance between indicated groups: ns, not significant; *, $P < 0.05$; **, $P < 0.01$.

level of these constructs but studied their surface turnover directly. The surface stability of EW_AS was obviously higher than that of HLA-E and similar to that of E7A (Fig.4.4.22B, C). In contrast, no difference was observed between the surface stability of 5C9 and HLA-E. This suggests that the fast surface turnover facilitated by the exon7 of HLA-E relies on the first two amino acids of exon7. The internalisation rates of these constructed were also assessed (Fig.4.4.22D, E). As expected, the 5C9 construct showed a fast internalisation rate resembling that of HLA-E, while the EW_AS construct showed a slower internalisation rate similar to E7A. Therefore, the motif crucial for the internalisation-promoting effect of the exon7 in HLA-E is embedded within the first two amino acids.

To explore the potential roles of the glutamic acid and the tryptophan at the start of the exon7 in the HLA-E cytoplasmic tail, I generated constructs with either of these mutated to the corresponding amino acids in HLA-A3 exon7 at the same position (Fig.4.4.23A), which were named E324A and W325S respectively. While the surface expression level of W325S was similar to that of EW_AS and significantly higher than that of HLA-E, the E324A mutation did not seem to increase HLA-E surface expression (Fig.4.4.23B), suggesting that the tryptophan at position 325 might be the key amino acid. In the BFA surface decay assay, W325S showed similar surface stability with EW_AS and HLA-E7A constructs, while E324A manifested a surface decay rate comparable to that of HLA-E (Fig.4.4.23C, D). This indicates that exon7 facilitates the low surface stability of HLA-E via a tryptophan-based motif. The internalisation rates were similar among W325S, EW_AS and E7A, with less than 20% internalised after one hour (Fig.4.4.23E, F). While the internalisation rate of E324A was still very high, it was slightly slower than that of HLA-E, which is probably because the glutamic acid-to-alanine amino acid change affected the function of the tryptophan-based motif. Therefore, the fast internalisation promoted

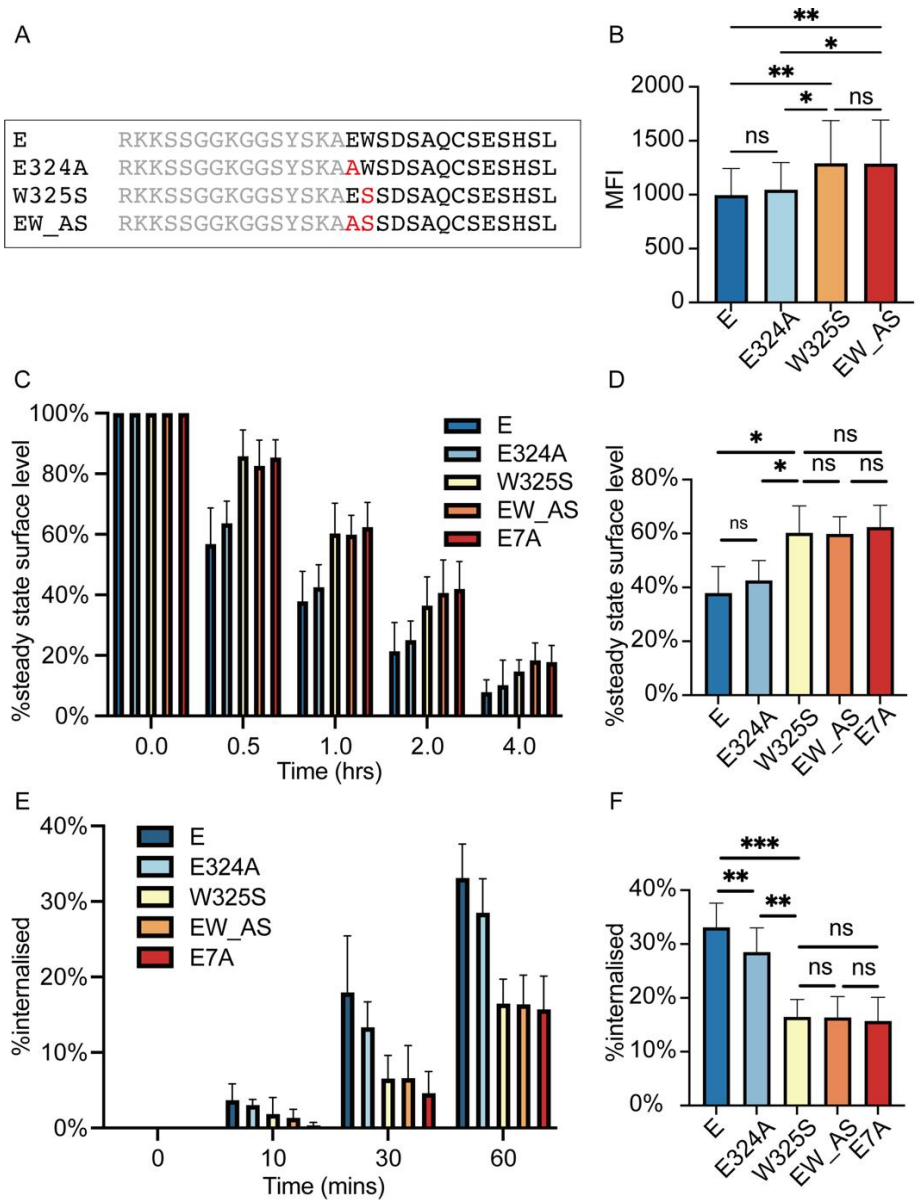

Figure 4.4.23 The internalisation-promoting effect of the exon7 of HLA-E depends on a tryptophan-based motif

A. Sequences of the cytoplasmic tail of different constructs with mutations in exon7. The mutations amino acids are highlighted in red.

B. HEK 293T cells were transiently transfected with different constructs. 24hrs after transfection, cells were collected for flow cytometry analysis (gated on EGFP+ cells), and surface expression of different constructs was assessed with anti-HLA-E antibody (3D12). MFIs were collected and plotted for eight biological runs, and data was shown as mean ± SD (error bars).

C, D. HEK 293T cells were transiently transfected with different constructs. 24hrs after transfection, cells were incubated in media containing BFA for different time points, and surface expression of different constructs was assessed with anti-HLA-E antibody (3D12). C, The average cell surface MFI for timepoint zero was set to 100% and the following values were normalised as its percentage. D, The percentage of HLA on the cell surface after BFA incubation for one hour. Data were collected for six biological runs and are shown as mean ± SD (error bars).

E, F. HEK 293T cells were transiently transfected with different constructs. 24hrs after transfection, surface HLA molecules were labeled with anti-HLA-E antibody 3D12, and then the cells were incubated in media containing primaquine. After different time points of internalisation, samples were collected, and uninternalised surface antibody-HLA complexes were stripped off using citric acid. E, The MFI of antibody-labeled cells without acid stripping was set to 100%, and the MFI of antibody-labeled cells with acid stripping but without internalisation was set to 0%. The percentage of internalisation was quantified by the normalisation of MFI increase accordingly. F, The percentage of HLA internalised after one hour. Data were collected for six biological runs and are shown as mean ± SD (error bars).

Statistical analysis was performed using one-way ANOVA with Tukey's post-hoc test. Asterisks show the statistical significance between indicated groups: ns, not significant; *, $P < 0.05$; **, $P < 0.01$.

by the HLA-E cytoplasmic tail requires either of the two HLA-E-unique lysines in

exon6 as well as a tryptophan-based motif in exon7.

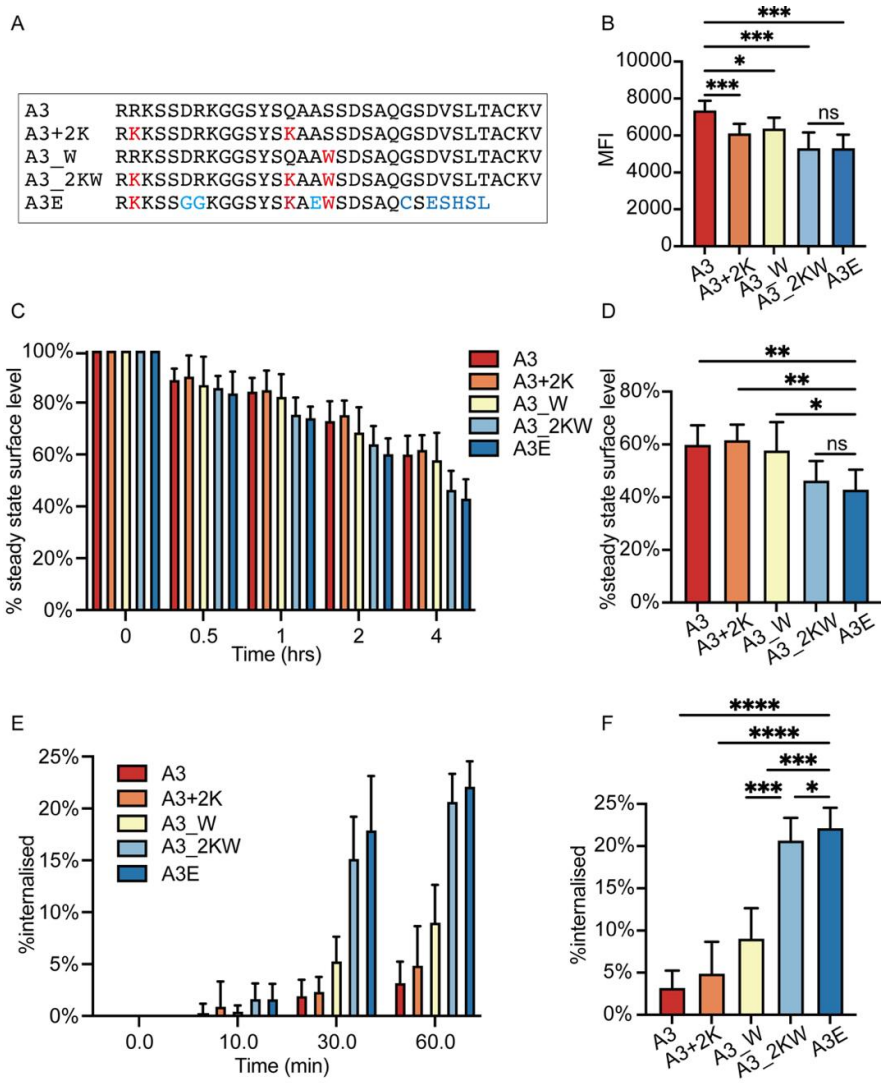

Figure 4.4.24 A lysine/tryptophan-based motif on the cytoplasmic tail is sufficient to elicit the fast internalisation of HLA-A3

A. Sequences of the cytoplasmic tail of different constructs with mutations. The target HLA-E-specific amino acids are highlighted in red, and other HLA-E-specific amino acids are highlighted in blue.

B. HEK 293T cells were transiently transfected with different constructs. 24hrs after transfection, cells were collected for flow cytometry analysis (gated on EGFP+ cells), and surface expression of different constructs was assessed with anti-HLA-A3 antibody (GAP.A3). MFIs were collected and plotted for nine biological runs, and data was shown as mean ± SD (error bars).

C, D. HEK 293T cells were transiently transfected with different constructs. 24hrs after transfection, cells were incubated in media containing BFA for different time points, and surface expression of different constructs was assessed with anti-HLA-A3 antibody (GAP.A3). C, The average cell surface MFI for timepoint zero was set to 100% and the following values were normalised as its percentage. D, The percentage of HLA on the cell surface after BFA incubation for one hour. Data were collected for six biological runs and are shown as mean ± SD (error bars).

E, F. HEK 293T cells were transiently transfected with different constructs. 24hrs after transfection, surface HLA molecules were labeled with anti-HLA-A3 antibody (GAP.A3), and then the cells were incubated in media containing primaquine. After different time points of internalisation, samples were collected, and uninternalised surface antibody-HLA complexes were stripped off using citric acid. E, The MFI of antibody-labelled cells without acid stripping was set to 100%, and the MFI of antibody-labeled cells with acid stripping but without internalisation was set to 0%. The percentage of internalisation was quantified by the normalisation of MFI increase accordingly. F, The percentage of HLA internalised after one hour. Data were collected for six

4.4.2.5 The lysine/tryptophan-based motif on the cytoplasmic tail is sufficient to elicit the fast internalisation of HLA-A3

After validating that a lysine/tryptophan-based motif is necessary for the fast internalisation of HLA-E, I then examined whether this motif is sufficient to elicit fast surface turnover of other HLA-I molecules. Therefore, I mutated the cytoplasmic tail of HLA-A3 to provide it with the HLA-E-unique lysines (A3+2K), the tryptophan on position 325 (A3_W) or both of them (A3_2KW) (Fig.4.4.24A). The acquisition of either the lysines or the tryptophan led to a decrease in the HLA-A3 surface level (Fig.4.4.24B), suggesting that either of these could promote the intracellular accumulation of HLA-A3 alone. The additive downregulating effect of the lysines and the tryptophan implied that they could downregulate HLA-A3 via different mechanisms. As the surface level of the A3_2KW construct was comparable to that of HLA-A3E, the lysine/tryptophan-based motif seemed sufficient for the down-regulatory effect of the HLA-E cytoplasmic tail.

I then examined how these mutations affect the surface turnover of HLA-A3. While the surface stability of A3+2K was similar to that of A3, the surface stability of A3_W was slightly lower than A3, though not significant (Fig.4.4.24C, D). However, the surface stability of HLA-A3_2KW was significantly lower than that of A3, A3+2K or A3_W, and paralleled that of HLA-A3E. This indicates that the lysine/tryptophan-based motif accounts for the destabilising effect of the HLA-E cytoplasmic tail. The tryptophan seems to be a crucial component of the motif, as the absence of tryptophan completely abolished the destabilising effect, whereas the tryptophan alone had a weak destabilising effect, though much less efficient than the complete motif. Internalisation rates of these constructs were examined simultaneously (Fig.4.4.24E, F). While around 3% of HLA-A3 was internalised in 60 mins, approximately 5% of A3+2K and 9% of A3_W were internalised in the same time frame, implying that both the lysines and the tryptophan could promote the

internalisation of surface HLA-A3, though the tryptophan seemed to be more effective. Around 20% of A3_2KW was internalised within 60 mins, which is much faster than A3+2K and A3_W and is very similar to that of A3E, implying that the lysines and the tryptophan are key amino acids on the cytoplasmic of HLA-E to promote internalisation. Thus, the internalisation-promoting effect of the HLA-E cytoplasmic tail depends on a unique lysine/tryptophan-based motif.

4.4.2.6 The lysine/tryptophan-based motif on the cytoplasmic tail affects HLA-I endosomal distribution

As the lysine/tryptophan-based motif accounts for the internalisation-promoting effect of the HLA-E cytoplasmic tail, I then examined how this motif may affect the endosomal distribution of HLA-I molecules (Fig.4.4.25). As the HLA-E cytoplasmic tail could lead to the enrichment of HLA-A3 in late endosomes and recycling endosomes (Fig.4.4.9), I co-localised these HLA-A3 constructs or HLA-E constructs without, with the complete or with part of the lysine/tryptophan-based motif with markers for late endosomes recycling line endosomes.

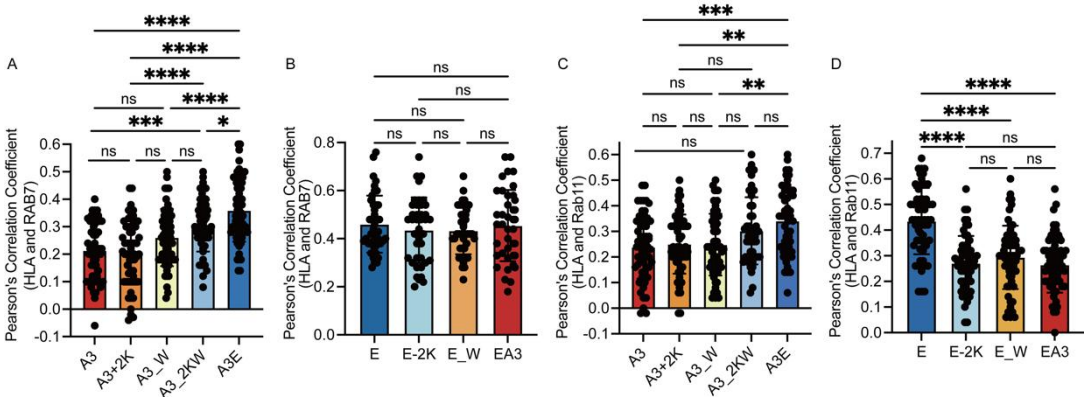

Figure 4.4.25 A lysine/tryptophan-based motif on the cytoplasmic tail affect the endosomal distribution of HLA-I molecules

HeLa cells were transiently transfected with different HLA-A3 (A, C) or HLA-E (B, D) constructs tagged with EGFP. 24hrs after transfection, cells were fixed, permeabilised, stained with Abs against the markers for late endosomes (Rab7, A, B) or recycling endosomes (Rab11, C, D), followed by detection with Alexa568-conjugated secondary antibody. Co-localisation of different constructs with endosomal markers was quantified by the calculation of the PCC value of each cell with 40-60 cells per sample. Statistical analysis was performed using one-way ANOVA with Tukey's post-hoc test. Asterisks show the statistical significance between indicated groups: ns, not significant; *, $P < 0.05$; **, $P < 0.01$; ***, $P < 0.001$; ****, $P < 0.0001$.

While there's no difference in late endosomal distribution between A3 and A3+2K, the obtainment of the tryptophan alone seemed to slightly enrich HLA-A3 in late endosomes, though not significant (Fig.4.4.25A). The possession of the complete lysine/tryptophan-based motif significantly increased the level of HLA-A3 in late endosomes, though the enrichment is slightly more pronounced with the complete HLA-E cytoplasmic tail. These data paralleled the internalisation rate of the constructs (Fig.4.4.24E, F). As expected, no difference was observed between HLA-E, HLA-E-2K, HLA-E_W and HLA-EA3 in late endosomal enrichment (Fig.4.4.25B). This is consistent with previous data (Fig.4.4.9B, F) and implies that factors other than the cytoplasmic tail could lead to the enrichment of HLA-E in late endosomes.

A3, A3+2K or A3_W were similarly distributed in the recycling endosomes (Fig.4.4.25C), suggesting that the lysines or the tryptophan alone did not affect the enrichment of HLA-A3 in the recycling endosomes. However, an elevation of localisation in the recycling endosomes could be observed for A3_2KW, though not statistically significant. Though HLA-E was enriched in the recycling endosomes, the enrichment was lost in the absence of either the lysines or the tryptophan and became similar to that of HLA-EA3 (Fig.4.4.25D). Therefore, the effect of the HLA-E cytoplasmic tail on enriching HLA-I molecules in the recycling endosomes depends on the integrity of the lysine/tryptophan-based motif.

Therefore, the lysine/tryptophan-based motif could enrich HLA-I molecules in late endosomes and the recycling endosomes. Although tryptophan alone has a slightly late endosomal enrichment effect, it could not enrich HLA-I molecules in recycling endosomes by itself. While HLA-E is enriched in late endosomes regardless of its cytoplasmic tail, its enrichment in recycling endosomes completely relies on the lysine/tryptophan-based motif.

In summary, the HLA-E cytoplasmic tail and the shortage of good peptide supply are the main regulators for the intracellular distribution and transport of HLA-E, though none of them seems to contribute to the TAP/tapasin-independent, non-canonical transport of HLA-E. While the shortage of peptide supply greatly reduces HLA-E surface expression by inhibiting its ER export, the cytoplasmic tail contributes moderately to HLA-E intracellular accumulation by promoting both ER retention and fast surface turnover. The ER-retaining effect of the cytoplasmic tail, which results from the lack of a C-terminal ER exit motif, is weak compared to the shortage of good peptides. The internalisation-promoting effect depends on a lysine/tryptophan motif on the cytoplasmic tail, which could lead to the enrichment of HLA-I molecules in late endosomes and recycling endosomes.

4.5 Discussion

In this chapter, I explored how HLA-E trafficking is regulated by different factors, including β2m, peptide, and the cytoplasmic tail. The low surface expression of HLA-E mainly results from ER retention, which is primarily due to the limited supply of high-affinity peptides and is reinforced by the absence of a C-terminal ER export motif. A lysine/tryptophan-based motif on the HLA-E cytoplasmic tail leads to fast internalisation of surface HLA-E, further decreasing its surface level and enriching HLA-E in late endosomes and recycling endosomes. While other regulatory factors, including β2m, also affect HLA-E surface level, the cytoplasmic tail and peptide are the two main factors shaping the unique transport patterns of HLA-E.

In the β2m titration experiments, I found that β2m overexpression did not significantly increase the HLA-A2 surface expression level (Fig.4.2B) but only increased the HLA-E surface level (Fig.4.2A). As there were sufficient high-affinity HLA-A2 peptides, most HLA-A2 may be already folded into HLA-A2_β2m_peptide trimers without β2m transfection. In contrast, most HLA-E might be in the form of

open conformers due to overexpression and the shortage of good peptides, so an extra supply of β2m may contribute to the refolding of the HLA-E_β2m_peptide trimer, thus promoting the ER export of HLA-E.

In the VL9 minigene titration experiments, I found that VL9 minigene transfection decreased the surface level of endogenous HLA-A2 (Fig.4.3.1B). The most possible explanation for the decrease of surface HLA-A2 is the lack of β2m. As the VL9 peptide helps to promote the refolding of the HLA-E trimer, at least in vitro (Walters et al. 2018; Walters et al. 2022), it may make HLA-E more competent for the endogenous β2m (Myers et al. 1996). Given the overexpression of the VL9 minigene and HLA-E, the supply of β2m is limited. In the presence of more high-affinity peptides to promote the refolding of HLA-E trimers, less HLA-A2 could fold into well-conformed trimers for the lack of β2m, leading to the decrease of HLA-A2 surface level. This is in line with the result that the overexpression of β2m alone does not affect HLA-A2 surface expression, as most HLA-A2 molecules are fully conformed.

In peptide pulsing, not only the weak peptides were less effective at promoting HLA-E surface expression, but also the surface accumulation of HLA-E reached a plateau quickly in the samples incubated with weak peptides (Fig.4.3.2). At the early stages of peptide pulsing, the surface level of HLA-E was low, so the amount of HLA-E arriving at the cell surface was higher than the amount internalised in the same timeframe, leading to the accumulation of HLA-E on the cell surface. While the velocity of surface arrival of HLA-E was relatively stable, its internalisation rate gradually increased with a higher surface HLA-E level. Therefore, the surface accumulation of HLA-E gradually reached a plateau, which signifies a dynamic equilibrium where the arrival and internalisation of HLA-E occur at equal rates. Although ER export could not be effectively promoted in peptide pulsing (Fig.4.3.7), the incubation with excessive high-affinity peptides could significantly enhance the

surface stability of HLA-E (Fig.4.3.5A, B), thus decreasing the internalisation rate of surface HLA-E. Therefore, it took longer for the surface arrival and internalisation of HLA-E to reach the equilibrium in the presence of high-affinity peptides.

Peptide binding facilitates the assembly of the trimer complex, which increases the surface expression of HLA-E. The magnitude of such surface increase depends on the peptide affinity, as the assembly of HLA-E trimers is more efficient when a high-affinity peptide is encoded into the SCT construct. Therefore, peptide affinity could be determined by the surface expression level of SCT. As β2m and the peptide are covalently linked to HLA-E in the SCT construct, the influence of β2m and potential difference in peptide supply and access could be excluded. Therefore, the surface HLA-E level entirely depends on the peptide affinity in SCTs. The linkage of β2m and the peptide enables SCTs to refold independent of the classical MHC-I assembly pathway, which increases the surface expression of HLA-E, thus allowing for sensitive detection of the potential binding of weak peptides. Therefore, HLA-E SCT is a useful tool for sensitive detection and quantitative comparison of the binding affinity of different HLA-E peptides. However, as the artificial linkage in the SCT constructs might distort the binding groove, the surface level of SCT might not reflect the real binding affinity of peptides, which may explain why several CLIP-derived peptides showed good binding in the SCTs but not on other assays (Table 7.4). Therefore, the peptide binding affinity measured in SCTs needs further validation.

Consistent with previous data (Braud et al. 1997; Braud et al. 1998b), I observed that VL9 peptide minigene expression can significantly promote the surface expression of HLA-E by effectively releasing HLA-E from the ER (Fig.4.3.3). As VL9 facilitates the refolding of the HLA-E complex (Walters et al. 2018; Walters et al. 2022), which is required to pass through the “quality selection” mediated by tapasin and TAPBPR (Thomas and Tampé 2019), VL9 enhances the ER export of HLA-E via the classical pathway, which depends on both TAP and tapasin (Fig.4.3.10). Weak peptides like

RL9 could not lead to effective ER export of HLA-E (Fig.4.3.4) for their incapability to refold HLA-E into a compact conformation (Walters et al. 2022).

However, while VL9 could effectively promote HLA-E ER export, it fails to significantly increase its surface stability under physiological conditions (Fig.4.3.5-6). This is consistent with the relatively modest binding affinity of the VL9 peptide as revealed by the lower thermostability of the HLA-E_β2m_VL9 complex (Hoare et al. 2008; Strong et al. 2003; Walters et al. 2022). The thermal melt (Tm) temperature measures the thermostability of the peptide-MHC-I complex, which is correlated to the binding affinity of the peptide (Hellman et al. 2016). While the Tm value is often around or over 65 ºC for MHC-Ia in complex with their strongest binding peptides (Hellman et al. 2016), the Tm values for the VL9-HLA-E trimer recorded were generally between 48 to 52 ºC depending on the assay employed (Hoare et al. 2008; Strong et al. 2003; Walters et al. 2022). Such a modest Tm value implies that the binding affinity of VL9 is comparatively not very high compared to good HLA-Ia peptides, though VL9 is among the best binding peptides for HLA-E. This explains why VL9 could not effectively stabilise surface HLA-E (Fig.4.3.5-6). However, the peptide affinity of VL9 is sufficient for the complete ER export of HLA-E (Fig.4.3.3), suggesting that the peptide affinity required for ER export is lower than that for efficient surface stabilisation. The precise affinity of the VL9 might be biologically important, as it allows for fast and sensitive detection of the change in endogenous VL9 level.

To explore the influence of peptides on the intracellular distribution of HLA-E, several different methods were applied to mimic the situation of sufficient supply of high-affinity HLA-E binding peptides where both the ER export and the surface stability of HLA-E were promoted, including coupling VL9 minigene transfection to low-temperature incubation or VL9 peptide pulsing and the usage of SCT_VL9 (Fig.4.3.7-8). The intracellular distribution of HLA-E resembles that of HLA-Ia

molecules, where high surface expression of HLA-E was observed, with a fraction in the endosomal compartments (Fig.4.3.8). Therefore, both the ER export and the surface stability are crucial for shaping the typical intracellular distribution of HLA-I molecules. The intracellular distribution of HLA-E is mainly shaped by its peptide repertoire, where the shortage of good peptides leads to its low surface expression and ER retention.

Co-expression of the VL9 peptide minigene enriched HLA-E in early endosomes and lysosomes but did not affect its accumulation in late endosomes or recycling endosomes (Fig.4.3.9). The enrichment of HLA-E in early endosomes may be caused by the large amount of HLA-E internalised from the cell surface, as VL9 failed to stabilise surface HLA-E (Fig.4.3.5-6). Rapid passage through the endocytic system might explain why late endosomal accumulation was not observed. The enrichment of HLA-E in lysosomes may be a combined result of the significant amount of HLA-E flushing into the endosomal pathway and the limited amount of HLA-E that could get recycled back to the cell surface, as no further enrichment of HLA-E in the recycling pathway was observed. As most HLA-E getting into the endosomal pathway could not get recycled, VL9 is likely to fall out of the HLA-E binding groove in the endosomal pathway, which is consistent with the fact that the binding affinity of VL9 is not very high.

Although VL9 peptide minigene could effectively promote HLA-E surface expression, the effect was completely blocked in the absence of TAP or tapasin (Fig.4.3.10). This suggests that VL9 peptide facilitates the ER export of HLA-E via the classical pathway, where TAP and tapasin are required for VL9 peptide binding. This is consistent with previous data where VL9 peptide loading is TAP-dependent (Braud et al. 1998b). Structural studies have shown that HLA-E refolds into a compact, fully folded form when bound to VL9 (Walters et al. 2018; Walters et al. 2022), which assists HLA-E to exit the ER through the classical pathway (Thomas and Tampé

2019). This reinforces the conclusion of the shortage of good HLA-E binding peptides under normal conditions in HEK293T cells, as HLA-E is transported to the cell surface in an unconventional pathway which is independent of TAP or tapasin (Fig.3.3.20).

The artificial fusion of EGFP at the C-terminus of HLA proteins might affect the interactions between the motifs on the cytoplasmic tail with proteins crucial for trafficking regulation. Therefore, I verified that EGFP tagging did not obstruct the functions of the cytoplasmic tail in regulating protein transport (Fig.4.4.7) before further characterisation of the functions, motifs, and mechanisms of the HLA-E cytoplasmic tail. The motifs embedded within the cytoplasmic sequence were not blocked in the presence of the EGFP tag, including the C-terminal motif (Fig.4.4.13; Fig.4.4.14). The protein interactions mediated by the HLA-E cytoplasmic tail are likely to be preserved in the presence of EGFP tapping, which may result from the short linker between the cytoplasmic tail and EGFP or the specific folding and structure of the proteins involved in the interactions.

Antibody cross-linking, like other protein-labelling techniques, may change the behaviour of surface class I molecules, and we could not rule out the effect of antibody cross-linking here. Besides, the binding affinity and conformational preference differ between antibodies, which may lead to systematic bias in measuring the surface stability and internalisation rate. This might be a big problem if we compare proteins labelled with different antibodies. However, a comparison between HLA-E and HLA-EA3 should be fine, as the same antibody was used to label them (antibody cross-linking should similarly affect them, thus ruling out the bias). Likewise, we could also compare between HLA-A3 and HLA-A3E. Therefore, although the surface decay rate and internalisation velocity measured here might not be accurate, as the result may vary between cell types and methods (Montealegre and van Endert 2018), the internalisation-promoting effect of HLA-E cytoplasmic tail

observed here should be genuine. Similarly, the facilitation of a fast-recycling pathway observed for the HLA-E cytoplasmic tail should be reliable, as the potential systematic bias should affect the constructs with swapped cytoplasmic tails in like manner.

The cytoplasmic tail plays a deciding role in regulating the surface turnover of HLA molecules, as tail swapping reversed the internalisation rates between HLA-E and HLA-A3 (Fig.4.4.8E, F). However, while the internalisation rate of HLA-A3E is higher than that of HLA-A3, it is still slightly lower than that of HLA-E, though insignificant. The difference in the peptide repertoire between HLA-A3E and HLA-E may explain this. The sufficient supply of high-affinity peptides enables most surface HLA-A3E to fold into a compact and stable conformation, while many HLA-E molecules exist as open conformers due to the shortage of high-affinity peptides, which are more unstable and get internalised quickly (Mahmutefendić et al. 2011; Zagorac et al. 2012). This fine-tuning effect of the peptide repertoire on the internalisation rate is further supported by the slightly higher internalisation rate of HLA-EA3 compared to that of HLA-A3 (Fig.4.4.8F).

Although the internalisation rate of HLA-A3E is higher than that of HLA-EA3, the surface stability of HLA-EA3 is lower than that of HLA-A3E. This is partly because many internalised HLA-A3E molecules can get recycled back to the cell surface, while the recycling of HLA-EA3 is ineffective (Fig.4.4.9). As the stability of HLA-A3E is still higher than HLA-EA3 when the recycling pathway is inhibited, there must be other factors influencing the surface stability of HLA-EA3, as has been discussed in section 3.6. Therefore, further exploration is necessary to determine the regulatory elements of HLA-E endosomal transport apart from peptides and the cytoplasmic tail.

While the obtainment of the HLA-E cytoplasmic tail enriches HLA-A3E in late endosomes, HLA-EA3 can accumulate in the late endosomes in the absence of the HLA-E cytoplasmic tail. Therefore, the HLA-E cytoplasmic tail is sufficient but not necessary for its accumulation in late endosomes, suggesting a redundant mechanism to ensure the late endosomal enrichment of HLA-E. The relative stability of HLA-E and HLA-EA3 under a mildly acidic pH might possibly contribute to their late endosomal enrichment (Camilli et al. 2016). This is in line with the importance of late endosomal structures where the loading of pathogen-derived peptides presumably occurs (Grotzke et al. 2009), which is crucial for the unconventional HLA-E-restricted CD8+ T cell response. Further studies are required to study the transport process regulated by the cytoplasmic tail as well as how it coordinates with other factors, most importantly peptides, to shape the endosomal transport of HLA-E.

VL9 minigene-mediated upregulation of HLA-E entirely depends on TAP and tapasin (Fig.4.3.10), suggesting that VL9 promotes the ER export of HLA-E via the classical peptide presentation pathway, which requires the loading of high-affinity peptides in the ER. While the surface expression of HLA-A3 and HLA-A3E were highly dependent on TAP and tapasin (Fig.4.4.10), the surface expression of neither HLA-E nor HLA-EA3 was affected in the absence of TAP or tapasin, indicating that the mechanisms through which the cytoplasmic tail regulates the surface expression of HLA-I do not require TAP or tapasin. Therefore, while the VL9 peptide minigene facilitates the classical ER export pathway to enhance the surface HLA-E level, the cytoplasmic tail of HLA-E regulates its surface expression via a TAP/tapasin-independent way.

Although the shortage of good peptides is the main cause for the ER retention of HLA-E (Fig.4.3.3), the lack of the C-terminal ER exit motif adds an extra layer of ER-retaining effect to allow for precise regulation of the antegrade transport of HLA-E (Fig.4.4.12-15). The C-terminal motif has been shown to promote the ER

export and surface expression of HLA-F molecules, though not capable of releasing HLA-F completely from the ER (Boyle et al. 2006). Similarly, while the obtainment of the C-terminal motif could assist the ER exit and surface expression of HLA-E, the majority was still retained in the ER (Fig.4.4.15). Deleting the C-terminal motif does not affect the steady-state surface expression of HLA-Ia molecules (Boyle et al. 2006). This seems to be due to the abundance of high-affinity peptides, which is more effective in promoting ER export compared to the C-terminal motif. Likewise, the acquisition of the C-terminal motif did not seem to promote further HLA-E surface expression in the presence of an ample supply of the VL9 peptide (Fig.4.4.15C-D). Although HLA-Ia molecules can exit the ER without the C-terminal motif (Boyle et al. 2006), the C-terminal motif enhances the efficiency of the process (Cho et al. 2011). This suggests that the lack of the C-terminal motif might keep HLA-E in the ER longer even when good peptides are abundant, thus reducing the possible escape of sub-optimally folded HLA-E from the ER. The absence of the C-terminal motif and the VL9-optimised peptide binding groove together ensure that HLA-E could only exit the ER when loaded with good peptides. Thus, the surface HLA-E level could sensitively reflect the change in VL9 peptide supply, which allows for regulating the activation of NK cells in an accurate and timely way.

Ubiquitination is a common signal for protein trafficking (Foot et al. 2017). The ubiquitination of the lysine residues on the cytoplasmic tail has been reported to downregulate the surface expression of HLA-Ia, HLA-II and CD1 molecules (De Angelis Rigotti et al. 2017; Maître et al. 2008; Shin et al. 2006). Apart from the two well-conserved lysines in exon 6, HLA-E has two unique lysine residues on position 310 and 322 (Fig.4.4.20A), in which the latter was reported to be ubiquitinated (Hornbeck et al. 2015). Thus, ubiquitination may be the mechanism of how these HLA-E-unique lysines facilitate the internalisation of surface HLA-I molecules (Fig.4.4.20-21). As many viral proteins also regulate the trafficking of HLA-I

molecules by targeting the ubiquitin conjugated to the lysines on the cytoplasmic tail (Boname et al. 2004; Boname and Stevenson 2001; Coscoy and Ganem 2000; Coscoy et al. 2001; Hewitt et al. 2002), the different ubiquitination pattern on the cytoplasmic tail of HLA-E may allow the virus to regulate HLA-E trafficking differently. Therefore, it would be interesting to explore whether the ubiquitination of the HLA-E-unique lysines may lead to the downregulation and fast surface turnover of surface HLA-E molecules, as well as whether viral proteins could target these lysines to regulate HLA-E transport.

Tryptophan-based motifs have been reported to facilitate endocytosis (Jarousse et al. 2003; Ritter et al. 2003). Consistent with previous data, I found that tryptophan is the key amino acid for the internalisation-promoting effect of the HLA-E cytoplasmic tail (Fig.4.4.23-24). While a tyrosine-based motif (YXXØ) and a dileucine-based motif (LI) have been well characterised to target surface MHC-I molecules to endosomal compartments (Bonifacino and Traub 2003; Schaefer et al. 2008; Sugita et al. 2004), this is the first study, to my knowledge, showing that a tryptophan-based motif can also promote the internalisation of MHC-I molecules.

The structural features may be crucial for the recognition of the tryptophan-based endocytosis signal, as it has been reported in other tryptophan-based motifs that the core tryptophan can be replaced by structurally related aromatic amino acids and that the mutation of the amino acids nearby may impair the function of the motif (Wu and Simister 2001). This explains why the mutation of the glutamic acid to alanine on position 324 slightly decreased the internalisation rate of HLA-E (Fig.4.4.23) as well as why the A3_2KW construct has a slightly slower internalisation rate and slightly less enriched in endosomal compartments compared to HLA-A3E (Fig.4.4.24-25).

Similar to the well-established dileucine- and tyrosine-based endocytosis signals, tryptophan-based internalisation signals have also been reported to be recognised by

the AP-2 complex (Wernick et al. 2005). Therefore, it's highly possible that the tryptophan-based motif on the cytoplasmic tail of HLA-E can also recruit the AP-2 complex to facilitate endocytosis. Considering that the AP-2 complex is the core component for clathrin-mediated endocytosis (Kaksonen and Roux 2018) and that HLA-Ia is internalised via a clathrin-independent pathway (Naslavsky et al. 2004), clathrin-mediated endocytosis might be a pathway unique to HLA-E, which might be important for the regulation for its surface turnover and endosomal localisation.

The obtainment of the lysine/tryptophan-based motif on the cytoplasmic tail could significantly facilitate the internalisation of HLA-A3 molecules and enrich them in late endosomes and recycling endosomes (Fig.4.4.24-25). While the motif still functioned weakly without the lysines, the absence of the tryptophan completely impaired the endocytosis motif. This suggests that the tryptophan is possibly the primary anchor for the lysine/tryptophan-based signal, and the lysines might have an auxiliary function to ensure the efficiency of endocytosis.

Although I have explored the general effect of peptides in regulating HLA-E transport, a lot of important questions remain unanswered, including where the HLA-E trimers possibly disassemble, where HLA-E could get reloaded with peptides, and how peptide binding affects the recycling and trafficking of HLA-E in the endosomal pathways. Besides, it is also necessary to explore how peptide delivery affects HLA-E transport, especially the pathogen-derived peptides delivered directly to the endosomal compartments. I have tried to track the location of internalised TAMRA-tagged peptides directly using imaging. However, the endocytosis of peptides seemed independent of HLA-I proteins, so the co-localisation of peptides and HLA-E does not signify peptide binding. Specific recognition of the HLA-E_β2m_peptide trimer complex is probably the best way to detect the association between the peptide and HLA-E. Our group is currently developing antibodies that could recognise the HLA-E trimer complex in a peptide-specific way.

Another approach is the usage of specific TCR, which is sensitive and ensures that such HLA-E trimer complex is functional. This will be discussed further in Chapter 5.

While a lysine/tryptophan-based endocytosis motif is identified here, it's possible that other surrounding residues also modulate the functions of the motif, though the effect of these amino acids may be less significant or redundant. While I have located and characterised the motifs embedded in the HLA-E cytoplasmic tail that promote ER export and surface internalisation, the exact mechanism and pathways involved remain unknown. I have shown that the HLA-E cytoplasmic tail can enrich HLA-I molecules in endosomal structures, but further characterisation of the dynamic process would be necessary for a clear idea of its regulatory functions. HLA-E cytoplasmic tail might also direct other intracellular events, though the effect might be hard to detect or only significant under abnormal conditions. As many viral proteins and cancer cells can target the motifs on HLA-I cytoplasmic tail to modulate their trafficking (Coscoy et al. 2001; Griffin et al. 2013; Le Gall et al. 1998; Wang et al. 2008), further investigation into how HLA-E cytoplasmic tail contributes to its differential transport regulation under abnormal conditions would be necessary.

Apart from components of the heterotrimer complex and the intrinsic specific motifs on the cytoplasmic tail, it would be interesting to explore the intracellular proteins that might interact with HLA-E and regulate its transport. CD74, a chaperone crucial for the regulation of MHC-II transport, can also bind to MHC-I molecules (Reber et al. 2002; Sugita and Brenner 1995) and MHC-I-like molecules (Huang et al. 2008; Jayawardena-Wolf et al. 2001) via the CLIP region (Powis 2006; van Luijn et al. 2012) and alter their transport. Some preliminary results show that some peptides derived from the CLIP region of CD74 bind to HLA-E, though the binding affinity is weak compared to VL9 (Table 7.4). This suggests that CD74 might potentially affect HLA-E trafficking. The peptide binding groove of HLA-F resembles that of HLA-II molecules and can accommodate long peptides (Hò et al. 2019). While HLA-F is not

directly involved in peptide presentation as most HLA-F exists in a peptide-free form (Goodridge et al. 2010), it can bind to open conformers of HLA-I molecules and facilitate cross-presentation (Goodridge et al. 2010; Goodridge et al. 2013), which resembles the functions of HLA-DM and CD1e. Given the interaction between HLA-F and HLA-E (Goodridge et al. 2010), HLA-F is a potential chaperone for HLA-E endosomal peptide loading.

Future work focusing on these questions would be crucial for a thorough understanding of the regulatory network of HLA-E, which would lay the basis for designing methods to manipulate its transport in potential immunotherapies.

Chapter 5: Establishment and optimisation of a CD8+ T cell activation system to assess peptide presentation pathways

5.1 Introduction

Blockage of the classical antigen presentation pathway of MHC-I molecules is common in pathogen infection (Antoniou and Powis 2008) and assists abnormal cells to escape from T cell-mediated immune responses. This creates a big obstacle for immunotherapies. However, HLA-E expression is usually resistant to such blockage upon infection to inhibit the activation of NK cells (McMichael and Picker 2017), which offers a great opportunity in the development of effective immunotherapies based around HLA-E-restricted presentation of pathogen-derived peptides.

An unconventional peptide loading and presentation pathway may be adopted by HLA-E to overcome the inhibition of the classical peptide transport process, as implied by studies in *Mtb* (Grotzke et al. 2009), S.typhi (Liss et al. 2017), and HCMV (Tomasec et al. 2000). Endosomal enrichment, rapid internalisation and recycling, and the existence of a TAP/tapasin-independent transport pathway for HLA-E also suggest an unconventional endosomal trafficking pathway, as shown in previous chapters. This hypothesis is further supported by the comparative stability of HLA-E dimers in a mildly acidic environment (unpublished data on in vitro HLA-E refolding from Max Quastel), which favours peptide exchange (Chefalo and Harding 2001; Saikia et al. 2022). In order to inform strategies to elicit effective HLA-E-restricted CD8+ T cell response, it will be crucial to understand the process and mechanism of HLA-E-restricted peptide loading and presentation.

As discussed in the introduction, an RhCMV-vectored vaccine could elicit effective and long-lasting protection against SIV in vaccinated RMs (Hansen et al. 2011;

Hansen et al. 2013a; Hansen et al. 2016), in which unconventional Mamu-E-restricted presentation of SIV-derived antigens is crucial (Hansen et al. 2016; Malouli et al. 2021). Considering the similarities between HLA-E and Mamu-E (Hansen et al. 2016; Walters et al. 2018; Wu et al. 2018) and that HLA-E-restricted CD8+ T cell response can be primed in vitro and inhibits HIV-1 replication (Yang et al. 2021), HLA-E seems to be a potential target for the development of an effective HIV vaccine. Unless a safe and equivalent version of HCMV can be found and tested, research into how HLA-E presents HIV-derived peptides would be critical for the transformation of the effective SIV vaccine into an HIV vaccine.

Apart from direct HIV infection, it will be essential to explore whether other peptide delivery systems can prime HLA-E-restricted presentation cell responses. Modified vaccinia Ankara virus (MVA) is a replication-deficient pox virus, and pre-existing immunity against MVA is not common since the cease of the smallpox vaccination (Orlova et al. 2022). The non-replicating simian (chimpanzee) adenovirus (ChAdOx1) is safe, easy to manipulate, and capable of inducing strong and sustained immune responses (Dicks et al. 2012). The pre-existing immunity towards the ChAdOx1 vector was rarely encountered (Dicks et al. 2012), though this is probably more common since the application of the ChAdOx1 nCov-19 vaccine from AstraZeneca. Recent studies in clinical trials have shown that vaccines delivering the Gag protein vectored by MVA and ChAdOx1 could elicit strong and broad T cell responses against HIV in vitro (Hanke 2019). CD74 can target MHC-I molecules to the endosomal pathway (Sugita and Brenner 1995), and specific epitopes embedded in the CLIP region of CD74 could be loaded effectively into MHC-I molecules and elicit CD8+ T cell response (Walchli et al. 2014). A recent study in an HCV clinical trial has reported that the fusion of CD74 into the viral vectors ChAd and MVA could effectively elevate HCV-specific CD8+ T cell response (Esposito et al. 2020). Therefore, exploration of whether and how HLA-E presents Gag-derived peptides in

these delivery systems would shed light on the ways to manipulate the peptide presentation of HLA-E, which might be crucial for vaccine design (Früh and Picker 2017; Hansen et al. 2016; Malouli et al. 2021).

Despite a thorough characterisation of the intracellular transport of HLA-E and its regulation in previous chapters, the peptide presentation process of HLA-E is far from clear. Conformation-specific antibodies can distinguish peptide-bound MHC molecules from peptide-free ones (Zagorac et al. 2012), and antibodies specific for a particular MHC-peptide complex could detect peptide presentation in a sensitive and precise way (Cohen et al. 2003), which are the most common tools to study the peptide loading and presentation process. Although our group is currently developing and characterising several HLA-E antibodies that could potentially distinguish between different HLA-E conformations and recognise the presentation of a specific peptide, the low surface expression of HLA-E and the short surface lifetime of HLA-E-peptide complexes challenge the sensitivity of an antibody-based system to detect HLA-E-restricted peptide presentation. As CD8+ T cells transduced with a certain TCR can recognise the presentation of the target peptide by the restricted HLA allele in a specific and sensitive way, it is possible to detect the surface presentation of HIV-derived peptide by HLA-E using CD8+ T cell activation as the readout. Therefore, in this chapter, I aim to establish and optimise a CD8+ T cell activation system to detect peptide presentation using different peptide delivery systems.

5.2 Results

5.2.1 Establishment of the SKW-3 cell activation system to assess peptide presentation

Given that the monocytic cell line THP1 resembles primary monocytes and the CD8+ cell line SKW-3 is TCRαβ negative, they were chosen to establish the CD8+ T cell activation system here. The best HLA-E-restricted, HIV-specific TCR (p13c7) that we

have, which recognises the HIV-1 $Gag_{275\text{-}283}$ RL9 peptide (RL9-TCR) (Yang et al. 2021), was chosen to enable the maximal sensitivity of the assay. The TCR that is specific for the HLA-A*0201 NY–ESO-$1_{157–165}$ peptide (1G4) was selected as the positive control to characterise SKW-3 cells.

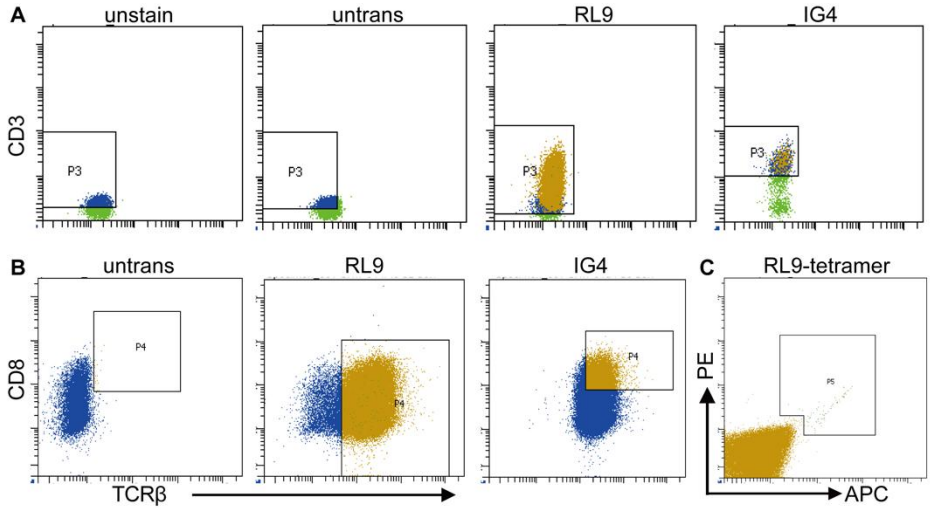

Figure 5.1 Construction of SKW-3 cells stably expressing RL9-TCR or 1G4
Gating strategy for FACS sorting of SKW-3 cells transduced with RL9-TCR or 1G4. After transduction, cells were sorted as CD3+ cells (A) and then as CD8+TCRβ+ cells (B). RL9-TCR transductants were further selected by tetramer staining (C).

After transduction with RL9-TCR or 1G4, SKW-3 cells positive for CD3, CD8 and mouseTCRβ were sorted (Fig5.1A). These TCR constructs contain specific Vα and Vβ segments fused to murine Cα and Cβ segments, so TCR+ cells can, therefore, be sorted based on the expression of mouse TCRβ. The expression of TCR enables the surface expression of CD3 (Ohashi et al. 1985; van Dongen et al. 1987; Weiss and Stobo 1984), which further ensures the successful transduction in SKW-3 cells. The transduction efficiency of SKW-3 cells was very high, as over 90% of cells were detected as TCRβ+ (Fig5.1B). RL9-TCR transductants were further selected by tetramer staining (Fig5.1C), in which HLA-E-RL9 tetramers conjugated to both PE and APC were used to obtain a clean population of SKW-3 cells expressing functional RL9-TCRs. The ones with low CD8 level were not excluded to enable the recovery of a larger population (Fig5.1B).

RL9-TCR and 1G4 were simultaneously transduced into primary CD8+ T cells as controls (Fig.5.2). Compared to SKW-3 cells, primary cells did not have the CD3 expression as a second layer for gating TCR transductants due to their endogenous expression of TCRαβ complex (Fig.5.2A). The transduction efficiency of primary

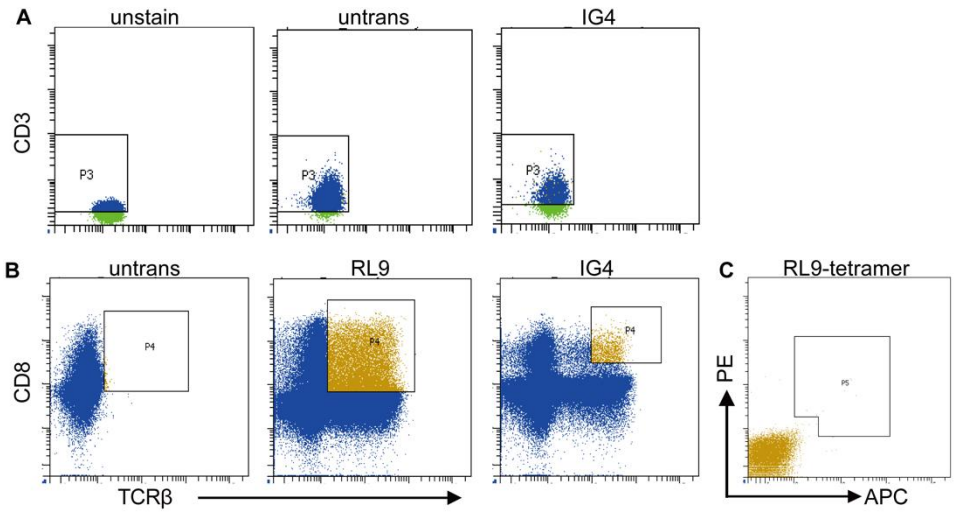

Figure 5.2 Transduction of RL9-TCR or 1G4 into primary CD8+ T cells
Gating strategy for FACS sorting of primary CD8+ T cells transduced with RL9-TCR or 1G4. After transduction, cells were sorted as CD3+ cells (A) and then as CD8+TCRβ+ cells (B). RL9-TCR transductants were further selected by tretramer staining (C).

CD8+ cells was approximately 40%, which was satisfactory, though lower than that of SKW-3 cells (Fig.5.2B). CD8 downregulation observed in a large population of primary cells is probably due to activation. Similar to SKW-3 cells, only a small population of RL9-TCR transductants were positive in the HLA-E-RL9 tetramer staining (Fig5.2C).

As the low surface expression of HLA-E might be a major restriction to the sensitility of the assay, I tested whether the incubation of IFN-γ and PMA could increase HLA-E surface expression. IFN-γ could stimulate the transcription of HLA-E (Barrett et al. 2004; Gustafson and Ginder 1996), and PMA could induce HLA-E surface expression in THP1 cells (Camilli et al. 2016). After a 24h incubation with IFN-γ at a final concentration of 1ng/ml, a three-fold increase of HLA-E surface expression was observed (Fig.5.3). However, the surface-promoting effect of IFN-γ quickly reached a

plateau, and no significant increase of HLA-E surface level was observed when the concentration of IFN-γ increased from 1ng/ml to 1000ng/ml. Although PMA incubation did not seem to increase HLA-E surface expression on its own, it appeared to enhance the promoting effect of IFN-γ, as the THP1 cells co-incubated with PMA showed higher HLA-E surface level at a high concentration of IFN-γ. An approximately 8-fold increase in surface HLA-E level was observed in THP1 cells after incubation with PMA (50ng/ml) and IFN-γ (100ng/ml). Therefore, the incubation of IFN-γ and PMA could effectively promote the surface expression of HLA-E in THP1 cells.

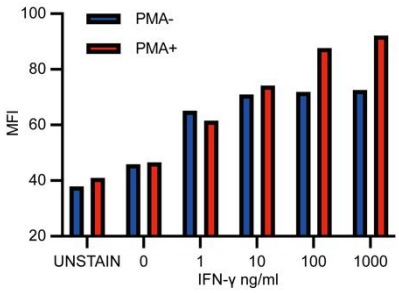

Figure 5.3 IFN-γ and PMA can increase HLA-E surface expression
THP1 cells were incubated with IFN-γ of different concentrations with (red) or without (blue) PMA addition (final: 50ng/mL). 24hrs after stimulation, surface expression of HLA-E was assessed with anti-HLA-E antibody (3D12). MFIs shown here are representative of observations made in two independent experiments.

T cell activation was examined using THP1 cells stimulated with both PMA (50ng/ml) and IFN-γ (100ng/ml), either of them or none of them (Fig.5.4). 24hrs after stimulation, THP1 cells were peptide-pulsed with RL9 or NY-ESO-1 peptide before co-incubation with SKW-3 cells or primary cells transduced with either 1G4 or RL9-TCR. In the positive control where THP1 cells peptide-pulsed with NY-ESO-1 were co-incubated with 1G4-transduced SKW-3 cells, the activation of SKW-3 cells could be detected by the upregulation of the activation markers CD25, CD69 and CD137 (Fig.5.4A, B). The increase in surface level was most significant for CD69, which is consistent with previous findings that CD69 seems to be a more sensitive activation marker than CD25 and CD137 in SKW-3 cells as well as others (Janssens et al. 2022; Satta et al. 2019). Pre-incubation with IFN-γ did not seem to affect the readout, and PMA pre-incubation seemed to lead to unspecific upregulation of CD69 in SKW-3 cells (Fig.5.4A). In contrast, despite the high concentration of RL9 peptide

kept in media during the co-incubation process, THP1 cells pulsed with RL9 could not activate SKW-3 cells transduced with the RL9-TCR (Fig.5.4A, B). This suggests the low binding affinity of RL9 to HLA-E as well as the low avidity of the RL9-TCR. In primary CD8+ T cells transduced with 1G4, the upregulation of all three surface markers seemed to be more remarkable compared to SKW-3 cells after co-incubation with NY-ESO-1-pulsed THP1 cells, though unspecific activation was observed in these 1G4 transductants after incubation with THP1 pulse with RL9 (Fig.5.4C, D). Similarly, IFN-γ did not make any difference, while PMA led to unspecific upregulation of CD69. HLA-E-RL9 complex failed to activate primary T cells transduced with the RL9-TCR.

To select the best indicator of SKW-3 cell activation, I also tested the secretion of a panel of cytokines apart from the surface markers (Fig.5.5). While TNF-α secretion was detectable for 1G4-transduced SKW-3 cells after co-incubation with THP1 cells pulsed with the NY-ESO-1 peptide, secretion of MIP-1 β or IFN-γ was not observed (Fig.5.5A, B). While IFN-γ did not seem to affect cytokine secretion, PMA promoted the secretion of TNF-α though adding a little background noise. No cytokine secretion was detected for SKW-3 cells transduced with the RL9-TCR after incubation with RL9-pulsed THP1 cells. In 1G4-transduced primary cells co-incubated with NY-ESO-1-pulsed THP1 cells, significant TNF-α secretion was detected, weak MIP-1 β secretion was detected, and no IFN-γ secretion was detected (Fig.5.5C, D). Pre-incubation with IFN-γ did not seem to affect the readout, but PMA pre-incubation led to unspecific secretion of both TNF-α and MIP-1 β. While the secretion of TNF-α was more pronounced in primary CD8+ T cells compared to SKW-3 cells, unspecific cytokine secretion was observed in 1G4-transduced primary cells incubated with RL9-pulsed THP1 cells, which is worsened after pre-incubation of THP1 cells with PMA.

To conclude, SKW-3 cells are comparable to primary CD8+ T cells and can thus be used to characterise peptide presentation in the following assays. Upregulation of the

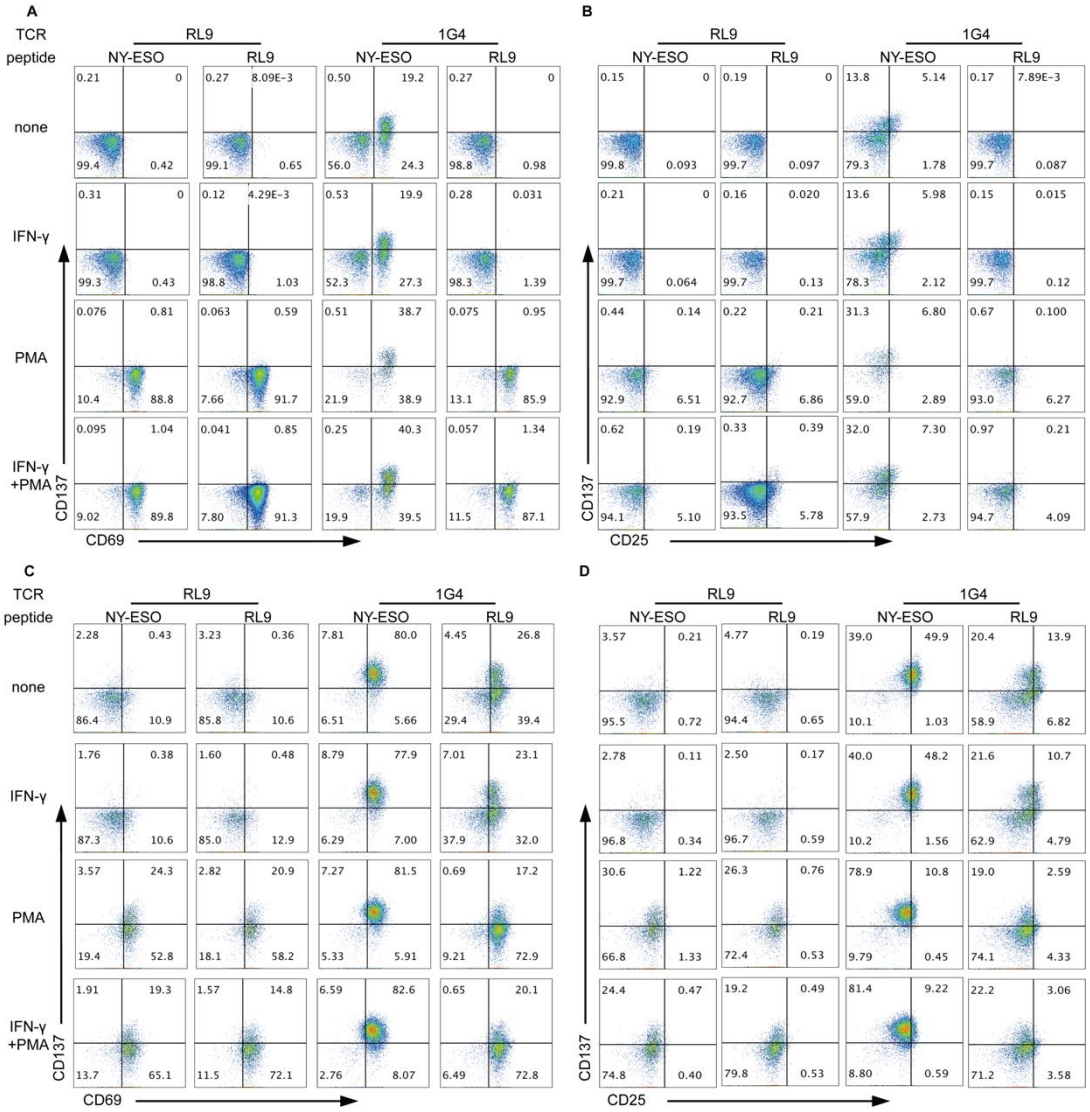

Figure 5.4 Assessment of the activation of SKW-3 cells and primary CD8+ cells with different activation markers
THP1 cells were stimulated with IFN-γ (final 100ng/mL) or PMA (final 50ng/mL) for 24hrs and then incubated with NY-ESO-1 (final 1μM) or RL9 (final 100μM) peptide for 2hrs. Peptide-pulsed THP1 cells were then incubated overnight with SKW-3 cells (A, B) or primary CD8+ cells (C, D) transduced with RL9-TCR or 1G4 at a 1:1 E:T ratio. NY-ESO-1 was washed away after peptide pulsing while RL9 was kept in media during the co-incubation. The activation of SKW-3 cells and primary CD8+ T cells were evaluated by the surface level of the activation markers CD25, CD69 and CD137. Dotplots are representative of two independent experiments (two replicates/run).

activation markers CD25, CD69, and CD137, as well as the secretion of TNF-α, are suitable readouts for measuring the activation of SKW-3 cells, among which CD69 and TNF-α are the best markers. RL9-TCR transduced T cells could not detect the presentation of the HLA-E-RL9 complex even when surface HLA-E was significantly

upregulated via IFN-γ and PMA pre-incubation and saturated with a high concentration of RL9 peptide.

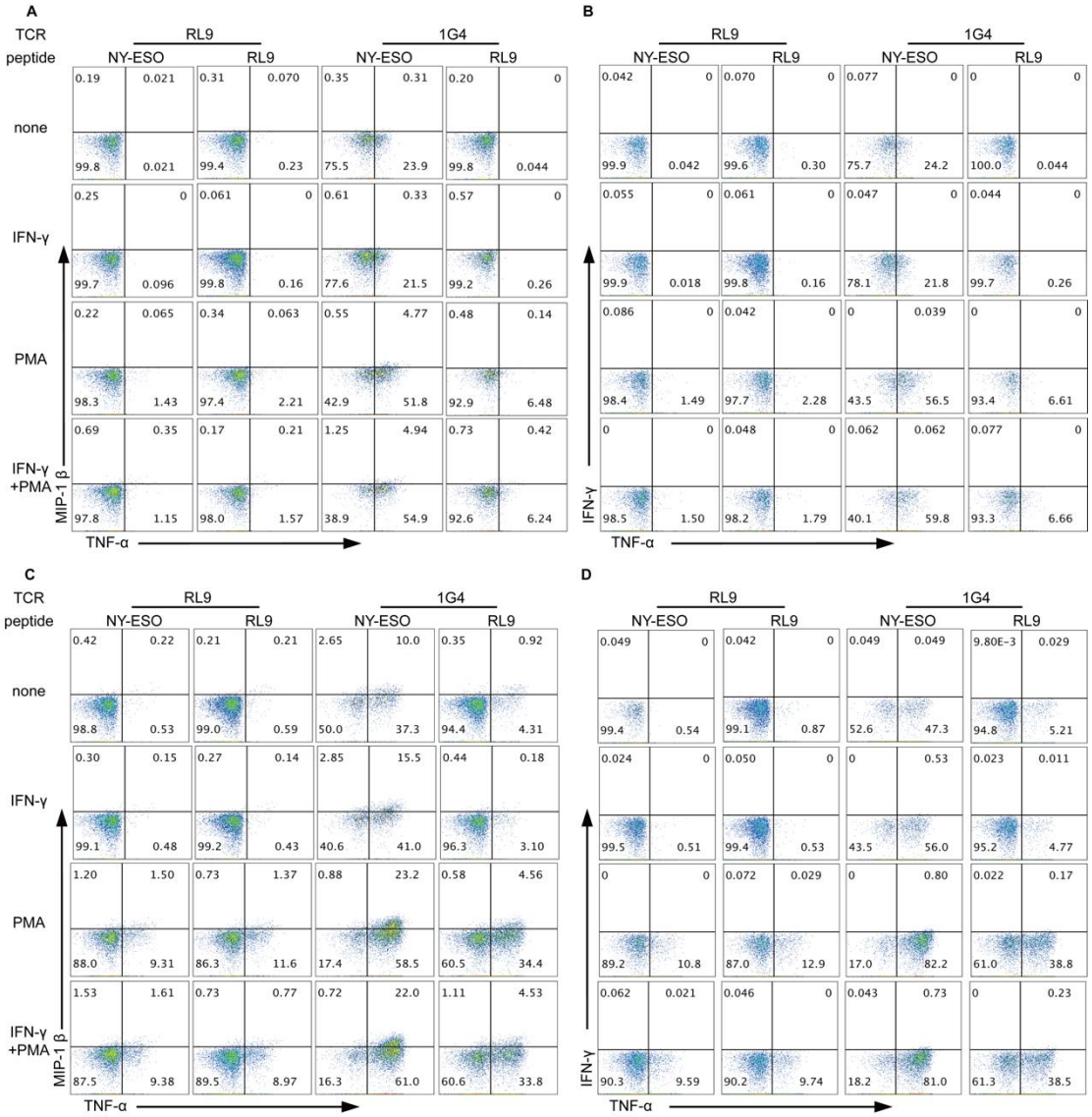

Figure 5.5 Assessment of the activation of SKW-3 cells and primary CD8+ cells with different cytokines
THP1 cells with or without a 24hrs pre-stimulation with IFN-γ (final 100ng/mL) or PMA (final 50ng/mL) were incubated with NY-ESO-1 (final 1μM) or RL9 (final 100μM) peptide for 2hrs. Peptide-pulsed THP1 cells were then incubated with SKW-3 cells (A, B) or primary CD8+ cells (C,D) transduced with RL9-TCR or 1G4 at a 1:1 E:T ratio for 8hrs in the presence of BFA (final 5μg/mL) and GolgiStop (final 5μg/mL). NY-ESO-1 was washed away after peptide pulsing while RL9 peptide was kept in media during the co-incubation. The activation of SKW-3 cells and primary CD8+ T cells were evaluated by the production of TNF-α, MIP-1 β and IFN-γ. Dotplots are representative of two independent experiments (two replicates/run).

5.2.2 Current system is not sensitive enough to detect the HLA-E-restricted presentation of RL9 peptide

As the system was not sensitive enough to detect RL9 presentation even if surface HLA-E molecules were effectively upregulated and artificially saturated with RL9 via peptide pulsing, it wouldn't be able to detect RL9 presentation under more physiological conditions like HIV infection where the surface level of the HLA-E-RL9 complex is even lower. Therefore, optimisation of the T cell activation assay is necessary.

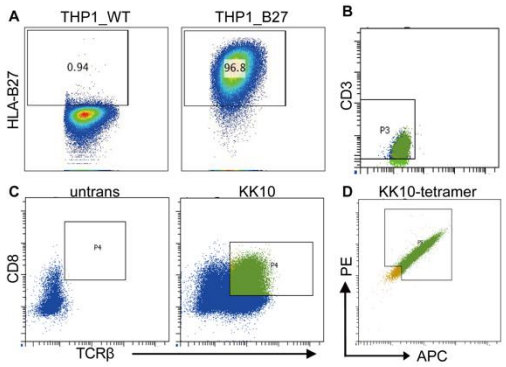

Figure 5.6 Construction of THP1_B27 and SKW-3 cells transduced with the HLA-B27-KK10 TCR
A. THP1 cells were transduced with HLA-B*2705 (THP1_B27), and surface expression of HLA-B27 was assessed with flow cytometry. Untransduced THP1 cells (THP1_WT) was used as the negative control.
B-D. SKW-3 cells were transduced with KK10-TCR, and sorted as CD3+ cells (B), CD8+TCRβ+ cells (C), and finally cells positive for HLA-B27-KK10 tetramer staining (D).

As I aim to assess RL9 presentation in HIV infection in the future, I switched the positive control from NY-ESO-1 to the HLA-B*2705-restricted HIV-1 $Gag_{263-272}$ KK10 peptide to improve the system. KK10 peptide could be presented after HIV infection and led to effective T cell activation (Iglesias et al. 2013), and is thus a sensitive and robust tool to optimise the conditions of the assay (Yang et al. 2021).

As THP1 does not express the HLA-B27 allele, I transduced HLA-B*27:05 into THP1 cells (THP1_B27) (Fig.5.6A). THP1_B27 cells have a satisfactory surface expression level of HLA-B27 and are, therefore, the ideal APCs for the optimisation process. HLA-B27-KK10-specific TCR (KK10-TCR) was transduced into SKW-3 cells and then sorted as CD3+CD8+TCRβ+ cells (Fig.5.6B, C) and further selected by tetramer staining (Fig5.6D). While less than 1% of TCRβ+ SKW3 cells transduced with the RL9-TCR were double positive in the tetramer staining, almost 100% of TCRβ+ SKW3 cells transduced with the KK10-TCR were double positive, which is consistent with the high avidity of the KK10-TCR and low avidity of the RL9-TCR

(Berger et al. 2011; Yang et al. 2021).

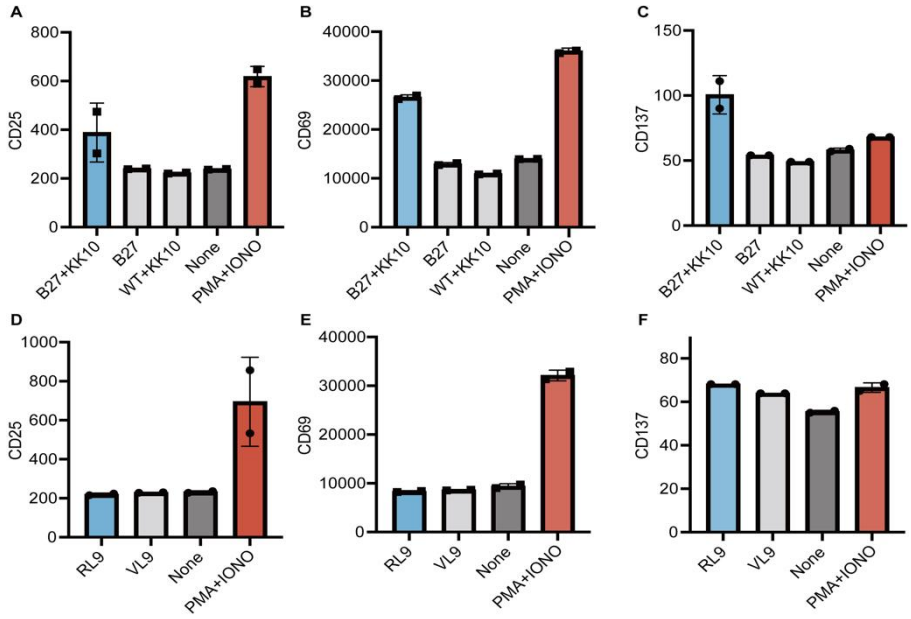

Figure 5.7 Assessment of the activation of SKW-3 cells with activation markers
A-C. THP1_B27 cells were incubated with KK10 peptide (final 1μM) for 2hrs (B27+KK10, blue) and then incubated overnight with SKW-3 cells transduced with KK10-TCR at a 1:1 E:T ratio. THP1_B27 cells without pre-incubation with KK10 peptide (B27), THP1 cells with KK10 incubation (WT+KK10), and the sample without THP1 addition (None) were used as negative controls (grey). SKW-3 directly stimulated overnight with PMA (final 50ng/mL) and IONO (final 40ng/mL) was used as the positive control (PMA+IONO, red).
D-F. SKW-3 cells transduced with RL9-TCR were co-incubated overnight with K562 cells stably transduced with SCT_HLA-E_RL9 (RL9, blue) at a 1:1 E:T ratio. K562 cells stably transduced with SCT_HLA-E_VL9 (VL9) or samples without K562 cells (None) were used as negative controls (grey). SKW-3 directly stimulated overnight with PMA (final 50ng/mL) and IONO (final 40ng/mL) was used as the positive control (PMA+IONO, red).
The activation of SKW-3 cells and primary CD8+ T cells was evaluated by the surface level of the activation markers CD25 (A, D), CD69 (B, E), and CD137 (C, F). MFIs were collected and plotted for two biological runs.

I then tested whether THP1_B27 cells could present the KK10 peptide to SKW-3 cells transduced with the KK10-TCR and activate them. As expected, KK10-pulsed THP1_B27 cells effectively upregulated the activation markers CD25, CD69 and CD137 in KK10-TCR transduced SKW-3 cells (Fig5.7A-C). No surface increase of the activation markers was observed in the absence of KK10 pulsing or HLA-B27 expression, suggesting that the activation of the SKW-3 cells was specific to the surface expression of the HLA-B27-KK10 complex. The combination of PMA and ionomycin (IONO), which could directly activate T cells without the involvement of TCRs (Takahama and Nakauchi 1996), was used as the positive control. Although activation with PMA and IONO significantly upregulated the surface level of CD25 and CD69, no increase in CD137 surface expression was observed. These results

suggest that KK10-TCR transduced SKW-3 cells could be activated effectively and specifically and could be used as the positive control in the following assay.

As RL9-pulsed THP1 cells failed to activate RL9-TCR transduced SKW-3 cells (Fig.5.4-5), I then tried K562 cells transduced with SCT_RL9, which should provide a considerably larger amount of HLA-E loaded with RL9 on the surface and may potentially activate T cells (Yang et al. 2021). K562 cells transduced with SCT_VL9 were used as the negative control, and PMA/IONO activation was used as the positive control. K562 cells transduced with the SCT_RL9 could not activate SKW-3 cells transduced with the RL9-TCR, as no obvious upregulation was observed for the activation markers (Fig.5.7D-F). In contrast, stimulation of PMA and IONO could lead to a pronounced increase in the surface expression of CD25 and CD69.

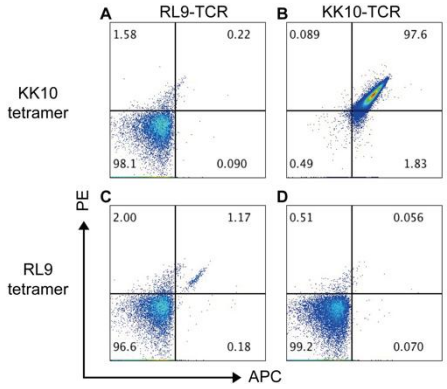

Figure 5.8 Tetramer staining of sorted SKW-3 cells transduced with different TCRs
Sorted SKW-3 cells transduced with TCRs specific for HLA-E-RL9 (A, C) or HLA-B27-KK10 (B, D) were stained with PE/APC-conjugated tetramers specific for HLA-B27-KK10 (A, B) or HLA-E-RL9 (C, D). Dotplots are representative of two independent experiments.

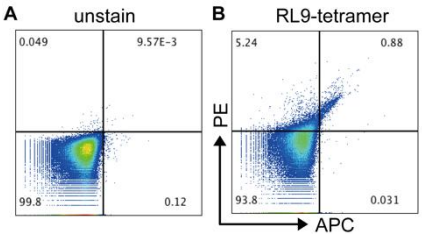

Figure 5.9 Tetramer staining of resorted SKW-3 cells transduced with RL9-TCR
Sorted SKW-3 cells transduced with specific for HLA-E-RL9 were expanded, resorted, and then stained again with PE/APC-conjugated tetramer specific for HLA-E-RL9 (B). unstained sample was used as the negative control (A).

As the artificial expression of SCT_RL9 is maximising the stability and amount of HLA-E-RL9 complex present on the cell surface of APCs, the failure of T cell activation may be due to the limited population of SKW-3 cells expressing a high level of RL9-TCR. To evaluate this hypothesis, I carried out tetramer staining for sorted SKW-3 cells transduced with RL9-TCR and KK10-TCR (Fig.5.8). As expected,

all sorted SKW-3 cells transduced with the KK10-TCR showed good staining for the KK10 tetramers. In contrast, only around 1% of SKW-3 cells transduced with the RL9-TCR were double positive in the RL9 tetramer staining, though the whole population was selected on tetramer staining during sorting.

The tetramer staining result implied poor expression of RL9-TCRs on the surface of SKW-3 cells, which may largely limit the sensibility of the detection of RL9 presentation. Therefore, I resorted the SKW-3 cells transduced with the RL9-TCR based on tetramer staining to enrich the population with a high level of functional RL9-TCRs. However, similar to the first round of sorting, the second round failed to enrich tetramer-positive SKW-3 cells (Fig.5.9). Given that the RL9-TCR has low avidity and is hard to manipulate from published and unpublished data in our group (Yang et al. 2021), a better HLA-E TCR is required to set up a robust and sensitive system to detect the regulation of HLA-E-restricted presentation of pathogen-derived peptides. Our group has recently got a promising high-affinity HLA-E-restricted TCR that is specific for an HPV E1 peptide which might fit into the system (unpublished data). Besides, we are also developing an antibody and CART cells that can specifically recognise the HLA-E-RL9 complex. Meantime, I tried to optimise the T cell activation system for peptide presentation pathway analysis based on the HLA-B27-KK10 system.

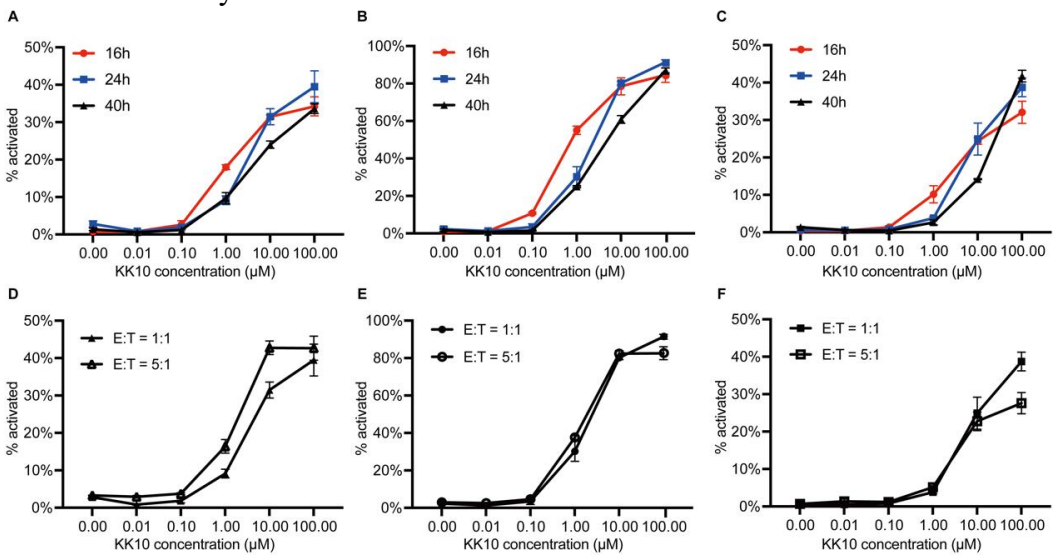

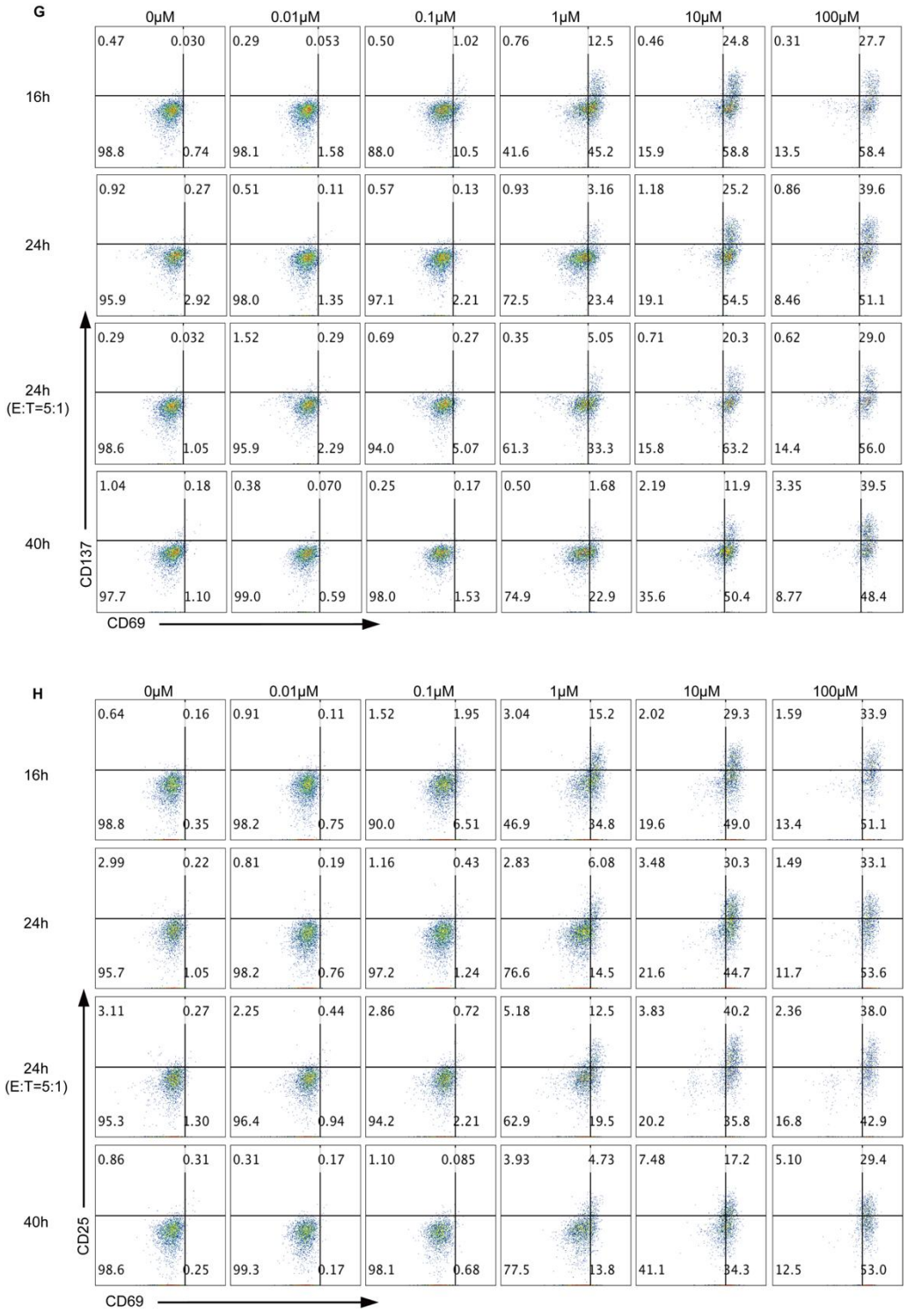

Figure 5.10 Optimisation of the activation of SKW-3 cells
THP1_B27 cells were incubated with different concentrations of KK10 peptide for 2hrs before incubation with SKW-3 cells transduced with KK10-TCR for different time lengths at a 1:1 E:T ratio (A-C), or for 24hrs at different E:T ratios (D-F). The activation of SKW-3 cells was evaluated by the surface level of the activation markers CD25 (A, D), CD69 (B, E), and CD137 (C, F). The percentage of activated cells under each condition was collected and plotted for three biological runs, and data are shown as mean ± SD (error bars) (A-F). Representative dotplots of each condition are shown (G, H).

5.2.3 Optimisation of the conditions to effectively elicit the response of SKW-3 cells

As it would be useful to characterise the conditions for the activation of SKW-3 cells for future manipulation of the system, I compared how activation time length, KK10 peptide concentration, and E:T ratio affected the activation of KK10-TCR transduced SKW-3 cells as well as the difference between different activation markers (Fig.5.10).

As the assessment of the expression kinetics of the activation markers would help to increase the sensitivity of the assay, I compared the surface expression of CD25, CD69 and CD137 after activation of SKW-3 cells for different time lengths. Similar trends were seen for different activation markers. Prolongation of the activation time length from 16hrs to 40hrs did not further increase the percentage of activated SKW-3 cells (Fig.5.10A-C, G, H). Besides, a slight decrease in signal was observed with the increase in activation time length. Therefore, 16hrs would be a suitable activation time length for SKW-3 cells.

As it is important to know the lowest peptide concentration to initiate the activation of SKW-3 cells or to enable robust activation of SKW-3 cells, I examined the surface expression of different activation markers with different concentrations of KK10 peptide. The lower limit of peptide concentration for the activation of SKW-3 cells is around 0.1μM, as no obvious T cell activation could be observed with a lower KK10 peptide concentration. A higher KK10 peptide concentration led to the activation of more SKW-3 cells, and over 80% of SKW-3 cells showed obvious upregulation of CD69 level when the peptide concentration reached 100μM (Fig.5.10B, G, H). When the KK10 concentration was 1μM, which was used in previous assays, upregulation of CD69 could be observed in around 60% of SKW-3 cells. Thus, 1μM would be the ideal concentration for the following assays.

As the E:T ratio also affects T cell activation (Yang et al. 2021), I also compared the surface expression of different activation markers between an E:T ratio of 1:1 and 5:1 (Fig.5.10D-H). A slightly higher percentage of SKW-3 cells upregulated CD25 at the 5:1 E: T ratio compared to 1:1, while no noticeable difference was observed for CD69 and CD137. Therefore, a 1:1 E:T ratio was applied in the following assays.

5.2.4 Establishment of KK10 peptide delivery via viral infection

After optimising the conditions for optimal activation of SKW-3 cells using peptide pulsing, I explored whether KK10 could be produced endogenously upon viral infection and activate SKW-3 cells.

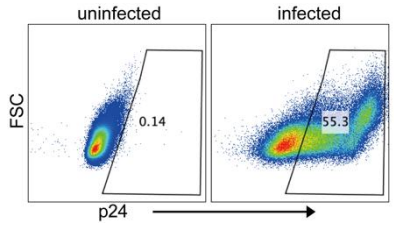

Figure 5.11 THP1 infection with HIV-1 (VSVG-BAL)
THP1 cells were infected with HIV-1 (VSVG-BAL), and infection efficiency was examined three days later via intracellular p24 staining. uninfected cells were used as the negative control, and representative dotplots are shown.

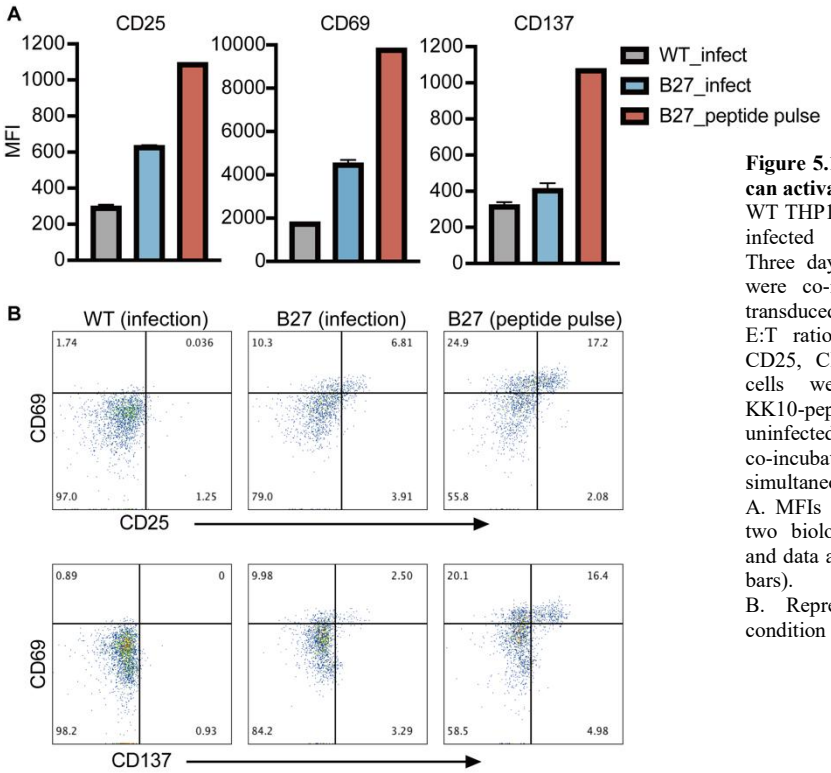

Figure 5.12 HIV-1-infected THP1 cells can activate SKW-3 cells
WT THP1 cells or THP1_B27 cells were infected with HIV-1 (VSVG-BAL). Three days after infection, THP1 cells were co-incubated with SKW-3 cells transduced with the KK10-TCR at a 1:1 E:T ratio, and surface expression of CD25, CD69 and CD137 on SKW-3 cells were examined after 16hrs. KK10-peptide pulsed (final 1μM), uninfected THP1_B27 cells were co-incubated with SKW-3 cells simultaneously as the positive control.
A. MFIs were collected and plotted for two biological runs (2 replicates/run), and data are shown as mean ± SD (error bars).
B. Representative dotplots of each condition are shown.

The effectiveness of direct HIV-1 infection was first assessed. To enable efficient infection, I chose the VSVG-pseudotyped HIV-1 NL4.3-BaL strain (HIV-1 (VSVG-BAL)), which was produced by Anna Kliszczak in our group. HIV-1 (VSVG-BAL) could infect THP1 cells effectively, as p24 was detected in over 50% of THP1 cells three days after infection (Fig.5.11). HIV-1 infected THP1_B27 cells could present the Gag-derived KK10 peptide and activate SKW-3 cells transduced with the KK10-TCR, as upregulation was observed for the activation markers CD25, CD69 and CD137 (Fig.5.12).

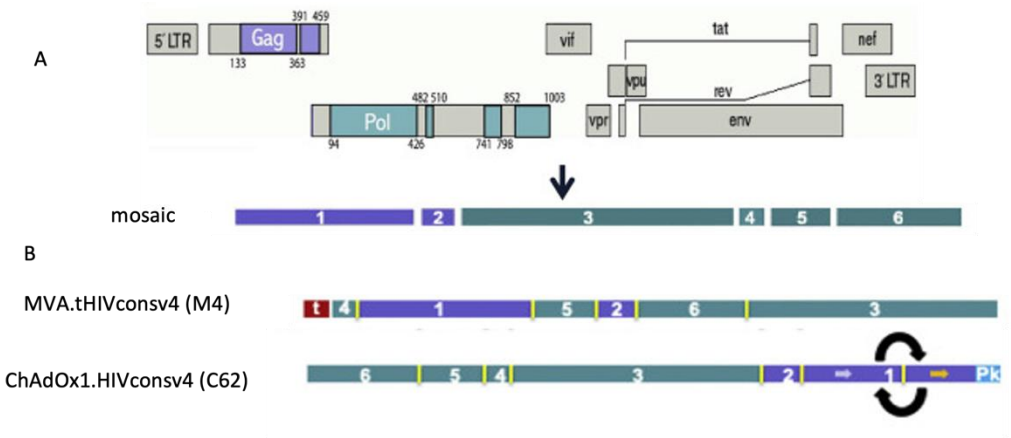

Figure 5.13 Design of the M4 and C62 constructs
A. Design of the bi-valent mosaics from six conserved regions in HIV-1 Gag (region 1-2, purple) and Pol (region 3-6, green) as described previously (Wee et al. 2021).
B. Design of the mosaics in the M4 and C62 constructs. C62 has p24 region in mosaic 1 rearranged. M4 contains the human tissue plasminogen activator (tPA) leader sequence at the start (t, red) while C62 has a C-terminal V5-tag that can be recognised by the monoclonal antibody SV5-Pk (Pk, blue). Figures reprinted from (Wee et al. 2021).

However, the level of T cell activation of HIV-infected THP1 cells was weaker than peptide-pulsed THP1 cells, implying the limited sensitivity of the assay. It takes more than 48h for HIV-infected cells to start to effectively produce the Gag protein (Pace et al. 2012), which makes it very challenging to introduce further manipulation of the peptide presentation pathways during the process, though the presentation of gag-derived epitopes from incoming viral particles has been reported (Kløverpris et al. 2013). Therefore, I also tested delivery of the Gag protein via non-replicating viral

vectors MVA and simian (chimpanzee) adenovirus ChAdOx1, which have provided encouraging results in recent clinical vaccine trials (Fig.5.13) (Wee et al. 2021).

The infection efficiency of these viral vectors was first examined. 24hrs after infection with M4 (Wee et al. 2021) at different MOI, the infection rate of THP1 cells was evaluated via intracellular p24 staining (Fig.5.14A). HeLa cells infected simultaneously at an MOI of 5 were used as the positive control (Fig.5.14B). Over 70% of THP1 cells were successfully infected at an MOI of 5, implying the high infection efficiency of M4. Further increase of MOI did not enhance the infection rate, suggesting that an MOI of 5 is enough for effective infection of THP1 cells.

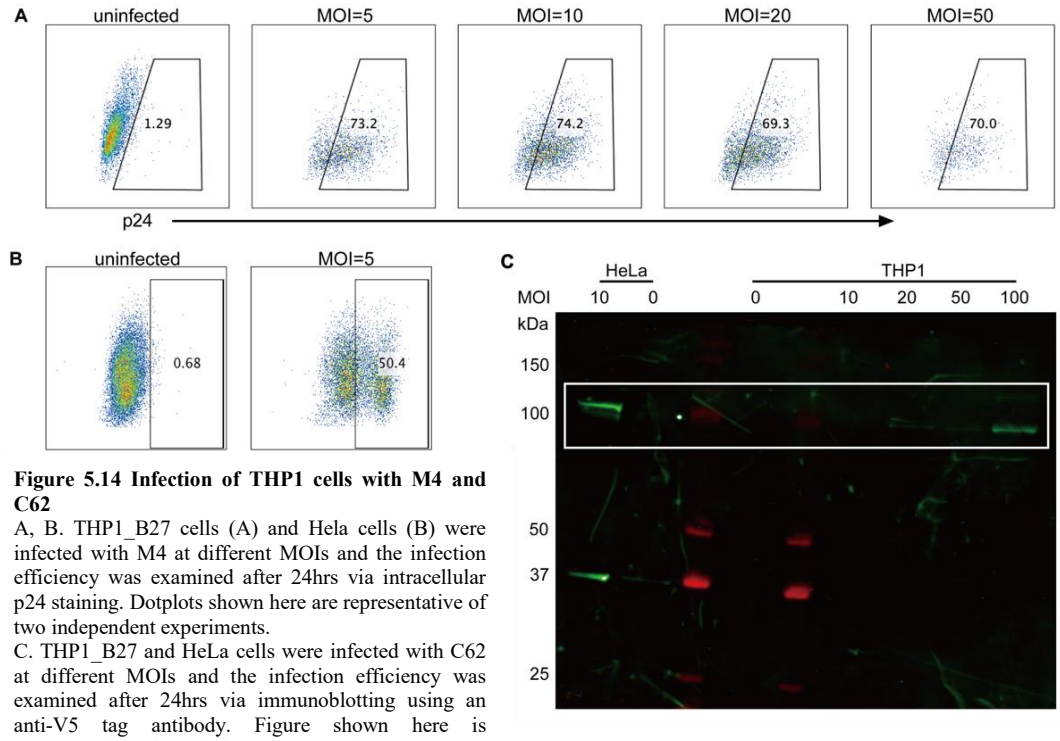

Figure 5.14 Infection of THP1 cells with M4 and C62

A, B. THP1_B27 cells (A) and Hela cells (B) were infected with M4 at different MOIs and the infection efficiency was examined after 24hrs via intracellular p24 staining. Dotplots shown here are representative of two independent experiments.

C. THP1_B27 and HeLa cells were infected with C62 at different MOIs and the infection efficiency was examined after 24hrs via immunoblotting using an anti-V5 tag antibody. Figure shown here is

The infection efficiency of ChAdOx1.HIVconsv62 (C62) in THP1 cells was also evaluated 24hrs after infection at different MOIs (Fig.5.14C). As the Gag p24 region was rearranged in C62, the infection efficiency was assessed by immunoblotting against the V5-tag, which is co-expressed on the construct (Wee et al. 2021). HeLa cells were infected simultaneously as the positive control. A bright band around

100kDa could be observed for infected HeLa cells, implying an effective infection of C62. In contrast, no band could be detected for the sample in which THP1 cells were infected at an MOI of 10, a very weak band was observed when the MOI was 20 or 50, and a clear band was only observed in the sample where the MOI was 100. This suggests that either C62 could not infect THP1 cells as effectively as HeLa cells or the synthesis of the Gag was less efficient in THP1 cells.

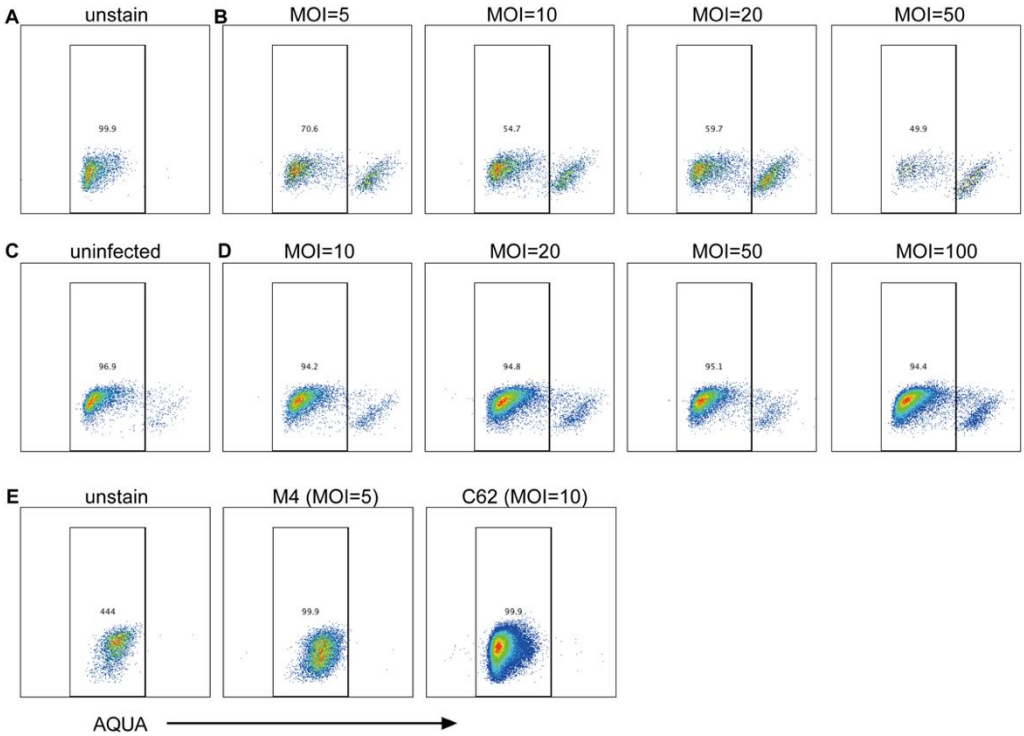

Figure 5.15 Viability of THP1_B27 cells and HeLa cells after infection with M4 or C62
THP1_B27 cells were infected with M4 (B) or C62 (D) at different MOIs and the viability was examined after 24hrs via staining with the Live/Dead Fixable Aqua dye (AQUA). Unstained cells (A) and uninfected cells (C) were used as negative controls. The viability of HeLa cells infected with M4 or C62 (E) were measured simultaneously. Dotplots shown here are representative of two independent experiments.

To select the optimal MOI, the viability of THP1 cells was assessed after infection with M4 or C62 at different MOIs (Fig.5.15). While the infection of M4 was effective, it seemed to be toxic to THP1 cells, as a higher MOI led to an increase in cell death (Fig.5.15B). The viability of THP1 cells dropped to around 70% when the MOI was 5 and to approximately 50% when the MOI was 50. In contrast, C62 did not seem to be toxic to THP1 cells, as the viability was over 90% even when the MOI was 100 (Fig.5.15D). The viability of HeLa cells was 100% when effectively infected with M4

or C62 (Fig.5.15E). Therefore, M4 infection was toxic to THP1 cells, while the infection of C62 did not affect its viability.

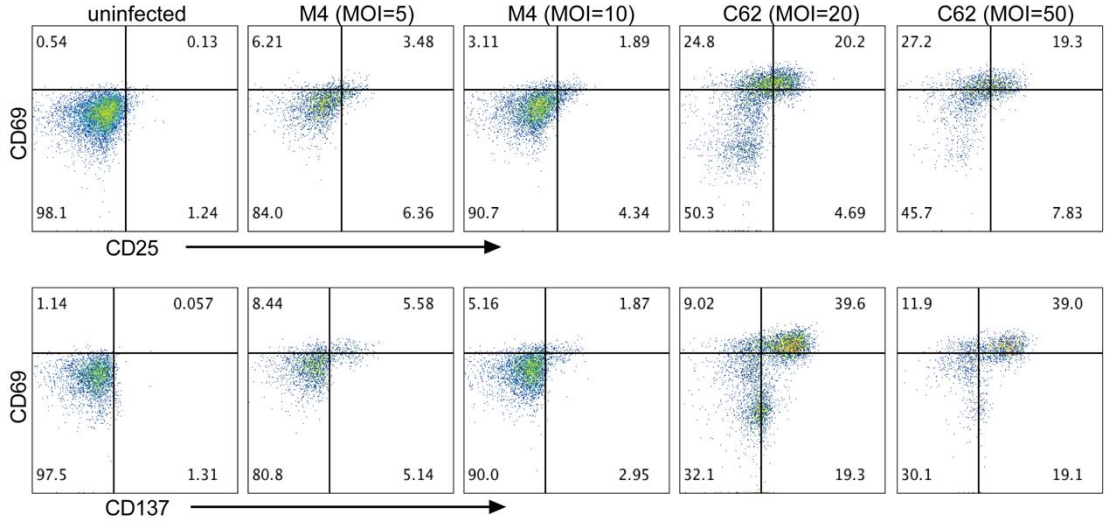

Figure 5.16 THP1 cells infected with M4 or C62 can activate SKW-3 cells
THP1_B27 cells were infected with M4 or C62 at different MOIs. 24hrs after infection, THP1 cells were co-incubated with SKW-3 cells transduced with the KK10-TCR at a 1:1 E:T ratio, and surface expression of CD25, CD69 and CD137 on SKW-3 cells were examined after 16hrs. Uninfected THP1_B27 cells were co-incubated with SKW-3 cells simultaneously as the negative control. Dotplots shown here are representative of two independent experiments.

After the evaluation of infection efficiency and toxicity, I then tested whether THP1_B27 cells infected with M4 or C62 could present the KK10 peptide to activate SKW-3 cells (Fig.5.16). An MOI of 5 and 10 was chosen for M4, while an MOI of 20 and 50 was chosen for C62 to ensure both the infection efficiency and cell viability. 24hrs after infection, THP1_B27 cells were co-incubated with SKW-3 cells transduced with the KK10-TCR. Infected THP1 cells in all the samples activate SKW-3 cells, as an increase of the activation markers CD25, CD69 and CD137 was observed. Although the infection rate of M4 was high (Fig.5.14A, B), less than 10% of SKW-3 was activated. While the Gag expression was weak in THP1 cells infected with C62 at an MOI of 20 or 50 (Fig.5.14C), the presentation of KK10 peptide seemed to be very efficient, as the upregulation of activation markers could be seen in most SKW-3 cells (Fig.5.16). Thus, while THP1 infected with either M4 or C62 could present the KK10 peptide and activate SKW-3 cells, C62 may be more effective.

Considering that C62 infection does not affect the viability of THP1 cells, C62 seem to be a better viral vector to deliver the Gag protein in this assay.

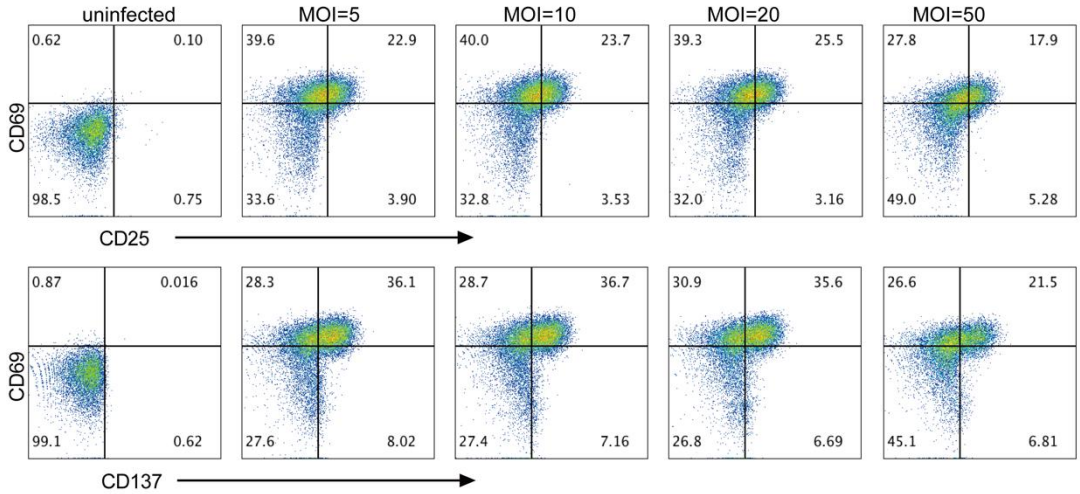

Figure 5.17 THP1_B27 cells infected with C62 can effectively activate SKW-3 cells
THP1_B27 cells were infected with C62 at different MOIs. 8hrs after infection, THP1 cells were co-incubated with SKW-3 cells transduced with the KK10-TCR at a 1:1 E:T ratio, and surface expression of CD25, CD69 and CD137 on SKW-3 cells were examined after 16hrs. Uninfected THP1_B27 cells were co-incubated with SKW-3 cells simultaneously as the negative control. Dotplots shown here are representative of two independent experiments.

As adenovirus could produce a marked level of transgene within a few hours after infection (Dumasius et al. 2003), I further tested if effective KK10 presentation could be detected 8hrs after C62 infection (Fig.5.17). Given that most SKW-3 cells could be activated when THP1 cells were infected with C62 at an MOI of 20, I also tested whether a lower MOI was sufficient to initiate the activation of SKW-3 cells. The majority of SKW-3 cells were activated in all the conditions, as shown by the upregulation of the activation markers CD25, CD69 and CD137. No difference was observed between THP1 cells infected with C62 of different MOIs, suggesting that an MOI of 5 is enough for effective KK10 presentation. Besides, an 8h infection before co-incubation seemed to be enough for the generation of sufficient KK10 peptide, as the activation level was comparable to that of a 16h infection (Fig.5.16; Fig.5.17). Therefore, the KK10 peptide could be efficiently presented in THP1 cells 8hrs after C62 infection at an MOI of 5.

In conclusion, while KK10 presentation could be detected in THP1 cells via infection of HIV-1 and M4, it is more effective in C62 infection. C62 seems to be a promising vector to use in the T cell activation assay, as it could effectively infect THP1 cells, induce quick production of target peptides and activate T cells efficiently, and does

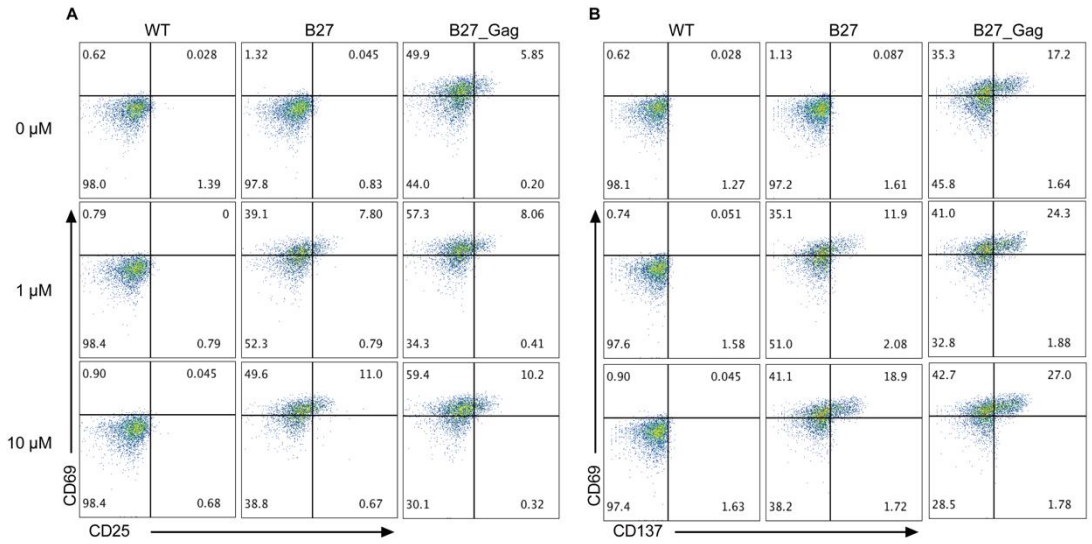

Figure 5.18 THP1 cells can present KK10 derived from endogenous Gag protein and activate SKW-3 cells
WT THP1 cells, THP1_B27 cells, and THP1_B27_Gag cells were incubated with different concentrations of KK10 peptide for 2hrs before incubation with SKW-3 cells transduced with KK10-TCR at a 1:1 E:T ratio. 16hrs after co-incubation, the activation of SKW-3 cells was evaluated by the surface level of the activation markers CD25, CD69, and CD137. Dotplots shown here are representative of three independent experiments.

not affect cell viability.

5.2.5 Establishment of KK10 peptide delivery via Gag or CD74

As viral proteins may play a role in the regulation of peptide presentation, it would be important to have an endogenous peptide delivery system as a control where KK10 could be generated while excluding the potential effects of other viral proteins. Therefore, HLA-B*27:05 and Gag were co-transduced into THP1 cells to generate a cell line stably expressing both HLA-B27 and Gag (THP1_B27_Gag). To evaluate if endogenous Gag expression could directly activate SKW-3 cells or increase the sensitivity of T cell activation, THP1, THP1_B27 and THP1_B27_Gag cells were peptide-pulsed with different concentrations of KK10 before co-incubation with SKW-3 cells transduced with the KK10-TCR (Fig.5.18). Endogenous Gag expression

in THP1_B27_Gag cells led to a significant upregulation of activation markers CD25, CD69 and CD137 on SKW-3 cells, implying sufficient generation of the KK10 peptide. In contrast, no T cell activation was observed in THP1 cells or THP1_B27 cells without peptide pulsing. Endogenous Gag expression and external KK10 peptide pulsing have a synergic effect on promoting KK10 presentation, as the activation was more evident for THP1_B27_Gag cells when coupled with peptide pulsing. Thus, the coupling of endogenous peptide generation and external peptide pulsing might be a useful tool in increasing the sensitivity of T cell activation, which might be particularly helpful in detecting the presentation of weak peptides, like the HLA-E-restricted RL9 peptide.

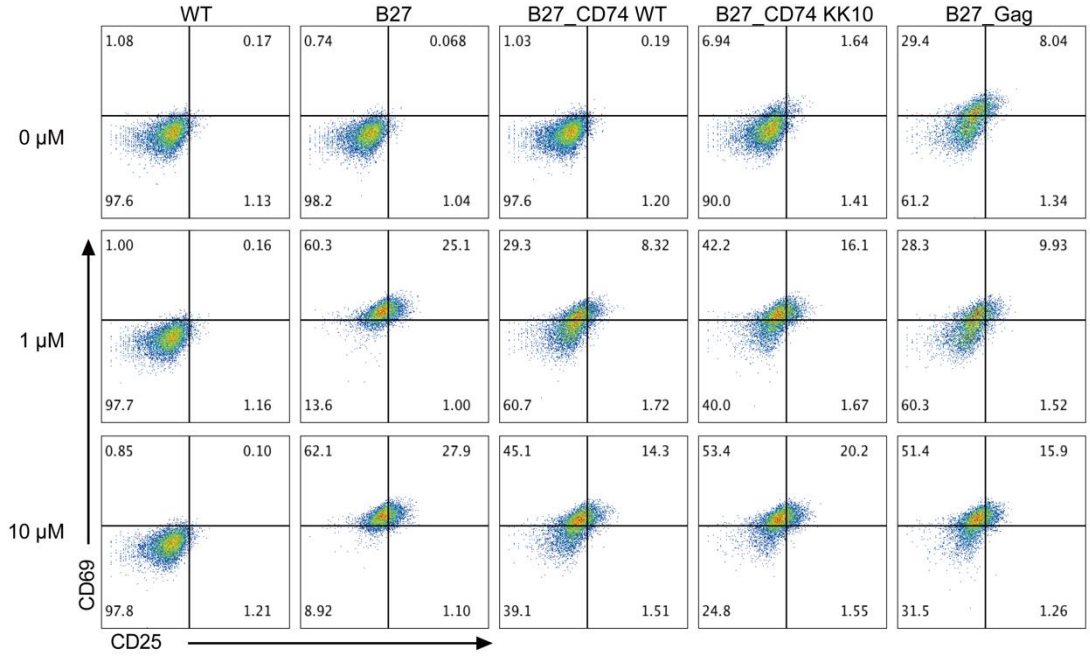

Figure 5.19 CD74 can deliver peptide to HLA-B27 and activate SKW-3 cells
THP1 cells, THP1_B27 cells, THP1_B27_CD74 WT cells, THP1_B27_CD74 KK10 cells or THP1_B27_Gag cells were incubated with different concentrations of KK10 peptide for 2hrs before incubation with SKW-3 cells transduced with KK10-TCR at a 1:1 E:T ratio. 16hrs after co-incubation, the activation of SKW-3 cells was evaluated by the surface level of the activation markers CD25 and CD69. Dotplots shown here are representative of three independent experiments.

CD74 may be a potential chaperone for endosomal peptide presentation, as antigen peptide embedded in the CLIP region of CD74 can be loaded onto HLA-I molecules and presented to CD8+ T cells in a non-canonical, TAP-independent pathway (Walchli et al. 2014). Therefore, I tested whether CD74 with the CLIP region replaced

with KK10 peptide can activate SKW-3 cells transduced with the KK10-TCR (Fig.5.19). HLA-B*27:05 and CD74 (CD74 WT) or CD74 with the CLIP region replaced with KK10 peptide (CD74 KK10) were co-transduced into THP1 cells to generate cell lines stably expressing both HLA-B27 and CD74 (THP1_B27_CD74 WT) or CD74 KK10 (THP1_B27_CD74 KK10). THP1, THP1_B27, THP1_B27_CD74 WT, THP1_B27_CD74 KK10 and THP1_B27_Gag cells were peptide-pulsed with different concentrations of KK10 before co-incubation with SKW-3 cells transduced with the KK10-TCR, and T cell activation was evaluated by the surface expression of CD25 and CD69 (Fig.5.19). Slight upregulation of CD25 and CD69 could be observed in SKW-3 cells co-incubated with THP1_B27_CD74 KK10 cells but not THP1_B27 cells or THP1_B27_CD74 WT cells, suggesting that KK10 peptide from the CLIP region of CD74 could be loaded into HLA-B27 and activate SKW-3 cells. The activation-promoting effect of CD74 KK10 was less effective than Gag, as CD25 and CD69 upregulation was observed in a significantly higher percentage of SKW-3 cells after co-incubation with THP1_B27_Gag cells.

As it should be easier for TCRs on T cells to engage with the MHC/peptide complex with an increase of APCs, I then tested whether the increase of the E:T ratio could enhance the activation of SKW-3 cells. When the ratio of THP1_B27_CD74 KK10: SKW-3 cells was 1:1, CD69 upregulation was observed in around 5% of SKW-3 cells (Fig.5.20). In contrast, around 10% of SKW-3 cells showed CD69 upregulation when the ratio was 5:1. Similarly, the change of E:T ratio from 1:1 to 5:1 also enhanced promoted the activation of SKW-3 cells after co-incubation with THP1_B27_Gag cells. The activation-promoting effect of the increase in the E:T ratio is less effective than peptide pulsing, which is possibly because only a small amount of KK10 was produced and presented endogenously from CD74_KK10 or Gag. THP1_WT, THP1_B27 or THP1_CD74 WT cells alone should not activate SKW-3 cells for lack of KK10 peptide and were thus used as the negative controls in the assay. However,

the rise of the E:T ratio led to a slight upregulation of CD25 and CD69 signals in SKW-3 cells. The background noise was more obvious for CD25, as 5% SKW-3 cells were unspecifically activated when the E:T ratio rose from 1:1 to 5:1. Thus, though the increase of the E:T ratio could promote the capability of THP1_B27_CD74 KK10 cells and THP1_B27_Gag cells in activating SKW-3 cells, it is not very effective and increased the background noise.

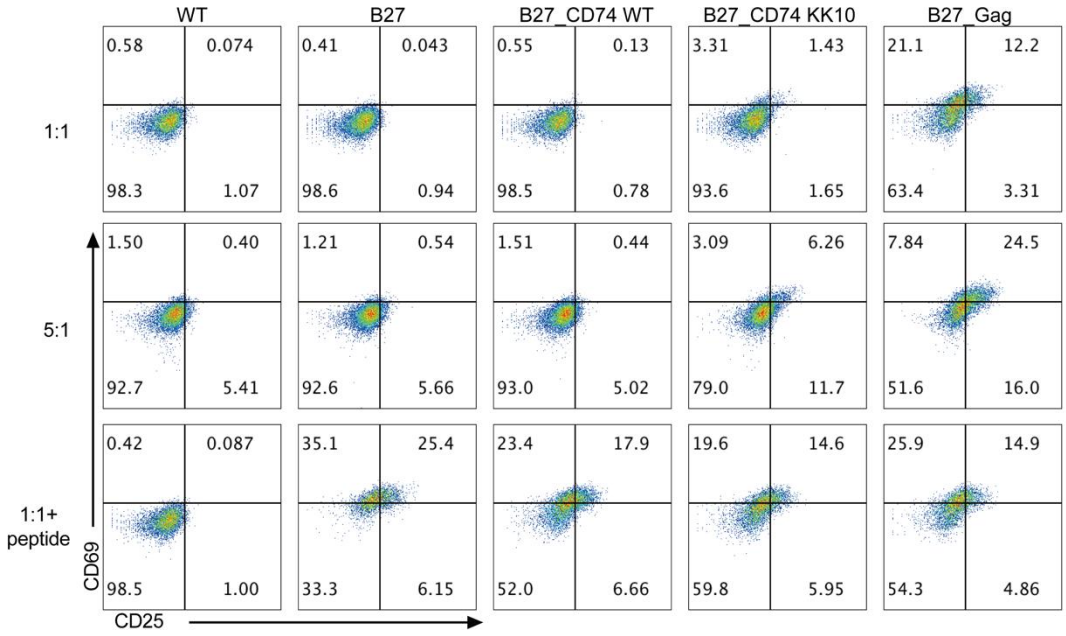

Figure 5.20 Effect of E:T ratio in the activation of SKW-3 cells
WT THP1 cells, THP1_B27 cells, THP1_B27_CD74 WT cells, THP1_B27_CD74 KK10 cells or THP1_B27_Gag cells were incubated with either preincubated with KK10 peptide (final 1μM) for 2hrs before incubation with SKW-3 cells transduced with KK10-TCR or directly incubated with SKW-3 cells at a 1:1 or 5:1 E:T ratio. 16hrs after co-incubation, the activation of SKW-3 cells was evaluated by the surface level of the activation markers CD25 and CD69. Dotplots shown here are representative of three independent experiments.

In summary, while endogenous expression of Gag or CD74 KK10 could generate KK10, the efficiency is significantly higher for Gag. Endogenous KK10 delivery and external KK10 peptide pulsing have a synergic effect on the activation of SKW-3 cells.

5.2.6 Fixed THP1 cells can't activate SKW-3 cells

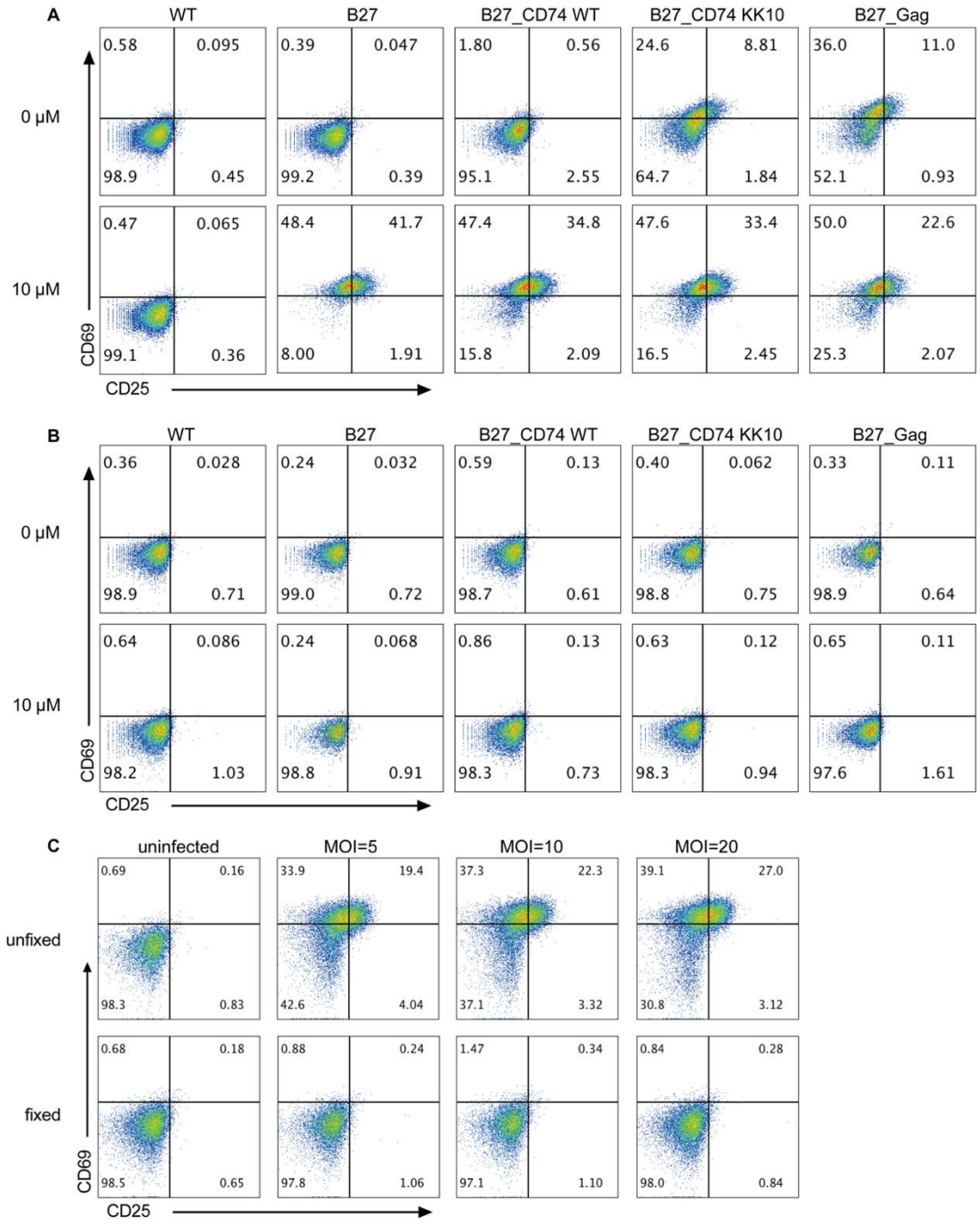

Figure 5.21 Fixed THP1 cells can't activate SKW-3 cells

A, B. WT THP1 cells, THP1_B27 cells, THP1_B27_CD74 WT cells, THP1_B27_CD74 KK10 cells or THP1_B27_Gag cells were incubated with different concentrations of KK10 peptide for 2hrs. THP1 cells were then either directly incubated with SKW-3 cells transduced with HLA-B27-KK10-TCR at a 1:1 E:T ratio (A) or fixed first before the co-incubation (B). 16hrs after co-incubation, the activation of SKW-3 cells was evaluated by the surface level of the activation markers CD25 and CD69. Dotplots shown here are representative of two independent experiments.

C. THP1_B27 cells were infected with C62 at different MOIs. 8hrsh after infection, THP1_B27 cells were either directly incubated with SKW-3 cells transduced with KK10-TCR at a 1:1 E:T ratio (unfixed) or fixed first before the co-incubation (fixed). 16hrs after co-incubation, the activation of SKW-3 cells was evaluated by the surface level of the activation markers CD25 and CD69. Dotplots shown here are representative of two independent experiments.

Some drugs could serve as transport inhibitors to block certain protein transport

pathways (Francia et al. 2019) and could thus be used to study the peptide presentation process. As drug addition may affect T cell activation, drug removal is necessary during co-incubation. However, as the effects of most drugs are reversible, it is necessary to keep APCs incubated with drugs all the time to enable effective pathway blockage. A possible solution is to initiate peptide presentation in APCs in the presence of drugs, fix the APCs, and then co-incubate them with T cells with drugs removed. As this method was shown to be practical in previous studies (Lewinsohn et al. 2006), I tested whether SKW-3 cells could be activated by the HLA-B27/KK10 complex on fixed THP1 with the peptide loading strategies mentioned above. While effective SKW-3 cell activation was observed after co-incubation with THP1_B27_CD74 KK10 or THP1_B27_Gag cells (Fig.5.21A), such effect disappeared when THP1 cells were fixed (Fig.5.21B), as no upregulation of CD25 or CD69 was detected. Though THP1 cells transduced with HLA-B27 could activate SKW-3 cells after KK10 peptide pulsing (Fig.5.21A), fixation completely blocked such activation (Fig.5.21B). Similarly, C62-infected THP1_B27 cells failed to activate SKW-3 cells upon fixation (Fig.5.21C). Therefore, fixed THP1 cells were incapable of activating SKW-3 cells transduced with KK10-TCR.

5.3 Discussion

In this chapter, I established and optimised a CD8+ T cell activation system to detect peptide presentation using the HLA-B2705-restricted KK10 peptide presentation as a model. CD25, CD69, CD137 and TNF-α are good activation markers to detect the activation of SKW-3 cells. Pre-incubation of THP1 cells with IFN-γ or PMA, increase of E:T ratio from 1:1 to 5:1, and elongation of co-incubation time from 16hrs to 24hrs or 40hrs did not obviously increase the effectiveness of T cell activation. KK10 peptide could be generated and presented via direct HIV-1 infection as well as infection of other viral vectors, including MVA and ChAdOx1. Compared to HIV-1 infection, MVA and ChAdOx1 have a higher infection rate and could generate KK10

peptide within 24hrs. While MVA infection affects the viability of THP1 cells and only stimulates weak activation of SKW-3 cells, ChAdOx1 infection does not affect cell viability and could induce robust T cell activation within a very short time at a low MOI. While endogenous KK10 peptide synthesis is successful via the expression of Gag or using CD74 to deliver the KK10 peptide by replacing the CLIP region with KK10, it is more effective for Gag. Although the current system can sensitively detect HLA-B27-restricted KK10 presentation, it fails to detect the presentation of HLA-E-restricted RL9 peptide, though various methods have been tried to increase the surface level of HLA-E/RL9 complex, including promotion of surface HLA-E level by pre-incubation IFN-γ or PMA, increase of peptide concentration in peptide pulsing, and the usage HLA-E/RL9 SCT.

Recent findings indicate that optimal priming of MHC-E restricted T cells requires myeloid cells, possibly macrophages (Hansen et al. 2022; Malouli et al. 2021), and that monocyte differentiation leads to HLA-E enrichment in autophagosomal-lysosomal pathways (Camilli et al. 2016). Therefore, the monocytic cell line THP1 was chosen as the APC to study peptide presentation, given its similarities to primary monocytes and the resemblance of PMA-differentiated THP1 cells to PBMC monocyte-derived macrophages (Chanput et al. 2014).

Primary CD8+ cells have been widely used to detect peptide presentation, as they are more sensitive than cell lines and better mimic physiological conditions. However, cell lines are more suitable for the exploration of HLA-E peptide presentation pathways. As I aim to assess how the inhibition of different peptide presentation pathways affects HLA-E-restricted peptide presentation, the T cell activation readouts must be consistent and comparable between different experiments to allow for quantitative analysis. Besides, I plan to do a screening to select the key regulatory proteins for HLA-E-restricted peptide presentation, which is hard to realise using primary T cells as the readout given the large scale. Therefore, SKW-3 cells were

chosen as the ideal CD8+T cells to assess peptide presentation, as they are easy to manipulate, clonally stable, do not express endogenous TCRαβ, and have been widely used to detect peptide presentation and in large-scale screening (Feng et al. 2022).

Given that untransduced SKW3+ cells do not express CD3 or TCRβ on the cell surface, the transduced SKW3 that are CD3+TCRβ+ should have the corresponding TCR present on the cell surface and should be positive in the tetramer staining. While all CD3+TCRβ+ SKW3 cells transduced with the KK10-TCR were positive in the tetramer staining (Fig.5.6D), only a small population of CD3+TCRβ+ SKW3 cells transduced with the RL9-TCR were (Fig.5.1C). Besides, most SKW3 cells transduced with the RL9-TCR were still negative in the RL9 tetramer staining after they were sorted based on tetramer staining (Fig.5.8-9). Similar RL9-tetramer staining was observed previously in our group (Yang et al. 2021). Although a weak enrichment of RL9-tetramer positive population could be obtained, the enrichment was transient and re-enrichment was impossible in these cells, which may be due to the downregulation of the TCRs, the cell growth was not selected through the TCR (unpublished data from our group).

The puzzling results obtained in RL9-tetramer staining may be partly explained by the instability of the HLA-E-RL9 complex, which might not fold correctly and might fall apart quickly, thus rendering the effectiveness of the tetramer staining (Walters et al. 2018). Difficulty in the pairing of RL9-TCR α and β chains or the clustering of RL9-TCRs, as well as the low surface level of the RL9-TCR, could also contribute to the failure of effective tetramer staining. The most likely reason is that the avidity of the RL9-TCR might be too weak to support effective tetramer binding, which may explain why no T cell activation was observed even after co-incubation with THP1 cells saturated with a high concentration of the RL9 peptide (Fig.5.4, 5), or with K562 cells stably expressing SCT_HLA-E_RL9 (Fig.5.10 D-F). The usage of HLA-E-RL9-SCT in isolating the RL9-TCR may contribute to its low binding affinity

towards the native HLA-E-β2m-RL9 complex, as the cysteine trap introduced in the SCT construct may alter the conformation of the trimer complex (Barber et al. 2022). Therefore, it's necessary to generate a TCR of higher affinity or to use a sensitive TCR detection system, like the spheromer platform (Mallajosyula et al. 2021). However, though the RL9-TCR may be of low affinity, T cells transduced with the RL9-TCR could inhibit HIV replication both in vitro (Yang et al. 2021) and in vivo in the mouse model (unpublished work from our group).

It was previously reported that PMA could effectively upregulate surface expression of HLA-E in THP1 cells (Camilli et al. 2016), which is different from my result here that PMA alone did not seem to affect HLA-E surface level (Fig.5.3). The failure to observe PMA-mediated HLA-E upregulation might be due to the limited incubation time, as I only incubated THP1 cells with PMA for 24hrs, while the PMA stimulation lasted 96hrs in the previous paper. IFN-γ could potently promote the surface expression of HLA-E in THP1 cells, as was reported for many other cells (Lee et al. 2022). The pre-stimulation of THP1 cells with PMA led to unspecific T cell activation (Fig.5.4, 5), which might be due to the trace of PMA introduced into the co-incubation system, as PMA could trigger T cell activation (Weiss et al. 1984). RL9 peptide-pulsed THP1 cells could not activate RL9-TCR transduced T cells even after the stimulation with IFN-γ, where the surface HLA-E level was effectively upregulated. One possible reason is that the surface level of HLA-E was still low after IFN-γ stimulation compared to that of HLA-Ia, despite being significantly higher than its original level. Another more likely reason seemed to be the low avidity of T cell activation, which may be caused by the instability of the HLA-E-RL9 complex and the low affinity of RL9-TCR.

An increase in the E:T ratio was reported to elevate the activation of CD8+ T cells (Yang et al. 2021). Consistently, a slightly higher level of CD25 signal was observed for SKW-3 cells after increase of E:T ratio during the co-culture of THP1_B27_CD74

KK10 cells, THP1_B27_Gag cells or peptide-pulsed THP1_B27 cells (Fig.5.10D; Fig.5.20), which is likely due to the engagement of more TCRs with the HLA-B27/KK10 complex. When peptide concentration is too low, the increase of THP1 cells may not significantly increase the level of the HLA-B27/KK10 complex to enable the effective activation of SKW-3 cells (Fig.5.10D). When the peptide concentration was too high, most SKW-3 cells were already activated (Fig.5.10D, E) at a 1:1 E:T ratio, so an increase in the ratio did not affect the activation level of SKW-3 cells. However, while the increase of the E:T ratio could moderately enhance the activation of SKW-3 cells, it also adds to some unspecific signals. Such a method could be considered to increase the sensitivity of the T cell activation assay, but the evaluation of background noise would be necessary.

Fixed THP1 cells failed to activate SKW-3 cells (Fig.5.21), which is probably because fixation masked the KK10 epitope or changed the structure of HLA-B27. As 1%PFA was reported in previous studies to fix the MHC-I/peptide complex (Lewinsohn et al. 2006), it's worth testing whether lowering the PFA concentration or using other fixation methods would preserve the HLA-B27/KK10 complex.

During HIV-1 infection, two populations of p24+ THP1 cells were observed, in which the population of cells larger in size showed better p24 staining (Fig.5.11). As cells in the G2/M phase of the cell cycle are larger, my result here is consistent with previous studies showing that HIV-1 proteins vif and vpr arrest cells at the G2 phase to allow for optimal replication (Goh et al. 1998; Gummuluru and Emerman 1999; Sakai et al. 2006). In contrast, the population of THP1 cells infected with M4 was uniform (Fig.5.14A).

As HIV-1 viral proteins might be involved in the regulation of peptide presentation, direct infection of THP1 cells with HIV-1 would be the ideal strategy to explore how HLA-E presents HIV-1-derived peptides upon infection. However, the difficulty in

manipulation, slow and inefficient protein production and ineffective T cell activation limit the usage of the HIV-1 infection system. Given that the direct presentation of epitopes from incoming viral particles has been reported (Kløverpris et al. 2013), it would be worth examining the presentation of gag-derived peptides at early time points upon HIV infection.

MVA and ChAdox1 are two widely used vaccine platforms and have corresponding HIV-1 vaccines currently in clinical trials (Wee et al. 2021). Therefore, it would be interesting and useful to know how HLA-E-restricted peptides are presented via antigen delivery through these viral vector systems and whether it is different from the antigen delivery via direct HIV-1 infection. Though further characterisation is required, my initial exploration has shown that C62 might be a particularly useful tool in future assays as it could overcome the major problems observed in HIV-1. As I plan to manipulate trafficking pathways in THP1 cells during the infection via drug incubation or knocking down key regulatory proteins, the high viability of THP1 cells as well as the effectiveness of the transport pathway control is necessary, which requires that THP1 cells quickly generate a considerable amount of transgene proteins and effectively activate SKW-3 cells upon infection. However, more than two days is required for effective Gag production upon HIV-1 infection (Pace et al. 2012), and HIV-1-infected THP1 cells only moderately activated SKW-3 cells (Fig.5.12). In contrast, THP1_B27 cells could effectively activate SKW-3 cells 8hrs after C62 infection (Fig.5.17), which is consistent with the capacity of the adenovirus to generate a large amount of target protein shortly upon infection (Dumasius et al. 2003). These advantages of C62 allow for quantification and future manipulation of different peptide presentation pathways.

Although the Gag expression was undetectable in THP1_B27 cells infected with C62 at an MOI of 10 (Fig.5.14C), effective SKW-3 cell activation could be observed even when THP1 cells were infected with C62 at an MOI of 5 (Fig.5.17). As T cell

activation is very sensitive, it is likely that the amount of KK10 peptide generated in THP1 cells infected with C62 at an MOI lower than 20, in which the Gag protein expression in THP1 could not be detected in immunoblotting, is sufficient for robust activation of SKW-3 cells.

CD74_KK10 construct can load the KK10 peptide into HLA-B27 molecules and elicit the activation of SKW-3 cells, which is consistent with previous results (Walchli et al. 2014). The activation-promoting effect of CD74 KK10 was less effective than Gag, implying that in the CD74 KK10 construct, either less KK10 peptide was produced or peptide was loaded via an unconventional pathway where they encountered less HLA-B27 molecules, as CD74 could facilitate endosomal peptide presentation of MHC-I molecules (Walchli et al. 2014). As the replacement of the CLIP peptide with KK10 could significantly enhance the interaction between CD74 and HLA-B27 (unpublished data), CD74 KK10 may likely direct HLA-B27 molecules to the endosomes, mimicking that of the HLA-II transport pathway. As CD74 is an encouraging adjuvant in vaccine design with a universal improvement of CD8+ T Cell response (Jensen et al. 2013), it would be important to further explore how CD74 manipulates the antigen presentation of MHC-I molecules, especially HLA-E.

Although I have established a robust system to detect peptide presentation, it is not sensitive enough to detect the presentation of the RL9 peptide by HLA-E. The low affinity of the corresponding TCR is likely to be the main cause of the failure, and other members of the group are currently trying to generate one with a higher affinity. We also have an agreement in progress to collaborate with Immunocore to use their high-affinity, HLA-E-RL9-specific immTav system, in which an antibody against CD3 is fused to the β chain of the soluble TCR specific to the HLA-E-RL9 complex (Wallace et al. 2022). Another strategy would be the development of an antibody that can recognise the HLA-E/RL9 complex with high affinity, and our group currently has a candidate under investigation. Once the system works for HLA-E, I will try to

explore the key proteins and pathways involved in peptide presentation upon HIV-1 infection and compare them to peptide delivery via other viral vectors or endogenous expression. siRNA screening would be the ideal method for the primary exploration of the potential targets, and further functional studies could be done in THP1 cells with these proteins knocked out. Validation of the target proteins will also be done in primary cells to rule out potential artefacts. I will also explore how CD74 as well as other potential proteins, if any discovered, could be utilised to regulate the peptide presentation of HLA-E, which could be useful for future therapeutic purposes.

Chapter 6: General discussion

The work presented in this thesis delineated the intracellular distribution and the dynamic trafficking process of HLA-E, as well as studied the underlying mechanisms of two pivotal regulatory factors. Different from HLA-Ia molecules, HLA-E predominantly resides intracellularly, which results from the ER retention after synthesis and the low surface stability upon surface arrival. These characteristics mainly stem from the specific motifs on the cytoplasmic tail of HLA-E and the deficiency in high-affinity peptides, collectively leading to its enrichment in ER and endosomal compartments. I also developed and optimised a CD8+ T cell-based methodology to detect target peptides presented via different means, though it proved ineffective in capturing the HLA-E-restricted presentation of the gag-derived RL9 peptide. In the chapter, I intend to explore how these data collectively enhance our understanding of the immune functions of HLA-E, conduct a comparative analysis of HLA-E transport to its homologues and other non-classical HLA-I molecules, and elucidate the implications of these findings on the development of an HLA-E-targeting HIV vaccine.

6.1 How HLA-E is fine-tuned for its immunological functions

6.1.1 The optimisation of HLA-E to fulfil its primary functions in regulating NK cell activity

Since the binding groove of HLA-E is tailored for VL9 (O'Callaghan et al. 1998), only VL9 could effectively facilitate the compact and stable refolding of HLA-E, which is a prerequisite for efficient ER export (Fig.4.3.3). Conversely, most other peptides are too weak to stabilise HLA-E (Walters et al. 2018; Walters et al. 2022). The absence of a C-terminal ER export motif further reduces the likelihood of sub-optimally loaded HLA-E exiting the ER (Fig.4.4.12-15). Consequently, HLA-E

could only achieve proficient ER exit and subsequently traffic to the cell surface when bound to VL9. This mechanism ensures that the surface-level HLA-E signal precisely mirrors the expression of HLA-Ia molecules and the integrity of the antigen processing machinery.

Meanwhile, considering the moderate binding affinity of VL9 compared to that of most HLA-Ia peptides (Hoare et al. 2008; Strong et al. 2003; Walters et al. 2022) and that the cytoplasmic tail of HLA-E contains a unique a lysine/tryptophan-based endocytosis motif (Fig.4.4.17-25), the surface stability of HLA-E is not very high (Fig.3.3.14). This ensures that the surface level of HLA-E provides a continuously updated and dynamic reflection of cellular HLA-I availability, thus facilitating the timely detection of aberrant cells by NK cells.

The endogenous expression of the VL9 peptide is limited and a substantial portion of intracellular HLA-E molecules are not loaded with the VL9 peptide, as overexpression of the VL9 peptide could significantly promote the release of HLA-E from the ER and dramatically upregulate the surface level of HLA-E (Fig.4.3.1). The stability of sub-optimally folded HLA-E might further contribute to its long-term survival in the ER in a peptide-receptive form. Such abundance of intracellular HLA-E guarantees its efficacy and sensitivity in monitoring the expression of HLA-Ia molecules and modulating the activity of NK cells (Strong et al. 2003).

To conclude, the precise affinity and availability of the VL9 peptide, in conjunction with the regulatory roles of the cytoplasmic tail, collaboratively refine the functionality of HLA-E, optimising its primary functions of modulating NK cell activation in an accurate, timely and sensitive way.

6.1.2 Unique features of HLA-E facilitate the non-canonical endosomal antigen presentation

Compared to HLA-Ia molecules, the peptide-receptive HLA-E/β2m dimers exhibit higher stability (Walters et al. 2018) and increased resistance to acidic conditions (Camilli et al. 2016). These properties facilitate the binding of HLA-E peptides in endosomes as well as the recycling of HLA-E back to the cell surface. Besides, the peptide binding groove of HLA-E is relatively broad and rigid (Walters et al. 2018). These attributes may be a disadvantage for the classical antigen presentation pathway, as high-affinity peptides are required to pass through the stringent peptide-editing stages for ER exit (Thomas and Tampé 2019). However, these features seem to be advantageous for endosomal peptide loading, enabling the binding and presentation of a diverse repertoire of pathogen-derived peptides with relatively low affinities. Thus, the structural characteristics of HLA-E facilitate the presentation of a wide array of antigens through the endosomal pathway.

The fast trafficking of HLA-E in the endosomal pathways and its enrichment in late endosomes and recycling endosomes result from a combination of different factors, including the shortage of high-affinity peptides (section 4.3), the unique endocytic motif on the cytoplasmic tail (section 4.4), the relative resistance to acidic environments (Camilli et al. 2016), and possibly other yet-to-be-identified regulatory elements. The fast internalisation and recycling of HLA-E facilitate the rapid presentation of pathogen-derived peptides, while the accumulation of HLA-E within endosomes establishes a sizable reservoir of HLA-E molecules ready for peptide loading. These attributes of endosomal trafficking collectively ensure that HLA-E is capable of presenting pathogen-derived peptides to CD8+ T cells in a timely and effective manner.

Inhibition of the classical antigen processing machinery, which is common during pathogen infection and cancers (Antoniou and Powis 2008; Hansen and Bouvier 2009; van de Weijer et al. 2015), may promote the endosomal peptide loading pathway of HLA-E. Such inhibition reduces competition from HLA-Ia by increasing β2m

availability (Myers et al. 1996; Shields et al. 1999; Townsend et al. 1990) and favours HLA-E expression (Fig.4.2). Moreover, it also disrupts the VL9-dominated peptide repertoire of HLA-E, thereby allowing for the presentation of a broader spectrum of weak peptides (van Hall et al. 2010). Consequently, the suppression of the conventional antigen presentation of HLA-Ia molecules promotes the non-canonical endosomal peptide loading of HLA-E.

In summary, the structural features and the distinct trafficking patterns of HLA-E, along with the inhibition of the classical peptide loading machinery under abnormal conditions collectively facilitate the unconventional endosomal peptide loading and presentation of HLA-E.

6.2 Comparison of HLA-E alleles, homologues and other non-classical HLA-I molecules

6.2.1 Differences between HLA-E allelic variants

Although the difference between two dominant alleles HLA-E*01:01 and HLA-E*01:03 resides in a single amino acid variation at position 107 (Geraghty et al. 1992), which is positioned within a loop region of the α2 domain and is not expected to affect the conformation of the peptide groove (Strong et al. 2003). Despite this apparent structural similarity, these two alleles exhibit different peptide repertoires (Celik et al. 2016; Kraemer et al. 2015). Besides, HLA-E*01:03 has a higher affinity for peptides and better thermal stability compared to HLA-E*01:01 (Strong et al. 2003), which results in its higher surface expression and stronger inhibition of NK cell activity.

The functional disparities between these two alleles of HLA-E are associated with increased risk or protection against different diseases (Kanevskiy et al. 2019). Homozygosity for HLA-E*01:01 is correlated with enhanced control of HCV

(Guzmán-Fulgencio et al. 2013; Schulte et al. 2009), better post-transplantation viral control (Guberina et al. 2018; Rohn et al. 2019), and decreased susceptibility of certain cancers (Martín et al. 2015; Wagner et al. 2017; Xu et al. 2019; Zheng et al. 2015). On the other hand, homozygosity for HLA-E*01:03 is linked to a reduced risk of HIV-1 infection (Guberina et al. 2018; Lajoie et al. 2006), better control of EBV infection (Vietzen et al. 2023), heightened resistance to severe bacterial infections (Tamouza et al. 2007; Tamouza et al. 2005), and a lower incidence of acute graft versus host disease following transplantation (Danzer et al. 2009; Hosseini et al. 2013; Tamouza et al. 2006).

HLA-E*01:03 was selected for investigation in this thesis as its comparatively higher surface expression level allows for easier detection of its surface expression. Considering the possibility that the peptide repertoires associated with these two HLA-E alleles are different, along with the reported correlation between the HLA-E genotype and clinical outcomes across various diseases, exploration of the transport and antigen presentation of the HLA-E *01:01 allele might be necessary.

6.2.2 HLA-E resembles its homologues Qa-1 and Mamu-E

Despite differences in sequence, the peptide-binding pockets of Qa1 and HLA-E exhibit similar structures and peptide-binding specificities (Braud et al. 1997; Kraft et al. 2000; O'Callaghan et al. 1998; van Hall et al. 2010; Zeng et al. 2012). The peptide repertoire of Qa-1 is optimised to accommodate the Qdm peptide derived from the leader sequence of H-2D/L(AMAPRTLLL) (Aldrich et al. 1994; DeCloux et al. 1997), which is crucial for its principal role in regulating NK cell activation (Aldrich et al. 1994; Salcedo et al. 1998; Vance et al. 1998). Similar to VL9 (section 4.3), the binding affinity of Qdm is moderate, as the Qa-1/Qdm complex is relatively unstable on the surface (Kambayashi et al. 2004). This may result from the substitution of tryptophans by serines at position 143 and 147, which reduces the stability of the Qa-1

trimer complex and impacts the C-terminus of the binding groove (Bouvier and Wiley 1994), as is the case of HLA-E (O'Callaghan et al. 1998). Impairment of the classical antigen-processing machinery inhibits the presentation of the dominant Qdm peptide, which is common in tumour and pathogen infections (Oliveira et al. 2010; van Hall et al. 2007). This allows Qa-1 to present a broad repertoire of peptides to CD8+ T cells, thereby inhibiting tumour growth and pathogenesis (Bouwer et al. 1998; Bouwer et al. 1994; Oliveira et al. 2010; van Hall et al. 2007; van Hall et al. 2006).

Mamu-E has around 30 alleles, which is slightly more diverse than HLA-E yet still considerably less polymorphic compared to MHC-Ia alleles (Wu et al. 2018). Mamu-E and HLA-E share pronounced similarities in their sequence and structure, particularly within their peptide binding grooves (Walters et al. 2018). This commonality allows Mamu-E and HLA-E to bind identical peptide ligands, enabling cross-species recognition of MHC-E-restricted CD8+T cells (Hansen et al. 2016; Walters et al. 2018; Wu et al. 2018). A consistent elevation of surface MHC-E level and downregulation of surface MHC-Ia expression were observed in SIV-infected RM and human CD4+ T cells, as well as in HIV-infected CD4+ T cells (Wu et al. 2018). Given the functional conservation between Mamu-E and HLA-E, RMs seem to be an appropriate animal model for investigating the functions and mechanisms for the unconventional HLA-E-restricted T cell response, especially in the context of HIV infection. As the RhCMV-vectored SIV vaccine can effectively induce robust CD8+ T cell responses restricted by Mamu-E and provides SIV protection in rhesus macaques (Burwitz et al. 2020; Hansen et al. 2019; Hansen et al. 2016), there is potential of developing a CMV-vectored HIV vaccine capable of eliciting HLA-E-restricted CD8+ T cell responses.

Therefore, the investigation into HLA-E orthologues expands the potential peptide repertoire of HLA-E, elucidates the structural and functional features of HLA-E, and

offers relevant models for conducting in vivo studies of MHC-E-restricted CD8+T cell response.

6.2.3 HLA-E shares many similarities with CD1

Structural data have revealed a broader lipid-binding groove for CD1e compared to other CD1 molecules (Garcia-Alles et al. 2011), a feature that permits loose contact with lipids and facilitates fast lipid exchange. Similarly, HLA-E has a comparatively broader and rigid binding groove compared to HLA-Ia molecules, resulting in a broad peptide repertoire and generally low binding affinity of HLA-E peptides (Walters et al. 2018). The structural properties of the HLA-E binding groove may facilitate fast peptide exchange of a wide range of pathogen-derived weak peptides in endosomes. The direct transport of CD1e, CD1a and HLA-Ia molecules from TGN to endosomes is mediated by its lysine-rich cytoplasmic tail, with ubiquitination serving as the key signal (De Angelis Rigotti et al. 2017; Maître et al. 2008). As the HLA-E cytoplasmic tail is also enriched in lysines which are crucial for its fast internalisation (section 4.4.2), these HLA-E-unique lysines might facilitate ubiquitination, which is potentially crucial for the endosomal transport regulation of HLA-E. Therefore, the structure and sequence of HLA-E seem tailored to facilitate the unconventional endosomal presentation of pathogen-derived peptides.

A mild acidic pH within the late endosomes is crucial for the lipid loading of CD1 molecules. The acidic environment in late endosomes not only activates lipid transfer proteins in the endosomes (Winau et al. 2004; Zhou et al. 2004) but also induces conformational changes in CD1b and CD1d, aiding in the facilitation of antigen binding (Cuevas-Zuviría et al. 2020; Relloso et al. 2008). CD1e exhibits even greater stability within an acidic environment in comparison to CD1b and CD1d (Bushmarina et al. 2011), which is probably crucial for its functions as a chaperone to facilitate lipid loading. In a parallel vein, the comparative resistance of HLA-E to an acidic pH

compared to classical class I molecules (Camilli et al. 2016) not only promotes its accumulation in late endosomes (section 3.3.3.5) but may also facilitate effective peptide exchange of HLA-E.

Hence, studies on other non-classical HLA-I molecules, especially CD1, not only enhance our understanding of how the structure and trafficking of HLA-E are optimised for its functions but also offer insights into the potential regulatory elements that might influence the transport and antigen presentation process of HLA-E.

6.3 Studies on HLA-E trafficking lays the basis for designing an HCMV-vectored HIV vaccine

Instead of the classical MHC-Ia-restricted CD8+ T cell responses, the RhCMV68.1 vector elicits unusual CD8+ T cell responses restricted by MHC-E and MHC-II (Hansen et al. 2013b; Hansen et al. 2016). Such modulation of the antigen processing machinery is crucial for the successful viral clearance of the RhCMV/SIV vaccine in over 50% of the vaccinated RMs, as the classical MHC-Ia-restricted CD8+ T cell responses fail to protect RMs against SIV.

Genetic rearrangement of the RhCMV is crucial for the unusual restrictions of the CD8+ T cell responses. Deletion of the Rh157.4-157.6 and Rh158-161 (orthologue of HCMV UL128/130/131 and UL146/147) gene regions from WT RhCMV is required for the immunological reprogramming (Malouli et al. 2021). Rh189 (orthologue of HCMV US11) is necessary for the suppression of the canonical MHC-Ia-restricted CD8+ T cell responses (Hansen et al. 2013b). Rh67 (orthologue of HCMV UL40) not only downregulates MHC-Ia expression but also upregulates the surface expression of MHC-E despite the dysfunction of TAP (Verweij et al. 2021), which ensures the efficacy of the MHC-E-restricted CD8+ T cell responses. Other RhCMV proteins may also play a role in the modulation of the antigen processing pathways, including

Rh182, Rh184 and Rh185 (orthologue of HCMV US2, US3, US6) (Pande et al. 2005), which are likely to work concertedly with Rh189 to inhibit the classical MHC-Ia antigen presentation. The RhCMV68.1 vector may also lead to specific modulation of MHC-II antigen presentation. While the underlying mechanisms through which the genetic modifications of the RhCMV vector elicit these unprecedented responses necessitate further analysis, it is evident that these modulations facilitate an atypical antigen presentation pathway of MHC-E, which is highly likely to resemble that of MHC-II. This hypothesis is not only supported by the immune reprogramming of the RhCMV68.1 vector but also by the structural and transport characteristics of MHC-E favouring endosomal peptide loading, which has been discussed throughout the thesis.

The facilitation of an alternative peptide presentation route not only circumvents the inhibition of the traditional antigen loading pathway but also modulates the repertoire of the SIV epitopes. The SIV-derived epitopes presented by MHC-E are broad, of low affinity, and do not contain a common motif (Hansen et al. 2016), which is likely due to the escape from the peptide quality control steps in the classical peptide presentation pathway. The diversity of the SIV peptides guarantees the breadth of the CD8+ T cell responses, which reduces the probability of the immune escape of SIV and facilitates effective early interception upon infection (Malouli et al. 2021). The relatively low peptide affinity enables an appropriate strength of peptide-TCR engagement, thus reducing T cell exhaustion and improving the overall immune control over chronic SIV infection (Collier et al. 2021). These two unusual features of the MHC-E-restricted peptide repertoire also seem to be crucial for the effective and long-term control of HIV.

Careful immune reprogramming is necessary to recapitulate the MHC-E-restricted CD8+ T cell responses against HIV in humans. Recently, four fibroblast-adapted, pentameric complex-deficient HCMV vaccines failed to elicit the atypical MHC-E/II-restricted CD8+ T cell responses in vaccinated humans (Murray et al.

2017). This suggests that further manipulation of the HCMV vector, particularly the deletion of UL146/147 (orthologue of HCMV Rh158-161) (Malouli et al. 2021), is necessary for the subversion of the conventional CD8+ T cell priming. Other factors apart from the vector itself might also be important, such as the induction and maintenance of IL-15 signalling (Barrenäs et al. 2021). Genetic differences within the immune systems between RMs and humans, as well as the disparities between RhCMV and HCMV, may further challenge the vaccine design. In addition to immunogenicity, safety considerations are crucial, as CMV infection may cause severe consequences in immunocompromised patients (Ramanan and Razonable 2013) and might promote cancer progression (Herbein 2018). Therefore, further development of an attenuated HCMV-based vaccine platform would be important (Caposio et al. 2019).

Considering all the difficulties in translating the SIV vaccine into an HIV vaccine, it's likely that a combination of different methods is required to elicit the non-canonical HLA-E-restricted CD8+ T cell responses. Understanding the transport patterns of HLA-E and the corresponding regulatory factors would enable future manipulation of the HLA-E transport process and the loading of pathogen-derived peptides, thus informing the recapture of the precise modulation of MHC-E-restricted peptide presentation to enable the unconventional CD8+ T cell priming. The provision of potent peptides like VL9 would be necessary for the effective release of HLA-E from the ER, which augments both the HLA-E surface level and the HLA-E pool in the endosomal pathway (section 4.3). The unique motifs in the cytoplasmic tail of HLA-E play a regulatory role in its transport process (section 4.4). The subtle variation of some key residues on the HLA-E cytoplasmic tail facilitates its resistance to viral downregulation, as has been reported for HIV Nef (Le Gall et al. 1998; Williams et al. 2002) and HCMV US11 (Barel et al. 2006). Hence, the cytoplasmic tail of HLA-E

emerges as a potential target to fine-tune the transport of HLA-E, especially in the context of viral infection.

Taken together, the findings presented in this thesis provide a comprehensive characterisation of HLA-E trafficking dynamics and how the regulatory role played by peptide availability and its cytoplasmic tail, which provide valuable insights into the advancement of immunotherapies targeting HLA-E-restricted CD8+ T cell responses. Further investigations will aim to explore other regulatory factors impacting HLA-E transport, as well as how HLA-E presents pathogen-derived peptides, particularly in situations where the classical antigen processing pathway is compromised or suppressed.

Appendix

Table 7.1 Primers used for plasmid construction

primer	sequence
pGEN HindIII F	ACCCAAGCTTGGTACCGAGCTCGGATCGA
pGEN NotI CD74 R	CTATGCGGCCGCGGATCCTCACATGGGGA
HLA-E HindIII F	GAAAGCTTGCCACCATGGTAGATGGAACCCTCCTTTTACTC
HLA-A3 HindIII F	GAAAGCTTGCCACCATGGCCGTCATGGCGCCCCGAACCCT
pGEN EGFP NotI R	AAGCGGCCGCTCACTTGTACAGCTCGTCCATGC
pGEN F	CTACCGGACTCAGATCTCGAGCTCA
PGEN TER R	GGTATGGCTGATTATGATCTAGAGTCGC
EA3 F	GAGCTGTGGTTGCTGCTGTGATATGGAGGAGGAAGAGCTCAGATAGAAAAGG
EA3 R	CCTTTTCTATCTGAGCTCTTCCTCCTCCATATCACAGCAGCAACCACAGCT
A3E F	GGTCGCTGCCGTGATGTGGAGGAAGAAGAGCTCAGGT
A3E R	ACCTGAGCTCTTCTTCCTCCACATCACGGCAGCGACC
E NotI R	TCGCGGCCGCTCACAAGCTGTGAGACTCAGACCCCTGG
A3 NotI R	TCGCGGCCGCTCACACTTTACAAGCTGTGAGGGACACATCAGA
E L337V NotI R	TCGCGGCCGCTCATACGCTGTGAGACTCAGACCCCTGG
A3 V337L NotI R	TCGCGGCCGCTCACAATTTACAAGCTGTGAGGGACACATCAGA
L337V EGFP F	GCGTATCGAATTCCCCTGCAGGTGTGAGCAAGGG
L337V EGFP R	ACACCTGCAGGGGAATTCGATACGCTGTGAGACTCAGACCCCTGG
V337L EGFP F	AATTG TCGAATTCC CCTGCAGGTGTGAGCAAGGG
V337L EGFP R	ACACCTGCAGG GGAATTCGA CAATTTACAAGCTGTGAGGGAC
Y320A F	GAAAAGGAGGGAGCGCATCTAAGGCTGAGTG
Y320A R	CACTCAGCCTTAGATGCGCTCCCTCCTTTTC
E7A F	GGAGCTACTCTAAGGCTGAGAGCAGTGACAGTGCCCAGG
E7A R	CCTGGGCACTGTCACTGCTCTCAGCCTTAGAGTAGCTCC
A7E F	GGAGTTACACTCAGGCTGCATGGAGCGACAGTGCCCAGG
A7E R	CCTGGGCACTGTCGCTCCATGCAGCCTGAGTGTAACTCC
K310R F	CTGTGATATGGAGGAGGAAGAGCTCAGGTGG
K310R R	CCACCTGAGCTCTTCCTCCTCCATATCACAG
K322Q F	AGGGAGCTACTCTCAgGCTGAGTGGAGC
K322Q R	GCTCCACTCAGCcTGAGAGTAGCTCCCT
A3+2K F	GCTCAGATAGAAAAGGAGGGAGTTACACTAAGGCTGCAAGCAGTGA
A3+2K R	AACTCCCTCCTTTTCTATCTGAGCTCTTCTTCCTCCACATCACGG
5C9 F	TGGAGCGACAGTGCCCAGGGCTCTGATG
5C9 R	AGCCCTGGGCACTGTCGCTCCA
EW-AS F	CTCTAAGGCTGCAAGCAGCGACAGTGCCCAGG
EW-AS R	CACTGTCGCTGCTTGCAGCCTTAGAGTAGCTC
E324A F	CTCTAAGGCTGCATGGAGCGACAGTGCCCAGG
E324A R	CACTGTCGCTCCATGCAGCCTTAGAGTAGCTC
W325S F	CTCTAAGGCTGAGAGCAGCGACAGTGCCCAGG
W325S R	CACTGTCGCTGCTCTCAGCCTTAGAGTAGCTC
A3_W F	AGGCTGCATGGAGTGACAGTGCCCAGGGCTCTG
A3_W R	CCTGGGCACTGTCACTCCATGCAGCCTGAGTGTAACTCC
A3_2KW R	CCTGGGCACTGTCACTCCATGCAGCCTTAGTGTAACTCC
P33 F	CGGACTCAGATCTCGAGCTCAAGCTTGCCACCATGGACGATCAGAGGGACCT
P33 R	GCTGATTATGATCTAGAGTCGCGGCCGCTCACATGGGGACTGGGCCCA
KK10 F	AGAAGCGCTGGATCATCCTGGGCCTGAACAAGCAGGCGCTGCCCATGGGAG
KK10 R	TGCTTGTTCAGGCCCAGGATGATCCAGCGCTTCTTGCTCACAGGCTTGGGAGGC
pLVX CD74 BamHI F	AGAAGACACCGACTCTAGAGAGGATCCGCCACCATGCACCGGAGGAGATCACGCT CTTGTA
pLVX CD74 SalI R	TGTAATCCAGAGGTTGATTGTCGACTCACATGGGGACTGGGCCCAGATCCT
pLVX HLA-E BamHI F	AGAAGACACCGACTCTAGAGGATCCGCCACCATGGTAGATGGAACCCTCCT
pLVX EGFP SalI R	TGTAATCCAGAGGTTGATTGTCGACTCACTTGTACAGCTCGTCCATGCCG
pLVX HLA-A3 BamHI F	AGAAGACACCGACTCTAGAGGATCCGCCACCATGGCCGTCATGGC
pLVX B27 BamHI F	AGAAGACACCGACTCTAGAGGATcCGCCACCATGCGGGTCACGGC
pLVX B27 SalI R	TGTAATCCAGAGGTTGATTGTCGACTCACGCTGTGAGAGACACATCAGAGCCC
pLVX GAG BamHI F	AGAAGACACCGACTCTAGAGGATcCGCCACCATGGGTGCCCGCGCCTCCGTT
pLVX GAG SalI R	TGTAATCCAGAGGTTGATTGTCGACTCACTTGGAGCCACCCTGGCTGGA
B27 P2A R	TCTCCAGCCTGCTTCAGCAGGCTGAAGTTAGTAGCTCCGCTTCCCGCTGTGAGAGA CACATCAGAGCC

P2A Kozak GAG F	GCCTGCTGAAGCAGGCTGGAGACGTGGAGGAGAACCCTGGACCTGCCACCATGGG TGCCCGCGCCT
P2A Kozak CD74 F	GCCTGCTGAAGCAGGCTGGAGACGTGGAGGAGAACCCTGGACCTGCCACCATGGA CGATCAGAGGG

Table 7.2 Antibodies for flow cytometry

Target	clone	fluorochrome	µl/sample	Source
HLA-E	3D12	APC	2	BioLegend, 342606
HLA-A3	GAP.A3	APC	2	Life Technologies, 17-5754-42
HLA-I	W6/32	APC	2	Life Technologies, 17-9983-42
HLA-A2	BB7.2	APC	2	BioLegend, 343308
CD3	SK7	APC- Cy7	2	BD Biosciences, 557832
CD8	RPA-T8	BV421	2	BioLegend, 301036
mouse TCRβ chain	H57-597	FITC	2	BioLegend, 109205
CD69	FN50	APC	2	BioLegend, 310910
CD25	2A3	BV711	2	BD Biosciences,563159
CD137	4B4-1	PE	2	BioLegend,309804
TNF-α	MAb11	PE	2	BioLegend,502909
IFN-γ	4S.B3	BV711	2	BioLegend,502540
MIP-1β	FL34Z3L	APC	2	Invitrogen, 17-7540-42
CD74	LN2	APC	2	BioLegend, 326812
HIV-1 p24	(KC57)	FITC	2	Beckman Coulter, 6604665
HLA-B27	REA176	APC	2	Miltenyi Biotec, 130-123-554

Table 7.3 Antibodies used for WB, co-IP, IF and ELISA

Antibody	Target	Per sample (ng/µL)	Assay	Source
anti-EGFP	EGFP	1	WB	Proteintech, 66002-1
		1µg	co-IP	
		10	ELISA	
MEM-E/02	HLA-E	1	WB	Enzo Life Sciences, ALX-805-701-C100
		10	IF	
VIC-Y1	CD74	1µg	co-IP	Invitrogen, 14-0747-82
HC10	HLA-I	0.5	WB	purified from hybridoma supernatant
IRDye 800CW donkey anti-mouse	mouse IgG	0.05	WB	LiCor, P/N: 926-32212
PIN.1	CD74	2	WB	Santa Cruz Biotechnology, sc-47742
SV5-Pk1	V5 tag	1	WB	Abcam, ab27671
anti-calnexin	calnexin	2	IF	Abcam, ab22595
anti-EEA1	EEA1	2	IF	Abcam, ab2900
anti-Rab7	Rab7	0.05	IF	Abcam, ab137029
anti-Rab11	Rab11	1	IF	Life Technologies, 71-5300
anti-LAMP1	LAMP1	1	IF	Abcam, ab24170
anti-GM130	GM130	0.25	IF	Abcam, ab52649
goat anti-rabbit Alexa Fluor 568	rabbit IgG	2	IF	Abcam, ab175471
donkey anti-rabbit Alexa Fluor 647	rabbit IgG	2	IF	Abcam, ab150075
goat anti-mouse Alexa Fluor 488	mouse IgG	2	IF	Abcam, ab150113
W6/32	HLA-I	2	IF	BioLegend, 311402
		10	ELISA	
S8E4	anti-streptavidin	1	IF	Novusbio, NB120-10023
3D12-APC	HLA-E	1:100	IF	BioLegend, 342606
GAP.A3-APC	HLA-A3	1:100	IF	Life Technologies, 17-5754-42
3D12	HLA-E	10	ELISA	BioLegend, 342602
anti-streptavidin (HRP-conjugated)	streptavidin	2.5	ELISA	Thermos Scientific, N100

*FC, flow cytometry; WB, western blotting; IF, immunofluorescence; co-IP: co-immunoprecipitation

Table 7.4 Summary of HLA-E binding affinity of CLIP-derived peptides

peptide	sequence	SCT	surface stabilisation	ELISA	DSF
VL9	VMAPRTLLL	***	***	***	**
Mtb	RLPAKAPLL			***	
RL9	RMYSPTSIL		**	**	
IG9	IHNFKRKGG	NS			
KL9	KMRMATPLL	**	**	**	*
KM10	KMRMATPLLM		*	*	*
KQ11	KMRMATPLLMQ		NS	NS	NS
KA12	KMRMATPLLMQA		NS	NS	NS
KL13	KMRMATPLLMQAL		NS	NS	NS
KP14	KMRMATPLLMQALP		NS	NS	NS
KM15	KMRMATPLLMQALPM		NS	NS	NS
MM9	MRMATPLLM	**	NS	NS	NS
MQ10	MRMATPLLMQ		NS		
MA11	MRMATPLLMQA		NS		
ML12	MRMATPLLMQAL		NS		
MP13	MRMATPLLMQALP		NS		
MM14	MRMATPLLMQALPM		NS		
RQ9	RMATPLLMQ	***	*	*	*
RA10	RMATPLLMQA		NS	NS	NS
RL11	RMATPLLMQAL		NS	*	*
RP12	RMATPLLMQALP		NS	NS	
RM13	RMATPLLMQALPM		*	*	*
MA9	MATPLLMQA	**	NS		
ML10	MATPLLMQAL		NS		
MP11	MATPLLMQALP		NS		
MM12	MATPLLMQALPM		NS		
AL9	ATPLLMQAL	NS	NS	NS	NS
AP10	ATPLLMQALP		NS		
AM11	ATPLLMQALPM		NS		
TP9	TPLLMQALP	**	NS	NS	
TM10	TPLLMQALPM		NS	NS	
PM9	PLLMQALPM	**	NS	NS	

***, high signal; **, medium signal; *, low signal; NS, no signal; grey block: not tested

#ELISA-based HLA-E peptide binding assay was carried out by Hong Sun following a previously published method developed by our group (Walters et al. 2020)

#Differential scanning fluorimetry (DSF) was performed by Max Quastel following a previously published methodology with minor modifications (Anjanappa et al. 2020)

References

Abd Hamid M, Wang RZ, Yao X, Fan P, Li X, Chang XM, Feng Y, Jones S, Maldonado-Perez D, Waugh C et al. 2019. Enriched hla-e and cd94/nkg2a interaction limits antitumor cd8 + tumor-infiltrating t lymphocyte responses. Cancer Immunol Res. 7(8):1293-1306.

Abdulhaqq SA, Wu H, Schell JB, Hammond KB, Reed JS, Legasse AW, Axthelm MK, Park BS, Asokan A, Früh K et al. 2019. Vaccine-mediated inhibition of the transporter associated with antigen processing is insufficient to induce major histocompatibility complex e-restricted cd8. J Virol. 93(19).

Ackerman AL, Cresswell P. 2003. Regulation of mhc class i transport in human dendritic cells and the dendritic-like cell line kg-1. J Immunol. 170(8):4178-4188.

Adiko AC, Babdor J, Gutierrez-Martinez E, Guermonprez P, Saveanu L. 2015. Intracellular transport routes for mhc i and their relevance for antigen cross-presentation. Front Immunol. 6:335.

Aldrich CJ, DeCloux A, Woods AS, Cotter RJ, Soloski MJ, Forman J. 1994. Identification of a tap-dependent leader peptide recognized by alloreactive t cells specific for a class ib antigen. Cell. 79(4):649-658.

Allard M, Oger R, Vignard V, Percier JM, Fregni G, Périer A, Caignard A, Charreau B, Bernardeau K, Khammari A et al. 2011. Serum soluble hla-e in melanoma: A new potential immune-related marker in cancer. PLoS One. 6(6):e21118.

Allen PM, Matsueda GR, Haber E, Unanue ER. 1985. Specificity of the t cell receptor: Two different determinants are generated by the same peptide and the i-ak molecule. J Immunol. 135(1):368-373.

Amiel J. 1967. Study of the leukocyte phenotypes in hodgkin's disease. Histocompatibility Testing.79-81.

Amigorena S, Bonnerot C, Drake JR, Choquet D, Hunziker W, Guillet JG, Webster P, Sautes C, Mellman I, Fridman WH. 1992. Cytoplasmic domain heterogeneity and functions of igg fc receptors in b lymphocytes. Science. 256(5065):1808-1812.

Androlewicz MJ, Anderson KS, Cresswell P. 1993. Evidence that transporters associated with antigen processing translocate a major histocompatibility

complex class i-binding peptide into the endoplasmic reticulum in an atp-dependent manner. Proc Natl Acad Sci U S A. 90(19):9130-9134.

Androlewicz MJ, Cresswell P. 1994. Human transporters associated with antigen processing possess a promiscuous peptide-binding site. Immunity. 1(1):7-14.

Angenieux C, Salamero J, Fricker D, Cazenave JP, Goud B, Hanau D, de La Salle H. 2000. Characterization of cd1e, a third type of cd1 molecule expressed in dendritic cells. J Biol Chem. 275(48):37757-37764.

Angénieux C, Fraisier V, Maître B, Racine V, van der Wel N, Fricker D, Proamer F, Sachse M, Cazenave JP, Peters P et al. 2005. The cellular pathway of cd1e in immature and maturing dendritic cells. Traffic. 6(4):286-302.

Anjanappa R, Garcia-Alai M, Kopicki JD, Lockhauserbäumer J, Aboelmagd M, Hinrichs J, Nemtanu IM, Uetrecht C, Zacharias M, Springer S et al. 2020. Structures of peptide-free and partially loaded mhc class i molecules reveal mechanisms of peptide selection. Nat Commun. 11(1):1314.

Antonini M, Lo Conte M, Sorini C, Falcone M. 2019. How the interplay between the commensal microbiota, gut barrier integrity, and mucosal immunity regulates brain autoimmunity. Front Immunol. 10:1937.

Antoniou AN, Powis SJ. 2008. Pathogen evasion strategies for the major histocompatibility complex class i assembly pathway. Immunology. 124(1):1-12.

Babbitt BP, Allen PM, Matsueda G, Haber E, Unanue ER. 1985. Binding of immunogenic peptides to ia histocompatibility molecules. Nature. 317(6035):359-361.

Barber C, De Souza VA, Paterson RL, Martin-Urdiroz M, Mulakkal NC, Srikannathasan V, Connolly M, Phillips G, Foong-Leong T, Pengelly R et al. 2022. Structure-guided stabilization of pathogen-derived peptide-hla-e complexes using non-natural amino acids conserves native tcr recognition. Eur J Immunol. 52(4):618-632.

Barel MT, Pizzato N, Le Bouteiller P, Wiertz EJ, Lenfant F. 2006. Subtle sequence variation among mhc class i locus products greatly influences sensitivity to hcmv us2- and us11-mediated degradation. Int Immunol. 18(1):173-182.

Barker DJ, Maccari G, Georgiou X, Cooper MA, Flicek P, Robinson J, Marsh SGE. 2023. The ipd-imgt/hla database. Nucleic Acids Res. 51(D1):D1053-D1060.

Barrenäs F, Hansen SG, Law L, Driscoll C, Green RR, Smith E, Chang J, Golez I, Urion T, Peng X et al. 2021. Interleukin-15 response signature predicts rhcmv/siv vaccine efficacy. PLoS Pathog. 17(7):e1009278.

Barrett DM, Gustafson KS, Wang J, Wang SZ, Ginder GD. 2004. A gata factor mediates cell type-restricted induction of hla-e gene transcription by gamma interferon. Mol Cell Biol. 24(14):6194-6204.

Barroso M, Tucker H, Drake L, Nichol K, Drake JR. 2015. Antigen-b cell receptor complexes associate with intracellular major histocompatibility complex (mhc) class ii molecules. J Biol Chem. 290(45):27101-27112.

Basha G, Omilusik K, Chavez-Steenbock A, Reinicke AT, Lack N, Choi KB, Jefferies WA. 2012. A cd74-dependent mhc class i endolysosomal cross-presentation pathway. Nat Immunol. 13(3):237-245.

Bashirova AA, Viard M, Naranbhai V, Grifoni A, Garcia-Beltran W, Akdag M, Yuki Y, Gao X, O'hUigin C, Raghavan M et al. 2020. Hla tapasin independence: Broader peptide repertoire and hiv control. Proc Natl Acad Sci U S A. 117(45):28232-28238.

Bauer S, Groh V, Wu J, Steinle A, Phillips JH, Lanier LL, Spies T. 1999. Activation of nk cells and t cells by nkg2d, a receptor for stress-inducible mica. Science. 285(5428):727-729.

Berger AC, Roche PA. 2009. Mhc class ii transport at a glance. J Cell Sci. 122(Pt 1):1-4.

Berger CT, Frahm N, Price DA, Mothe B, Ghebremichael M, Hartman KL, Henry LM, Brenchley JM, Ruff LE, Venturi V et al. 2011. High-functional-avidity cytotoxic t lymphocyte responses to hla-b-restricted gag-derived epitopes associated with relative hiv control. J Virol. 85(18):9334-9345.

Bjorkman PJ, Saper MA, Samraoui B, Bennett WS, Strominger JL, Wiley DC. 1987a. Structure of the human class i histocompatibility antigen, hla-a2. Nature. 329(6139):506-512.

Bjorkman PJ, Saper MA, Samraoui B, Bennett WS, Strominger JL, Wiley DC. 1987b. The foreign antigen binding site and t cell recognition regions of class i histocompatibility antigens. Nature. 329(6139):512-518.

Bolitho P, Voskoboinik I, Trapani JA, Smyth MJ. 2007. Apoptosis induced by the lymphocyte effector molecule perforin. Curr Opin Immunol. 19(3):339-347.

Boname JM, de Lima BD, Lehner PJ, Stevenson PG. 2004. Viral degradation of the mhc class i peptide loading complex. Immunity. 20(3):305-317.

Boname JM, Stevenson PG. 2001. Mhc class i ubiquitination by a viral phd/lap finger protein. Immunity. 15(4):627-636.

Boncompain G, Divoux S, Gareil N, de Forges H, Lescure A, Latreche L, Mercanti V, Jollivet F, Raposo G, Perez F. 2012. Synchronization of secretory protein traffic in populations of cells. Nat Methods. 9(5):493-498.

Bonifacino JS, Traub LM. 2003. Signals for sorting of transmembrane proteins to endosomes and lysosomes. Annu Rev Biochem. 72:395-447.

Bonifaz L, Bonnyay D, Mahnke K, Rivera M, Nussenzweig MC, Steinman RM. 2002. Efficient targeting of protein antigen to the dendritic cell receptor dec-205 in the steady state leads to antigen presentation on major histocompatibility complex class i products and peripheral cd8+ t cell tolerance. J Exp Med. 196(12):1627-1638.

Borrego F, Ulbrecht M, Weiss EH, Coligan JE, Brooks AG. 1998. Recognition of human histocompatibility leukocyte antigen (hla)-e complexed with hla class i signal sequence-derived peptides by cd94/nkg2 confers protection from natural killer cell-mediated lysis. J Exp Med. 187(5):813-818.

Borst J, Ahrends T, Bąbała N, Melief CJM, Kastenmüller W. 2018. Cd4 + t cell help in cancer immunology and immunotherapy. Nat Rev Immunol. 18(10):635-647.

Bouvier M, Wiley DC. 1994. Importance of peptide amino and carboxyl termini to the stability of mhc class i molecules. Science. 265(5170):398-402.

Bouwer HG, Bai A, Forman J, Gregory SH, Wing EJ, Barry RA, Hinrichs DJ. 1998. Listeria monocytogenes-infected hepatocytes are targets of major histocompatibility complex class ib-restricted antilisterial cytotoxic t lymphocytes. Infect Immun. 66(6):2814-2817.

Bouwer HG, Lindahl KF, Baldridge JR, Wagner CR, Barry RA, Hinrichs DJ. 1994. An h2-t mhc class ib molecule presents listeria monocytogenes-derived antigen to immune cd8+ cytotoxic t cells. J Immunol. 152(11):5352-5360.

Boyle LH, Gillingham AK, Munro S, Trowsdale J. 2006. Selective export of hla-f by its cytoplasmic tail. J Immunol. 176(11):6464-6472.

Boyle LH, Hermann C, Boname JM, Porter KM, Patel PA, Burr ML, Duncan LM, Harbour ME, Rhodes DA, Skjodt K et al. 2013. Tapasin-related protein tapbpr is an additional component of the mhc class i presentation pathway. Proc Natl Acad Sci U S A. 110(9):3465-3470.

Bradley SD, Chen Z, Melendez B, Talukder A, Khalili JS, Rodriguez-Cruz T, Liu S, Whittington M, Deng W, Li F et al. 2015. Brafv600e co-opts a conserved mhc class i internalization pathway to diminish antigen presentation and cd8+ t-cell recognition of melanoma. Cancer Immunol Res. 3(6):602-609.

Braud V, Jones EY, McMichael A. 1997. The human major histocompatibility complex class ib molecule hla-e binds signal sequence-derived peptides with primary anchor residues at positions 2 and 9. Eur J Immunol. 27(5):1164-1169.

Braud VM, Allan DS, O'Callaghan CA, Söderström K, D'Andrea A, Ogg GS, Lazetic S, Young NT, Bell JI, Phillips JH et al. 1998a. Hla-e binds to natural killer cell receptors cd94/nkg2a, b and c. Nature. 391(6669):795-799.

Braud VM, Allan DS, Wilson D, McMichael AJ. 1998b. Tap- and tapasin-dependent hla-e surface expression correlates with the binding of an mhc class i leader peptide. Curr Biol. 8(1):1-10.

Brehm MA, Daniels KA, Welsh RM. 2005. Rapid production of tnf-alpha following tcr engagement of naive cd8 t cells. J Immunol. 175(8):5043-5049.

Breitfeld D, Ohl L, Kremmer E, Ellwart J, Sallusto F, Lipp M, Förster R. 2000. Follicular b helper t cells express cxc chemokine receptor 5, localize to b cell follicles, and support immunoglobulin production. J Exp Med. 192(11):1545-1552.

Bremnes B, Madsen T, Gedde-Dahl M, Bakke O. 1994. An li and ml motif in the cytoplasmic tail of the mhc-associated invariant chain mediate rapid internalization. J Cell Sci. 107 (Pt 7):2021-2032.

Briken V, Jackman RM, Dasgupta S, Hoening S, Porcelli SA. 2002. Intracellular trafficking pathway of newly synthesized cd1b molecules. EMBO J. 21(4):825-834.

Briley GP, Hissong MA, Chiu ML, Lee DC. 1997. The carboxyl-terminal valine residues of protgf alpha are required for its efficient maturation and intracellular routing. Mol Biol Cell. 8(8):1619-1631.

Brown JH, Jardetzky TS, Gorga JC, Stern LJ, Urban RG, Strominger JL, Wiley DC. 1993. Three-dimensional structure of the human class ii histocompatibility antigen hla-dr1. Nature. 364(6432):33-39.

Bukur J, Malenica B, Huber C, Seliger B. 2003. Altered expression of nonclassical hla class ib antigens in human renal cell carcinoma and its association with impaired immune response. Hum Immunol. 64(11):1081-1092.

Burgdorf S, Kautz A, Bohnert V, Knolle PA, Kurts C. 2007. Distinct pathways of antigen uptake and intracellular routing in cd4 and cd8 t cell activation. Science. 316(5824):612-616.

Burgdorf S, Lukacs-Kornek V, Kurts C. 2006. The mannose receptor mediates uptake of soluble but not of cell-associated antigen for cross-presentation. J Immunol. 176(11):6770-6776.

Burian A, Wang KL, Finton KA, Lee N, Ishitani A, Strong RK, Geraghty DE. 2016. Hla-f and mhc-i open conformers bind natural killer cell ig-like receptor kir3ds1. PLoS One. 11(9):e0163297.

Burrows CK, Kosova G, Herman C, Patterson K, Hartmann KE, Velez Edwards DR, Stephenson MD, Lynch VJ, Ober C. 2016. Expression quantitative trait locus mapping studies in mid-secretory phase endometrial cells identifies hla-f and tap2 as fecundability-associated genes. PLoS Genet. 12(7):e1005858.

Burwitz BJ, Hashiguchi PK, Mansouri M, Meyer C, Gilbride RM, Biswas S, Womack JL, Reed JS, Wu HL, Axthelm MK et al. 2020. Mhc-e-restricted cd8 + t cells target hepatitis b virus-infected human hepatocytes. J Immunol. 204(8):2169-2176.

Bushmarina N, Tourne S, Giacometti G, Signorino-Gelo F, Garcia-Alles LF, Cazenave JP, Hanau D, de la Salle H. 2011. Increased flexibility and liposome-binding capacity of cd1e at endosomal ph. FEBS J. 278(12):2022-2033.

Caccamo N, Pietra G, Sullivan LC, Brooks AG, Prezzemolo T, La Manna MP, Di Liberto D, Joosten SA, van Meijgaarden KE, Di Carlo P et al. 2015. Human cd8 t lymphocytes recognize mycobacterium tuberculosis antigens presented by hla-e during active tuberculosis and express type 2 cytokines. Eur J Immunol. 45(4):1069-1081.

Camilli G, Cassotta A, Battella S, Palmieri G, Santoni A, Paladini F, Fiorillo MT, Sorrentino R. 2016. Regulation and trafficking of the hla-e molecules during monocyte-macrophage differentiation. J Leukoc Biol. 99(1):121-130.

Campeau E, Ruhl VE, Rodier F, Smith CL, Rahmberg BL, Fuss JO, Campisi J, Yaswen P, Cooper PK, Kaufman PD. 2009. A versatile viral system for expression and depletion of proteins in mammalian cells. PLoS One. 4(8):e6529.

Caposio P, van den Worm S, Crawford L, Perez W, Kreklywich C, Gilbride RM, Hughes CM, Ventura AB, Ratts R, Marshall EE et al. 2019. Characterization of a live-attenuated hcmv-based vaccine platform. Sci Rep. 9(1):19236.

Carter RW, Thompson C, Reid DM, Wong SY, Tough DF. 2006. Preferential induction of cd4+ t cell responses through in vivo targeting of antigen to dendritic cell-associated c-type lectin-1. J Immunol. 177(4):2276-2284.

Cebrian I, Visentin G, Blanchard N, Jouve M, Bobard A, Moita C, Enninga J, Moita LF, Amigorena S, Savina A. 2011. Sec22b regulates phagosomal maturation and antigen crosspresentation by dendritic cells. Cell. 147(6):1355-1368.

Celik AA, Kraemer T, Huyton T, Blasczyk R, Bade-Döding C. 2016. The diversity of the hla-e-restricted peptide repertoire explains the immunological impact of the arg107gly mismatch. Immunogenetics. 68(1):29-41.

Chanput W, Mes JJ, Wichers HJ. 2014. Thp-1 cell line: An in vitro cell model for immune modulation approach. Int Immunopharmacol. 23(1):37-45.

Chefalo PJ, Grandea AG, Van Kaer L, Harding CV. 2003. Tapasin-/- and tap1-/- macrophages are deficient in vacuolar alternate class i mhc (mhc-i) processing due to decreased mhc-i stability at phagolysosomal ph. J Immunol. 170(12):5825-5833.

Chefalo PJ, Harding CV. 2001. Processing of exogenous antigens for presentation by class i mhc molecules involves post-golgi peptide exchange influenced by peptide-mhc complex stability and acidic ph. J Immunol. 167(3):1274-1282.

Chen M, Bouvier M. 2007. Analysis of interactions in a tapasin/class i complex provides a mechanism for peptide selection. EMBO J. 26(6):1681-1690.

Cho KJ, Ishido S, Eisenlohr LC, Roche PA. 2020. Activation of dendritic cells alters the mechanism of mhc class ii antigen presentation to cd4 t cells. J Immunol. 204(6):1621-1629.

Cho S, Ryoo J, Jun Y, Ahn K. 2011. Receptor-mediated er export of human mhc class i molecules is regulated by the c-terminal single amino acid. Traffic. 12(1):42-55.

Chua WJ, Kim S, Myers N, Huang S, Yu L, Fremont DH, Diamond MS, Hansen TH. 2011. Endogenous mhc-related protein 1 is transiently expressed on the plasma membrane in a conformation that activates mucosal-associated invariant t cells. J Immunol. 186(8):4744-4750.

Chua WJ, Truscott SM, Eickhoff CS, Blazevic A, Hoft DF, Hansen TH. 2012. Polyclonal mucosa-associated invariant t cells have unique innate functions in bacterial infection. Infect Immun. 80(9):3256-3267.

Clemens DL, Lee BY, Horwitz MA. 2002. The mycobacterium tuberculosis phagosome in human macrophages is isolated from the host cell cytoplasm. Infect Immun. 70(10):5800-5807.

Cohen CJ, Denkberg G, Lev A, Epel M, Reiter Y. 2003. Recombinant antibodies with mhc-restricted, peptide-specific, t-cell receptor-like specificity: New tools to study antigen presentation and tcr-peptide-mhc interactions. J Mol Recognit. 16(5):324-332.

Cohen GB, Gandhi RT, Davis DM, Mandelboim O, Chen BK, Strominger JL, Baltimore D. 1999. The selective downregulation of class i major histocompatibility complex proteins by hiv-1 protects hiv-infected cells from nk cells. Immunity. 10(6):661-671.

Colbert JD, Cruz FM, Rock KL. 2020. Cross-presentation of exogenous antigens on mhc i molecules. Curr Opin Immunol. 64:1-8.

Collier JL, Weiss SA, Pauken KE, Sen DR, Sharpe AH. 2021. Not-so-opposite ends of the spectrum: Cd8 + t cell dysfunction across chronic infection, cancer and autoimmunity. Nat Immunol. 22(7):809-819.

Collins EJ, Garboczi DN, Karpusas MN, Wiley DC. 1995. The three-dimensional structure of a class i major histocompatibility complex molecule missing the alpha 3 domain of the heavy chain. Proc Natl Acad Sci U S A. 92(4):1218-1221.

Complete sequence and gene map of a human major histocompatibility complex. The mhc sequencing consortium. 1999. Nature. 401(6756):921-923.

Coscoy L, Ganem D. 2000. Kaposi's sarcoma-associated herpesvirus encodes two proteins that block cell surface display of mhc class i chains by enhancing their endocytosis. Proc Natl Acad Sci U S A. 97(14):8051-8056.

Coscoy L, Sanchez DJ, Ganem D. 2001. A novel class of herpesvirus-encoded membrane-bound e3 ubiquitin ligases regulates endocytosis of proteins involved in immune recognition. J Cell Biol. 155(7):1265-1273.

Coupel S, Moreau A, Hamidou M, Horejsi V, Soulillou JP, Charreau B. 2007. Expression and release of soluble hla-e is an immunoregulatory feature of endothelial cell activation. Blood. 109(7):2806-2814.

Cuevas-Zuviría B, Mínguez-Toral M, Díaz-Perales A, Garrido-Arandia M, Pacios LF. 2020. Dynamic plasticity of the lipid antigen-binding site of cd1d is crucially favoured by acidic ph and helper proteins. Sci Rep. 10(1):5714.

Danzer M, Polin H, Pröll J, Haunschmid R, Hofer K, Stabentheiner S, Hackl C, Kasparu H, König J, Hauser H et al. 2009. Clinical significance of hla-e*0103 homozygosity on survival after allogeneic hematopoietic stem-cell transplantation. Transplantation. 88(4):528-532.

Dausset J. 1958. Iso-leuco-anticorps. A*cta Haematol*.

Davidson B, Elstrand MB, McMaster MT, Berner A, Kurman RJ, Risberg B, Trope CG, Shih IM. 2005. Hla-g expression in effusions is a possible marker of tumor susceptibility to chemotherapy in ovarian carcinoma. Gynecol Oncol. 96(1):42-47.

De Angelis Rigotti F, De Gassart A, Pforr C, Cano F, N'Guessan P, Combes A, Camossetto V, Lehner PJ, Pierre P, Gatti E. 2017. March9-mediated ubiquitination regulates mhc i export from the tgn. Immunol Cell Biol. 95(9):753-764.

De Gassart A, Camosseto V, Thibodeau J, Ceppi M, Catalan N, Pierre P, Gatti E. 2008. Mhc class ii stabilization at the surface of human dendritic cells is the result of maturation-dependent march i down-regulation. Proc Natl Acad Sci U S A. 105(9):3491-3496.

de Kruijf EM, Sajet A, van Nes JG, Natanov R, Putter H, Smit VT, Liefers GJ, van den Elsen PJ, van de Velde CJ, Kuppen PJ. 2010. Hla-e and hla-g expression in classical hla class i-negative tumors is of prognostic value for clinical outcome of early breast cancer patients. J Immunol. 185(12):7452-7459.

De Libero G, Mori L. 2012. Novel insights into lipid antigen presentation. Trends Immunol. 33(3):103-111.

DeCloux A, Woods AS, Cotter RJ, Soloski MJ, Forman J. 1997. Dominance of a single peptide bound to the class i(b) molecule, qa-1b. J Immunol. 158(5):2183-2191.

Delneste Y, Magistrelli G, Gauchat J, Haeuw J, Aubry J, Nakamura K, Kawakami-Honda N, Goetsch L, Sawamura T, Bonnefoy J et al. 2002. Involvement of lox-1 in dendritic cell-mediated antigen cross-presentation. Immunity. 17(3):353-362.

Demaria S, Schwab R, Gottesman SR, Bushkin Y. 1994. Soluble beta 2-microglobulin-free class i heavy chains are released from the surface of activated and leukemia cells by a metalloprotease. J Biol Chem. 269(9):6689-6694.

Denzin LK, Cresswell P. 1995. Hla-dm induces clip dissociation from mhc class ii alpha beta dimers and facilitates peptide loading. Cell. 82(1):155-165.

Denzin LK, Sant'Angelo DB, Hammond C, Surman MJ, Cresswell P. 1997. Negative regulation by hla-do of mhc class ii-restricted antigen processing. Science. 278(5335):106-109.

Derré L, Corvaisier M, Charreau B, Moreau A, Godefroy E, Moreau-Aubry A, Jotereau F, Gervois N. 2006. Expression and release of hla-e by melanoma cells and melanocytes: Potential impact on the response of cytotoxic effector cells. J Immunol. 177(5):3100-3107.

Dicks MD, Spencer AJ, Edwards NJ, Wadell G, Bojang K, Gilbert SC, Hill AV, Cottingham MG. 2012. A novel chimpanzee adenovirus vector with low human seroprevalence: Improved systems for vector derivation and comparative immunogenicity. PLoS One. 7(7):e40385.

Djurisic S, Hviid TV. 2014. Hla class ib molecules and immune cells in pregnancy and preeclampsia. Front Immunol. 5:652.

Donaldson JG, Williams DB. 2009. Intracellular assembly and trafficking of mhc class i molecules. Traffic. 10(12):1745-1752.

Dulberger CL, McMurtrey CP, Hölzemer A, Neu KE, Liu V, Steinbach AM, Garcia-Beltran WF, Sulak M, Jabri B, Lynch VJ et al. 2017. Human leukocyte

antigen f presents peptides and regulates immunity through interactions with nk cell receptors. Immunity. 46(6):1018-1029.e1017.

Dumasius V, Jameel M, Burhop J, Meng FJ, Welch LC, Mutlu G GM, Factor P. 2003. In vivo timing of onset of transgene expression following adenoviral-mediated gene transfer. Virology. 308(2):243-249.

Dunn KW, Kamocka MM, McDonald JH. 2011. A practical guide to evaluating colocalization in biological microscopy. Am J Physiol Cell Physiol. 300(4):C723-742.

Durgeau A, Virk Y, Corgnac S, Mami-Chouaib F. 2018. Recent advances in targeting cd8 t-cell immunity for more effective cancer immunotherapy. Front Immunol. 9:14.

Engering A, Geijtenbeek TB, van Vliet SJ, Wijers M, van Liempt E, Demaurex N, Lanzavecchia A, Fransen J, Figdor CG, Piguet V et al. 2002. The dendritic cell-specific adhesion receptor dc-sign internalizes antigen for presentation to t cells. J Immunol. 168(5):2118-2126.

Esposito I, Cicconi P, D'Alise AM, Brown A, Esposito M, Swadling L, Holst PJ, Bassi MR, Stornaiuolo M, Mori F et al. 2020. Mhc class ii invariant chain-adjuvanted viral vectored vaccines enhances t cell responses in humans. Sci Transl Med. 12(548).

Fahnestock ML, Tamir I, Narhi L, Bjorkman PJ. 1992. Thermal stability comparison of purified empty and peptide-filled forms of a class i mhc molecule. Science. 258(5088):1658-1662.

Farmery MR, Allen S, Allen AJ, Bulleid NJ. 2000. The role of erp57 in disulfide bond formation during the assembly of major histocompatibility complex class i in a synchronized semipermeabilized cell translation system. J Biol Chem. 275(20):14933-14938.

Farrand KJ, Dickgreber N, Stoitzner P, Ronchese F, Petersen TR, Hermans IF. 2009. Langerin+ cd8alpha+ dendritic cells are critical for cross-priming and il-12 production in response to systemic antigens. J Immunol. 183(12):7732-7742.

Feng Y, Zhao X, White AK, Garcia KC, Fordyce PM. 2022. A bead-based method for high-throughput mapping of the sequence- and force-dependence of t cell activation. Nat Methods. 19(10):1295-1305.

Figdor CG, van Kooyk Y, Adema GJ. 2002. C-type lectin receptors on dendritic cells and langerhans cells. Nat Rev Immunol. 2(2):77-84.

Foot N, Henshall T, Kumar S. 2017. Ubiquitination and the regulation of membrane proteins. Physiol Rev. 97(1):253-281.

Francia V, Reker-Smit C, Boel G, Salvati A. 2019. Limits and challenges in using transport inhibitors to characterize how nano-sized drug carriers enter cells. Nanomedicine (Lond). 14(12):1533-1549.

Franciszkiewicz K, Salou M, Legoux F, Zhou Q, Cui Y, Bessoles S, Lantz O. 2016. Mhc class i-related molecule, mr1, and mucosal-associated invariant t cells. Immunol Rev. 272(1):120-138.

Früh K, Picker L. 2017. Cd8+ t cell programming by cytomegalovirus vectors: Applications in prophylactic and therapeutic vaccination. Curr Opin Immunol. 47:52-56.

Fujii T, Ishitani A, Geraghty DE. 1994. A soluble form of the hla-g antigen is encoded by a messenger ribonucleic acid containing intron 4. J Immunol. 153(12):5516-5524.

Gagnon E, Duclos S, Rondeau C, Chevet E, Cameron PH, Steele-Mortimer O, Paiement J, Bergeron JJ, Desjardins M. 2002. Endoplasmic reticulum-mediated phagocytosis is a mechanism of entry into macrophages. Cell. 110(1):119-131.

Garbi N, Tanaka S, Momburg F, Hammerling GJ. 2006. Impaired assembly of the major histocompatibility complex class i peptide-loading complex in mice deficient in the oxidoreductase erp57. Nat Immunol. 7(1):93-102.

Garcia-Alles LF, Giacometti G, Versluis C, Maveyraud L, de Paepe D, Guiard J, Tranier S, Gilleron M, Prandi J, Hanau D et al. 2011. Crystal structure of human cd1e reveals a groove suited for lipid-exchange processes. Proc Natl Acad Sci U S A. 108(32):13230-13235.

Garcia-Beltran WF, Hölzemer A, Martrus G, Chung AW, Pacheco Y, Simoneau CR, Rucevic M, Lamothe-Molina PA, Pertel T, Kim TE et al. 2016. Open conformers of hla-f are high-affinity ligands of the activating nk-cell receptor kir3ds1. Nat Immunol. 17(9):1067-1074.

Garstka MA, Fritzsche S, Lenart I, Hein Z, Jankevicius G, Boyle LH, Elliott T, Trowsdale J, Antoniou AN, Zacharias M et al. 2011. Tapasin dependence of

major histocompatibility complex class i molecules correlates with their conformational flexibility. FASEB J. 25(11):3989-3998.

Georgel P, Radosavljevic M, Macquin C, Bahram S. 2011. The non-conventional mhc class i mr1 molecule controls infection by klebsiella pneumoniae in mice. Mol Immunol. 48(5):769-775.

Geraghty DE, Stockschleader M, Ishitani A, Hansen JA. 1992. Polymorphism at the hla-e locus predates most hla-a and -b polymorphism. Hum Immunol. 33(3):174-184.

Giodini A, Rahner C, Cresswell P. 2009. Receptor-mediated phagocytosis elicits cross-presentation in nonprofessional antigen-presenting cells. Proc Natl Acad Sci U S A. 106(9):3324-3329.

Gocher AM, Workman CJ, Vignali DAA. 2022. Interferon-γ: Teammate or opponent in the tumour microenvironment? Nat Rev Immunol. 22(3):158-172.

Goh WC, Rogel ME, Kinsey CM, Michael SF, Fultz PN, Nowak MA, Hahn BH, Emerman M. 1998. Hiv-1 vpr increases viral expression by manipulation of the cell cycle: A mechanism for selection of vpr in vivo. Nat Med. 4(1):65-71.

Goodridge JP, Burian A, Lee N, Geraghty DE. 2010. Hla-f complex without peptide binds to mhc class i protein in the open conformer form. J Immunol. 184(11):6199-6208.

Goodridge JP, Lee N, Burian A, Pyo CW, Tykodi SS, Warren EH, Yee C, Riddell SR, Geraghty DE. 2013. Hla-f and mhc-i open conformers cooperate in a mhc-i antigen cross-presentation pathway. J Immunol. 191(4):1567-1577.

Gorer PA, Lyman S, Snell GD, . 1948. Studies on the genetic and antigenic basis of tumour transplantation linkage between a histocompatibility gene and 'fused' in mice. Proc. R. Soc. B. p. 499-505.

Goulmy E, Termijtelen A, Bradley BA, van Rood JJ. 1977. Y-antigen killing by t cells of women is restricted by hla. Nature. 266(5602):544-545.

Grandea AG, Lehner PJ, Cresswell P, Spies T. 1997. Regulation of mhc class i heterodimer stability and interaction with tap by tapasin. Immunogenetics. 46(6):477-483.

Greenfield JJ, High S. 1999. The sec61 complex is located in both the er and the er-golgi intermediate compartment. J Cell Sci. 112 (Pt 10):1477-1486.

Griffin BD, Gram AM, Mulder A, Van Leeuwen D, Claas FH, Wang F, Ressing ME, Wiertz E. 2013. Ebv bilf1 evolved to downregulate cell surface display of a wide range of hla class i molecules through their cytoplasmic tail. J Immunol. 190(4):1672-1684.

Grotzke JE, Harriff MJ, Siler AC, Nolt D, Delepine J, Lewinsohn DA, Lewinsohn DM. 2009. The mycobacterium tuberculosis phagosome is a hla-i processing competent organelle. PLoS Pathog. 5(4):e1000374.

Guberina H, da Silva Nardi F, Michita RT, Dolff S, Bienholz A, Heinemann FM, Wilde B, Trilling M, Horn PA, Kribben A et al. 2018. Susceptibility of hla-e*01:03 allele carriers to develop cytomegalovirus replication after living-donor kidney transplantation. J Infect Dis. 217(12):1918-1922.

Guce AI, Mortimer SE, Yoon T, Painter CA, Jiang W, Mellins ED, Stern LJ. 2013. Hla-do acts as a substrate mimic to inhibit hla-dm by a competitive mechanism. Nat Struct Mol Biol. 20(1):90-98.

Guild BC, Strominger JL. 1984. Human and murine class i mhc antigens share conserved serine 335, the site of hla phosphorylation in vivo. J Biol Chem. 259(14):9235-9240.

Gummuluru S, Emerman M. 1999. Cell cycle- and vpr-mediated regulation of human immunodeficiency virus type 1 expression in primary and transformed t-cell lines. J Virol. 73(7):5422-5430.

Gumperz JE. 2006. The ins and outs of cd1 molecules: Bringing lipids under immunological surveillance. Traffic. 7(1):2-13.

Gupta M, Wahi A, Sharma P, Nagpal R, Raina N, Kaurav M, Bhattacharya J, Rodrigues Oliveira SM, Dolma KG, Paul AK et al. 2022. Recent advances in cancer vaccines: Challenges, achievements, and futuristic prospects. Vaccines (Basel). 10(12).

Gustafson KS, Ginder GD. 1996. Interferon-gamma induction of the human leukocyte antigen-e gene is mediated through binding of a complex containing stat1alpha to a distinct interferon-gamma-responsive element. J Biol Chem. 271(33):20035-20046.

Guzmán-Fulgencio M, Berenguer J, Rallón N, Fernández-Rodríguez A, Miralles P, Soriano V, Jiménez-Sousa MA, Cosín J, Medrano J, García-Álvarez M et al. 2013. Hla-e variants are associated with sustained virological response in

hiv/hepatitis c virus-coinfected patients on hepatitis c virus therapy. AIDS. 27(8):1231-1238.

Hafstrand I, Aflalo A, Boyle LH. 2021. Why tapbpr? Implications of an additional player in mhc class i peptide presentation. Curr Opin Immunol. 70:90-94.

Hanke T. 2019. Aiming for protective t-cell responses: A focus on the first generation conserved-region hivconsv vaccines in preventive and therapeutic clinical trials. Expert Rev Vaccines. 18(10):1029-1041.

Hannoun Z, Lin Z, Brackenridge S, Kuse N, Akahoshi T, Borthwick N, McMichael A, Murakoshi H, Takiguchi M, Hanke T. 2018. Identification of novel hiv-1-derived hla-e-binding peptides. Immunol Lett. 202:65-72.

Hansen SG, Ford JC, Lewis MS, Ventura AB, Hughes CM, Coyne-Johnson L, Whizin N, Oswald K, Shoemaker R, Swanson T et al. 2011. Profound early control of highly pathogenic siv by an effector memory t-cell vaccine. Nature. 473(7348):523-527.

Hansen SG, Hancock MH, Malouli D, Marshall EE, Hughes CM, Randall KT, Morrow D, Ford JC, Gilbride RM, Selseth AN et al. 2022. Myeloid cell tropism enables mhc-e-restricted cd8. Sci Immunol. 7(72):eabn9301.

Hansen SG, Piatak M, Ventura AB, Hughes CM, Gilbride RM, Ford JC, Oswald K, Shoemaker R, Li Y, Lewis MS et al. 2013a. Immune clearance of highly pathogenic siv infection. Nature. 502(7469):100-104.

Hansen SG, Sacha JB, Hughes CM, Ford JC, Burwitz BJ, Scholz I, Gilbride RM, Lewis MS, Gilliam AN, Ventura AB et al. 2013b. Cytomegalovirus vectors violate cd8+ t cell epitope recognition paradigms. Science. 340(6135):1237874.

Hansen SG, Womack J, Scholz I, Renner A, Edgel KA, Xu G, Ford JC, Grey M, St Laurent B, Turner JM et al. 2019. Cytomegalovirus vectors expressing plasmodium knowlesi antigens induce immune responses that delay parasitemia upon sporozoite challenge. PLoS One. 14(1):e0210252.

Hansen SG, Wu HL, Burwitz BJ, Hughes CM, Hammond KB, Ventura AB, Reed JS, Gilbride RM, Ainslie E, Morrow DW et al. 2016. Broadly targeted $cd8^+$ t cell responses restricted by major histocompatibility complex e. Science. 351(6274):714-720.

Hansen TH, Bouvier M. 2009. Mhc class i antigen presentation: Learning from viral evasion strategies. Nat Rev Immunol. 9(7):503-513.

Harriff MJ, Karamooz E, Burr A, Grant WF, Canfield ET, Sorensen ML, Moita LF, Lewinsohn DM. 2016. Endosomal mr1 trafficking plays a key role in presentation of mycobacterium tuberculosis ligands to mait cells. PLoS Pathog. 12(3):e1005524.

Harrington LE, Hatton RD, Mangan PR, Turner H, Murphy TL, Murphy KM, Weaver CT. 2005. Interleukin 17-producing cd4+ effector t cells develop via a lineage distinct from the t helper type 1 and 2 lineages. Nat Immunol. 6(11):1123-1132.

Haworth KB, Leddon JL, Chen CY, Horwitz EM, Mackall CL, Cripe TP. 2015. Going back to class i: Mhc and immunotherapies for childhood cancer. Pediatr Blood Cancer. 62(4):571-576.

He W, Gea-Mallorquí E, Colin-York H, Fritzsche M, Gillespie GM, Brackenridge S, Borrow P, McMichael AJ. 2023. Intracellular trafficking of hla-e and its regulation. J Exp Med. 220(8).

Heinzel AS, Grotzke JE, Lines RA, Lewinsohn DA, McNabb AL, Streblow DN, Braud VM, Grieser HJ, Belisle JT, Lewinsohn DM. 2002. Hla-e-dependent presentation of mtb-derived antigen to human cd8+ t cells. J Exp Med. 196(11):1473-1481.

Hellman LM, Yin L, Wang Y, Blevins SJ, Riley TP, Belden OS, Spear TT, Nishimura MI, Stern LJ, Baker BM. 2016. Differential scanning fluorimetry based assessments of the thermal and kinetic stability of peptide-mhc complexes. J Immunol Methods. 432:95-101.

Herbein G. 2018. The human cytomegalovirus, from oncomodulation to oncogenesis. Viruses. 10(8).

Hershko A. 1988. Ubiquitin-mediated protein degradation. J Biol Chem. 263(30):15237-15240.

Hewitt EW, Duncan L, Mufti D, Baker J, Stevenson PG, Lehner PJ. 2002. Ubiquitylation of mhc class i by the k3 viral protein signals internalization and tsg101-dependent degradation. EMBO J. 21(10):2418-2429.

Hewitt EW, Gupta SS, Lehner PJ. 2001. The human cytomegalovirus gene product us6 inhibits atp binding by tap. EMBO J. 20(3):387-396.

Hinks TSC, Zhang XW. 2020. Mait cell activation and functions. Front Immunol. 11:1014.

Hoare HL, Sullivan LC, Clements CS, Ely LK, Beddoe T, Henderson KN, Lin J, Reid HH, Brooks AG, Rossjohn J. 2008. Subtle changes in peptide conformation profoundly affect recognition of the non-classical mhc class i molecule hla-e by the cd94-nkg2 natural killer cell receptors. J Mol Biol. 377(5):1297-1303.

Hornbeck PV, Zhang B, Murray B, Kornhauser JM, Latham V, Skrzypek E. 2015. Phosphositeplus, 2014: Mutations, ptms and recalibrations. Nucleic Acids Res. 43(Database issue):D512-520.

Hosseini E, Schwarer AP, Jalali A, Ghasemzadeh M. 2013. The impact of hla-e polymorphisms on relapse following allogeneic hematopoietic stem cell transplantation. Leuk Res. 37(5):516-519.

Houde M, Bertholet S, Gagnon E, Brunet S, Goyette G, Laplante A, Princiotta MF, Thibault P, Sacks D, Desjardins M. 2003. Phagosomes are competent organelles for antigen cross-presentation. Nature. 425(6956):402-406.

HoWangYin KY, Loustau M, Wu J, Alegre E, Daouya M, Caumartin J, Sousa S, Horuzsko A, Carosella ED, LeMaoult J. 2012. Multimeric structures of hla-g isoforms function through differential binding to lilrb receptors. Cell Mol Life Sci. 69(23):4041-4049.

Huang S, Gilfillan S, Kim S, Thompson B, Wang X, Sant AJ, Fremont DH, Lantz O, Hansen TH. 2008. Mr1 uses an endocytic pathway to activate mucosal-associated invariant t cells. J Exp Med. 205(5):1201-1211.

Hughes EA, Cresswell P. 1998. The thiol oxidoreductase erp57 is a component of the mhc class i peptide-loading complex. Curr Biol. 8(12):709-712.

Hurwitz JL. 2018. Antiviral vaccines: Successes and prospects. Viral Immunol. 31(2):79.

Hò GT, Heinen FJ, Huyton T, Blasczyk R, Bade-Döding C. 2019. Hla-f*01:01 presents peptides with n-terminal flexibility and a preferred length of 16 residues. Immunogenetics. 71(5-6):353-360.

Iglesias MC, Briceno O, Gostick E, Moris A, Meaudre C, Price DA, Ungeheuer MN, Saez-Cirion A, Mallone R, Appay V. 2013. Immunodominance of hla-b27-restricted hiv kk10-specific cd8(+) t-cells is not related to naïve precursor frequency. Immunol Lett. 149(1-2):119-122.

Ilca FT, Drexhage LZ, Brewin G, Peacock S, Boyle LH. 2019. Distinct polymorphisms in hla class i molecules govern their susceptibility to peptide editing by tapbpr. Cell Rep. 29(6):1621-1632.e1623.

Ilca FT, Neerincx A, Hermann C, Marcu A, Stevanović S, Deane JE, Boyle LH. 2018. Tapbpr mediates peptide dissociation from mhc class i using a leucine lever. Elife. 7.

Iodice L, Sarnataro S, Bonatti S. 2001. The carboxyl-terminal valine is required for transport of glycoprotein cd8 alpha from the endoplasmic reticulum to the intermediate compartment. J Biol Chem. 276(31):28920-28926.

Jackson MR, Cohen-Doyle MF, Peterson PA, Williams DB. 1994. Regulation of mhc class i transport by the molecular chaperone, calnexin (p88, ip90). Science. 263(5145):384-387.

Janssens I, Campillo Davó D, Van den Bos J, De Reu H, Berneman ZN, Wens I, Cools N. 2022. Engineering of regulatory t cells by means of mrna electroporation in a gmp-compliant manner. Cytotherapy. 24(6):659-672.

Jardetzky TS, Brown JH, Gorga JC, Stern LJ, Urban RG, Chi YI, Stauffacher C, Strominger JL, Wiley DC. 1994. Three-dimensional structure of a human class ii histocompatibility molecule complexed with superantigen. Nature. 368(6473):711-718.

Jarousse N, Wilson JD, Arac D, Rizo J, Kelly RB. 2003. Endocytosis of synaptotagmin 1 is mediated by a novel, tryptophan-containing motif. Traffic. 4(7):468-478.

Jayawardena-Wolf J, Benlagha K, Chiu YH, Mehr R, Bendelac A. 2001. Cd1d endosomal trafficking is independently regulated by an intrinsic cd1d-encoded tyrosine motif and by the invariant chain. Immunity. 15(6):897-908.

Jensen S, Steffensen MA, Jensen BA, Schlüter D, Christensen JP, Thomsen AR. 2013. Adenovirus-based vaccine against listeria monocytogenes: Extending the concept of invariant chain linkage. J Immunol. 191(8):4152-4164.

Jhunjhunwala S, Hammer C, Delamarre L. 2021. Antigen presentation in cancer: Insights into tumour immunogenicity and immune evasion. Nat Rev Cancer. 21(5):298-312.

Jones PP, Murphy DB, Hewgill D, McDevitt HO. 1979. Detection of a common polypeptide chain in i--a and i--e sub-region immunoprecipitates. Mol Immunol. 16(1):51-60.

Joosten SA, van Meijgaarden KE, van Weeren PC, Kazi F, Geluk A, Savage ND, Drijfhout JW, Flower DR, Hanekom WA, Klein MR et al. 2010. Mycobacterium tuberculosis peptides presented by hla-e molecules are targets for human cd8 t-cells with cytotoxic as well as regulatory activity. PLoS Pathog. 6(2):e1000782.

Jouand N, Bressollette-Bodin C, Gerard N, Giral M, Guerif P, Rodallec A, Oger R, Parrot T, Allard M, Cesbron-Gautier A et al. 2018. Hcmv triggers frequent and persistent ul40-specific unconventional hla-e-restricted cd8 t-cell responses with potential autologous and allogeneic peptide recognition. PLoS Pathog. 14(4):e1007041.

Kaiser BK, Pizarro JC, Kerns J, Strong RK. 2008. Structural basis for nkg2a/cd94 recognition of hla-e. Proc Natl Acad Sci U S A. 105(18):6696-6701.

Kaksonen M, Roux A. 2018. Mechanisms of clathrin-mediated endocytosis. Nat Rev Mol Cell Biol. 19(5):313-326.

Kambayashi T, Kraft-Leavy JR, Dauner JG, Sullivan BA, Laur O, Jensen PE. 2004. The nonclassical mhc class i molecule qa-1 forms unstable peptide complexes. J Immunol. 172(3):1661-1669.

Kanevskiy L, Erokhina S, Kobyzeva P, Streltsova M, Sapozhnikov A, Kovalenko E. 2019. Dimorphism of hla-e and its disease association. Int J Mol Sci. 20(21).

Kang SJ, Cresswell P. 2002. Regulation of intracellular trafficking of human cd1d by association with mhc class ii molecules. EMBO J. 21(7):1650-1660.

Karamooz E, Harriff MJ, Lewinsohn DM. 2018. Mr1-dependent antigen presentation. Semin Cell Dev Biol. 84:58-64.

Karamooz E, Harriff MJ, Narayanan GA, Worley A, Lewinsohn DM. 2019. Mr1 recycling and blockade of endosomal trafficking reveal distinguishable antigen presentation pathways between mycobacterium tuberculosis infection and exogenously delivered antigens. Sci Rep. 9(1):4797.

Kasper MR, Roeth JF, Williams M, Filzen TM, Fleis RI, Collins KL. 2005. Hiv-1 nef disrupts antigen presentation early in the secretory pathway. J Biol Chem. 280(13):12840-12848.

Kirana C, Ruszkiewicz A, Stubbs RS, Hardingham JE, Hewett PJ, Maddern GJ, Hauben E. 2017. Soluble hla-g is a differential prognostic marker in sequential colorectal cancer disease stages. Int J Cancer. 140(11):2577-2586.

Klechevsky E, Flamar AL, Cao Y, Blanck JP, Liu M, O'Bar A, Agouna-Deciat O, Klucar P, Thompson-Snipes L, Zurawski S et al. 2010. Cross-priming cd8+ t cells by targeting antigens to human dendritic cells through dcir. Blood. 116(10):1685-1697.

Kleijmeer MJ, Ossevoort MA, van Veen CJ, van Hellemond JJ, Neefjes JJ, Kast WM, Melief CJ, Geuze HJ. 1995. Mhc class ii compartments and the kinetics of antigen presentation in activated mouse spleen dendritic cells. J Immunol. 154(11):5715-5724.

Kløverpris HN, Payne RP, Sacha JB, Rasaiyaah JT, Chen F, Takiguchi M, Yang OO, Towers GJ, Goulder P, Prado JG. 2013. Early antigen presentation of protective hiv-1 kf11gag and kk10gag epitopes from incoming viral particles facilitates rapid recognition of infected cells by specific cd8+ t cells. J Virol. 87(5):2628-2638.

Koch M, Stronge VS, Shepherd D, Gadola SD, Mathew B, Ritter G, Fersht AR, Besra GS, Schmidt RR, Jones EY et al. 2005. The crystal structure of human cd1d with and without alpha-galactosylceramide. Nat Immunol. 6(8):819-826.

Kovacsovics-Bankowski M, Rock KL. 1995. A phagosome-to-cytosol pathway for exogenous antigens presented on mhc class i molecules. Science. 267(5195):243-246.

Kraemer T, Celik AA, Huyton T, Kunze-Schumacher H, Blasczyk R, Bade-Döding C. 2015. Hla-e: Presentation of a broader peptide repertoire impacts the cellular immune response-implications on hsct outcome. Stem Cells Int. 2015:346714.

Kraft JR, Vance RE, Pohl J, Martin AM, Raulet DH, Jensen PE. 2000. Analysis of qa-1(b) peptide binding specificity and the capacity of cd94/nkg2a to discriminate between qa-1-peptide complexes. J Exp Med. 192(5):613-624.

Kreer C, Rauen J, Zehner M, Burgdorf S. 2011. Cross-presentation: How to get there - or how to get the er. Front Immunol. 2:87.

Krieger V, Liebl D, Zhang Y, Rajashekar R, Chlanda P, Giesker K, Chikkaballi D, Hensel M. 2014. Reorganization of the endosomal system in salmonella-infected cells: The ultrastructure of salmonella-induced tubular compartments. PLoS Pathog. 10(9):e1004374.

Kropshofer H, Arndt SO, Moldenhauer G, Hämmerling GJ, Vogt AB. 1997. Hla-dm acts as a molecular chaperone and rescues empty hla-dr molecules at lysosomal ph. Immunity. 6(3):293-302.

Kropshofer H, Vogt AB, Moldenhauer G, Hammer J, Blum JS, Hämmerling GJ. 1996. Editing of the hla-dr-peptide repertoire by hla-dm. EMBO J. 15(22):6144-6154.

Lafon M, Prehaud C, Megret F, Lafage M, Mouillot G, Roa M, Moreau P, Rouas-Freiss N, Carosella ED. 2005. Modulation of hla-g expression in human neural cells after neurotropic viral infections. J Virol. 79(24):15226-15237.

Lajoie J, Hargrove J, Zijenah LS, Humphrey JH, Ward BJ, Roger M. 2006. Genetic variants in nonclassical major histocompatibility complex class i human leukocyte antigen (hla)-e and hla-g molecules are associated with susceptibility to heterosexual acquisition of hiv-1. J Infect Dis. 193(2):298-301.

Lamb CA, Yewdell JW, Bennink JR, Cresswell P. 1991. Invariant chain targets hla class ii molecules to acidic endosomes containing internalized influenza virus. Proc Natl Acad Sci U S A. 88(14):5998-6002.

Lamichhane R, Ussher JE. 2017. Expression and trafficking of mr1. Immunology. 151(3):270-279.

Lampen MH, Hassan C, Sluijter M, Geluk A, Dijkman K, Tjon JM, de Ru AH, van der Burg SH, van Veelen PA, van Hall T. 2013. Alternative peptide repertoire of hla-e reveals a binding motif that is strikingly similar to hla-a2. Mol Immunol. 53(1-2):126-131.

Le Bourhis L, Martin E, Péguillet I, Guihot A, Froux N, Coré M, Lévy E, Dusseaux M, Meyssonnier V, Premel V et al. 2010. Antimicrobial activity of mucosal-associated invariant t cells. Nat Immunol. 11(8):701-708.

Le Gall S, Erdtmann L, Benichou S, Berlioz-Torrent C, Liu L, Benarous R, Heard JM, Schwartz O. 1998. Nef interacts with the mu subunit of clathrin adaptor complexes and reveals a cryptic sorting signal in mhc i molecules. Immunity. 8(4):483-495.

Lee J, Keam B, Park HR, Park JE, Kim S, Kim M, Kim TM, Kim DW, Heo DS. 2022. Monalizumab efficacy correlates with hla-e surface expression and nk cell

activity in head and neck squamous carcinoma cell lines. J Cancer Res Clin Oncol.

Lee N, Geraghty DE. 2003. Hla-f surface expression on b cell and monocyte cell lines is partially independent from tapasin and completely independent from tap. J Immunol. 171(10):5264-5271.

Lee N, Goodlett DR, Ishitani A, Marquardt H, Geraghty DE. 1998a. Hla-e surface expression depends on binding of tap-dependent peptides derived from certain hla class i signal sequences. J Immunol. 160(10):4951-4960.

Lee N, Llano M, Carretero M, Ishitani A, Navarro F, López-Botet M, Geraghty DE. 1998b. Hla-e is a major ligand for the natural killer inhibitory receptor cd94/nkg2a. Proc Natl Acad Sci U S A. 95(9):5199-5204.

Lee SY, Kang MG, Park JS, Lee G, Ting AY, Rhee HW. 2016. Apex fingerprinting reveals the subcellular localization of proteins of interest. Cell Rep. 15(8):1837-1847.

Lehner PJ, Hewitt EW, Romisch K. 2000. Antigen presentation: Peptides and proteins scramble for the exit. Curr Biol. 10(22):R839-842.

Lehner PJ, Karttunen JT, Wilkinson GW, Cresswell P. 1997. The human cytomegalovirus us6 glycoprotein inhibits transporter associated with antigen processing-dependent peptide translocation. Proc Natl Acad Sci U S A. 94(13):6904-6909.

Lemberg MK, Bland FA, Weihofen A, Braud VM, Martoglio B. 2001. Intramembrane proteolysis of signal peptides: An essential step in the generation of hla-e epitopes. J Immunol. 167(11):6441-6446.

Lewinsohn DM, Grotzke JE, Heinzel AS, Zhu L, Ovendale PJ, Johnson M, Alderson MR. 2006. Secreted proteins from mycobacterium tuberculosis gain access to the cytosolic mhc class-i antigen-processing pathway. J Immunol. 177(1):437-442.

Li P, Wang N, Zhang Y, Wang C, Du L. 2021. Hla-g/shla-g and hla-g-bearing extracellular vesicles in cancers: Potential role as biomarkers. Front Immunol. 12:791535.

Lila N, Carpentier A, Amrein C, Khalil-Daher I, Dausset J, Carosella ED. 2000. Implication of hla-g molecule in heart-graft acceptance. Lancet. 355(9221):2138.

LILLY F, BOYSE EA, OLD LJ. 1964. Genetic basis of susceptibility to viral leukaemogenesis. Lancet. 2(7371):1207-1209.

Lima-Junior JaC, Pratt-Riccio LR. 2016. Major histocompatibility complex and malaria: Focus on plasmodium vivax infection. Front Immunol. 7:13.

Lin A, Yan WH. 2019. The emerging roles of human leukocyte antigen-f in immune modulation and viral infection. Front Immunol. 10:964.

Lion J, Debuysscher V, Wlodarczyk A, Hodroge A, Serriari NE, Choteau L, Ouled-haddou H, Plistat M, Lassoued K, Lantz O et al. 2013. Mr1b, a natural spliced isoform of the mhc-related 1 protein, is expressed as homodimers at the cell surface and activates mait cells. Eur J Immunol. 43(5):1363-1373.

Liss V, Swart AL, Kehl A, Hermanns N, Zhang Y, Chikkaballi D, Bohles N, Deiwick J, Hensel M. 2017. Salmonella enterica remodels the host cell endosomal system for efficient intravacuolar nutrition. Cell Host Microbe. 21(3):390-402.

Liu Q, Sun Z, Chen L. 2020. Memory t cells: Strategies for optimizing tumor immunotherapy. Protein Cell. 11(8):549-564.

Lizée G, Basha G, Tiong J, Julien JP, Tian M, Biron KE, Jefferies WA. 2003. Control of dendritic cell cross-presentation by the major histocompatibility complex class i cytoplasmic domain. Nat Immunol. 4(11):1065-1073.

Ljunggren HG, Kärre K. 1990. In search of the 'missing self': Mhc molecules and nk cell recognition. Immunol Today. 11(7):237-244.

Ljunggren HG, Stam NJ, Ohlén C, Neefjes JJ, Höglund P, Heemels MT, Bastin J, Schumacher TN, Townsend A, Kärre K. 1990. Empty mhc class i molecules come out in the cold. Nature. 346(6283):476-480.

Lopez JA, Susanto O, Jenkins MR, Lukoyanova N, Sutton VR, Law RH, Johnston A, Bird CH, Bird PI, Whisstock JC et al. 2013. Perforin forms transient pores on the target cell plasma membrane to facilitate rapid access of granzymes during killer cell attack. Blood. 121(14):2659-2668.

Lotteau V, Teyton L, Peleraux A, Nilsson T, Karlsson L, Schmid SL, Quaranta V, Peterson PA. 1990. Intracellular transport of class ii mhc molecules directed by invariant chain. Nature. 348(6302):600-605.

Lunemann S, Schöbel A, Kah J, Fittje P, Hölzemer A, Langeneckert AE, Hess LU, Poch T, Martrus G, Garcia-Beltran WF et al. 2018. Interactions between

kir3ds1 and hla-f activate natural killer cells to control hcv replication in cell culture. Gastroenterology. 155(5):1366-1371.e1363.

Lázaro-Sánchez AD, Salces-Ortiz P, Velásquez LI, Orozco-Beltrán D, Díaz-Fernández N, Juárez-Marroquí A. 2020. Hla-g as a new tumor biomarker: Detection of soluble isoforms of hla-g in the serum and saliva of patients with colorectal cancer. Clin Transl Oncol. 22(7):1166-1171.

Ma J, Becker C, Lowell CA, Underhill DM. 2012. Dectin-1-triggered recruitment of light chain 3 protein to phagosomes facilitates major histocompatibility complex class ii presentation of fungal-derived antigens. J Biol Chem. 287(41):34149-34156.

Ma W, Zhang Y, Vigneron N, Stroobant V, Thielemans K, van der Bruggen P, Van den Eynde BJ. 2016. Long-peptide cross-presentation by human dendritic cells occurs in vacuoles by peptide exchange on nascent mhc class i molecules. J Immunol. 196(4):1711-1720.

Machamer CE, Cresswell P. 1982. Biosynthesis and glycosylation of the invariant chain associated with hla-dr antigens. J Immunol. 129(6):2564-2569.

Mahmutefendic H, Zagorac GB, Tomas MI, Groettrup M, Momburg F, Lucin P. 2013. Endosomal trafficking of open major histocompatibility class i conformers--implications for presentation of endocytosed antigens. Mol Immunol. 55(2):149-152.

Mahmutefendić H, Blagojević G, Kucić N, Lucin P. 2007. Constitutive internalization of murine mhc class i molecules. J Cell Physiol. 210(2):445-455.

Mahmutefendić H, Blagojević G, Tomaš MI, Kučić N, Lučin P. 2011. Segregation of open major histocompatibility class i conformers at the plasma membrane and during endosomal trafficking reveals conformation-based sorting in the endosomal system. Int J Biochem Cell Biol. 43(4):504-515.

Mahmutefendić H, Blagojević Zagorac G, Grabušić K, Karleuša L, Maćešić S, Momburg F, Lučin P. 2017. Late endosomal recycling of open mhc-i conformers. J Cell Physiol. 232(4):872-887.

Mahmutefendić H, Zagorac GB, Tomaš MI, Groettrup M, Momburg F, Lučin P. 2013. Endosomal trafficking of open major histocompatibility class i conformers--implications for presentation of endocytosed antigens. Mol Immunol. 55(2):149-152.

Mahnke K, Guo M, Lee S, Sepulveda H, Swain SL, Nussenzweig M, Steinman RM. 2000. The dendritic cell receptor for endocytosis, dec-205, can recycle and enhance antigen presentation via major histocompatibility complex class ii-positive lysosomal compartments. J Cell Biol. 151(3):673-684.

Mallajosyula V, Ganjavi C, Chakraborty S, McSween AM, Pavlovitch-Bedzyk AJ, Wilhelmy J, Nau A, Manohar M, Nadeau KC, Davis MM. 2021. Cd8. Sci Immunol. 6(61).

Malouli D, Hansen SG, Hancock MH, Hughes CM, Ford JC, Gilbride RM, Ventura AB, Morrow D, Randall KT, Taher H et al. 2021. Cytomegaloviral determinants of cd8+ t cell programming and rhcmv/siv vaccine efficacy. Sci Immunol. 6(57).

Marshall JS, Warrington R, Watson W, Kim HL. 2018. An introduction to immunology and immunopathology. Allergy Asthma Clin Immunol. 14(Suppl 2):49.

Martín P, Krsnik I, Navarro B, Provencio M, García JF, Bellas C, Vilches C, Gomez-Lozano N. 2015. Hla allele e*01:01 is associated with a reduced risk of ebv-related classical hodgkin lymphoma independently of hla-a*01/*02. PLoS One. 10(8):e0135512.

Martín-Villa JM, Vaquero-Yuste C, Molina-Alejandre M, Juarez I, Suárez-Trujillo F, López-Nares A, Palacio-Gruber J, Barrera-Gutiérrez L, Fernández-Cruz E, Rodríguez-Sainz C et al. 2022. Hla-g: Too much or too little? Role in cancer and autoimmune disease. Front Immunol. 13:796054.

Marín R, Ruiz-Cabello F, Pedrinaci S, Méndez R, Jiménez P, Geraghty DE, Garrido F. 2003. Analysis of hla-e expression in human tumors. Immunogenetics. 54(11):767-775.

Mazzarino P, Pietra G, Vacca P, Falco M, Colau D, Coulie P, Moretta L, Mingari MC. 2005. Identification of effector-memory cmv-specific t lymphocytes that kill cmv-infected target cells in an hla-e-restricted fashion. Eur J Immunol. 35(11):3240-3247.

Maître B, Angénieux C, Salamero J, Hanau D, Fricker D, Signorino F, Proamer F, Cazenave JP, Goud B, Tourne S et al. 2008. Control of the intracellular pathway of cd1e. Traffic. 9(4):431-445.

McDevitt HO, Sela M. 1967. Genetic control of the antibody response. Ii. Further analysis of the specificity of determinant-specific control, and genetic analysis of the response to (h,g)-a--l in cba and c57 mice. J Exp Med. 126(5):969-978.

McMichael AJ, Picker LJ. 2017. Unusual antigen presentation offers new insight into hiv vaccine design. Curr Opin Immunol. 46:75-81.

McMurtrey C, Harriff MJ, Swarbrick GM, Duncan A, Cansler M, Null M, Bardet W, Jackson KW, Lewinsohn DA, Hildebrand W et al. 2017. T cell recognition of mycobacterium tuberculosis peptides presented by hla-e derived from infected human cells. PLoS One. 12(11):e0188288.

McShan AC, Natarajan K, Kumirov VK, Flores-Solis D, Jiang J, Badstubner M, Toor JS, Bagshaw CR, Kovrigin EL, Margulies DH et al. 2018. Peptide exchange on mhc-i by tapbpr is driven by a negative allostery release cycle. Nat Chem Biol. 14(8):811-820.

McWilliam HE, Birkinshaw RW, Villadangos JA, McCluskey J, Rossjohn J. 2015. Mr1 presentation of vitamin b-based metabolite ligands. Curr Opin Immunol. 34:28-34.

McWilliam HE, Eckle SB, Theodossis A, Liu L, Chen Z, Wubben JM, Fairlie DP, Strugnell RA, Mintern JD, McCluskey J et al. 2016. The intracellular pathway for the presentation of vitamin b-related antigens by the antigen-presenting molecule mr1. Nat Immunol. 17(5):531-537.

McWilliam HE, Villadangos JA. 2018. Mr1 antigen presentation to mait cells: New ligands, diverse pathways? Curr Opin Immunol. 52:108-113.

McWilliam HEG, Villadangos JA. 2017. How mr1 presents a pathogen metabolic signature to mucosal-associated invariant t (mait) cells. Trends Immunol. 38(9):679-689.

Medhasi S, Chantratita N. 2022. Human leukocyte antigen (hla) system: Genetics and association with bacterial and viral infections. J Immunol Res. 2022:9710376.

Medina F, Ramos M, Iborra S, de León P, Rodríguez-Castro M, Del Val M. 2009. Furin-processed antigens targeted to the secretory route elicit functional tap1-/-cd8+ t lymphocytes in vivo. J Immunol. 183(7):4639-4647.

Mellins ED, Stern LJ. 2014. Hla-dm and hla-do, key regulators of mhc-ii processing and presentation. Curr Opin Immunol. 26:115-122.

Miley MJ, Truscott SM, Yu YY, Gilfillan S, Fremont DH, Hansen TH, Lybarger L. 2003. Biochemical features of the mhc-related protein 1 consistent with an immunological function. J Immunol. 170(12):6090-6098.

Milner CM, Campbell RD. 2001. Genetic organization of the human mhc class iii region. Front Biosci. 6:D914-926.

Momburg F, Roelse J, Howard JC, Butcher GW, Hammerling GJ, Neefjes JJ. 1994. Selectivity of mhc-encoded peptide transporters from human, mouse and rat. Nature. 367(6464):648-651.

Montealegre S, van Endert PM. 2018. Endocytic recycling of mhc class i molecules in non-professional antigen presenting and dendritic cells. Front Immunol. 9:3098.

Moody DB, Cotton RN. 2017. Four pathways of cd1 antigen presentation to t cells. Curr Opin Immunol. 46:127-133.

Morales PJ, Pace JL, Platt JS, Phillips TA, Morgan K, Fazleabas AT, Hunt JS. 2003. Placental cell expression of hla-g2 isoforms is limited to the invasive trophoblast phenotype. J Immunol. 171(11):6215-6224.

Morandi F, Cangemi G, Barco S, Amoroso L, Giuliano M, Gigliotti AR, Pistoia V, Corrias MV. 2013. Plasma levels of soluble hla-e and hla-f at diagnosis may predict overall survival of neuroblastoma patients. Biomed Res Int. 2013:956878.

Moreau P, Rousseau P, Rouas-Freiss N, Le Discorde M, Dausset J, Carosella ED. 2002. Hla-g protein processing and transport to the cell surface. Cell Mol Life Sci. 59(9):1460-1466.

Morgan CS, Holton JM, Olafson BD, Bjorkman PJ, Mayo SL. 1997. Circular dichroism determination of class i mhc-peptide equilibrium dissociation constants. Protein Sci. 6(8):1771-1773.

Moris A, Nobile C, Buseyne F, Porrot F, Abastado JP, Schwartz O. 2004. Dc-sign promotes exogenous mhc-i-restricted hiv-1 antigen presentation. Blood. 103(7):2648-2654.

Morrice NA, Powis SJ. 1998. A role for the thiol-dependent reductase erp57 in the assembly of mhc class i molecules. Curr Biol. 8(12):713-716.

Murphy K, Weaver C, Janeway C. 2016. Janeway's immunobiology.

Murray SE, Nesterenko PA, Vanarsdall AL, Munks MW, Smart SM, Veziroglu EM, Sagario LC, Lee R, Claas FHJ, Doxiadis IIN et al. 2017. Fibroblast-adapted human cmv vaccines elicit predominantly conventional cd8 t cell responses in humans. J Exp Med. 214(7):1889-1899.

Myers NB, Wormstall E, Hansen TH. 1996. Differences among various class i molecules in competition for beta2m in vivo. Immunogenetics. 43(6):384-387.

Napier RJ, Adams EJ, Gold MC, Lewinsohn DM. 2015. The role of mucosal associated invariant t cells in antimicrobial immunity. Front Immunol. 6:344.

Naslavsky N, Weigert R, Donaldson JG. 2004. Characterization of a nonclathrin endocytic pathway: Membrane cargo and lipid requirements. Mol Biol Cell. 15(8):3542-3552.

Nattermann J, Nischalke HD, Hofmeister V, Kupfer B, Ahlenstiel G, Feldmann G, Rockstroh J, Weiss EH, Sauerbruch T, Spengler U. 2005. Hiv-1 infection leads to increased hla-e expression resulting in impaired function of natural killer cells. Antivir Ther. 10(1):95-107.

Neefjes JJ, Momburg F, Hämmerling GJ. 1993. Selective and atp-dependent translocation of peptides by the mhc-encoded transporter. Science. 261(5122):769-771.

Neerincx A, Hermann C, Antrobus R, van Hateren A, Cao H, Trautwein N, Stevanović S, Elliott T, Deane JE, Boyle LH. 2017. Tapbpr bridges udp-glucose:Glycoprotein glucosyltransferase 1 onto mhc class i to provide quality control in the antigen presentation pathway. Elife. 6.

Nufer O, Guldbrandsen S, Degen M, Kappeler F, Paccaud JP, Tani K, Hauri HP. 2002. Role of cytoplasmic c-terminal amino acids of membrane proteins in er export. J Cell Sci. 115(Pt 3):619-628.

O'Callaghan CA, Tormo J, Willcox BE, Braud VM, Jakobsen BK, Stuart DI, McMichael AJ, Bell JI, Jones EY. 1998. Structural features impose tight peptide binding specificity in the nonclassical mhc molecule hla-e. Mol Cell. 1(4):531-541.

Ohashi PS, Mak TW, Van den Elsen P, Yanagi Y, Yoshikai Y, Calman AF, Terhorst C, Stobo JD, Weiss A. 1985. Reconstitution of an active surface t3/t-cell antigen receptor by dna transfer. Nature. 316(6029):606-609.

Oliveira CC, van Hall T. 2015. Alternative antigen processing for mhc class i: Multiple roads lead to rome. Front Immunol. 6:298.

Oliveira CC, van Veelen PA, Querido B, de Ru A, Sluijter M, Laban S, Drijfhout JW, van der Burg SH, Offringa R, van Hall T. 2010. The nonpolymorphic mhc qa-1b mediates cd8+ t cell surveillance of antigen-processing defects. J Exp Med. 207(1):207-221.

Orlova OV, Glazkova DV, Bogoslovskaya EV, Shipulin GA, Yudin SM. 2022. Development of modified vaccinia virus ankara-based vaccines: Advantages and applications. Vaccines (Basel). 10(9).

Ortmann B, Copeman J, Lehner PJ, Sadasivan B, Herberg JA, Grandea AG, Riddell SR, Tampe R, Spies T, Trowsdale J et al. 1997. A critical role for tapasin in the assembly and function of multimeric mhc class i-tap complexes. Science. 277(5330):1306-1309.

Osterloh A. 2022. Vaccination against bacterial infections: Challenges, progress, and new approaches with a focus on intracellular bacteria. Vaccines (Basel). 10(5).

Pace MJ, Graf EH, Agosto LM, Mexas AM, Male F, Brady T, Bushman FD, O'Doherty U. 2012. Directly infected resting cd4+t cells can produce hiv gag without spreading infection in a model of hiv latency. PLoS Pathog. 8(7):e1002818.

Pande NT, Powers C, Ahn K, Früh K. 2005. Rhesus cytomegalovirus contains functional homologues of us2, us3, us6, and us11. J Virol. 79(9):5786-5798.

Parham P. 1988. Function and polymorphism of human leukocyte antigen-a,b,c molecules. Am J Med. 85(6A):2-5.

Park B, Kim Y, Shin J, Lee S, Cho K, Fruh K, Lee S, Ahn K. 2004a. Human cytomegalovirus inhibits tapasin-dependent peptide loading and optimization of the mhc class i peptide cargo for immune evasion. Immunity. 20(1):71-85.

Park B, Lee S, Kim E, Chang S, Jin M, Ahn K. 2001. The truncated cytoplasmic tail of hla-g serves a quality-control function in post-er compartments. Immunity. 15(2):213-224.

Park GM, Lee S, Park B, Kim E, Shin J, Cho K, Ahn K. 2004b. Soluble hla-g generated by proteolytic shedding inhibits nk-mediated cell lysis. Biochem Biophys Res Commun. 313(3):606-611.

Perrin-Cocon LA, Villiers CL, Salamero J, Gabert F, Marche PN. 2004. B cell receptors and complement receptors target the antigen to distinct intracellular compartments. J Immunol. 172(6):3564-3572.

Pierre P, Turley SJ, Gatti E, Hull M, Meltzer J, Mirza A, Inaba K, Steinman RM, Mellman I. 1997. Developmental regulation of mhc class ii transport in mouse dendritic cells. Nature. 388(6644):787-792.

Pietra G, Romagnani C, Mazzarino P, Falco M, Millo E, Moretta A, Moretta L, Mingari MC. 2003. Hla-e-restricted recognition of cytomegalovirus-derived peptides by human cd8+ cytolytic t lymphocytes. Proc Natl Acad Sci U S A. 100(19):10896-10901.

Pober JS, Guild BC, Strominger JL. 1978. Phosphorylation in vivo and in vitro of human histocompatibility antigens (hla-a and hla-b) in the carboxy-terminal intracellular domain. Proc Natl Acad Sci U S A. 75(12):6002-6006.

Poluektov YO, Kim A, Hartman IZ, Sadegh-Nasseri S. 2013. Hla-do as the optimizer of epitope selection for mhc class ii antigen presentation. PLoS One. 8(8):e71228.

Pos W, Sethi DK, Call MJ, Schulze MS, Anders AK, Pyrdol J, Wucherpfennig KW. 2012. Crystal structure of the hla-dm-hla-dr1 complex defines mechanisms for rapid peptide selection. Cell. 151(7):1557-1568.

Powers C, DeFilippis V, Malouli D, Fruh K. 2008. Cytomegalovirus immune evasion. Curr Top Microbiol Immunol. 325:333-359.

Powis SJ. 2006. Clip-region mediated interaction of invariant chain with mhc class i molecules. FEBS Lett. 580(13):3112-3116.

Prezzemolo T, van Meijgaarden KE, Franken KLMC, Caccamo N, Dieli F, Ottenhoff THM, Joosten SA. 2018. Detailed characterization of human mycobacterium tuberculosis specific hla-e restricted cd8 + t cells. Eur J Immunol. 48(2):293-305.

Rajagopalan S, Bryceson YT, Kuppusamy SP, Geraghty DE, van der Meer A, Joosten I, Long EO. 2006. Activation of nk cells by an endocytosed receptor for soluble hla-g. PLoS Biol. 4(1):e9.

Ramanan P, Razonable RR. 2013. Cytomegalovirus infections in solid organ transplantation: A review. Infect Chemother. 45(3):260-271.

Rashidi S, Vieira C, Tuteja R, Mansouri R, Ali-Hassanzadeh M, Muro A, Nguewa P, Manzano-Román R. 2022. Immunomodulatory potential of non-classical hla-g in infections including covid-19 and parasitic diseases. Biomolecules. 12(2).

Raskov H, Orhan A, Christensen JP, Gögenur I. 2021. Cytotoxic cd8 + t cells in cancer and cancer immunotherapy. Br J Cancer. 124(2):359-367.

Reber AJ, Turnquist HR, Thomas HJ, Lutz CT, Solheim JC. 2002. Expression of invariant chain can cause an allele-dependent increase in the surface expression of mhc class i molecules. Immunogenetics. 54(2):74-81.

Reche PA, Reinherz EL. 2003. Sequence variability analysis of human class i and class ii mhc molecules: Functional and structural correlates of amino acid polymorphisms. J Mol Biol. 331(3):623-641.

Reina-Campos M, Scharping NE, Goldrath AW. 2021. Cd8 + t cell metabolism in infection and cancer. Nat Rev Immunol. 21(11):718-738.

Relloso M, Cheng TY, Im JS, Parisini E, Roura-Mir C, DeBono C, Zajonc DM, Murga LF, Ondrechen MJ, Wilson IA et al. 2008. Ph-dependent interdomain tethers of cd1b regulate its antigen capture. Immunity. 28(6):774-786.

Riera Romo M, Pérez-Martínez D, Castillo Ferrer C. 2016. Innate immunity in vertebrates: An overview. Immunology. 148(2):125-139.

Riteau B, Rouas-Freiss N, Menier C, Paul P, Dausset J, Carosella ED. 2001. Hla-g2, -g3, and -g4 isoforms expressed as nonmature cell surface glycoproteins inhibit nk and antigen-specific ctl cytolysis. J Immunol. 166(8):5018-5026.

Ritter B, Philie J, Girard M, Tung EC, Blondeau F, McPherson PS. 2003. Identification of a family of endocytic proteins that define a new alpha-adaptin ear-binding motif. EMBO Rep. 4(11):1089-1095.

Roche PA, Cresswell P. 1990. Invariant chain association with hla-dr molecules inhibits immunogenic peptide binding. Nature. 345(6276):615-618.

Roche PA, Furuta K. 2015. The ins and outs of mhc class ii-mediated antigen processing and presentation. Nat Rev Immunol. 15(4):203-216.

Rock KL, Reits E, Neefjes J. 2016. Present yourself! By mhc class i and mhc class ii molecules. Trends Immunol. 37(11):724-737.

Rodríguez-Cruz TG, Liu S, Khalili JS, Whittington M, Zhang M, Overwijk W, Lizée G. 2011. Natural splice variant of mhc class i cytoplasmic tail enhances dendritic cell-induced cd8+ t-cell responses and boosts anti-tumor immunity. PLoS One. 6(8):e22939.

Roeth JF, Williams M, Kasper MR, Filzen TM, Collins KL. 2004. Hiv-1 nef disrupts mhc-i trafficking by recruiting ap-1 to the mhc-i cytoplasmic tail. J Cell Biol. 167(5):903-913.

Rohn H, Michita RT, Schramm S, Dolff S, Gäckler A, Korth J, Heinemann FM, Wilde B, Trilling M, Horn PA et al. 2019. Hla-e polymorphism determines susceptibility to bk virus nephropathy after living-donor kidney transplant. Cells. 8(8).

Romagnani S. 1995. Biology of human th1 and th2 cells. J Clin Immunol. 15(3):121-129.

Rouas-Freiss N, Gonçalves RM, Menier C, Dausset J, Carosella ED. 1997. Direct evidence to support the role of hla-g in protecting the fetus from maternal uterine natural killer cytolysis. Proc Natl Acad Sci U S A. 94(21):11520-11525.

Sadasivan B, Lehner PJ, Ortmann B, Spies T, Cresswell P. 1996. Roles for calreticulin and a novel glycoprotein, tapasin, in the interaction of mhc class i molecules with tap. Immunity. 5(2):103-114.

Sagert L, Hennig F, Thomas C, Tampé R. 2020. A loop structure allows tapbpr to exert its dual function as mhc i chaperone and peptide editor. Elife. 9.

Saikia A, Hadeler A, Prasad P, Zacharias M, Springer S. 2022. Fast peptide exchange on major histocompatibility complex class i molecules by acidic stabilization of a peptide-empty intermediate. Protein Sci. 31(12):e4478.

Sakaguchi S, Fukuma K, Kuribayashi K, Masuda T. 1985. Organ-specific autoimmune diseases induced in mice by elimination of t cell subset. I. Evidence for the active participation of t cells in natural self-tolerance; deficit of a t cell subset as a possible cause of autoimmune disease. J Exp Med. 161(1):72-87.

Sakai K, Dimas J, Lenardo MJ. 2006. The vif and vpr accessory proteins independently cause hiv-1-induced t cell cytopathicity and cell cycle arrest. Proc Natl Acad Sci U S A. 103(9):3369-3374.

Salcedo M, Bousso P, Ljunggren HG, Kourilsky P, Abastado JP. 1998. The qa-1b molecule binds to a large subpopulation of murine nk cells. Eur J Immunol. 28(12):4356-4361.

Salerno-Goncalves R, Fernandez-Vina M, Lewinsohn DM, Sztein MB. 2004. Identification of a human hla-e-restricted cd8+ t cell subset in volunteers immunized with salmonella enterica serovar typhi strain ty21a typhoid vaccine. J Immunol. 173(9):5852-5862.

Salerno-Goncalves R, Wahid R, Sztein MB. 2010. Ex vivo kinetics of early and long-term multifunctional human leukocyte antigen e-specific cd8+ cells in volunteers immunized with the ty21a typhoid vaccine. Clin Vaccine Immunol. 17(9):1305-1314.

Salerno-Gonçalves R, Fernandez-Viña M, Lewinsohn DM, Sztein MB. 2004. Identification of a human hla-e-restricted cd8+ t cell subset in volunteers immunized with salmonella enterica serovar typhi strain ty21a typhoid vaccine. J Immunol. 173(9):5852-5862.

Salio M, Awad W, Veerapen N, Gonzalez-Lopez C, Kulicke C, Waithe D, Martens AWJ, Lewinsohn DM, Hobrath JV, Cox LR et al. 2020. Ligand-dependent downregulation of mr1 cell surface expression. Proc Natl Acad Sci U S A. 117(19):10465-10475.

Sallusto F, Cella M, Danieli C, Lanzavecchia A. 1995. Dendritic cells use macropinocytosis and the mannose receptor to concentrate macromolecules in the major histocompatibility complex class ii compartment: Downregulation by cytokines and bacterial products. J Exp Med. 182(2):389-400.

Sambi M, Bagheri L, Szewczuk MR. 2019. Current challenges in cancer immunotherapy: Multimodal approaches to improve efficacy and patient response rates. J Oncol. 2019:4508794.

Santos SG, Antoniou AN, Sampaio P, Powis SJ, Arosa FA. 2006. Lack of tyrosine 320 impairs spontaneous endocytosis and enhances release of hla-b27 molecules. J Immunol. 176(5):2942-2949.

Saric T, Chang SC, Hattori A, York IA, Markant S, Rock KL, Tsujimoto M, Goldberg AL. 2002. An ifn-gamma-induced aminopeptidase in the er, erap1, trims precursors to mhc class i-presented peptides. Nat Immunol. 3(12):1169-1176.

Satta A, Grazia G, Caroli F, Frigerio B, Di Nicola M, Raspagliesi F, Mezzanzanica D, Zaffaroni N, Gianni AM, Anichini A et al. 2019. A bispecific antibody to link a trail-based antitumor approach to immunotherapy. Front Immunol. 10:2514.

Saveanu L, Carroll O, Weimershaus M, Guermonprez P, Firat E, Lindo V, Greer F, Davoust J, Kratzer R, Keller SR et al. 2009. Irap identifies an endosomal compartment required for mhc class i cross-presentation. Science. 325(5937):213-217.

Schaefer MR, Williams M, Kulpa DA, Blakely PK, Yaffee AQ, Collins KL. 2008. A novel trafficking signal within the hla-c cytoplasmic tail allows regulated expression upon differentiation of macrophages. J Immunol. 180(12):7804-7817.

Schaerli P, Willimann K, Lang AB, Lipp M, Loetscher P, Moser B. 2000. Cxc chemokine receptor 5 expression defines follicular homing t cells with b cell helper function. J Exp Med. 192(11):1553-1562.

Scharf L, Li NS, Hawk AJ, Garzón D, Zhang T, Fox LM, Kazen AR, Shah S, Haddadian EJ, Gumperz JE et al. 2010. The 2.5 å structure of cd1c in complex with a mycobacterial lipid reveals an open groove ideally suited for diverse antigen presentation. Immunity. 33(6):853-862.

Schmid D, Pypaert M, Münz C. 2007. Antigen-loading compartments for major histocompatibility complex class ii molecules continuously receive input from autophagosomes. Immunity. 26(1):79-92.

Schreibelt G, Klinkenberg LJ, Cruz LJ, Tacken PJ, Tel J, Kreutz M, Adema GJ, Brown GD, Figdor CG, de Vries IJ. 2012. The c-type lectin receptor clec9a mediates antigen uptake and (cross-)presentation by human blood bdca3+ myeloid dendritic cells. Blood. 119(10):2284-2292.

Schröder B. 2016. The multifaceted roles of the invariant chain cd74--more than just a chaperone. Biochim Biophys Acta. 1863(6 Pt A):1269-1281.

Schulte D, Vogel M, Langhans B, Krämer B, Körner C, Nischalke HD, Steinberg V, Michalk M, Berg T, Rockstroh JK et al. 2009. The hla-e(r)/hla-e(r) genotype affects the natural course of hepatitis c virus (hcv) infection and is associated with hla-e-restricted recognition of an hcv-derived peptide by interferon-gamma-secreting human cd8(+) t cells. J Infect Dis. 200(9):1397-1401.

Schuurhuis DH, Ioan-Facsinay A, Nagelkerken B, van Schip JJ, Sedlik C, Melief CJ, Verbeek JS, Ossendorp F. 2002. Antigen-antibody immune complexes empower dendritic cells to efficiently prime specific cd8+ ctl responses in vivo. J Immunol. 168(5):2240-2246.

Schwartz O, Marechal V, Le Gall S, Lemonnier F, Heard JM. 1996. Endocytosis of major histocompatibility complex class i molecules is induced by the hiv-1 nef protein. Nat Med. 2(3):338-342.

Schwich E, Hò GT, LeMaoult J, Bade-Döding C, Carosella ED, Horn PA, Rebmann V. 2020. Soluble hla-g and hla-g bearing extracellular vesicles affect ilt-2 positive and ilt-2 negative cd8 t cells complementary. Front Immunol. 11:2046.

Seifert U, Marañón C, Shmueli A, Desoutter JF, Wesoloski L, Janek K, Henklein P, Diescher S, Andrieu M, de la Salle H et al. 2003. An essential role for tripeptidyl peptidase in the generation of an mhc class i epitope. Nat Immunol. 4(4):375-379.

Seliger B, Jasinski-Bergner S, Quandt D, Stoehr C, Bukur J, Wach S, Legal W, Taubert H, Wullich B, Hartmann A. 2016. Hla-e expression and its clinical relevance in human renal cell carcinoma. Oncotarget. 7(41):67360-67372.

Sengupta D, Graham M, Liu X, Cresswell P. 2019. Proteasomal degradation within endocytic organelles mediates antigen cross-presentation. EMBO J. 38(16):e99266.

Serwold T, Gonzalez F, Kim J, Jacob R, Shastri N. 2002. Eraap customizes peptides for mhc class i molecules in the endoplasmic reticulum. Nature. 419(6906):480-483.

Shakushiro K, Yamasaki Y, Nishikawa M, Takakura Y. 2004. Efficient scavenger receptor-mediated uptake and cross-presentation of negatively charged soluble antigens by dendritic cells. Immunology. 112(2):211-218.

Shankaran V, Ikeda H, Bruce AT, White JM, Swanson PE, Old LJ, Schreiber RD. 2001. Ifngamma and lymphocytes prevent primary tumour development and shape tumour immunogenicity. Nature. 410(6832):1107-1111.

Shankarkumar U. 2010. Complexities and similarities of hla antigen distribution in asian subcontinent. Indian J Hum Genet. 16(3):108-110.

Sharpe HR, Bowyer G, Brackenridge S, Lambe T. 2019. Hla-e: Exploiting pathogen-host interactions for vaccine development. Clin Exp Immunol. 196(2):167-177.

Shen L, Sigal LJ, Boes M, Rock KL. 2004. Important role of cathepsin s in generating peptides for tap-independent mhc class i crosspresentation in vivo. Immunity. 21(2):155-165.

Sherman MA, Weber DA, Jensen PE. 1995. Dm enhances peptide binding to class ii mhc by release of invariant chain-derived peptide. Immunity. 3(2):197-205.

Shields MJ, Hodgson W, Ribaudo RK. 1999. Differential association of beta2-microglobulin mutants with mhc class i heavy chains and structural analysis demonstrate allele-specific interactions. Mol Immunol. 36(9):561-573.

Shiina T, Ando A, Suto Y, Kasai F, Shigenari A, Takishima N, Kikkawa E, Iwata K, Kuwano Y, Kitamura Y et al. 2001. Genomic anatomy of a premier major histocompatibility complex paralogous region on chromosome 1q21-q22. Genome Res. 11(5):789-802.

Shiina T, Hosomichi K, Inoko H, Kulski JK. 2009. The hla genomic loci map: Expression, interaction, diversity and disease. J Hum Genet. 54(1):15-39.

Shin JS, Ebersold M, Pypaert M, Delamarre L, Hartley A, Mellman I. 2006. Surface expression of mhc class ii in dendritic cells is controlled by regulated ubiquitination. Nature. 444(7115):115-118.

Shiroishi M, Tsumoto K, Amano K, Shirakihara Y, Colonna M, Braud VM, Allan DS, Makadzange A, Rowland-Jones S, Willcox B et al. 2003. Human inhibitory receptors ig-like transcript 2 (ilt2) and ilt4 compete with cd8 for mhc class i binding and bind preferentially to hla-g. Proc Natl Acad Sci U S A. 100(15):8856-8861.

Singh B, Schwartz JA, Sandrock C, Bellemore SM, Nikoopour E. 2013. Modulation of autoimmune diseases by interleukin (il)-17 producing regulatory t helper (th17) cells. Indian J Med Res. 138(5):591-594.

Sloan VS, Cameron P, Porter G, Gammon M, Amaya M, Mellins E, Zaller DM. 1995. Mediation by hla-dm of dissociation of peptides from hla-dr. Nature. 375(6534):802-806.

Song R, Harding CV. 1996. Roles of proteasomes, transporter for antigen presentation (tap), and beta 2-microglobulin in the processing of bacterial or particulate antigens via an alternate class i mhc processing pathway. J Immunol. 156(11):4182-4190.

Song S, Miranda CJ, Braun L, Meyer K, Frakes AE, Ferraiuolo L, Likhite S, Bevan AK, Foust KD, McConnell MJ et al. 2016. Major histocompatibility complex class i molecules protect motor neurons from astrocyte-induced toxicity in amyotrophic lateral sclerosis. Nat Med. 22(4):397-403.

Stagg HR, Thomas M, van den Boomen D, Wiertz EJ, Drabkin HA, Gemmill RM, Lehner PJ. 2009. The trc8 e3 ligase ubiquitinates mhc class i molecules before dislocation from the er. J Cell Biol. 186(5):685-692.

Steele-Mortimer O. 2008. The salmonella-containing vacuole: Moving with the times. Curr Opin Microbiol. 11(1):38-45.

Story CM, Furman MH, Ploegh HL. 1999. The cytosolic tail of class i mhc heavy chain is required for its dislocation by the human cytomegalovirus us2 and us11 gene products. Proc Natl Acad Sci U S A. 96(15):8516-8521.

Strasser A, Jost PJ, Nagata S. 2009. The many roles of fas receptor signaling in the immune system. Immunity. 30(2):180-192.

Strong RK, Holmes MA, Li P, Braun L, Lee N, Geraghty DE. 2003. Hla-e allelic variants. Correlating differential expression, peptide affinities, crystal structures, and thermal stabilities. J Biol Chem. 278(7):5082-5090.

Sugita M, Brenner MB. 1995. Association of the invariant chain with major histocompatibility complex class i molecules directs trafficking to endocytic compartments. J Biol Chem. 270(3):1443-1448.

Sugita M, Cao X, Watts GF, Rogers RA, Bonifacino JS, Brenner MB. 2002. Failure of trafficking and antigen presentation by cd1 in ap-3-deficient cells. Immunity. 16(5):697-706.

Sugita M, Cernadas M, Brenner MB. 2004. New insights into pathways for cd1-mediated antigen presentation. Curr Opin Immunol. 16(1):90-95.

Sugita M, Grant EP, van Donselaar E, Hsu VW, Rogers RA, Peters PJ, Brenner MB. 1999. Separate pathways for antigen presentation by cd1 molecules. Immunity. 11(6):743-752.

Takahama Y, Nakauchi H. 1996. Phorbol ester and calcium ionophore can replace tcr signals that induce positive selection of cd4 t cells. J Immunol. 157(4):1508-1513.

Tamouza R, Busson M, Fortier C, Diagne I, Diallo D, Sloma I, Contouris H, Krishnamoorthy R, Labie D, Girot R et al. 2007. Hla-e*0101 allele in homozygous state favors severe bacterial infections in sickle cell anemia. Hum Immunol. 68(10):849-853.

Tamouza R, Busson M, Rocha V, Fortier C, Haddad Y, Brun M, Boukouaci W, Bleux H, Socié G, Krishnamoorthy R et al. 2006. Homozygous status for hla-e*0103 confers protection from acute graft-versus-host disease and transplant-related mortality in hla-matched sibling hematopoietic stem cell transplantation. Transplantation. 82(11):1436-1440.

Tamouza R, Rocha V, Busson M, Fortier C, El Sherbini SM, Esperou H, Filion A, Socié G, Dulphy N, Krishnamoorthy R et al. 2005. Association of hla-e polymorphism with severe bacterial infection and early transplant-related mortality in matched unrelated bone marrow transplantation. Transplantation. 80(1):140-144.

Tang D, Kang R, Coyne CB, Zeh HJ, Lotze MT. 2012. Pamps and damps: Signal 0s that spur autophagy and immunity. Immunol Rev. 249(1):158-175.

ten Broeke T, Wubbolts R, Stoorvogel W. 2013. Mhc class ii antigen presentation by dendritic cells regulated through endosomal sorting. Cold Spring Harb Perspect Biol. 5(12):a016873.

Teyton L. 2018. Role of lipid transfer proteins in loading cd1 antigen-presenting molecules. J Lipid Res. 59(8):1367-1373.

Thomas C, Tampe R. 2017. Structure of the tapbpr-mhc i complex defines the mechanism of peptide loading and editing. Science. 358(6366):1060-1064.

Thomas C, Tampé R. 2019. Mhc i chaperone complexes shaping immunity. Curr Opin Immunol. 58:9-15.

Tomasec P, Braud VM, Rickards C, Powell MB, McSharry BP, Gadola S, Cerundolo V, Borysiewicz LK, McMichael AJ, Wilkinson GW. 2000. Surface expression of hla-e, an inhibitor of natural killer cells, enhanced by human cytomegalovirus gpul40. Science. 287(5455):1031.

Townsend A, Elliott T, Cerundolo V, Foster L, Barber B, Tse A. 1990. Assembly of mhc class i molecules analyzed in vitro. Cell. 62(2):285-295.

Townsend AR, Rothbard J, Gotch FM, Bahadur G, Wraith D, McMichael AJ. 1986. The epitopes of influenza nucleoprotein recognized by cytotoxic t lymphocytes can be defined with short synthetic peptides. Cell. 44(6):959-968.

Trowsdale J. 2001. Genetic and functional relationships between mhc and nk receptor genes. Immunity. 15(3):363-374.

Turvy DN, Blum JS. 2001. Biotin labeling and quantitation of cell-surface proteins. Curr Protoc Immunol. Chapter 18:Unit 18.17.

Ulbrecht M, Couturier A, Martinozzi S, Pla M, Srivastava R, Peterson PA, Weiss EH. 1999. Cell surface expression of hla-e: Interaction with human beta2-microglobulin and allelic differences. Eur J Immunol. 29(2):537-547.

Ulbrecht M, Kellermann J, Johnson JP, Weiss EH. 1992. Impaired intracellular transport and cell surface expression of nonpolymorphic hla-e: Evidence for inefficient peptide binding. J Exp Med. 176(4):1083-1090.

Ulbrecht M, Martinozzi S, Grzeschik M, Hengel H, Ellwart JW, Pla M, Weiss EH. 2000. Cutting edge: The human cytomegalovirus ul40 gene product contains a ligand for hla-e and prevents nk cell-mediated lysis. J Immunol. 164(10):5019-5022.

Ureña JM, Merlos-Suárez A, Baselga J, Arribas J. 1999. The cytoplasmic carboxy-terminal amino acid determines the subcellular localization of protgf-(alpha) and membrane type matrix metalloprotease (mt1-mmp). J Cell Sci. 112 (Pt 6):773-784.

van de Weijer ML, Luteijn RD, Wiertz EJ. 2015. Viral immune evasion: Lessons in mhc class i antigen presentation. Semin Immunol. 27(2):125-137.

van den Boomen DJ, Timms RT, Grice GL, Stagg HR, Skødt K, Dougan G, Nathan JA, Lehner PJ. 2014. Tmem129 is a derlin-1 associated erad e3 ligase essential for virus-induced degradation of mhc-i. Proc Natl Acad Sci U S A. 111(31):11425-11430.

van Dongen JJ, Quertermous T, Bartram CR, Gold DP, Wolvers-Tettero IL, Comans-Bitter WM, Hooijkaas H, Adriaansen HJ, de Klein A, Raghavachar A. 1987. T cell receptor-cd3 complex during early t cell differentiation. Analysis

of immature t cell acute lymphoblastic leukemias (t-all) at dna, rna, and cell membrane level. J Immunol. 138(4):1260-1269.

van Endert P. 2016. Intracellular recycling and cross-presentation by mhc class i molecules. Immunol Rev. 272(1):80-96.

van Hall T, Laban S, Koppers-Lalic D, Koch J, Precup C, Asmawidjaja P, Offringa R, Wiertz EJ. 2007. The varicellovirus-encoded tap inhibitor ul49.5 regulates the presentation of ctl epitopes by qa-1b1. J Immunol. 178(2):657-662.

van Hall T, Oliveira CC, Joosten SA, Ottenhoff TH. 2010. The other janus face of qa-1 and hla-e: Diverse peptide repertoires in times of stress. Microbes Infect. 12(12-13):910-918.

van Hall T, Wolpert EZ, van Veelen P, Laban S, van der Veer M, Roseboom M, Bres S, Grufman P, de Ru A, Meiring H et al. 2006. Selective cytotoxic t-lymphocyte targeting of tumor immune escape variants. Nat Med. 12(4):417-424.

Van Kaer L, Wu L, Joyce S. 2016. Mechanisms and consequences of antigen presentation by cd1. Trends Immunol. 37(11):738-754.

van Luijn MM, van de Loosdrecht AA, Lampen MH, van Veelen PA, Zevenbergen A, Kester MG, de Ru AH, Ossenkoppele GJ, van Hall T, van Ham SM. 2012. Promiscuous binding of invariant chain-derived clip peptide to distinct hla-i molecules revealed in leukemic cells. PLoS One. 7(4):e34649.

van Meijgaarden KE, Haks MC, Caccamo N, Dieli F, Ottenhoff TH, Joosten SA. 2015. Human cd8+ t-cells recognizing peptides from mycobacterium tuberculosis (mtb) presented by hla-e have an unorthodox th2-like, multifunctional, mtb inhibitory phenotype and represent a novel human t-cell subset. PLoS Pathog. 11(3):e1004671.

van Niel G, Wubbolts R, Ten Broeke T, Buschow SI, Ossendorp FA, Melief CJ, Raposo G, van Balkom BW, Stoorvogel W. 2006. Dendritic cells regulate exposure of mhc class ii at their plasma membrane by oligoubiquitination. Immunity. 25(6):885-894.

van Stigt Thans T, Akko JI, Niehrs A, Garcia-Beltran WF, Richert L, Sturzel CM, Ford CT, Li H, Ochsenbauer C, Kappes JC et al. 2019. Primary hiv-1 strains use nef to downmodulate hla-e surface expression. J Virol. 93(20).

van Vliet SJ, Aarnoudse CA, Broks-van den Berg VC, Boks M, Geijtenbeek TB, van Kooyk Y. 2007. Mgl-mediated internalization and antigen presentation by dendritic cells: A role for tyrosine-5. Eur J Immunol. 37(8):2075-2081.

Vance RE, Kraft JR, Altman JD, Jensen PE, Raulet DH. 1998. Mouse cd94/nkg2a is a natural killer cell receptor for the nonclassical major histocompatibility complex (mhc) class i molecule qa-1(b). J Exp Med. 188(10):1841-1848.

Vega MA, Strominger JL. 1989. Constitutive endocytosis of hla class i antigens requires a specific portion of the intracytoplasmic tail that shares structural features with other endocytosed molecules. Proc Natl Acad Sci U S A. 86(8):2688-2692.

Verweij MC, Hansen SG, Iyer R, John N, Malouli D, Morrow D, Scholz I, Womack J, Abdulhaqq S, Gilbride RM et al. 2021. Modulation of mhc-e transport by viral decoy ligands is required for rhcmv/siv vaccine efficacy. Science. 372(6541).

Vietzen H, Furlano PL, Cornelissen JJ, Böhmig GA, Jaksch P, Puchhammer-Stöckl E. 2023. Hla-e-restricted immune responses are crucial for the control of ebv infections and the prevention of ptld. Blood. 141(13):1560-1573.

Vigna JL, Smith KD, Lutz CT. 1996. Invariant chain association with mhc class i: Preference for hla class i/beta 2-microglobulin heterodimers, specificity, and influence of the mhc peptide-binding groove. J Immunol. 157(10):4503-4510.

Wagner B, da Silva Nardi F, Schramm S, Kraemer T, Celik AA, Dürig J, Horn PA, Dührsen U, Nückel H, Rebmann V. 2017. Hla-e allelic genotype correlates with hla-e plasma levels and predicts early progression in chronic lymphocytic leukemia. Cancer. 123(5):814-823.

Wainwright SD, Biro PA, Holmes CH. 2000. Hla-f is a predominantly empty, intracellular, tap-associated mhc class ib protein with a restricted expression pattern. J Immunol. 164(1):319-328.

Walchli S, Kumari S, Fallang LE, Sand KM, Yang W, Landsverk OJ, Bakke O, Olweus J, Gregers TF. 2014. Invariant chain as a vehicle to load antigenic peptides on human mhc class i for cytotoxic t-cell activation. Eur J Immunol. 44(3):774-784.

Wallace Z, Singh PK, Dorrell L. 2022. Combination strategies to durably suppress hiv-1: Soluble t cell receptors. J Virus Erad. 8(3):100082.

Walseng E, Bakke O, Roche PA. 2008. Major histocompatibility complex class ii-peptide complexes internalize using a clathrin- and dynamin-independent endocytosis pathway. J Biol Chem. 283(21):14717-14727.

Walters LC, Harlos K, Brackenridge S, Rozbesky D, Barrett JR, Jain V, Walter TS, O'Callaghan CA, Borrow P, Toebes M et al. 2018. Pathogen-derived hla-e bound epitopes reveal broad primary anchor pocket tolerability and conformationally malleable peptide binding. Nat Commun. 9(1):3137.

Walters LC, McMichael AJ, Gillespie GM. 2020. Detailed and atypical hla-e peptide binding motifs revealed by a novel peptide exchange binding assay. Eur J Immunol.

Walters LC, Rozbesky D, Harlos K, Quastel M, Sun H, Springer S, Rambo RP, Mohammed F, Jones EY, McMichael AJ et al. 2022. Primary and secondary functions of hla-e are determined by stability and conformation of the peptide-bound complexes. Cell Rep. 39(11):110959.

Wang Z, Zhang L, Qiao A, Watson K, Zhang J, Fan GH. 2008. Activation of cxcr4 triggers ubiquitination and down-regulation of major histocompatibility complex class i (mhc-i) on epithelioid carcinoma hela cells. J Biol Chem. 283(7):3951-3959.

Wee EG, Moyo N, Hannoun Z, Giorgi EE, Korber B, Hanke T. 2021. Effect of epitope variant co-delivery on the depth of cd8 t cell responses induced by hiv-1 conserved mosaic vaccines. Mol Ther Methods Clin Dev. 21:741-753.

Weiss A, Stobo JD. 1984. Requirement for the coexpression of t3 and the t cell antigen receptor on a malignant human t cell line. J Exp Med. 160(5):1284-1299.

Weiss A, Wiskocil RL, Stobo JD. 1984. The role of t3 surface molecules in the activation of human t cells: A two-stimulus requirement for il 2 production reflects events occurring at a pre-translational level. J Immunol. 133(1):123-128.

Wernick NL, Haucke V, Simister NE. 2005. Recognition of the tryptophan-based endocytosis signal in the neonatal fc receptor by the mu subunit of adaptor protein-2. J Biol Chem. 280(8):7309-7316.

Wiertz EJ, Jones TR, Sun L, Bogyo M, Geuze HJ, Ploegh HL. 1996a. The human cytomegalovirus us11 gene product dislocates mhc class i heavy chains from the endoplasmic reticulum to the cytosol. Cell. 84(5):769-779.

Wiertz EJ, Tortorella D, Bogyo M, Yu J, Mothes W, Jones TR, Rapoport TA, Ploegh HL. 1996b. Sec61-mediated transfer of a membrane protein from the endoplasmic reticulum to the proteasome for destruction. Nature. 384(6608):432-438.

Williams M, Roeth JF, Kasper MR, Fleis RI, Przybycin CG, Collins KL. 2002. Direct binding of human immunodeficiency virus type 1 nef to the major histocompatibility complex class i (mhc-i) cytoplasmic tail disrupts mhc-i trafficking. J Virol. 76(23):12173-12184.

Winau F, Schwierzeck V, Hurwitz R, Remmel N, Sieling PA, Modlin RL, Porcelli SA, Brinkmann V, Sugita M, Sandhoff K et al. 2004. Saposin c is required for lipid presentation by human cd1b. Nat Immunol. 5(2):169-174.

Wonderlich ER, Williams M, Collins KL. 2008. The tyrosine binding pocket in the adaptor protein 1 (ap-1) mu1 subunit is necessary for nef to recruit ap-1 to the major histocompatibility complex class i cytoplasmic tail. J Biol Chem. 283(6):3011-3022.

Wu HL, Wiseman RW, Hughes CM, Webb GM, Abdulhaqq SA, Bimber BN, Hammond KB, Reed JS, Gao L, Burwitz BJ et al. 2018. The role of mhc-e in t cell immunity is conserved among humans, rhesus macaques, and cynomolgus macaques. J Immunol. 200(1):49-60.

Wu Z, Simister NE. 2001. Tryptophan- and dileucine-based endocytosis signals in the neonatal fc receptor. J Biol Chem. 276(7):5240-5247.

Xu YP, Wieten L, Wang SX, Cai Y, Olieslagers T, Zhang L, He LM, Tilanus MGJ, Hong WX. 2019. Clinical significance of hla-e genotype and surface/soluble expression levels between healthy individuals and patients with acute leukemia. Leuk Lymphoma. 60(1):208-215.

Yang H, Rei M, Brackenridge S, Brenna E, Sun H, Abdulhaqq S, Liu MKP, Ma W, Kurupati P, Xu X et al. 2021. Hla-e-restricted, gag-specific cd8. Sci Immunol. 6(57).

Yang H, Yorke E, Hancock G, Clutton G, Sande N, Angus B, Smyth R, Mak J, Dorrell L. 2013. Improved quantification of hiv-1-infected cd4+ t cells using an optimised method of intracellular hiv-1 gag p24 antigen detection. J Immunol Methods. 391(1-2):174-178.

Ye SR, Yang H, Li K, Dong DD, Lin XM, Yie SM. 2007. Human leukocyte antigen g expression: As a significant prognostic indicator for patients with colorectal cancer. Mod Pathol. 20(3):375-383.

Zagorac GB, Mahmutefendić H, Tomaš MI, Kučić N, Le Bouteiller P, Lučin P. 2012. Early endosomal rerouting of major histocompatibility class i conformers. J Cell Physiol. 227(7):2953-2964.

Zajonc DM, Elsliger MA, Teyton L, Wilson IA. 2003. Crystal structure of cd1a in complex with a sulfatide self antigen at a resolution of 2.15 a. Nat Immunol. 4(8):808-815.

Zehner M, Marschall AL, Bos E, Schloetel JG, Kreer C, Fehrenschild D, Limmer A, Ossendorp F, Lang T, Koster AJ et al. 2015. The translocon protein sec61 mediates antigen transport from endosomes in the cytosol for cross-presentation to cd8(+) t cells. Immunity. 42(5):850-863.

Zeng L, Sullivan LC, Vivian JP, Walpole NG, Harpur CM, Rossjohn J, Clements CS, Brooks AG. 2012. A structural basis for antigen presentation by the mhc class ib molecule, qa-1b. J Immunol. 188(1):302-310.

Zheng H, Lu R, Xie S, Wen X, Wang H, Gao X, Guo L. 2015. Human leukocyte antigen-e alleles and expression in patients with serous ovarian cancer. Cancer Sci. 106(5):522-528.

Zhou D, Cantu C, Sagiv Y, Schrantz N, Kulkarni AB, Qi X, Mahuran DJ, Morales CR, Grabowski GA, Benlagha K et al. 2004. Editing of cd1d-bound lipid antigens by endosomal lipid transfer proteins. Science. 303(5657):523-527.

Zhu CB, Wang CX, Zhang X, Zhang J, Li W. 2011. Serum shla-g levels: A useful indicator in distinguishing colorectal cancer from benign colorectal diseases. Int J Cancer. 128(3):617-622.

Zinkernagel RM, Doherty PC. 1974a. Immunological surveillance against altered self components by sensitised t lymphocytes in lymphocytic choriomeningitis. Nature. 251(5475):547-548.

Zinkernagel RM, Doherty PC. 1974b. Restriction of in vitro t cell-mediated cytotoxicity in lymphocytic choriomeningitis within a syngeneic or semiallogeneic system. Nature. 248(5450):701-702.